Properties of the Vortex Lattice of an Abelian Topological Superconductor

A thesis submitted to the
College of Graduate and Postdoctoral Studies
in partial fulfillment of the requirements
for the degree of Master of Science
in the Department of Physics and Engineering Physics
University of Saskatchewan
Saskatoon

By
Victoria Howse

Permission to Use

In presenting this thesis in partial fulfillment of the requirements for a Postgraduate degree from the University of Saskatchewan, I agree that the Libraries of this University may make it freely available for inspection. I further agree that permission for copying of this thesis in any manner, in whole or in part, for scholarly purposes may be granted by the professor or professors who supervised my thesis work or, in their absence, by the Head of the Department or the Dean of the College in which my thesis work was done. It is understood that any copying or publication or use of this thesis or parts thereof for financial gain shall not be allowed without my written permission. It is also understood that due recognition shall be given to me and to the University of Saskatchewan in any scholarly use which may be made of any material in my thesis.

Disclaimer

Reference in this thesis to any specific commercial products, process, or service by trade name, trademark, manufacturer, or otherwise, does not constitute or imply its endorsement, recommendation, or favoring by the University of Saskatchewan. The views and opinions of the author expressed herein do not state or reflect those of the University of Saskatchewan, and shall not be used for advertising or product endorsement purposes.

Requests for permission to copy or to make other uses of materials in this thesis in whole or part should be addressed to:

Head of the Department of Physics and Engineering Physics
University of Saskatchewan
116 Science Place
Saskatoon, Saskatchewan S7N 5E2
Canada

OR

Dean

College of Graduate and Postdoctoral Studies

University of Saskatchewan

116 Thorvaldson Building, 110 Science Place

Saskatoon, Saskatchewan S7N 5C9 Canada

Abstract

Topological materials exhibit behaviour very different from conventional materials. Due to an integer invariant characteristic of the material, topologically-protected zero-energy excitations are guaranteed to exist at a boundary or topological defect – such as a vortex in a topological superconductor – of such a material. Topological insulators, materials which are insulating in the bulk but metallic at the surface, host massless Dirac fermions at the surface, excitations with a relativistic, helical nature. In topological superconductors, due to the intrinsic particle-hole symmetry of superconductivity, these surface states become Majorana fermions. The existence of Majorana fermions as condensed matter excitations provides not only a unique opportunity to study properties of this type of excitation, but the possibility of utilizing them for fault-tolerant topological quantum computation.

In this thesis, we study two-dimensional topological superconductivity (TSC) with broken time-reversal symmetry. Extensive research has been done on the non-Abelian phase of TSC, and an index theorem showing the existence of a single Majorana fermion in a vortex core has been derived based on the continuum model of TSC. The Abelian phase, which is allowed in the tight-binding model of TSC and is still topologically distinct from the trivial phase, has been much less studied than the non-Abelian phase. Using the tight-binding model of TSC, we derive an analogous index theorem in the Abelian phase. Our index theorem predicts that a vortex core in the Abelian phase of this system hosts two Majorana fermions as zero-energy bound states, one of which is composed mainly of quasiparticles with momentum near the Γ point and the other of quasiparticles with momentum near the M point in the Brillouin zone. We attempt to discern the relation between these two modes, in particular, if they are similar – and hence will annihilate each other – or orthogonal.

In contrast with our analytical results, we find no Majorana zero modes numerically in a vortex core in the Abelian phase. Solving the Bogoliubov-de Gennes (BdG) equations self-consistently for the superconducting order parameter, we study how the various ingredients for TSC interact in practice in this system. We use efficient, recently-developed numerical methods designed for large-scale parallel computation, namely, the Chebyshev polynomial method to solve for the mean fields without direct diagonalization of the BdG matrix, and

the Sakurai-Sugiura method to find the quasiparticle excitation energies and wave functions within an energy window of one's choice. Calculations were performed on Compute Canada clusters. Our numerical results, lacking any Majorana modes in a vortex core in the Abelian phase, are an indication that the Majorana modes in this phase are not orthogonal to each other, so that when confined in a vortex core they annihilate each other.

Acknowledgements

I would like to thank my supervisor Kaori Tanaka sincerely for her continual guidance, support, and friendship. I have learned innumerable things I consider valuable during my time as her student. I would also like to thank my supervisor's collaborator Yuki Nagai and my committee members Rainier Dick, Robert Green, and Jacek Szmigielski for their contributions. I am grateful to the Natural Sciences and Engineering Research Council of Canada as well as the University of Saskatchewan for their financial support. Compute Canada's resources were instrumental in this work.

To my sisters, and especially to my friend Matt, for their friendship and support. To my nieces, who are growing up – may they have the courage and ability to try whatever they wish to do.

Contents

List of Tables

List of Figures

List of Abbreviations

BCS	Bardeen-Cooper-Schriefer
BdG	Bogoliubov-de Gennes
BZ	Brillouin zone
LDOS	local density of states
PHS	particle-hole symmetry
SC	superconductor
SLS	sublattice or 'chiral' symmetry
SS	Sakurai-Sugiura
TI	topological insulator
TQC	topological quantum computation
TRS	time-reversal symmetry
TSC	topological superconductivity

1 Introduction

1.1 Topological Materials

In the last 15 years, the field of topological materials has undergone a huge expansion, with the discovery of many three-dimensional (3D) topological insulators (TIs), the discovery of topological superconductivity (TSC), and the convincing detection of Majorana modes in various topological superconducting materials. Three-dimensional TIs, materials which are insulating in the bulk but exhibit exotic metallic states on the surface, were first predicted in 2007 [1] and subsequently discovered in bismuth-based compounds [2, 3, 4, 5, 6, 7, 8, 9]; their novel properties are made possible by strong spin-orbit coupling, which coordinates an electron's spin with its momentum. A TI can turn into a 3D topological superconductor upon carrier doping, or present two-dimensional (2D) TSC on the surface in proximity to a conventional superconductor [8, 9]. In a topological material, *bulk-edge correspondence* says that there is a topological invariant in the bulk which is equal to the number of protected zero-energy bound states on the surface or in topological defects such as magnetic vortices [8, 9]. There have been convincing experimental observations of Majorana modes at the ends of one-dimensional (1D) superconducting wires [10, 11, 12] and on the surface of a 3D topological superconductor [9, 13], as well as a recent claim of observing Majorana modes in vortices in a TI thin film in proximity to a conventional superconductor [14]. More recently, Majorana fermions have also been detected in a 2D TSC system [15] for which the model of Sato *et al.* [16, 17] used in our study is applicable.

The first known topological material, the 2D *quantum Hall system*, was recognized as such in 1982 by Thouless, Kohomoto, Nightingale, and den Nijs (TKNN) [18], and its place in a theory of topological materials later expanded on by Wen [19]. The topological properties of this TI, like those of all currently known topological materials, emerge at low temperature,

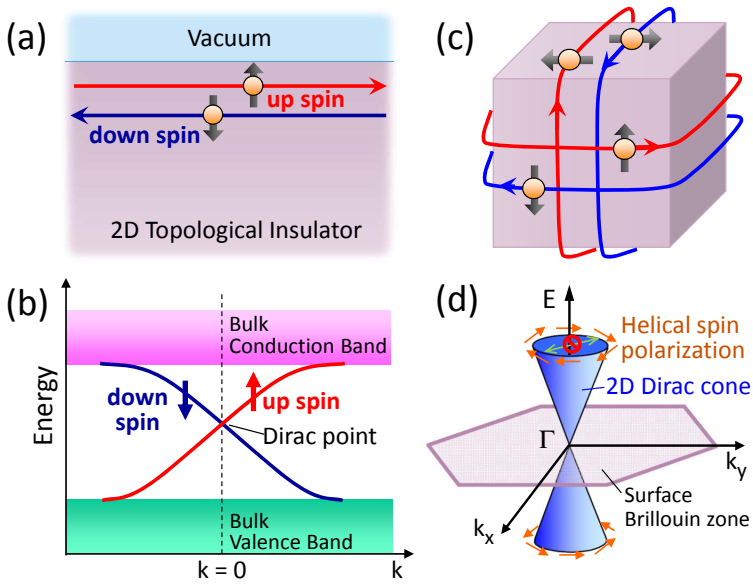

Figure 1.1: Edge and surface states of TIs. (a) Schematic of the 1D helical edge states of a 2D TI. (b) Energy dispersion of the spin non-degenerate edge states of a 2D TI forming a 1D Dirac cone. (c) Schematic of the 2D helical surface states of a 3D TI. (d) Energy dispersion of the spin non-degenerate surface states of a 3D TI forming a 2D Dirac cone; back scattering from $\boldsymbol{k}$ to $-\boldsymbol{k}$ is prohibited due to the helical spin polarization. [6] The Physical Society of Japan © (2013). http://dx.doi.org/10.7566/JPSJ.82.102001

where the system is well described by its low-energy modes. (In the case of the quantum Hall system, these modes are the Landau levels, due to the strong magnetic field giving rise to this topological state.) In the quantum Hall state, electrons propagate along the edge of the material in a single direction determined by the magnetic field, and cannot be localized by disorder as in Anderson localization due to impurities, because there are no states available for backscattering. This protected metallic edge state is due to a topological integer invariant – the first *Chern* (or *TKNN*) *number* – which measures the 'twist' of the bulk occupied states in Hilbert space (see Appendix A).

In a topological state of matter, wave functions are not adiabatically deformable into the trivial state. All topological materials have an integer invariant which characterizes the topology of the map from some parameter space (usually momentum space) to the Hilbert space of electronic wave functions. Although the topology is often discussed in momentum space, requiring a system with translational invariance, this discussion also holds for disordered materials. As long as a perturbation, representing disorder for example, does not change the particular symmetry of the *topological class* or close the bulk gap between occupied and higher-energy unoccupied states of a material, the topological properties remain unchanged.

When two materials with different invariants are in contact with each other (including a non-trivial topological material in vacuum), then, as the topological invariant must change at the boundary between them, the bulk gap must close there [20]. The presence of the bulk gap

is in this sense what gives rise to the "holographic" nature of topological materials, with the boundary reflecting the nature of the bulk via topologically-protected, gapless (zero-energy) excitations on a material's surface.

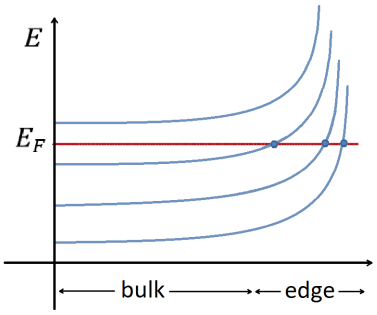

Figure 1.2: Energy bands (Landau levels) in the bulk and at the edge of a quantum Hall system. States at the Fermi energy E_F (defined as the zero of energy) arise at the material's edge.

In general these edge states are (massless) Dirac fermions, with spin locked to momentum in a chiral nature. The existence of Dirac point(s) in the boundary spectrum is protected by the bulk topology. At a Dirac point or 'Dirac cone', the energy dispersion is linear ('conical') with momentum for low energies, leading to quasiparticles with a relativistic nature. Quasiparticles travel at a constant velocity, acting massless, and are described by the Dirac equation for half-integer spin particles. In a topological superconductor, these Dirac fermion quasiparticles become Majorana fermions due to particle-hole symmetry.

The *topological* (or *symmetry*) *class* determines the type and number of these gapless edge states. All possible topological phases of single-particle Hamiltonians can be described in terms of presence or absence of time reversal symmetry (TRS), particle-hole symmetry (PHS), and sublattice or 'chiral' symmetry (SLS) [21], as shown in Table 1.1. For example, the (2D) *integer quantum Hall state* previously described is given by class A, in which all of these Hamiltonian symmetries are absent. In particular, TRS is broken in this state by the magnetic field. There is a similar but topologically different state called the *quantum spin Hall state*, in which TRS is preserved, described by an integer modulo 2 ($\mathbb{Z}_2$) invariant. In the quantum spin Hall system, the protected edge states consist of a single pair of time-reversed modes propagating in opposite directions. When a component of spin is conserved, these modes correspond to spin-up electrons propagating in one direction and spin-down electrons in the other direction.

The ten Altland-Zirnbauer (AZ) classes of random matrices describe all possible topological phases of single-particle Hamiltonians. They are given in terms of the generic symme-

Table 1.1: The ten Altland-Zirnbauer symmetry classes of single-particle Hamiltonians. Absence of symmetries is denoted by 0, while +1 and −1 refer to whether the antiunitary operator implementing the symmetry squares to $+\mathbf{1}$ or $-\mathbf{1}$. The mathematical space of all topologically non-trivial ground states for each class is given in the last three columns. [21]

		TRS	PHS	SLS	$d=1$	$d=2$	$d=3$
Standard	A (unitary)	0	0	0	-	$\mathbb{Z}$	-
(Wigner-Dyson)	AI (orthogonal)	+1	0	0	-	-	-
	AII (symplectic)	−1	0	0	-	$\mathbb{Z}_2$	$\mathbb{Z}_2$
Chiral	AIII (chiral unitary)	0	0	1	$\mathbb{Z}$	-	$\mathbb{Z}$
(sublattice)	BDI (chiral orthogonal)	+1	+1	1	$\mathbb{Z}$	-	-
	CII (chiral symplectic)	−1	−1	1	$\mathbb{Z}$	-	$\mathbb{Z}_2$
BdG	D	0	+1	0	$\mathbb{Z}_2$	$\mathbb{Z}$	-
	C	0	−1	0	-	$\mathbb{Z}$	-
	DIII	−1	+1	1	$\mathbb{Z}_2$	$\mathbb{Z}_2$	$\mathbb{Z}$
	CI	+1	−1	1	-	-	$\mathbb{Z}$

tries allowed under unitary or anti-unitary operations, TRS, PHS and SLS. Symmetries of a Hamiltonian are necessarily given by a unitary or antiunitary operator, as these are the only operators which preserve the magnitude of the inner product between states. Under TRS, momentum and spin are reversed. Under PHS, particles and holes behave equally and opposite, and the energy spectrum is symmetric about zero. SLS, which also gives energies symmetric about zero, is so-called because it often arises on a bipartite lattice, where a change of sign of wave functions on all sites of one of the two sublattices leaves the energies invariant [21].

Topological classes are well-understood in the limit of non-interacting fermion systems. Although these classes are described solely in terms of single-particle energy bands, the results also apply to interacting fermions as long as the interaction is sufficiently small compared to the size of the bulk gap [21]. When viewed as mean-field ground states, these classes can also naturally describe strongly-correlated states – the non-interacting fermions in the case of TSC are the Bogoliubov-de Gennes (BdG) quasiparticles in a superconductor.

The standard topological superconductors live in the BdG classes, which are the classes realizable only in superconducting systems. (The BdG class DIII can also describe the superfluid ^{3}He-B Balian-Werthamer state, in the limit of non-interacting quasiparticles [21].) These classes are described by the superconducting BdG Hamiltonian which uses a mean-field

theory of Cooper pairing. Mean-field theory essentially averages out the interactions between BdG quasiparticles, giving an average pairing potential ('gap function') for electrons to form into the Cooper pairs of the superconducting condensate. In reality, the pairing potential is a dynamic quantity; however, as long as the superconducting gap is large enough, the results of topological theory are the same for the true interacting-quasiparticle case as for the mean-field case.

The relation between fractional quantum Hall (FQH) states and many-body aspects of superconductors allows insight into strongly-correlated phases [21]. Under full interaction in a topological superconductor, charge fractionalization and non-trivial ground state degeneracies are thought to occur in the strongly-correlated case, providing non-Abelian properties of quasiparticles which we will discuss. The FQH effect describes a partially-filled Landau level, where interactions between electrons are strong [22]. The electron states here experience strong interactions similarly to how Cooper pairs form in a superconductor, leading to FQH quasiparticles with charges a fraction of the electron charge, among other things. Electrons (or holes) can 'carry' magnetic flux quanta around with them, leading to correlation into quasiparticles with these strange properties.

It was once thought that TSC was limited to p-wave superconductors (SCs), in which electrons form into Cooper pairs with spin-triplet pairing and an odd orbital angular momentum ($l = 1$), giving a pairing potential with the proper symmetry for topological order to appear in the standard BdG Hamiltonian. However, it was recently realized that there should be ways to 'engineer' TSC using more conventional s-wave (spin-singlet, $l = 0$) SCs in conjunction with other materials. In particular, to 'freeze' out the spin degree of freedom at the Fermi energy in a typical SC, spin-orbit coupling and Zeeman splitting under a magnetic field can be used. There are proposals for engineering TSC in this way in one, two and three dimensions, using nanowires, sandwiched 2D layers, or SCs in proximity to a 3D TI [8, 16]. In the model of Sato, Takahashi, and Fujimoto [16] first described in the context of ultracold fermionic atoms in an optical lattice [17], a 2D semiconductor material is layered next to a ferromagnetic insulator and an s-wave (or d-wave) SC, to give the ingredients necessary for TSC. Superconductivity is induced in the semiconductor by the proximity effect (tunneling of Cooper pairs), and the Zeeman field originates from the ferromagnetic material. The Zeeman

field must be larger than the size of the gap for the s-wave case in order to transition into the non-trivial topological phase. The Hamiltonian of this system can be shown to be similar to a chiral $p \pm ip$-wave superconductor under a unitary transformation [16].

The possibility of topologically-protected, Majorana zero-modes is a highly exciting prospect for topological quantum computation. Majorana fermions – charge-neutral, spin-1/2 particles that are their own antiparticles – have long been of theoretical interest in particle physics, with neutrinos and dark-matter particles as candidates, although they have not yet been detected in this context [23]. As elementary excitations in condensed-matter systems, these zero-energy modes have exciting properties: as well as being highly stable due to topological protection, they obey what are known as *non-Abelian exchange statistics*, wherein exchange of particles is non-commutative.

In two dimensions, Majorana fermion modes are a special form of what are called *anyons*, a type of particle which obeys neither the regular fermion nor boson statistics [24, 25, 23]. In a many-body wave function of identical particles, exchange of any two bosons gives back the same wave function, while exchange of any two fermions changes the sign of the wave function. In the case of Abelian anyons, the wave function is instead changed by some phase factor anywhere between 1 and -1. Anyons are particles which only exist in effectively 2D systems, where interchange of particles can occur in more than one distinct way – rotating particles counter-clockwise versus clockwise around each other gives topologically distinct paths. *Non-Abelian* anyons, realized by Majorana fermions in TSC, instead are *non-commutative* under exchange, rotating the wave function in Hilbert space. The non-Abelian property requires that the ground state of the system is degenerate, as zero-modes can be added at no extra energy cost. The exchange of Majorana modes in 2D rotates the ground state within the space of degenerate ground states. This property makes Majorana modes promising candidates for use as fault-tolerant qubits in a quantum computer [9, 26, 27]. Using two well-separated anyons as a single qubit, computations can be done by 'braiding' pairs of anyons from different qubits around each other (where the anyons' worldlines in 2D space plus time is what is referred to by a 'braid') giving a final outcome which is dependent only on the topology of the braid and not the precise paths of the anyons [24, 25, 23].

1.2 Motivation for Research

The 2D model of Sato *et al.* [16] is a very promising candidate for providing Majorana modes useful for topological qubits, with these modes pinned in vortex cores which can potentially be manipulated. In addition to the materials used in s-wave TSC being much more common than p-wave SCs, these s-wave topological superconductors in general have much more stable topological phases than p-wave SCs [16]. Thermal noise is more of a problem in p-wave SCs, as the superconducting gap is generally much smaller than for s-wave SCs. In the case of Majorana modes trapped in vortex cores of the vortex lattice in a 2D SC, the Majorana modes have a larger-than typical separation in energy from the next excited vortex state and they may be particularly stable against decoherence from intervortex tunneling. According to Sato *et al.* [16], whose model of 2D s-wave TSC we adopt, this stability is due to the fact that the Majorana mode in a vortex core may be formed mainly by quasiparticles with momentum $k \sim 0$ (near the Γ point) or $\boldsymbol{k} \sim (\pi, \pi)$ (the M point), especially far from the vortex.

We hope to elucidate the lesser-studied Abelian phase of this TSC model. The existence of *charge-density wave* states, with a wavevector near $\pm(\pi, \pi)$ (the M-point), has been studied numerically for the Abelian phase [28, 29], but analytic studies of the Abelian phase have not been done. In particular, the existence of a Majorana mode in a vortex core has been shown analytically for the non-Abelian phase [30], but it is unknown whether or how many Majorana modes exist in a vortex core in the Abelian phase. In the non-Abelian phase, with Chern number ± 1, there exists a single Majorana fermion mode in a vortex core. The Abelian phase in this model has Chern number -2, meaning that bulk-boundary correspondence would predict the existence of two Majorana modes per vortex. However, this correspondence has only been proven in a few cases [31] such as for quantum Hall systems and for a vortex core in the non-Abelian phase of Sato *et al.'s* model. If there are indeed two Majorana modes per vortex core in the Abelian phase, another question to answer would be what the relationship between these hypothetical Majorana modes is, in particular, whether they are orthogonal to each other or not, and hence whether or not they can coexist in a vortex.

1.3 Layout of Thesis

In this thesis, our aim is to study the properties of the Abelian TSC phase for the vortex lattice, in particular whether Majorana modes exist in the vortex core in this topological phase. We first present the theoretical background necessary to understand superconductivity, both in its original Bardeen-Cooper-Schrieffer (BCS) momentum-space formulation and later more-general Bogoliubov-de Gennes (BdG) formulation, as well as the theoretical background of the vortex lattice, in chapter 2. In chapter 3, we cover the 2D model of topological superconductivity (TSC) of Sato *et al.* [16] that we adopt, including the real-space BdG equations for TSC in the final section of chapter 3. In chapter 4 the numerical methods we use for efficient parallel computation are covered: the Chebyshev method for self-consistent calculation of the superconducting mean fields, the Sakurai-Sugiura (SS) method to study the energies and wave functions within an energy window of choice, and the implementation of the vortex lattice. In chapter 5 we derive an index theorem showing that the Abelian phase of this system hosts two Majorana fermion zero-modes per vortex core. Numerical results are presented in chapter 6, in which we find indication that the Majorana modes in a vortex in the Abelian phase annihilate each other – we find no Majorana modes in the vortex core numerically in this phase. Finally, chapter 7 concludes and provides a discussion of this thesis.

2 Superconductivity Theory

Superconductivity is a phenomenon occurring at low temperature, in which a material has a direct-current resistance of zero and perfect diamagnetism. This phenomenon is a powerful example of quantum-mechanical effects on a macroscopic scale. In a superconducting state, electrons form together into a system-wide condensate and behave as a collective whole, similarly to constituents of a superfluid. This condensate is described by a kind of 'wave function' called the (superconducting) order parameter, which essentially represents the fraction of electrons participating in the condensate at each point. This effect occurs below a certain temperature, T_c, the critical temperature of the material, with the fraction of electrons in the condensate increasing as temperature is lowered until all electrons are included at zero temperature.

In this chapter we cover the basics of superconductivity theory, including the original Bardeen-Cooper-Schrieffer (BCS) theory formulated in momentum space and the more general Bogoliubov-de Gennes (BdG) theory. In the final section we describe the theory of the Abrikosov vortex lattice in a type-II superconductor, including the Caroli-de Gennes-Matricon (CdGM) bound states in the vortex core.

2.1 The BCS Theory of Superconductivity

The very first microscopic theory of superconductivity was formulated by Bardeen, Cooper, and Schrieffer (BCS) in 1957 [32]. It was formulated in momentum space, for translationally-invariant systems only, though is still a powerful theory for homogeneous superconductors with no applied external field. The theory relies on the idea of 'pairing' of electrons into a macroscopic condensate. In this model, electrons form into bound states called 'Cooper pairs', in which one electron has spin up and one spin down (spin-singlet pairing). In terms of expectation values, the probability for these two single-electron states to be occupied at

the same time in the superconducting state, S, is given by,

$$P_{\boldsymbol{k}\boldsymbol{k}'} = \langle S|n_{\boldsymbol{k}\uparrow}n_{\boldsymbol{k}'\downarrow}|S\rangle, \tag{2.1}$$

where $P_{\boldsymbol{k}\boldsymbol{k}'}$ is a smoothly-varying function of $\boldsymbol{k}$ and $\boldsymbol{k}'$ *except* when $\boldsymbol{k}$ and $\boldsymbol{k}'$ are states that 'pair' (here $n_{\boldsymbol{k}\sigma}$ is the number operator counting the number of electrons in state $\boldsymbol{k}\sigma$). In the case that they pair, the probability is larger by some finite amount than for non-pairing states with nearby momenta. For the case of Cooper pairs with zero center-of-mass momentum, the electron states that pair are $\boldsymbol{k}\uparrow$ and $-\boldsymbol{k}\downarrow$ [32].

The problem Cooper first considered was that of a pair of electrons interacting above a filled Fermi sea of non-interacting electrons, where the 'sea' interacts with this electron pair only through Pauli exclusion, blocking the states below the Fermi surface. One finds from this that electrons inevitably form a bound state and that they tend to pair most strongly into the state with zero relative angular momentum. Bardeen, Cooper and Schrieffer then studied this problem, considering interacting normal-state electrons with a different effective mass (rather than "bare" electrons) and assuming only pairs with zero relative angular momentum. Taking a velocity-dependent potential V, and using the formalism of second quantization, the Hamiltonian for this problem is [32],

$$H = \sum_{\boldsymbol{k},\sigma} \epsilon_{\boldsymbol{k}} n_{\boldsymbol{k}\sigma} + \sum_{\boldsymbol{k},\boldsymbol{k}'} V_{\boldsymbol{k}'\boldsymbol{k}} b^{\dagger}_{\boldsymbol{k}'} b_{\boldsymbol{k}}, \tag{2.2}$$

where $\epsilon_{\boldsymbol{k}}$ is the kinetic energy of a normal-state electron in the state with momentum $\boldsymbol{k}$ and spin σ. The matrix element $V_{\boldsymbol{k}'\boldsymbol{k}}$ is given by,

$$V_{\boldsymbol{k}'\boldsymbol{k}} = \langle \boldsymbol{k}', -\boldsymbol{k}'|V|\boldsymbol{k}, -\boldsymbol{k}\rangle, \tag{2.3}$$

and the operator $b^{\dagger}_{\boldsymbol{k}}$ ($b_{\boldsymbol{k}}$) creates (annihilates) a *pair* of electrons with states $\boldsymbol{k}\uparrow$ and $-\boldsymbol{k}\downarrow$,

$$b^{\dagger}_{\boldsymbol{k}} = c^{\dagger}_{\boldsymbol{k}\uparrow} c^{\dagger}_{-\boldsymbol{k}\downarrow}, \tag{2.4}$$

$$b_{\boldsymbol{k}} = c_{-\boldsymbol{k}\downarrow} c_{\boldsymbol{k}\uparrow}, \tag{2.5}$$

with c and $c^{\dagger}$ representing creation and annihilation operators for single-electron (with effective mass) states. $V_{\boldsymbol{k}'\boldsymbol{k}}$ then measures the probability that a two-electron state $(\boldsymbol{k}\uparrow, -\boldsymbol{k}\downarrow)$ will be scattered into the state $(\boldsymbol{k}'\uparrow, -\boldsymbol{k}'\downarrow)$, giving an effective interaction between electrons with opposite momenta and spins.

Remarkably, as long as the interaction is attractive, that is $V_{\boldsymbol{k}'\boldsymbol{k}}$ is negative near the Fermi surface, superconductivity emerges. The effective attraction between electrons in conventional s-wave superconductivity is due to what is called *electron-phonon coupling*, where interactions between electrons and the much heavier ions in the crystal lattice cause oscillations in the ions' positions. Essentially, as an electron passes by, it pulls the nearby, positively-charged ions towards it, creating a region of greater positive charge which then attracts another electron. (The ions, being much heavier, move much more slowly than the electrons.) This effective interaction is only strong enough to overcome thermal effects counteracting it at low enough temperatures.

In the ground state of this Hamiltonian, at zero temperature, all electrons are paired. In this case, the operator $n_{\boldsymbol{k}\uparrow} + n_{-\boldsymbol{k}\downarrow}$ is equal to $2b^\dagger_{\boldsymbol{k}} b_{\boldsymbol{k}}$, twice the number of Cooper pairs. This gives the Hamiltonian of the ground state [32],

$$H_g = \sum_{\boldsymbol{k}} 2\epsilon_{\boldsymbol{k}} b^\dagger_{\boldsymbol{k}} b_{\boldsymbol{k}} + \sum_{\boldsymbol{k},\boldsymbol{k}'} V_{\boldsymbol{k}'\boldsymbol{k}} b^\dagger_{\boldsymbol{k}'} b_{\boldsymbol{k}}. \tag{2.6}$$

By using the variational principle, the approximate ground-state energy can be solved for by minimization of the total energy of the system, along with the constraint that the average number of electrons N_0 is conserved,

$$\langle\psi_0|\hat{N}_0|\psi_0\rangle \equiv \langle\psi_0| \sum_{\boldsymbol{k}\sigma} n_{\boldsymbol{k}\sigma}|\psi_0\rangle = N_0, \tag{2.7}$$

where ψ_0 is the normalized trial ground state,

$$|\psi_0\rangle = \prod_{\boldsymbol{k}} (u_{\boldsymbol{k}} + v_{\boldsymbol{k}} b^\dagger_{\boldsymbol{k}})|0\rangle, \tag{2.8}$$

with $|u_{\boldsymbol{k}}|^2 + |v_{\boldsymbol{k}}|^2 = 1$. Using the method of Lagrange multipliers, minimization is given by setting

$$\delta W \equiv \delta\langle\psi_0|H - \mu\hat{N}_0|\psi_0\rangle = 0. \tag{2.9}$$

The quantity to be minimized is then [32],

$$W = \sum_{\boldsymbol{k}} 2(\epsilon_{\boldsymbol{k}} - \mu)v^2_{\boldsymbol{k}} + \sum_{\boldsymbol{k},\boldsymbol{k}'} V_{\boldsymbol{k}'\boldsymbol{k}} u_{\boldsymbol{k}} v_{\boldsymbol{k}} u_{\boldsymbol{k}'} v_{\boldsymbol{k}'}, \tag{2.10}$$

where it has been assumed that $u_{\boldsymbol{k}}$ and $v_{\boldsymbol{k}}$ are real. Physically, $u_{\boldsymbol{k}}$ and $v_{\boldsymbol{k}}$ represent probability amplitudes for a Cooper pair in state $(\boldsymbol{k}\uparrow, -\boldsymbol{k}\downarrow)$ to be absent or present in the

superconducting condensate, respectively, and are equivalent to the particle and hole amplitudes of a quasiparticle excitation in this state. The physical meaning of the multiplier μ is the chemical potential that controls the filling factor.

On minimization with $u_{\boldsymbol{k}}$ or $v_{\boldsymbol{k}}$ as variational parameters, assuming $V_{\boldsymbol{k}'\boldsymbol{k}}$ is real (and therefore symmetric), one finds the amplitudes [32],

$$u_{\boldsymbol{k}}^2 = \frac{1}{2}\left(1 + \frac{\epsilon_{\boldsymbol{k}} - \mu}{E_{\boldsymbol{k}}}\right), \tag{2.11}$$

$$v_{\boldsymbol{k}}^2 = \frac{1}{2}\left(1 - \frac{\epsilon_{\boldsymbol{k}} - \mu}{E_{\boldsymbol{k}}}\right), \tag{2.12}$$

where,

$$E_{\boldsymbol{k}} = \frac{\Delta_{\boldsymbol{k}}}{2u_{\boldsymbol{k}}v_{\boldsymbol{k}}}, \qquad\qquad \Delta_{\boldsymbol{k}} = -\sum_{\boldsymbol{k}'} V_{\boldsymbol{k}'\boldsymbol{k}} u_{\boldsymbol{k}'} v_{\boldsymbol{k}'}. \tag{2.13}$$

The quantity $E_{\boldsymbol{k}}$ can be shown (for example by multiplying Eq. (2.11) and Eq. (2.12) together, and using Eq. (2.13) to eliminate the amplitudes $u_{\boldsymbol{k}}$ and $v_{\boldsymbol{k}}$) to be,

$$E_{\boldsymbol{k}} = +[(\epsilon_{\boldsymbol{k}} - \mu)^2 + \Delta_{\boldsymbol{k}}^2]^{1/2}. \tag{2.14}$$

As shown below, $E_{\boldsymbol{k}}$ is the energy needed to create a quasiparticle excitation of momentum $\boldsymbol{k}$ from the superconducting ground state. Using Eqs. (2.11) and (2.12) and the first of Eqs. (2.13), $E_{\boldsymbol{k}}$ satisfies the equation in matrix form,

$$\begin{pmatrix} \epsilon_{\boldsymbol{k}} - \mu & \Delta_{\boldsymbol{k}} \\ \Delta_{\boldsymbol{k}} & -(\epsilon_{\boldsymbol{k}} - \mu) \end{pmatrix} \begin{pmatrix} u_{\boldsymbol{k}} \\ v_{\boldsymbol{k}} \end{pmatrix} = E_{\boldsymbol{k}} \begin{pmatrix} u_{\boldsymbol{k}} \\ v_{\boldsymbol{k}} \end{pmatrix}. \tag{2.15}$$

The parameter $\Delta_{\boldsymbol{k}}$, which satisfies the BCS *gap equation*,

$$\Delta_{\boldsymbol{k}} = -\sum_{\boldsymbol{k}'} V_{\boldsymbol{k}\boldsymbol{k}'} \frac{\Delta_{\boldsymbol{k}'}}{2E_{\boldsymbol{k}'}}, \tag{2.16}$$

can be shown to be 1/2 the energy difference between the highest occupied and lowest unoccupied states in the ground state of this system, also known as the *energy gap*. In the BCS theory for isotropic s-wave superconductivity, the potential $V_{\boldsymbol{k}'\boldsymbol{k}}$ is assumed to be constant for energies $\epsilon_{\boldsymbol{k}}$ within the Debye energy of the Fermi surface and zero otherwise, giving $\Delta_{\boldsymbol{k}} = \Delta_0$ a constant.

These equations must be solved self-consistently in order to find $u_{\boldsymbol{k}},\ v_{\boldsymbol{k}},\ E_{\boldsymbol{k}}$ and $\Delta_{\boldsymbol{k}}$. In general one assumes a starting order parameter $\{\Delta_{\boldsymbol{k}}\}$, from which $\{E_{\boldsymbol{k}}\}$ can be found and a new $\{\Delta_{\boldsymbol{k}}\}$ calculated from the gap equation, repeating until convergence is reached.

To study the energies of quasiparticle excitations of the superconducting state, Schreiffer imagined adding a single electron in state $\boldsymbol{p}\uparrow$ to this ground state. The electron in state $\boldsymbol{p}\uparrow$ will have no pair, and deleting the pair state $(\boldsymbol{p}\uparrow,\ -\boldsymbol{p}\downarrow)$ from the ground state changes the energy (assuming $\mu = 0$) in Eq. (2.10) by

$$-2\epsilon_{\boldsymbol{p}} v_{\boldsymbol{p}}^2 - 2\left[\sum_{\boldsymbol{k}'} V_{\boldsymbol{p}\boldsymbol{k}'} u_{\boldsymbol{k}'} v_{\boldsymbol{k}'}\right] u_{\boldsymbol{p}} v_{\boldsymbol{p}}, \tag{2.17}$$

while the energy of the added electron is given by $\epsilon_{\boldsymbol{p}}$. The total excitation energy is then,

$$\epsilon_{\boldsymbol{p}}(1 - 2v_{\boldsymbol{p}}^2) + 2\Delta_{\boldsymbol{p}} u_{\boldsymbol{p}} v_{\boldsymbol{p}} = \frac{\epsilon_{\boldsymbol{p}}^2}{E_{\boldsymbol{p}}} + \frac{\Delta_{\boldsymbol{p}}^2}{E_{\boldsymbol{p}}} = E_{\boldsymbol{p}}, \tag{2.18}$$

where we find this excitation energy to be nothing but $E_{\boldsymbol{p}}$. Therefore adding an electron to the system with energy above the Fermi surface (equivalently, removing an electron below the Fermi surface) with momentum $\boldsymbol{p}$ requires energy $E_{\boldsymbol{p}}$. The minimum value of $E_{\boldsymbol{p}}$, when $\epsilon_{\boldsymbol{p}} = 0$, is $\Delta_{\boldsymbol{p}}$. In the case of instead exciting an electron from below the Fermi surface to a state above it, equivalent to both removing an electron below the Fermi energy and adding one above, the minimum energy required is $2\Delta_{\boldsymbol{p}}$.

This equivalence of adding an electron above the Fermi energy or removing one below it is reflected in the fact that

$$c_{\boldsymbol{p}\uparrow}^\dagger |\psi_0\rangle = u_{\boldsymbol{p}} |\psi_{\boldsymbol{p}\uparrow}\rangle, \tag{2.19}$$

$$c_{-\boldsymbol{p}\downarrow} |\psi_0\rangle = -v_{\boldsymbol{p}} |\psi_{\boldsymbol{p}\uparrow}\rangle, \tag{2.20}$$

where $\psi_{\boldsymbol{p}\uparrow}$ is the state with one electron added to the ground state. The Bogoliubov-Valatin (B-V) transformation, given by [32]

$$\gamma_{\boldsymbol{p}\uparrow} = u_{\boldsymbol{p}} c_{\boldsymbol{p}\uparrow} - v_{\boldsymbol{p}} c_{-\boldsymbol{p}\downarrow}^\dagger, \tag{2.21}$$

$$\gamma_{-\boldsymbol{p}\downarrow}^\dagger = u_{\boldsymbol{p}} c_{-\boldsymbol{p}\downarrow}^\dagger + v_{\boldsymbol{p}} c_{\boldsymbol{p}\uparrow}, \tag{2.22}$$

uses this fact to define the quasiparticle operators $\gamma,\ \gamma^\dagger$ of the superconducting system – equivalent to diagonalizing Eq. (2.15). In particular, we see that the quasiparticles in the

superconducting state are combinations of particles and holes. The operators γ, $\gamma^\dagger$ can be shown to be fermion operators, satisfying by direct calculation the Fermi-Dirac anticommutation relations,

$$\{\gamma^\dagger_{\boldsymbol{p}\sigma}, \gamma_{\boldsymbol{p}'\sigma'}\} = \delta_{\boldsymbol{p}\boldsymbol{p}'}\delta_{\sigma\sigma'}, \tag{2.23}$$

$$\{\gamma_{\boldsymbol{p}\sigma}, \gamma_{\boldsymbol{p}'\sigma'}\} = \{\gamma^\dagger_{\boldsymbol{p}\sigma}, \gamma^\dagger_{\boldsymbol{p}'\sigma'}\} = 0. \tag{2.24}$$

2.2 The BdG Theory of Superconductivity and the Extended Hubbard Model

Following the BCS theory came the Bogoliubov-de Gennes (BdG) [33] theory of superconductivity. The BdG formulation generalizes the BCS theory to real space, for systems not necessarily translationally-invariant; it can naturally incorporate the presence of inhomogeneities such as impurities, surfaces, or magnetic fields, for which momentum is not a good quantum number.

In real space, following the notation of de Gennes [33], one has the creation and annihilation operators,

$$\begin{aligned} \Psi^\dagger(\boldsymbol{r}\alpha) &= \sum_{\boldsymbol{k}} e^{-i\boldsymbol{k}\cdot\boldsymbol{r}} a^\dagger_{\boldsymbol{k}\alpha}, \\ \Psi(\boldsymbol{r}\alpha) &= \sum_{\boldsymbol{k}} e^{i\boldsymbol{k}\cdot\boldsymbol{r}} a_{\boldsymbol{k}\alpha}, \end{aligned} \tag{2.25}$$

where α denotes spin and a, $a^\dagger$'s are the operators in momentum space. The BdG formulation essentially generalizes the Hartree-Fock equations of a many-body system to the superconducting state. In the case of isotropic s-wave superconductivity, the full Hamiltonian can be given by

$$H = H_0 + H_1, \tag{2.26}$$

$$H_0 = \int d\boldsymbol{r} \sum_\alpha \Psi^\dagger(\boldsymbol{r}\alpha) \left[\frac{1}{2m}\left(\boldsymbol{p} - \frac{e}{c}\boldsymbol{A}\right)^2 + U_0(\boldsymbol{r})\right] \Psi(\boldsymbol{r}\alpha), \tag{2.27}$$

$$H_1 = -\frac{1}{2}V \int d\boldsymbol{r} \sum_{\alpha,\beta} \Psi^\dagger(\boldsymbol{r}\alpha)\Psi^\dagger(\boldsymbol{r}\beta)\Psi(\boldsymbol{r}\beta)\Psi(\boldsymbol{r}\alpha), \tag{2.28}$$

where $U_0(\boldsymbol{r})$ is an arbitrary, spin-independent external potential, and the interaction potential V is a constant in the isotropic case. Similarly to the BCS theory, a *mean field* approximation is used – here the interaction in H_1 is replaced by an average potential acting on only one particle at a time (therefore containing only two operators Ψ or $\Psi^\dagger$). Also defining the single-electron Hamiltonian

$$H_e(\boldsymbol{r}) = \frac{1}{2m}\left(-i\hbar\nabla - \frac{e}{c}\boldsymbol{A}\right)^2 + U_0(\boldsymbol{r}) - \mu, \tag{2.29}$$

this gives an effective Hamiltonian,

$$\begin{aligned} H_{\text{eff}} = \int d\boldsymbol{r} \Bigg[&\sum_\alpha \left(\Psi^\dagger(\boldsymbol{r}\alpha) H_e(\boldsymbol{r}) \Psi(\boldsymbol{r}\alpha) + U(\boldsymbol{r})\Psi^\dagger(\boldsymbol{r}\alpha)\Psi(\boldsymbol{r}\alpha)\right) \\ &+ \Delta(\boldsymbol{r})\Psi^\dagger(\boldsymbol{r}\uparrow)\Psi^\dagger(\boldsymbol{r}\downarrow) + \Delta^*(\boldsymbol{r})\Psi(\boldsymbol{r}\downarrow)\Psi(\boldsymbol{r}\uparrow)\Big]. \end{aligned} \tag{2.30}$$

We model the BdG theory using the extended (attractive) Hubbard model, in conjunction with a minimal tight-binding approximation (in which electrons are modelled as being tightly-bound to atoms at lattice sites). We will find a similar effective Hamiltonian. The Hubbard model was first developed in 1963 by J. Hubbard and naturally describes the interactions of electrons in a solid [34]. Using the second-quantized formalism, the most general Hubbard Hamiltonian is given by

$$H = \sum_{\langle \boldsymbol{ij}\rangle}\sum_\sigma t_{\boldsymbol{ij}} c^\dagger_{\boldsymbol{i}\sigma} c_{\boldsymbol{j}\sigma} + \sum_{\boldsymbol{i},\sigma}(\varepsilon_{\boldsymbol{i}\sigma} - \mu) n_{\boldsymbol{i}\sigma} + \sum_{\boldsymbol{i}} U_{\boldsymbol{ii}} n_{\boldsymbol{i}\uparrow} n_{\boldsymbol{i}\downarrow} + \sum_{\langle \boldsymbol{ij}\rangle}\sum_{\sigma,\sigma'} U_{\boldsymbol{ij}} n_{\boldsymbol{i}\sigma} n_{\boldsymbol{j}\sigma'}, \tag{2.31}$$

where $\langle \boldsymbol{ij}\rangle$ denotes all pairs of sites $\boldsymbol{i}$ and $\boldsymbol{j}$. Here $t_{\boldsymbol{ij}}$ is the *hopping amplitude* or probability amplitude for an electron to hop from site $\boldsymbol{j}$ to site $\boldsymbol{i}$, represented by destroying an electron at site $\boldsymbol{j}$ and creating one at site $\boldsymbol{i}$. The spin is σ, and $n_{\boldsymbol{i}\sigma} = c^\dagger_{\boldsymbol{i}\sigma} c_{\boldsymbol{i}\sigma}$ is the number operator which counts the number of electrons at site $\boldsymbol{i}$.

The energy of the system is described by both 'onsite' and 'offsite' terms. Onsite terms include energy contributions from electrons at the same site, such as the chemical potential, μ, impurity potentials, $\varepsilon_{\boldsymbol{i}\sigma}$ for a (possibly spin-dependent) impurity at site $\boldsymbol{i}$, and the coupling constant $U_{\boldsymbol{ii}}$ describing the strength of Cooper pairing between electrons at the same site. Offsite terms include the kinetic energy, from electrons 'hopping' between sites, and the longer-range coupling $U_{\boldsymbol{ij}}$, $\boldsymbol{i} \neq \boldsymbol{j}$.

In the original Hubbard model, $U_{ii} = +U > 0$ represents the screened Coulomb interaction of the band. In the extended Hubbard model, the repulsive interaction given by U_{ii} (and U_{ij}) can be changed to an *attractive* one, $U_{ii} = -U < 0$, modelling the electron-phonon or other attractive interaction giving rise to (isotropic) superconductivity. In this way, the onsite interaction, U_{ii}, can model s-wave superconductivity and the longer-range interactions U_{ij} between electrons at different sites can model p- or d-wave, etc, superconductivity.

The Hamiltonian in Eq. (2.31) can be approximated with the mean-field decomposition by rewriting,

$$c^\dagger_{i\sigma} c_{i\sigma} = \langle c^\dagger_{i\sigma} c_{i\sigma}\rangle - (\langle c^\dagger_{i\sigma} c_{i\sigma}\rangle - c^\dagger_{i\sigma} c_{i\sigma}), \tag{2.32}$$

$$c^\dagger_{i\uparrow} c^\dagger_{i\downarrow} = \langle c^\dagger_{i\uparrow} c^\dagger_{i\downarrow}\rangle - (\langle c^\dagger_{i\uparrow} c^\dagger_{i\downarrow}\rangle - c^\dagger_{i\uparrow} c^\dagger_{i\downarrow}), \tag{2.33}$$

$$c_{i\downarrow} c_{i\uparrow} = \langle c_{i\downarrow} c_{i\uparrow}\rangle - (\langle c_{i\downarrow} c_{i\uparrow}\rangle - c_{i\downarrow} c_{i\uparrow}), \tag{2.34}$$

and considering the difference between the c operator pairs and their average values to be small. Then, neglecting higher-order terms,

$$\begin{aligned} c^\dagger_{i\uparrow} c_{i\uparrow} c^\dagger_{i\downarrow} c_{i\downarrow} &= [\langle c^\dagger_{i\uparrow} c_{i\uparrow}\rangle - (\langle c^\dagger_{i\uparrow} c_{i\uparrow}\rangle - c^\dagger_{i\uparrow} c_{i\uparrow})][\langle c^\dagger_{i\downarrow} c_{i\downarrow}\rangle - (\langle c^\dagger_{i\downarrow} c_{i\downarrow}\rangle - c^\dagger_{i\downarrow} c_{i\downarrow})] \\ &\simeq -\langle c^\dagger_{i\uparrow} c_{i\uparrow}\rangle\langle c^\dagger_{i\downarrow} c_{i\downarrow}\rangle + \langle c^\dagger_{i\uparrow} c_{i\uparrow}\rangle c^\dagger_{i\downarrow} c_{i\downarrow} + c^\dagger_{i\uparrow} c_{i\uparrow}\langle c^\dagger_{i\downarrow} c_{i\downarrow}\rangle, \end{aligned} \tag{2.35}$$

and similarly,

$$c^\dagger_{i\uparrow} c^\dagger_{i\downarrow} c_{i\downarrow} c_{i\uparrow} \simeq -\langle c^\dagger_{i\uparrow} c^\dagger_{i\downarrow}\rangle\langle c_{i\downarrow} c_{i\uparrow}\rangle + \langle c^\dagger_{i\uparrow} c^\dagger_{i\downarrow}\rangle c_{i\downarrow} c_{i\uparrow} + c^\dagger_{i\uparrow} c^\dagger_{i\downarrow}\langle c_{i\downarrow} c_{i\uparrow}\rangle. \tag{2.36}$$

The Hamiltonian (2.31), neglecting longer-range interactions U_{ij} and constant terms contributing to the ground-state energy, and considering only non-magnetic impurities, can then be written as

$$\begin{aligned} H_{\text{eff}} &= H_0 + \sum_{i,\sigma} V^{(H)}_{ii} n_{i\sigma} + \sum_i \left(\Delta_{ii} c^\dagger_{i\uparrow} c^\dagger_{i\downarrow} + \Delta^*_{ii} c_{i\downarrow} c_{i\uparrow}\right) \\ &= \sum_{\langle ij\rangle,\sigma} t_{ij} c^\dagger_{i\sigma} c_{j\sigma} + \sum_{i,\sigma} (\varepsilon_i - \mu + V^{(H)}_{ii}) n_{i\sigma} + \sum_i \left(\Delta_{ii} c^\dagger_{i\uparrow} c^\dagger_{i\downarrow} + \Delta^*_{ii} c_{i\downarrow} c_{i\uparrow}\right), \end{aligned} \tag{2.37}$$

where the (onsite) Hartree and pairing potentials are given by

$$V^{(H)}_{ii} = U_{ii}\langle c^\dagger_{i\uparrow} c_{i\uparrow}\rangle = U_{ii}\langle c^\dagger_{i\downarrow} c_{i\downarrow}\rangle, \qquad \Delta_{ii} = U_{ii}\langle c_{i\downarrow} c_{i\uparrow}\rangle. \tag{2.38}$$

These can also be found by minimizing the free energy of the system. Using the fermion operator anticommutation relations, in matrix form this becomes

$$H_{\text{eff}} = \sum_{\boldsymbol{ij}} \begin{pmatrix} c^\dagger_{\boldsymbol{i}\uparrow} & c_{\boldsymbol{i}\downarrow} \end{pmatrix} \begin{pmatrix} t_{\boldsymbol{ij}} + (\epsilon_{\boldsymbol{i}} - \mu + V^{(H)}_{\boldsymbol{ii}}) & \Delta_{\boldsymbol{ii}} \\ \Delta^*_{\boldsymbol{ii}} & -t^*_{\boldsymbol{ij}} - (\epsilon_{\boldsymbol{i}} - \mu + V^{(H)}_{\boldsymbol{ii}}) \end{pmatrix} \begin{pmatrix} c_{\boldsymbol{j}\uparrow} \\ c^\dagger_{\boldsymbol{j}\downarrow} \end{pmatrix}, \tag{2.39}$$

where the Kronecker delta $\delta_{\boldsymbol{ij}}$ is implicit in $V^{\text{diag}}_{\boldsymbol{ii}} = \epsilon_{\boldsymbol{i}} - \mu + V^{(H)}_{\boldsymbol{ii}}$ and $\Delta_{\boldsymbol{ii}}$. The right-hand side sum in Eq. (2.39) can also be expressed using a matrix of size $2N \times 2N$, where N is the number of lattice sites, with vectors of operators running over all lattice sites.

The Hamiltonian (2.39) can be diagonalized by a unitary transformation,

$$c_{\boldsymbol{i}\uparrow} = \sum_{n=1}^{N} \left(\gamma_{n\uparrow} u_n(\boldsymbol{i}) - \gamma^\dagger_{n\downarrow} v^*_n(\boldsymbol{i}) \right), \tag{2.40}$$

$$c_{\boldsymbol{i}\downarrow} = \sum_{n=1}^{N} \left(\gamma_{n\downarrow} u_n(\boldsymbol{i}) + \gamma^\dagger_{n\uparrow} v^*_n(\boldsymbol{i}) \right), \tag{2.41}$$

so that,

$$H_{\text{eff}} = E_g + \sum_{n,\sigma} \varepsilon_n \gamma^\dagger_{n\sigma} \gamma_{n\sigma}, \tag{2.42}$$

where E_g is the ground-state energy. This can also be written as

$$[H_{\text{eff}}, \gamma_{n\sigma}] = -\varepsilon_n \gamma_{n\sigma}, \tag{2.43}$$

$$[H_{\text{eff}}, \gamma^\dagger_{n\sigma}] = \varepsilon_n \gamma^\dagger_{n\sigma}. \tag{2.44}$$

Finally, evaluating these commutators, and using $\Psi = (u_n, v_n)^T$, gives the *BdG equations*,

$$H_{\text{BdG}}\Psi \equiv \begin{pmatrix} \hat{T} + \hat{V}^{(H)} & \hat{\Delta} \\ \hat{\Delta}^* & -\left(\hat{T}^* + \hat{V}^{(H)} \right) \end{pmatrix} \begin{pmatrix} u_n \\ v_n \end{pmatrix} = \varepsilon_n \begin{pmatrix} u_n \\ v_n \end{pmatrix}, \tag{2.45}$$

where H_{BdG} is a $2N \times 2N$ matrix, with $\hat{T}$ the kinetic energy or "hopping" matrix, and $\hat{V}^{(H)}$ represents the diagonal terms including the Hartree potential. For off-site interactions U_{ij} with $\boldsymbol{i} \neq \boldsymbol{j}$, the Hartree potential is joined by the off-diagonal Fock potential $\hat{V}^{(F)}$, describing exchange correlation effects.

The BdG Hamiltonian has what is known as particle-hole symmetry (PHS), meaning that for every eigenstate Ψ with energy E, the particle-hole conjugate state $\Xi\Psi$ is also an eigenstate, with energy $-E$. PHS of the BdG Hamiltonian can be expressed as

$$\Xi H_{\text{BdG}} \Xi^{-1} = -H^*_{\text{BdG}}. \tag{2.46}$$

For the BdG matrix as above,

$$\Xi = \begin{pmatrix} 0 & 1 \\ -1 & 0 \end{pmatrix} \hat{K},$$

where $\hat{K}$ is the complex conjugation operator. For the BdG matrix in the case of TSC, derived in section 3.3, one has $\Xi = \tau_x \hat{K}$, where τ_x is a Pauli matrix representing particle-hole space.

The mean-field potentials can be written in terms of the normalized eigenvectors and eigenvalues by

$$V_{\boldsymbol{ii}}^{(H)} = U_{\boldsymbol{ii}} \sum_n \left[|u_n(\boldsymbol{j})|^2 f_n + |v_n(\boldsymbol{j})|^2 (1 - f_n) \right], \tag{2.47}$$

$$\Delta_{\boldsymbol{ii}} = -\frac{1}{2} U_{\boldsymbol{ii}} \sum_n \left[u_n(\boldsymbol{i}) v_n^*(\boldsymbol{j}) + u_n(\boldsymbol{j}) v_n^*(\boldsymbol{i}) \right] (1 - 2f_n), \tag{2.48}$$

where f_n is the Fermi-Dirac distribution function – or occupation probability – for filling of the single-particle energy level ε_n,

$$f_n = \frac{1}{e^{\varepsilon_n/\tau} + 1}, \tag{2.49}$$

at fundamental temperature τ, where ε_n is measured from μ.

To solve the BdG equations, one starts with a guess for the values of the mean fields, then diagonalizes the BdG matrix to obtain the eigenvalues and eigenvectors $\{\varepsilon_n,\ (u_n,\ v_n)\}$, which can then be used to recompute the mean fields using Eqs. (2.47) and (2.48). One continues on until convergence of a desired precision is reached.

2.3 Type II Superconductivity and the Vortex Lattice

A *type-I superconductor* is defined by the fact that no magnetic field can penetrate the bulk of the material. The superfluid-like nature of the electron condensate causes it to have irrotational flow, whereas the magnetic field intrinsically tends to cause rotational flow. The electron condensate of a SC will react in a way so as to cancel the magnetic field inside, leading to what is known as the *Meissner effect* or perfect diamagnetism. Under this effect, a SC will levitate in a magnetic field. In a *type-II superconductor*, however, the magnetic field can partially penetrate, leading to what is known as the Abrikosov vortex lattice [32, 33].

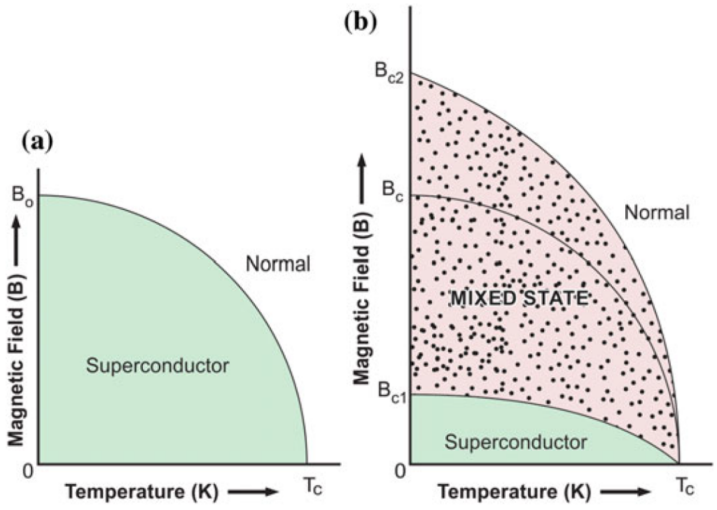

Figure 2.1: (a) Phase diagram of a type-I SC. The material is superconducting up to its critical temperature T_c and magnetic field strength B_0. (b) Phase diagram of a type-II SC. The SC now has two critical magnetic field strengths B_{c_1} and B_{c_2}. Below B_{c_1}, no magnetic field penetrates the bulk. Between B_{c_1} and the upper critical field B_{c_2}, the magnetic field penetrates at isolated vortex lines, forming the Abrikosov vortex lattice. [35] Reprinted by permission from Copyright Clearace Center: Springer, Superconductivity by R. G. Sharma © (2015). http://dx.doi.org/10.1007/978-3-319-13713-1

The order parameter goes to zero at the center of a vortex, decreasing from the bulk value over a characteristic length, ξ, known as the *coherence length* or roughly speaking the average size of a Cooper pair.

An understanding of the vortex lattice begins with the condition that the order parameter, $\Delta(\boldsymbol{r})$, must be single-valued. In polar coordinates about the vortex center, this means

$$\Delta(\boldsymbol{r}) = |\Delta(r)|e^{im\theta}, \tag{2.50}$$

where m must be an integer. The single-electron Hamiltonian, described in the notation of de Gennes [33] in Eq. (2.29),

$$H_e(\boldsymbol{A}) = \frac{1}{2m}\left(\boldsymbol{p} - \frac{e\boldsymbol{A}}{c}\right)^2 + U_0 - \mu, \tag{2.51}$$

and its complex conjugate,

$$H_e^*(\boldsymbol{A}) = \frac{1}{2m}\left(\boldsymbol{p} + \frac{e\boldsymbol{A}}{c}\right)^2 + U_0 - \mu, \tag{2.52}$$

which are equivalent to the hopping, impurity and chemical potential part of our Hamiltonian, act on the particle and hole components of the BdG eigenstates respectively:

$$\begin{aligned} \varepsilon u(\boldsymbol{r}) &= (H_e + U(\boldsymbol{r}))u(\boldsymbol{r}) + \Delta(\boldsymbol{r})v(\boldsymbol{r}), \\ \varepsilon v(\boldsymbol{r}) &= -(H_e^* + U(\boldsymbol{r}))v(\boldsymbol{r}) + \Delta^*(\boldsymbol{r})u(\boldsymbol{r}), \end{aligned} \tag{2.53}$$

where $U(\boldsymbol{r})$ is the Hartree potential.

Hamiltonians (2.51) and (2.52) depend on the choice of the vector potential $\boldsymbol{A}$ giving rise to a magnetic field. The gauge for $\boldsymbol{A}$ can be changed, for example by replacing $\boldsymbol{A}$ by $\boldsymbol{A}'$,

$$\boldsymbol{A}' = \boldsymbol{A} + \nabla\chi(\boldsymbol{r}), \tag{2.54}$$

which gives the same magnetic field (and observables) $\boldsymbol{B} = \nabla \times \boldsymbol{A} = \nabla \times \boldsymbol{A}'$. If the BdG eigenstates and order parameter in the original gauge, with $\boldsymbol{A}$, are $(u_n, v_n)^T$ and $\Delta(\boldsymbol{r})$, then changing $\boldsymbol{A}$ to $\boldsymbol{A}'$ in the BdG equations above yields the eigenfunctions,

$$\begin{aligned} u_n' &= u_n(\boldsymbol{r}) \exp\left[\frac{ie}{\hbar c}\chi(\boldsymbol{r})\right], \\ v_n' &= v_n(\boldsymbol{r}) \exp\left[-\frac{ie}{\hbar c}\chi(\boldsymbol{r})\right], \end{aligned} \tag{2.55}$$

and the order parameter

$$\Delta' = \Delta(\boldsymbol{r}) \exp\left[\frac{2ie}{\hbar c}\chi(\boldsymbol{r})\right]. \tag{2.56}$$

However, one can now see that the choice of $\chi(\boldsymbol{r})$ is not completely arbitrary, as $\Delta(\boldsymbol{r})$ must be single-valued. In particular, in winding around any loop enclosing the vortex center, one must get back the same phase factor. Taking $\Delta(\boldsymbol{r}) = |\Delta(r)|e^{im\theta}$, we therefore find

$$\chi = \frac{\hbar c}{2e} m'\theta, \tag{2.57}$$

where m' is an integer. The consequence of this is that the *magnetic flux* a vortex is allowed to carry is *quantized*. To see this, note that the magnetic flux over a region C is

$$\Phi \equiv \int_C d\boldsymbol{a}(\nabla \times \boldsymbol{A}) = \oint_{\partial C} d\boldsymbol{l} \cdot \boldsymbol{A}, \tag{2.58}$$

so that

$$\int_C d\boldsymbol{a}(\nabla \times \boldsymbol{A}') = \oint_{\partial C} d\boldsymbol{l} \cdot (\boldsymbol{A} + \nabla\chi) = \Phi + 2\pi \cdot \frac{\hbar c}{2e} m'. \tag{2.59}$$

In other words, the flux can only vary by an integer multiple of

$$\Phi_0 = \frac{hc}{2e}. \tag{2.60}$$

Namely, each vortex can carry a quantum of the magnetic flux. This can be thought of as a type-II SC's way of 'expelling' the magnetic field, by only allowing it to penetrate at isolated vortices where the superconducting order parameter is suppressed.

2.3.1 CdGM Vortex Bound States

The low-energy bound states in a vortex core, distinct from true zero-energy Majorana bound states, were first described by Caroli, de Gennes, and Matricon (CdGM) in 1964 [36]. Around a vortex, the superconducting gap $\Delta(\boldsymbol{r})$ decreases to zero at the vortex center over a length scale of the coherence length, ξ. Therefore the vortex can have localized bound states with energies lower than the bulk Δ. The energies of these bound states are the positive eigenvalues of the BdG system:

$$\begin{aligned} \varepsilon u(\boldsymbol{r}) &= \left[\frac{1}{2m}\left(\boldsymbol{p} - \tfrac{e\boldsymbol{A}}{c}\right)^2 - \mu\right] u(\boldsymbol{r}) + \Delta(\boldsymbol{r}) v(\boldsymbol{r}), \\ \varepsilon v(\boldsymbol{r}) &= \left[-\frac{1}{2m}\left(\boldsymbol{p} + \tfrac{e\boldsymbol{A}}{c}\right)^2 + \mu\right] v(\boldsymbol{r}) + \Delta(\boldsymbol{r}) u(\boldsymbol{r}). \end{aligned} \tag{2.61}$$

Choosing a gauge where $\Delta(\boldsymbol{r}) = \Delta(r)e^{-i\theta}$ ($\Delta(r)$ real), where (r, θ, z) are cylindrical coordinates around the axis of the vortex line, the phase of $\Delta(\boldsymbol{r})$ can be eliminated by setting

$$\psi \equiv \begin{pmatrix} \psi_1 \\ \psi_2 \end{pmatrix} = \begin{pmatrix} e^{i\theta/2} u \\ e^{-i\theta/2} v \end{pmatrix}. \tag{2.62}$$

Then Eq. (2.61) becomes

$$\begin{aligned} \left[\frac{1}{2m}\left(\boldsymbol{p} - \tfrac{e\boldsymbol{A}}{c} - \tfrac{1}{2}\hbar\nabla\theta\right)^2 - \mu\right] \psi_1 + \Delta(r)\psi_2 &= \varepsilon\psi_1, \\ -\left[\frac{1}{2m}\left(\boldsymbol{p} + \tfrac{e\boldsymbol{A}}{c} + \tfrac{1}{2}\hbar\nabla\theta\right)^2 - \mu\right] \psi_2 + \Delta(r)\psi_1 &= \varepsilon\psi_2, \end{aligned} \tag{2.63}$$

or

$$\sigma_z\left[\frac{1}{2m}\left(\boldsymbol{p} - \sigma_z\tfrac{e\boldsymbol{A}}{c} - \sigma_z\tfrac{1}{2}\hbar\nabla\theta\right)^2 - \mu\right]\psi + \sigma_x\Delta(r)\psi = \varepsilon\psi. \tag{2.64}$$

The CdGM bound states are found by looking for these 2-spinor solutions of the form

$$\psi = \exp(ik_F z\cos(\alpha))\exp(i\beta\theta) f(r), \tag{2.65}$$

where k_F is the Fermi momentum magnitude, α an arbitrary angle, and β a positive or negative integer. Caroli *et al.* assumed that $H_Z \ll H_{C_2}$, that is the applied Zeeman magnetic field was much smaller than the upper critical field at which type-II superconductivity is

destroyed, so that the gauge field $\frac{e\boldsymbol{A}}{c}$ can be neglected compared to $\frac{1}{2}\hbar\boldsymbol{\nabla}\theta$ [36]. Using the expression above for ψ and this assumption, Eq. (2.64) becomes

$$\sigma_z \frac{\hbar^2}{2m}\left[-\frac{d^2 f}{dr^2} - \frac{1}{r}\frac{df}{dr} + (\beta - \tfrac{1}{2}\sigma_z)^2 \frac{f}{r^2} - k_F^2 \sin^2(\alpha) f\right] + \sigma_x \Delta(r) f = \varepsilon f, \tag{2.66}$$

which Caroli *et al.* were able to solve exactly in the region $0 < \beta \ll k_F\xi$, by neglecting the Δ term for $r < r_c$, with r_c a critical radius, $(\beta + \frac{1}{2})/k_F \ll r_c \ll \xi$.

For $r < r_c$, the upper $(+)$ and lower $(-)$ components of f are found to be

$$f_\pm(r) = A_\pm J_{\beta \mp 1/2}((k_F \pm \varepsilon/v_F)\sin(\alpha) r), \tag{2.67}$$

where J is a Bessel function and $A_\pm$ normalization coefficients, while for $r > r_c$, f is found to be given by

$$f = g(r) H_m(k_F r \sin(\alpha)) + c.c., \qquad\qquad m = \sqrt{\beta^2 + \tfrac{1}{4}}, \tag{2.68}$$

where H is a Hankel function and $g(r)$ a slowly-varying envelope. Caroli *et al.* then matched the solutions at $r = r_c$ by using the asymptotic forms of the Bessel and Hankel functions. (This type of vortex bound-state solution is explored for TSC in the tight-binding model in Appendix D.)

3 Formulation of Model: Two-Dimensional Topological Superconductivity

The model of 2D s-wave TSC we study in this thesis is adopted from Sato *et al.* [16], who first described it for modelling ultracold fermionic atoms in an optical lattice [17]. One way of realizing this model experimentally is with a sandwich heterostructure. One typically uses a material exhibiting spin-orbit coupling (such as a semiconductor), under which an electron's spin is coupled to its momentum, layered next to a superconductor and a ferromagnetic insulator, to induce superconductivity and Zeeman splitting by proximity. Alternatively, a case which is more applicable to our method of self-consistently solving for the superconducting order parameter, one can use a material with both strong spin-orbit coupling and intrinsic superconductivity (such as lead) layered next to a ferromagnetic insulator [15]. We study the s-wave case only.

In real space, the tight-binding Hamiltonian for this system is

$$H_{\text{eff}} = H_K + H_{SO} + H_Z + H_s, \tag{3.1}$$

where

$$H_K = -t \sum_{\langle \boldsymbol{ij} \rangle, \sigma} c^\dagger_{\boldsymbol{i}\sigma} c_{\boldsymbol{j}\sigma} + \sum_{\boldsymbol{i},\sigma} (\varepsilon_{\boldsymbol{i}} - \mu + V^{(H)}_{\boldsymbol{ii}\bar{\sigma}}) c^\dagger_{\boldsymbol{i}\sigma} c_{\boldsymbol{i}\sigma}, \tag{3.2}$$

$$H_{SO} = -\frac{\alpha}{2} \sum_{\boldsymbol{i}} \left[\left(c^\dagger_{\boldsymbol{i}-\hat{x},\downarrow} c_{\boldsymbol{i}\uparrow} - c^\dagger_{\boldsymbol{i}+\hat{x},\downarrow} c_{\boldsymbol{i}\uparrow} \right) + i \left(c^\dagger_{\boldsymbol{i}-\hat{y},\downarrow} c_{\boldsymbol{i}\uparrow} - c^\dagger_{\boldsymbol{i}+\hat{y},\downarrow} c_{\boldsymbol{i}\uparrow} \right) + H.c. \right], \tag{3.3}$$

$$H_Z = -h \sum_{\boldsymbol{i}} \left(c^\dagger_{\boldsymbol{i}\uparrow} c_{\boldsymbol{i}\uparrow} - c^\dagger_{\boldsymbol{i}\downarrow} c_{\boldsymbol{i}\downarrow} \right), \tag{3.4}$$

$$H_s = \sum_{\boldsymbol{i}} \left(\Delta_{\boldsymbol{ii}} c^\dagger_{\boldsymbol{i}\uparrow} c^\dagger_{\boldsymbol{i}\downarrow} + \Delta^*_{\boldsymbol{ii}} c_{\boldsymbol{i}\downarrow} c_{\boldsymbol{i}\uparrow} \right), \tag{3.5}$$

where $H.c.$ stands for Hermitian conjugate, and we use a nearest-neighbour hopping approximation in which $\boldsymbol{i}$ and $\boldsymbol{j}$ are nearest neighbours only, with $\langle \boldsymbol{ij} \rangle$ now standing for pairs of nearest neighbours (see chapter 2, Eqs. (2.31) to (2.37)).

The (onsite) Hartree potentials and the pairing potential are given by

$$V_{\boldsymbol{ii}\bar{\sigma}}^{(H)} = U_{\boldsymbol{ii}}\langle c_{\boldsymbol{i}\bar{\sigma}}^{\dagger} c_{\boldsymbol{i}\bar{\sigma}}\rangle, \qquad \Delta_{\boldsymbol{ii}} = U_{\boldsymbol{ii}}\langle c_{\boldsymbol{i}\downarrow} c_{\boldsymbol{i}\uparrow}\rangle. \tag{3.6}$$

In chapter 2, we saw that the Hartree potential (average on-site attraction) in the BdG formalism was given by $V_{\boldsymbol{ii}}^{(H)} = U_{\boldsymbol{ii}}\langle c_{\boldsymbol{i}\uparrow}^{\dagger} c_{\boldsymbol{i}\uparrow}\rangle = U_{\boldsymbol{ii}}\langle c_{\boldsymbol{i}\downarrow}^{\dagger} c_{\boldsymbol{i}\downarrow}\rangle$. In the case that there are spin-dependent potentials, however, the expectation values $\langle n_{\boldsymbol{i}\uparrow}\rangle$ and $\langle n_{\boldsymbol{i}\downarrow}\rangle$ are in general not the same. In this case we have

$$V_{\boldsymbol{ii}\sigma}^{(H)} = U_{\boldsymbol{ii}}\langle n_{\boldsymbol{i}\sigma}\rangle = U_{\boldsymbol{ii}}\langle c_{\boldsymbol{i}\sigma}^{\dagger} c_{\boldsymbol{i}\sigma}\rangle, \tag{3.7}$$

where $V_{\boldsymbol{ii}\sigma}^{(H)}$ is the Hartree potential created by an electron with spin σ and felt by an electron with opposite spin $\bar{\sigma}$. As in chapter 2, we assume uniform coupling constant $U_{\boldsymbol{ii}} = -U$.

3.1 Ingredients for TSC

We now study the ingredients necessary for TSC in our 2D s-wave system. To understand spin-orbit coupling, a key ingredient of TSC in which an electron's spin is coupled to its momentum, we must look at the dispersion relation for our 2D system. With nearest-neighbour hopping only, and uniform hopping amplitude $t_{\boldsymbol{ij}} = -t$, the hopping part of the Hamiltonian is

$$\sum_{\langle \boldsymbol{ij}\rangle,\sigma} t_{\boldsymbol{ij}} c_{\boldsymbol{i}\sigma}^{\dagger} c_{\boldsymbol{j}\sigma} = -t \sum_{\boldsymbol{i},\sigma} \left(c_{\boldsymbol{i}\sigma}^{\dagger} c_{\boldsymbol{i}+\hat{x},\sigma} + c_{\boldsymbol{i}\sigma}^{\dagger} c_{\boldsymbol{i}-\hat{x},\sigma} + c_{\boldsymbol{i}\sigma}^{\dagger} c_{\boldsymbol{i}+\hat{y},\sigma} + c_{\boldsymbol{i}\sigma}^{\dagger} c_{\boldsymbol{i}-\hat{y},\sigma} \right). \tag{3.8}$$

For translationally-invariant systems, one can transform to momentum space, which requires the Fourier transform of an electron operator at lattice site $\boldsymbol{i}$ into delocalized Bloch states of momenta $\boldsymbol{k}$,

$$c_{\boldsymbol{i}\sigma}^{\dagger} = \frac{1}{\sqrt{N}} \sum_{\boldsymbol{k}\in BZ} e^{i\boldsymbol{k}\cdot\boldsymbol{R}_i} c_{\boldsymbol{k}\sigma}^{\dagger}, \tag{3.9}$$

Here $\boldsymbol{R}_i$ denotes the vector coordinate of lattice site $\boldsymbol{i}$, and $N = N_x N_y$ is the total number of sites in two dimensions. Then the hopping or kinetic energy term transforms to

$$\sum_{\langle \boldsymbol{ij}\rangle,\sigma} t_{\boldsymbol{ij}} c_{\boldsymbol{i}\sigma}^{\dagger} c_{\boldsymbol{j}\sigma} = \sum_{\boldsymbol{k},\sigma} \left[-2t(\cos k_x + \cos k_y)\right] c_{\boldsymbol{k}\sigma}^{\dagger} c_{\boldsymbol{k}\sigma}, \tag{3.10}$$

where lattice spacing $a \equiv 1$, and the representation of a delta function has been used, $\delta_{\boldsymbol{k},\boldsymbol{p}} = \frac{1}{N}\sum_{\boldsymbol{i}} e^{i(\boldsymbol{k}-\boldsymbol{p})\cdot\boldsymbol{R}_i}$. This gives the dispersion relation for a nearest-neighbour hopping Hamiltonian, measured from chemical potential μ,

$$\varepsilon(\boldsymbol{k}) = -2t(\cos k_x + \cos k_y) - \mu. \tag{3.11}$$

Spin-orbit coupling results from an effective electric field in the crystal that the electrons feel. Relativistic correction for the electron's motion results in an effective magnetic field, $\boldsymbol{B} \sim \boldsymbol{v_k} \times \boldsymbol{E}/c$, which acts differently on electrons of differing spin. In spin space the energy of this interaction is given by

$$\boldsymbol{\sigma}\cdot\boldsymbol{B} \sim \boldsymbol{\sigma}\cdot\left(\frac{1}{c}\boldsymbol{v_k}\times\boldsymbol{E}\right) = \frac{1}{c}\boldsymbol{E}\cdot(\boldsymbol{\sigma}\times\boldsymbol{v_k}), \tag{3.12}$$

where $\boldsymbol{\sigma}$ is the triplet of Pauli (spin) matrices, $\sigma_x,\ \sigma_y$ and σ_z.

A type of spin-orbit coupling known as Rashba spin-orbit coupling exists in a system with broken inversion symmetry,

$$\boldsymbol{E} = E\hat{z}. \tag{3.13}$$

In such a case, we have

$$\boldsymbol{E}\cdot(\boldsymbol{\sigma}\times\boldsymbol{v_k}) = E\left(\boldsymbol{\sigma}\times\boldsymbol{v_k}\right)_z = E\left(\sigma_x(\boldsymbol{v_k})_y - \sigma_y(\boldsymbol{v_k})_x\right). \tag{3.14}$$

The velocity $\boldsymbol{v_k}$, however, is just given by the gradient of the dispersion,

$$\boldsymbol{v_k} = \frac{1}{\hbar}\nabla_{\boldsymbol{k}}\varepsilon(\boldsymbol{k}) = \frac{1}{\hbar}2t(\sin k_x, \sin k_y). \tag{3.15}$$

The energy contribution of Rashba spin-orbit coupling in a 2D system is therefore given by

$$\begin{aligned} H_{SO} &= \alpha\sum_{\boldsymbol{k},\sigma,\sigma'}(\sigma_x\sin k_y - \sigma_y\sin k_x)_{\sigma\sigma'}c^\dagger_{\boldsymbol{k}\sigma}c_{\boldsymbol{k}\sigma'} \\ &= \alpha\sum_{\boldsymbol{k}}\begin{pmatrix}c^\dagger_{\boldsymbol{k}\uparrow} & c^\dagger_{\boldsymbol{k}\downarrow}\end{pmatrix}\begin{pmatrix}0 & \sin k_y + i\sin k_x \\ \sin k_y - i\sin k_x & 0\end{pmatrix}\begin{pmatrix}c_{\boldsymbol{k}\uparrow} \\ c_{\boldsymbol{k}\downarrow}\end{pmatrix}, \end{aligned} \tag{3.16}$$

where α is the spin-orbit coupling constant, defining the strength of the interaction, and additionally one often defines $\mathcal{L}_0(\boldsymbol{k}) = (\sin k_y, -\sin k_x, 0)$, so that H_{SO} can be written as

$$H_{SO} = \alpha\sum_{\boldsymbol{k},\sigma,\sigma'}(\mathcal{L}_0(\boldsymbol{k})\cdot\boldsymbol{\sigma})_{\sigma\sigma'}\,c^\dagger_{\boldsymbol{k}\sigma}c_{\boldsymbol{k}\sigma'}. \tag{3.17}$$

Equation (3.3) gives the spin-orbit part of the Hamiltonian in real space.

Another ingredient necessary for TSC in our system is *Zeeman splitting*. Zeeman splitting arises from an effective magnetic field perpendicular to the 2D system, for example from a ferromagnetic insulator layered next to the other materials. The Zeeman energy is given by

$$H_Z = -h \sum_{\boldsymbol{k}} \left(c^\dagger_{\boldsymbol{k}\uparrow} c_{\boldsymbol{k}\uparrow} - c^\dagger_{\boldsymbol{k}\downarrow} c_{\boldsymbol{k}\downarrow} \right) = -h \sum_{\boldsymbol{k}} (\sigma_z)_{\sigma\sigma'} c^\dagger_{\boldsymbol{k}\sigma} c_{\boldsymbol{k}\sigma'}, \tag{3.18}$$

or by Eq. (3.4) in real space.

The Pauli depairing effect, in which Zeeman splitting tends to break up Cooper pairs and destroy spin-singlet superconductivity, affects all spin-singlet superconducting systems. With larger Zeeman magnetic field, the spins of electrons become increasingly aligned with the field direction, tending to break up spin-singlet Cooper pairs. However, a larger Zeeman splitting is also desirable for maintaining the topological order of the system, as will be seen in the next section. The spin-orbit coupling tends to mitigate the Pauli depairing effect.

Finally, for completeness the superconducting s-wave order parameter is Fourier transformed to momentum space by

$$\begin{aligned} \Delta_s &= -\frac{U}{N} \sum_{\boldsymbol{i}} \langle c_{\boldsymbol{i}\downarrow} c_{\boldsymbol{i}\uparrow} \rangle = -\frac{U}{N} \frac{1}{N} \sum_{\boldsymbol{i}} \sum_{\boldsymbol{k},\boldsymbol{k}'} e^{-i\boldsymbol{k}\cdot\boldsymbol{R}_i} e^{-i\boldsymbol{k}'\cdot\boldsymbol{R}_i} \langle c_{\boldsymbol{k}\downarrow} c_{\boldsymbol{k}'\uparrow} \rangle \\ &= -\frac{U}{N} \sum_{\boldsymbol{k}} \langle c_{-\boldsymbol{k}\downarrow} c_{\boldsymbol{k}\uparrow} \rangle, \end{aligned} \tag{3.19}$$

giving the superconducting part of the Hamiltonian in momentum space,

$$H_S = \sum_{\boldsymbol{k}} \Delta_s \left(c^\dagger_{\boldsymbol{k}\uparrow} c^\dagger_{-\boldsymbol{k}\downarrow} - c_{-\boldsymbol{k}\downarrow} c_{\boldsymbol{k}\uparrow} \right) = \Delta_s \sum_{\boldsymbol{k}} (i\sigma_y)_{\sigma\sigma'} c^\dagger_{\boldsymbol{k}\sigma} c^\dagger_{-\boldsymbol{k}\sigma'} + H.c. \tag{3.20}$$

3.2 Topological regions

The topological properties of electronic wave functions in a condensed matter system are determined by the electronic band structure below the Fermi surface. With the proper ingredients, the band structure can give rise to interesting topological states even for regular s-wave superconductivity. Topological regions are defined in terms of the bulk of a system, where translational invariance exists and the system can be formulated in momentum space.

(a) $\alpha = 0$, $h = 0$.

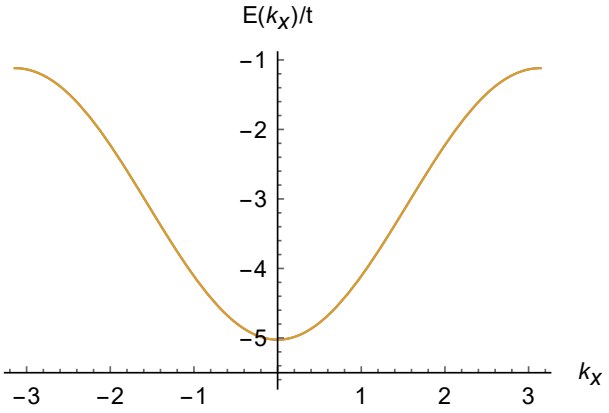

(b) $\alpha = 1.0t$, $h = 0$.

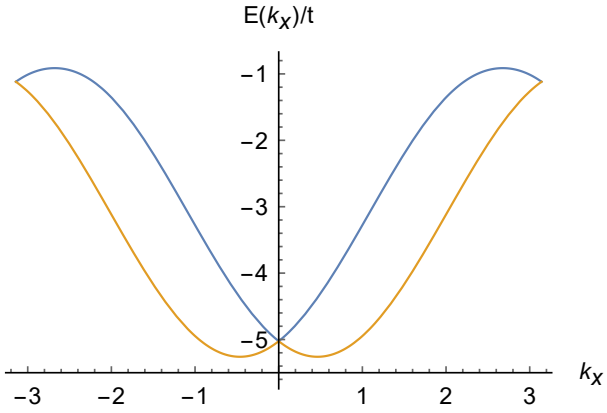

(c) $\alpha = 1.0t$, $h = 0.2t$.

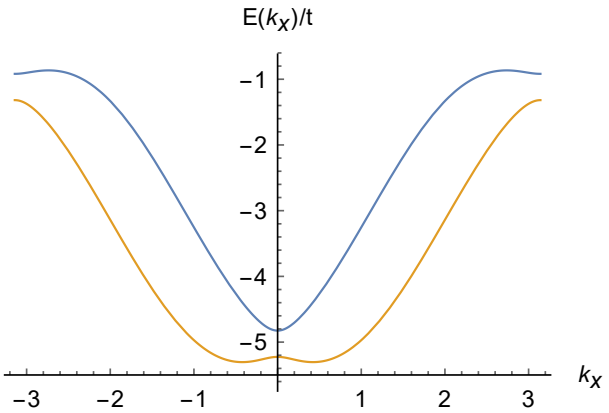

(d) $\alpha = 1.0t$, $h = 1.0t$.

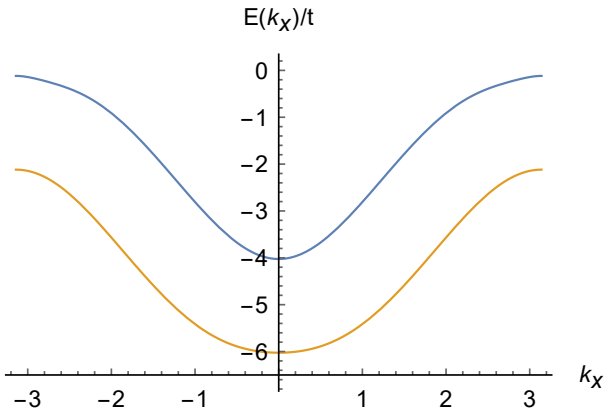

Figure 3.1: Electronic energy bands E_+ (blue) and E_- (orange) as a function of momentum k_x with $k_y = 0$, for $\mu = 1.0t$ and $\Delta = 0.5t$. The spin-orbit coupling is given by α, and the Zeeman splitting by h.

The energy bands of the ordinary (non-topological) superconducting system are everywhere spin-degenerate. Rashba spin-orbit coupling splits the spin degeneracy of the bands everywhere except at $\boldsymbol{k} = (0,0), \pm(0,\pi), \pm(\pi,0)$, and $\pm(\pi,\pi)$, giving two different bands for different spin polarizations, as in Fig. 3.1(b). Zeeman splitting from an external magnetic field breaks TRS, taking care of the remaining degeneracies so that a gap opens up between the bands, as in Fig. 3.1(c) and (d). When the Fermi energy lies in-between the bands, the spin degree of freedom is essentially locked out there (as only states in the lower band will be filled). This guarantees the existence of a single Majorana fermion mode at an edge or topological defect.

The total Hamiltonian for this system in momentum space, combining Eqs. (3.10), (3.17),

(3.18), and (3.20), is given by [16]

$$H_{\text{eff}} = \sum_{\boldsymbol{k},\sigma} \varepsilon(\boldsymbol{k}) c^\dagger_{\boldsymbol{k}\sigma} c_{\boldsymbol{k}\sigma} + \alpha \sum_{\boldsymbol{k},\sigma,\sigma'} \left(\mathcal{L}_0(\boldsymbol{k}) \cdot \boldsymbol{\sigma}\right)_{\sigma\sigma'} c^\dagger_{\boldsymbol{k}\sigma} c_{\boldsymbol{k}\sigma'} - h \sum_{\boldsymbol{k}} (\sigma_z)_{\sigma\sigma'} c^\dagger_{\boldsymbol{k}\sigma} c_{\boldsymbol{k}\sigma'} + \frac{1}{2} \sum_{\boldsymbol{k},\sigma,\sigma'} \Delta_{\sigma\sigma'}(\boldsymbol{k}) c^\dagger_{\boldsymbol{k}\sigma} c^\dagger_{-\boldsymbol{k}\sigma'} + \frac{1}{2} \sum_{\boldsymbol{k},\sigma,\sigma'} \Delta^*_{\sigma'\sigma}(\boldsymbol{k}) c_{-\boldsymbol{k}\sigma} c_{\boldsymbol{k}\sigma'}, \tag{3.21}$$

where the dispersion is $\varepsilon(\boldsymbol{k}) = -2t(\cos k_x + \cos k_y) - \mu$, the spin-orbit coupling is $\alpha\mathcal{L}_0(\boldsymbol{k}) = \alpha(\sin k_y, -\sin k_x, 0)$, and for spin-singlet – s-wave or d-wave – superconductivity, with up spins paired to down spins,

$$\Delta_{\sigma\sigma'}(\boldsymbol{k}) = i\Delta(\boldsymbol{k})(\sigma_y)_{\sigma\sigma'}. \tag{3.22}$$

In analogy with Eq. (2.39) in chapter 2, the total Hamiltonian can be rewritten in short form as

$$H_{\text{eff}} = \frac{1}{2} \sum_{\boldsymbol{k}} \Psi^\dagger_{\boldsymbol{k}} \mathcal{H}(\boldsymbol{k}) \Psi_{\boldsymbol{k}}, \qquad \Psi_{\boldsymbol{k}} = \begin{pmatrix} c_{\boldsymbol{k}\uparrow} & c_{\boldsymbol{k}\downarrow} & c^\dagger_{-\boldsymbol{k}\uparrow} & c^\dagger_{-\boldsymbol{k}\downarrow} \end{pmatrix}^T, \tag{3.23}$$

where $\mathcal{H}(\boldsymbol{k})$ is the 4×4 matrix

$$\mathcal{H}(\boldsymbol{k}) = \begin{pmatrix} \varepsilon(\boldsymbol{k}) - h\sigma_z + \alpha\mathcal{L}_0(\boldsymbol{k}) \cdot \boldsymbol{\sigma} & i\Delta(\boldsymbol{k})\sigma_y \\ -i\Delta^*(\boldsymbol{k})\sigma_y & -\varepsilon(\boldsymbol{k}) + h\sigma_z + \alpha\mathcal{L}_0(\boldsymbol{k}) \cdot \boldsymbol{\sigma}^* \end{pmatrix}. \tag{3.24}$$

As the Chern (or TKNN) number is a topological property protected by the existence of the bulk gap, it can only change when the bulk gap closes. As in Ref. [16], diagonalizing the BdG Hamiltonian (3.24) gives the bulk energy spectrum,

$$E(\boldsymbol{k}) = \sqrt{\varepsilon(\boldsymbol{k})^2 + \alpha^2\mathcal{L}_0(\boldsymbol{k})^2 + h^2 + |\Delta(\boldsymbol{k})|^2 \pm 2\sqrt{\varepsilon(\boldsymbol{k})^2\alpha^2\mathcal{L}_0(\boldsymbol{k})^2 + [\varepsilon(\boldsymbol{k})^2 + |\Delta(\boldsymbol{k})|^2]h^2}}, \tag{3.25}$$

with minimum value E_0 referred to as the bulk spectral gap. Therefore this bulk gap can only close, i.e., $E(\boldsymbol{k}) = 0$, when

$$\varepsilon(\boldsymbol{k})^2 + \alpha^2\mathcal{L}_0(\boldsymbol{k})^2 + h^2 + |\Delta(\boldsymbol{k})|^2 = 2\sqrt{\varepsilon(\boldsymbol{k})^2\alpha^2\mathcal{L}_0(\boldsymbol{k})^2 + [\varepsilon(\boldsymbol{k})^2 + |\Delta(\boldsymbol{k})|^2]h^2},$$

or

$$\varepsilon(\boldsymbol{k})^2 + |\Delta(\boldsymbol{k})|^2 = h^2 + \alpha^2\mathcal{L}_0(\boldsymbol{k})^2, \qquad |\Delta(\boldsymbol{k})|\alpha\mathcal{L}_0(\boldsymbol{k}) = 0. \tag{3.26}$$

Table 3.1: Topological regions for a 2D s-wave topological superconductor with Rashba spin-orbit coupling and Zeeman splitting, h. Odd TKNN number I_{TKNN} corresponds to the *non-Abelian* phase, and non-zero, even I_{TKNN} corresponds to the *Abelian* phase (here given by $I_{\mathrm{TKNN}} = -2$, for $|\mu| \leq 2t$ only). [16]

(a) $|\mu| \leq 2t$

Region	$(-1)^{I_{TKNN}}$	I_{TKNN}
$0 < h^2 < \mu^2 + \Delta_s^2$	1	0
$\mu^2 + \Delta_s^2 < h^2 < (4t - \lvert\mu\rvert)^2 + \Delta_s^2$	1	-2
$(4t - \lvert\mu\rvert)^2 + \Delta_s^2 < h^2 < (4t + \lvert\mu\rvert)^2 + \Delta_s^2$	-1	-1
$(4t + \lvert\mu\rvert)^2 + \Delta_s^2 < h^2$	1	0

(b) $|\mu| \geq 2t$

Region	$(-1)^{I_{TKNN}}$	I_{TKNN}
$0 < h^2 < (4t - \lvert\mu\rvert)^2 + \Delta_s^2$	1	0
$(4t - \lvert\mu\rvert)^2 + \Delta_s^2 < h^2 < \mu^2 + \Delta_s^2$	-1	1
$\mu^2 + \Delta_s^2 < h^2 < (4t + \lvert\mu\rvert)^2 + \Delta_s^2$	-1	-1
$(4t + \lvert\mu\rvert)^2 + \Delta_s^2 < h^2$	1	0

For isotropic s-wave pairing, the order parameter $|\Delta(\boldsymbol{k})| = \Delta_s$ is a constant, and the second equation is only satisfied when $\mathcal{L}_0(\boldsymbol{k}) = 0$. Therefore the gap closes only at $\boldsymbol{k} = (0, 0)$, $\pm(0, \pi)$, $\pm(\pi, 0)$, and $\pm(\pi, \pi)$. Substituting these values into the first of Eqs. (3.26), one finds three different gap-closing conditions, given by

$$(4t + \mu)^2 + \Delta_s^2 = h^2, \qquad \mu^2 + \Delta_s^2 = h^2, \qquad (4t - \mu)^2 + \Delta_s^2 = h^2. \tag{3.27}$$

These conditions mark the boundaries between (bulk) topological regions. Topological regions are listed by Chern (TKNN) number in Table 3.1.

3.3 The BdG equations for TSC

The BdG equations for TSC, as in Eqs. (2.43) and (2.44) in chapter 2, can be found from the commutators of the Hamiltonian with its eigenstates,

$$[H_{\text{eff}}, \gamma_{\tilde{n}}] = -\varepsilon_{\tilde{n}}\gamma_{\tilde{n}}, \tag{3.28}$$

$$[H_{\text{eff}}, \gamma_{\tilde{n}}^\dagger] = \varepsilon_{\tilde{n}}\gamma_{\tilde{n}}^\dagger. \tag{3.29}$$

Due to lifted spin degeneracy – each quasiparticle excitation will have both spin-up and spin-down components – the index $\tilde{n}$ runs from 1 to $2N$ (over all positive energies). There are now $4N$ equations and therefore $4N$ energy eigenvalues (symmetric about 0, due to PHS), with N the number of lattice sites.

Using the fact that the Hamiltonian is Hermitian, it can be written as

$$\begin{aligned} H_{\text{eff}} = &\frac{1}{2}\sum_{\langle \boldsymbol{ij}\rangle,\sigma} t_{\boldsymbol{ij}} c_{\boldsymbol{i}\sigma}^\dagger c_{\boldsymbol{j}\sigma} + \frac{1}{2}\sum_{\langle \boldsymbol{ij}\rangle,\sigma} t_{\boldsymbol{ij}}^* c_{\boldsymbol{j}\sigma}^\dagger c_{\boldsymbol{i}\sigma} + \sum_{\boldsymbol{i},\sigma}\left(\varepsilon_{\boldsymbol{i}\sigma} - \mu + h_\sigma + V_{\boldsymbol{ii}\bar{\sigma}}^{(H)}\right) c_{\boldsymbol{i}\sigma}^\dagger c_{\boldsymbol{i}\sigma} \\ &+ \frac{\alpha}{2}\sum_{\langle \boldsymbol{ij}\rangle} s_{\boldsymbol{ij}} c_{\boldsymbol{i}\downarrow}^\dagger c_{\boldsymbol{j}\uparrow} + \frac{\alpha}{2}\sum_{\langle \boldsymbol{ij}\rangle} s_{\boldsymbol{ij}}^* c_{\boldsymbol{j}\uparrow}^\dagger c_{\boldsymbol{i}\downarrow} + \frac{1}{2}\sum_{\boldsymbol{i}}\left(\Delta_{\boldsymbol{ii}}^{\downarrow\uparrow} c_{\boldsymbol{i}\uparrow}^\dagger c_{\boldsymbol{i}\downarrow}^\dagger + (\Delta_{\boldsymbol{ii}}^{\downarrow\uparrow})^* c_{\boldsymbol{i}\downarrow} c_{\boldsymbol{i}\uparrow}\right) \\ &+ \frac{1}{2}\sum_{\boldsymbol{i}}\left(\Delta_{\boldsymbol{ii}}^{\uparrow\downarrow} c_{\boldsymbol{i}\downarrow}^\dagger c_{\boldsymbol{i}\uparrow}^\dagger + (\Delta_{\boldsymbol{ii}}^{\uparrow\downarrow})^* c_{\boldsymbol{i}\uparrow} c_{\boldsymbol{i}\downarrow}\right), \end{aligned} \tag{3.30}$$

where $t_{\boldsymbol{ij}}$ is a hopping coefficient, $s_{\boldsymbol{ij}}$ is a spin-orbit coefficient, $\varepsilon_{\boldsymbol{i}\sigma}$ is a (possibly spin-dependent) single-impurity potential, $h_\uparrow = -h$ and $h_\downarrow = h$ is the Zeeman energy, and

$$\Delta_{\boldsymbol{ii}}^{\uparrow\downarrow} = U_{\boldsymbol{ii}}\langle c_{\boldsymbol{i}\uparrow} c_{\boldsymbol{i}\downarrow}\rangle = -U_{\boldsymbol{ii}}\langle c_{\boldsymbol{i}\downarrow} c_{\boldsymbol{i}\uparrow}\rangle = -\Delta_{\boldsymbol{ii}}^{\downarrow\uparrow}. \tag{3.31}$$

Computing the commutators of $c_{\boldsymbol{i}\uparrow}$ and $c_{\boldsymbol{i}\downarrow}$ with H_{eff} yields

$$\begin{aligned} [c_{\boldsymbol{i}\uparrow}, H_{\text{eff}}] = &\frac{1}{2}\sum_{\boldsymbol{j}} t_{\boldsymbol{ij}} c_{\boldsymbol{j}\uparrow} + \frac{1}{2}\sum_{\boldsymbol{j}} t_{\boldsymbol{ji}}^* c_{\boldsymbol{j}\uparrow} + \left(\varepsilon_{\boldsymbol{i}\uparrow} - \mu - h + V_{\boldsymbol{ii}\downarrow}^{(H)}\right) c_{\boldsymbol{i}\uparrow} \\ &+ \frac{\alpha}{2}\sum_{\boldsymbol{j}} s_{\boldsymbol{ji}}^* c_{\boldsymbol{j}\downarrow} + \Delta_{\boldsymbol{ii}}^{\downarrow\uparrow} c_{\boldsymbol{i}\downarrow}^\dagger, \end{aligned} \tag{3.32}$$

$$\begin{aligned} [c_{\boldsymbol{i}\downarrow}, H_{\text{eff}}] = &\frac{1}{2}\sum_{\boldsymbol{j}} t_{\boldsymbol{ij}} c_{\boldsymbol{j}\downarrow} + \frac{1}{2}\sum_{\boldsymbol{j}} t_{\boldsymbol{ji}}^* c_{\boldsymbol{j}\downarrow} + \left(\varepsilon_{\boldsymbol{i}\downarrow} - \mu + h + V_{\boldsymbol{ii}\uparrow}^{(H)}\right) c_{\boldsymbol{i}\downarrow} \\ &+ \frac{\alpha}{2}\sum_{\boldsymbol{j}} s_{\boldsymbol{ij}} c_{\boldsymbol{j}\uparrow} - \Delta_{\boldsymbol{ii}}^{\downarrow\uparrow} c_{\boldsymbol{i}\uparrow}^\dagger. \end{aligned} \tag{3.33}$$

We now take a unitary transformation of the c operators,

$$c_{\boldsymbol{i}\uparrow} = \sum_{\tilde{n}=1}^{2N} \left(u_{\tilde{n}\uparrow}(\boldsymbol{i})\gamma_{\tilde{n}} - v^*_{\tilde{n}\uparrow}(\boldsymbol{i})\gamma^\dagger_{\tilde{n}} \right), \tag{3.34}$$

$$c_{\boldsymbol{i}\downarrow} = \sum_{\tilde{n}=1}^{2N} \left(u_{\tilde{n}\downarrow}(\boldsymbol{i})\gamma_{\tilde{n}} - v^*_{\tilde{n}\downarrow}(\boldsymbol{i})\gamma^\dagger_{\tilde{n}} \right), \tag{3.35}$$

where the u's and v's are particle and hole amplitudes of the eigenstates, respectively, and normalization of c operators gives

$$\sum_{\tilde{n}=1}^{2N} \left[|u_{\tilde{n}\uparrow}(\boldsymbol{i})|^2 + |v_{\tilde{n}\uparrow}(\boldsymbol{i})|^2 \right] = 1, \qquad \sum_{\tilde{n}=1}^{2N} \left[|u_{\tilde{n}\downarrow}(\boldsymbol{i})|^2 + |v_{\tilde{n}\downarrow}(\boldsymbol{i})|^2 \right] = 1. \tag{3.36}$$

This unitary transformation can also be expressed as

$$\begin{pmatrix} c_\uparrow \\ c_\downarrow \\ c^\dagger_\uparrow \\ c^\dagger_\downarrow \end{pmatrix} = \begin{pmatrix} u_{1\uparrow} & u_{2\uparrow} & -v^*_{1\uparrow} & -v^*_{2\uparrow} \\ u_{1\downarrow} & u_{2\downarrow} & -v^*_{1\downarrow} & -v^*_{2\downarrow} \\ -v_{1\uparrow} & -v_{2\uparrow} & u^*_{1\uparrow} & u^*_{2\uparrow} \\ -v_{1\downarrow} & -v_{2\downarrow} & u^*_{1\downarrow} & u^*_{2\downarrow} \end{pmatrix} \begin{pmatrix} \gamma_1 \\ \gamma_2 \\ \gamma^\dagger_1 \\ \gamma^\dagger_2 \end{pmatrix},$$

where $c_\sigma = (c_{1\sigma}, \ldots, c_{N\sigma})^T$ for example runs over all lattice sites $\boldsymbol{i} = 1$ to N, while $\gamma_\alpha = (\gamma_{1\alpha}, \ldots, \gamma_{N\alpha})^T$ for example runs over states $n\alpha$, for $n = 1$ to N and $\alpha = 1, 2$ (breaking up index $\tilde{n}$ into indices $n1$ and $n2$). Equivalently, one has

$$\begin{pmatrix} \gamma_1 \\ \gamma_2 \\ \gamma^\dagger_1 \\ \gamma^\dagger_2 \end{pmatrix} = \begin{pmatrix} u^*_{1\uparrow} & u^*_{1\downarrow} & -v^*_{1\uparrow} & -v^*_{1\downarrow} \\ u^*_{2\uparrow} & u^*_{2\downarrow} & -v^*_{2\uparrow} & -v^*_{2\downarrow} \\ -v_{1\uparrow} & -v_{1\downarrow} & u_{1\uparrow} & u_{1\downarrow} \\ -v_{2\uparrow} & -v_{2\downarrow} & u_{2\uparrow} & u_{2\downarrow} \end{pmatrix} \begin{pmatrix} c_\uparrow \\ c_\downarrow \\ c^\dagger_\uparrow \\ c^\dagger_\downarrow \end{pmatrix},$$

showing explicitly that each excitation, with creation operator $\gamma^\dagger$, has a spin-up particle, a spin-down particle, a spin-up hole, and a spin-down hole part. In addition to normalization over states for each site $\boldsymbol{i}$ (Eq. (3.36)), unitarity of the transformation also gives

$$\sum_{i=1}^{N} \left[|u_{\tilde{n}\uparrow}(\boldsymbol{i})|^2 + |u_{\tilde{n}\downarrow}(\boldsymbol{i})|^2 + |v_{\tilde{n}\uparrow}(\boldsymbol{i})|^2 + |v_{\tilde{n}\downarrow}(\boldsymbol{i})|^2 \right] = 1, \tag{3.37}$$

that is, normalization over lattice sites for each state $\tilde{n}$. (Other relations between the u's and v's can be found from anticommutation relations between operators.)

Comparing the commutators (3.32) and (3.33) with their expressions when substituting in terms of γ operators, and using Eqs. (3.28) and (3.29), one finds

$$\begin{aligned}
\varepsilon_{\tilde{n}} u_{\tilde{n}\uparrow}(\boldsymbol{i}) &= \sum_{\boldsymbol{j}} t_{\boldsymbol{ij}} u_{\tilde{n}\uparrow}(\boldsymbol{j}) + \left(\varepsilon_{\boldsymbol{i}\uparrow} - \mu - h + V^{(H)}_{\boldsymbol{ii}\downarrow}\right) u_{\tilde{n}\uparrow}(\boldsymbol{i}) + \frac{\alpha}{2}\sum_{\boldsymbol{j}} s^*_{\boldsymbol{ji}} u_{\tilde{n}\downarrow}(\boldsymbol{j}) \\
&- \Delta^{\downarrow\uparrow}_{\boldsymbol{ii}} v_{\tilde{n}\downarrow}(\boldsymbol{i}), \qquad (3.38)\\
\varepsilon_{\tilde{n}} u_{\tilde{n}\downarrow}(\boldsymbol{i}) &= \sum_{\boldsymbol{j}} t_{\boldsymbol{ij}} u_{\tilde{n}\downarrow}(\boldsymbol{j}) + \left(\varepsilon_{\boldsymbol{i}\downarrow} - \mu + h + V^{(H)}_{\boldsymbol{ii}\uparrow}\right) u_{\tilde{n}\downarrow}(\boldsymbol{i}) + \frac{\alpha}{2}\sum_{\boldsymbol{j}} s_{\boldsymbol{ij}} u_{\tilde{n}\uparrow}(\boldsymbol{j}) \\
&+ \Delta^{\downarrow\uparrow}_{\boldsymbol{ii}} v_{\tilde{n}\uparrow}(\boldsymbol{i}), \qquad (3.39)\\
\varepsilon_{\tilde{n}} v_{\tilde{n}\uparrow}(\boldsymbol{i}) &= -\sum_{\boldsymbol{j}} t^*_{\boldsymbol{ij}} v_{\tilde{n}\uparrow}(\boldsymbol{j}) - \left(\varepsilon_{\boldsymbol{i}\uparrow} - \mu - h + V^{(H)}_{\boldsymbol{ii}\downarrow}\right) v_{\tilde{n}\uparrow}(\boldsymbol{i}) - \frac{\alpha}{2}\sum_{\boldsymbol{j}} s_{\boldsymbol{ji}} v_{\tilde{n}\downarrow}(\boldsymbol{j}) \\
&+ (\Delta^{\downarrow\uparrow}_{\boldsymbol{ii}})^* u_{\tilde{n}\downarrow}(\boldsymbol{i}), \qquad (3.40)\\
\varepsilon_{\tilde{n}} v_{\tilde{n}\downarrow}(\boldsymbol{i}) &= -\sum_{\boldsymbol{j}} t^*_{\boldsymbol{ij}} v_{\tilde{n}\downarrow}(\boldsymbol{j}) - \left(\varepsilon_{\boldsymbol{i}\downarrow} - \mu + h + V^{(H)}_{\boldsymbol{ii}\uparrow}\right) v_{\tilde{n}\downarrow}(\boldsymbol{i}) - \frac{\alpha}{2}\sum_{\boldsymbol{j}} s^*_{\boldsymbol{ij}} v_{\tilde{n}\uparrow}(\boldsymbol{j}) \\
&- (\Delta^{\downarrow\uparrow}_{\boldsymbol{ii}})^* u_{\tilde{n}\uparrow}(\boldsymbol{i}). \qquad (3.41)
\end{aligned}$$

Thus the BdG equations are found in their eigen-equation form,

$$\begin{pmatrix}
\hat{T} + \hat{V}^{\mathrm{diag}}_{\uparrow} & (V^{SO})^\dagger & 0 & -\Delta^{\downarrow\uparrow} \\
V^{SO} & \hat{T} + \hat{V}^{\mathrm{diag}}_{\downarrow} & \Delta^{\downarrow\uparrow} & 0 \\
0 & (\Delta^{\downarrow\uparrow})^* & -\hat{T}^* - \hat{V}^{\mathrm{diag}}_{\uparrow} & -(V^{SO})^T \\
-(\Delta^{\downarrow\uparrow})^* & 0 & -(V^{SO})^* & -\hat{T}^* - \hat{V}^{\mathrm{diag}}_{\downarrow}
\end{pmatrix}
\begin{pmatrix} u_{\tilde{n}\uparrow} \\ u_{\tilde{n}\downarrow} \\ v_{\tilde{n}\uparrow} \\ v_{\tilde{n}\downarrow} \end{pmatrix}
= \varepsilon_{\tilde{n}}
\begin{pmatrix} u_{\tilde{n}\uparrow} \\ u_{\tilde{n}\downarrow} \\ v_{\tilde{n}\uparrow} \\ v_{\tilde{n}\downarrow} \end{pmatrix}, \qquad (3.42)$$

where $\hat{T}$ is the hopping matrix, V^{SO} is the spin-orbit coupling matrix, $\hat{V}^{\mathrm{diag}}_{\boldsymbol{ii}\sigma} = \varepsilon_{\boldsymbol{i}\sigma} - \mu + h_\sigma + V^{(H)}_{\boldsymbol{ii}\bar{\sigma}}$ and the Kronecker delta $\delta_{\boldsymbol{ij}}$ is implicit for $\hat{V}^{\mathrm{diag}}_{\boldsymbol{ii}\sigma}$ and $\Delta^{\downarrow\uparrow}_{\boldsymbol{ii}}$ (in other words $\hat{V}^{\mathrm{diag}}_{\sigma}$ and $\Delta^{\downarrow\uparrow}$ are diagonal matrices). In the eigenstates, particle and hole amplitudes run over all lattice sites, for example $u_{\tilde{n}\uparrow} \equiv (u_{\tilde{n}\uparrow}(1), ..., u_{\tilde{n}\uparrow}(N))^T$.

To solve Eq. (3.42) self-consistently, the order parameter $\Delta^{\downarrow\uparrow}$ (and Hartree potentials if desired) must be recalculated from Eq. (3.42)'s solution and substituted back in. One should keep in mind that if self-consistently solving for the Hartree potentials, the topological regions defined in Table 3.1 should be thought of in terms of the effective or "shifted" chemical potential and Zeeman splitting, $\tilde{\mu}$ and $\tilde{h}$. To find $\tilde{\mu}$ and $\tilde{h}$, first define the average spin-up

and spin-down Hartree potentials,

$$\bar{V}_{\uparrow}^{(H)} = \frac{1}{N}\sum_{\boldsymbol{i}} V_{\boldsymbol{ii}\uparrow}^{(H)}, \qquad\qquad \bar{V}_{\downarrow}^{(H)} = \frac{1}{N}\sum_{\boldsymbol{i}} V_{\boldsymbol{ii}\downarrow}^{(H)}. \tag{3.43}$$

Then the term $\hat{V}_{\boldsymbol{ii}\sigma}^{\mathrm{diag}} = \varepsilon_{\boldsymbol{i}\sigma} - \mu + h_{\sigma} + V_{\boldsymbol{ii}\bar{\sigma}}^{(H)}$ can be re-written as

$$\hat{V}_{\boldsymbol{ii}\uparrow}^{\mathrm{diag}} = \varepsilon_{\boldsymbol{i}\uparrow} - (\mu - \frac{\bar{V}_{\uparrow}^{(H)} + \bar{V}_{\downarrow}^{(H)}}{2}) - (h + \frac{\bar{V}_{\uparrow}^{(H)} - \bar{V}_{\downarrow}^{(H)}}{2}) + V_{\boldsymbol{ii}\downarrow}^{(H)} - \bar{V}_{\downarrow}^{(H)}, \tag{3.44}$$

$$\hat{V}_{\boldsymbol{ii}\downarrow}^{\mathrm{diag}} = \varepsilon_{\boldsymbol{i}\downarrow} - (\mu - \frac{\bar{V}_{\uparrow}^{(H)} + \bar{V}_{\downarrow}^{(H)}}{2}) + (h + \frac{\bar{V}_{\uparrow}^{(H)} - \bar{V}_{\downarrow}^{(H)}}{2}) + V_{\boldsymbol{ii}\uparrow}^{(H)} - \bar{V}_{\uparrow}^{(H)}. \tag{3.45}$$

Thus the effective chemical potential is measured from the average of the Hartree potentials, by

$$\tilde{\mu} = \mu - \frac{\bar{V}_{\uparrow}^{(H)} + \bar{V}_{\downarrow}^{(H)}}{2}, \tag{3.46}$$

and the effective Zeeman splitting is given by

$$\tilde{h} = h + \frac{\bar{V}_{\uparrow}^{(H)} - \bar{V}_{\downarrow}^{(H)}}{2}. \tag{3.47}$$

The simplest method of solving the BdG equations is through direct diagonalization, where all eigenvectors and eigenvalues are found. To calculate the mean fields by direct diagonalization, one uses the definitions,

$$V_{\boldsymbol{ii}\sigma}^{(H)} = U_{\boldsymbol{ii}}\langle c_{\boldsymbol{i}\sigma}^{\dagger} c_{\boldsymbol{i}\sigma}\rangle, \tag{3.48}$$

$$\Delta_{\boldsymbol{ii}}^{\downarrow\uparrow} = U_{\boldsymbol{ii}}\langle c_{\boldsymbol{i}\downarrow} c_{\boldsymbol{i}\uparrow}\rangle. \tag{3.49}$$

In terms of diagonalized γ operators, one has

$$\begin{aligned}
\langle c_{\boldsymbol{i}\sigma}^{\dagger} c_{\boldsymbol{i}\sigma}\rangle &= \left\langle \sum_{\tilde{n}=1}^{2N} \left(u_{\tilde{n}\sigma}^{*}(\boldsymbol{i})\gamma_{\tilde{n}}^{\dagger} - v_{\tilde{n}\sigma}(\boldsymbol{i})\gamma_{\tilde{n}} \right) \sum_{\tilde{m}=1}^{2N} \left(u_{\tilde{m}\sigma}(\boldsymbol{i})\gamma_{\tilde{m}} - v_{\tilde{m}\sigma}^{*}(\boldsymbol{i})\gamma_{\tilde{m}}^{\dagger} \right) \right\rangle \\
&= \sum_{\tilde{m},\tilde{n}=1}^{2N} \left[|u_{\tilde{n}\sigma}(\boldsymbol{i})|^2 \left\langle \gamma_{\tilde{n}}^{\dagger}\gamma_{\tilde{m}} \right\rangle + |v_{\tilde{n}\sigma}(\boldsymbol{i})|^2 \left\langle \gamma_{\tilde{n}}\gamma_{\tilde{m}}^{\dagger} \right\rangle \right] \\
&= \sum_{\tilde{n}=1}^{2N} \left[|u_{\tilde{n}\sigma}(\boldsymbol{i})|^2 f_{\tilde{n}} + |v_{\tilde{n}\sigma}(\boldsymbol{i})|^2 (1 - f_{\tilde{n}}) \right],
\end{aligned} \tag{3.50}$$

where $f_{\tilde{n}}$ is the Fermi-Dirac distribution, or occupation probability, for eigenstate $\tilde{n}$. Similarly, one has

$$\langle c_{\boldsymbol{i}\downarrow} c_{\boldsymbol{i}\uparrow}\rangle = \sum_{\tilde{n}=1}^{2N} \left[-u_{\tilde{n}\downarrow}(\boldsymbol{i}) v_{\tilde{n}\downarrow}^{*}(\boldsymbol{i})(1 - f_{\tilde{n}}) + v_{\tilde{n}\uparrow}^{*}(\boldsymbol{i}) u_{\tilde{n}\uparrow}(\boldsymbol{i}) f_{\tilde{n}} \right]. \tag{3.51}$$

Therefore, if all eigenvectors and eigenvalues in Eq. (3.42) are found from an initial guess, all $\Delta_{\boldsymbol{ii}}^{\downarrow\uparrow}$ and $V_{\boldsymbol{ii}\sigma}^{(H)}$ can be recalculated using Eq. (3.48) and Eq. (3.49). This method works well for smaller lattice sizes, though at larger lattice sizes it is computationally more efficient to avoid direct diagonalization of the BdG matrix, which becomes very costly numerically for large N. Numerical methods are covered in chapter 4.

4 Numerical Methods

This chapter discusses the numerical methods used to study our system, including the Chebyshev polynomial expansion method, the Sakurai-Sugiura method, and implementation of the vortex lattice.

Although direct diagonalization of Eq. (3.42) to find all energies and eigenstates works well for small lattice sizes, this method is not easy to parallelize, and it becomes very computationally demanding for large lattice sizes. The Chebyshev method [37, 38], based on Green functions, avoids diagonalization of the BdG matrix, instead finding the mean fields directly. In addition this method is easy to parallelize, as the mean fields at different lattice sites can be calculated independently. As opposed to direct diagonalization, in which computation time increases as $\mathcal{O}(N^3)$ with N the number of lattice sites, the Chebyshev method takes $\mathcal{O}(N^2)$ time. The Sakurai-Sugiura (SS) method [39], also based on Green functions, allows one to find the quasiparticle energies and wave functions within an energy window of one's choice. The SS method is useful alongside the Chebyshev method (which does not find the eigenpairs directly), especially to check the existence of any zero-energy excitations and whether they are truly Majorana fermions or not.

4.1 Chebyshev Polynomial Method

The Chebyshev polynomial method is useful for calculating the mean fields as well as the local density of states (LDOS) without diagonalizing the BdG matrix. This method expands either the Green function or the spectral density of the Green function by Chebyshev polynomials. The idea of expansion by a set of orthonormal polynomials is called *kernel polynomial expansion*. Chebyshev polynomials work particularly well for expansion, and can be efficiently found by a recursive formula. Both expansions, for the mean fields and LDOS, can be easily implemented in parallel, as calculations for each lattice site can be performed

separately. Lattice points near inhomogeneities such as impurities and vortex cores, which tend to converge more slowly, can therefore also be sampled with higher frequency.

The Chebyshev expansion is closest in efficiency to the Lanczos procedure, another recursive method using Green functions. However, the Lanczos method can become unstable numerically with round-off errors causing loss of orthogonality between the calculated basis vectors, while the Chebyshev expansion is stable, with its moments decaying exponentially above a given number of iterations [38]. Unlike the Lanczos procedure, the Chebyshev expansion can also find all off-diagonal elements (e.g. correlations between nearest neighbours) for a site i using only one iteration. Other benefits of the Chebyshev expansion include the fact that it is a Fourier transform with a change of variables, meaning that any integration of the Green functions components over energy variables can be calculated numerically with a fast Fourier transform.

We first describe the method to find the mean fields, in which the spectral density of the Green function is expanded, following the notation of Nagai *et al* [37]. We then describe expansion of the Green function to find the local density of states, following Covaci *et al* [38].

4.1.1 Hamiltonian and Spectral Density of the Green Function

The Hamiltonian is described by [37],

$$H = \frac{1}{2}\Psi^\dagger \hat{\mathcal{H}} \Psi, \qquad \Psi = (\{c_j\}, \{c_j^\dagger\})^T, \tag{4.1}$$

where $\{c_j\} = (c_1, c_2, ..., c_N)$, with j a quantum index depending on spatial site, spin, orbital, etc. Here, the size N is only equal to the number of lattice sites in the case of ordinary superconductivity in our model; otherwise it is doubled to include spin.

The BdG equations are

$$\hat{\mathcal{H}} \begin{pmatrix} u_{(\gamma)} \\ v_{(\gamma)} \end{pmatrix} = \varepsilon_\gamma \begin{pmatrix} u_{(\gamma)} \\ v_{(\gamma)} \end{pmatrix}, \qquad \gamma = 1, 2, ..., N \tag{4.2}$$

and are diagonalized by a unitary transformation $U^\dagger \mathcal{H} U = D$, where

$$U_{j\gamma} = u_{(\gamma),j}, \qquad U_{j+N,\gamma} = v_{(\gamma),j}. \tag{4.3}$$

Introducing notation for the set of $2N$ standard unit vectors $\boldsymbol{e}(j) \equiv |c_j\rangle$ and $\boldsymbol{h}(j) \equiv |c_j^\dagger\rangle$ $(j = 1, 2, ..., N)$, defined as

$$[\boldsymbol{e}(j)]_\gamma = \delta_{j,\gamma}, \qquad\qquad [\boldsymbol{h}(j)]_\gamma = \delta_{j+N,\gamma}, \tag{4.4}$$

one can express the particle and hole amplitudes by

$$u_{(\gamma),j} = [\boldsymbol{e}(j)^T U]_\gamma, \qquad\qquad v^*_{(\gamma),j} = [U^\dagger \boldsymbol{h}(j)]_\gamma. \tag{4.5}$$

The Green function, $\hat{G}(z) = (z - \hat{\mathcal{H}})^{-1}$, is given by

$$\hat{G}_{\alpha\beta}(z) = \sum_{\gamma=1}^{2N} U_{\alpha\gamma} U^*_{\beta\gamma} \frac{1}{z - \varepsilon_\gamma}. \tag{4.6}$$

The *spectral density* of the Green function is given by the difference between the retarded and advanced Green functions, $\hat{d}(\omega) = \hat{G}^R(\omega) - \hat{G}^A(\omega) = \lim_{\eta\to 0^+}(\hat{G}(\omega + i\eta) - \hat{G}(\omega - i\eta))$. Using the Sokhotsky-Plemelj relations for the real line,

$$\lim_{\eta\to 0^+} \int_a^b \frac{f(x)}{x \pm i\eta} dx = \mp i\pi f(0) + \mathcal{P} \int_a^b \frac{f(x)}{x} dx,$$

with $f(x) = \delta(x)$ giving $\lim_{\eta\to 0^+} 1/(x \pm i\eta) = \mp i\pi\delta(x) + \mathcal{P}(1/x)$, this yields

$$[\hat{d}(\omega)]_{\alpha\beta} = -2\pi i \sum_{\gamma=1}^{2N} U_{\alpha\gamma} U^*_{\beta\gamma} \delta(\omega - \varepsilon_\gamma). \tag{4.7}$$

The local density of states for a particular quantum index, j, is then given in terms of this spectral density by

$$\begin{aligned} N(\omega, j) &= \sum_{j'=1}^{N} |u_{(j'),j}|^2 \delta(\omega - \varepsilon_{j'}) + \sum_{j'=1}^{N} |v_{(j'),j}|^2 \delta(\omega + \varepsilon_{j'}) \\ &= -\frac{1}{2\pi i} \boldsymbol{e}(j)^T \hat{d}(\omega) \boldsymbol{e}(j). \end{aligned} \tag{4.8}$$

Similarly, the mean fields (the Hartree potential(s) and superconducting order parameter) are found from $\langle c_j^\dagger c_{j'}\rangle$ and $\langle c_j c_{j'}\rangle$, which can be expressed as

$$\langle c_j^\dagger c_{j'}\rangle = -\frac{1}{2\pi i} \int_{-\infty}^{\infty} d\omega\, f(\omega) \boldsymbol{e}(j')^T \hat{d}(\omega) \boldsymbol{e}(j), \tag{4.9}$$

$$\langle c_j c_{j'}\rangle = -\frac{1}{2\pi i} \int_{-\infty}^{\infty} d\omega\, f(\omega) \boldsymbol{e}(j')^T \hat{d}(\omega) \boldsymbol{h}(j), \tag{4.10}$$

with $f(x) = 1/(e^{x/\tau} + 1)$ the Fermi-Dirac distribution.

4.1.2 Expansion by Chebyshev Polynomials

A set of orthonormal polynomials $\phi_n(x)$, defined on $x \in (a, b)$, is given in general by

$$\delta(x - x') = \sum_{n=0}^{\infty} \frac{W(x)}{w_n} \phi_n(x)\phi_n(x'), \tag{4.11}$$

$$w_n \delta_{n,m} = \int_a^b \phi_n(x)\phi_m(x)W(x)dx, \tag{4.12}$$

with weights w_n and weighting function $W(x)$. The Chebyshev polynomials, which are defined on the interval $[-1, 1]$, are given by

$$\phi_n(x) = \cos\left[n \arccos\left(x\right)\right], \tag{4.13}$$

$$W(x) = \frac{1}{\sqrt{1 - x^2}}, \qquad w_n = \frac{\pi}{2}(1 + \delta_{n0}). \tag{4.14}$$

Additionally, the Chebyshev polynomials can easily be defined recursively by

$$\phi_{n+1}(x) = 2x\phi_n(x) - \phi_{n-1}(x) \quad (n \geq 2), \tag{4.15}$$

$$\phi_1(x) = x, \qquad \phi_0(x) = 1. \tag{4.16}$$

In order to contain the energy eigenvalues within the interval $[-1, 1]$ on which Chebyshev polynomials are defined, the Hamiltonian and corresponding energies are rescaled as

$$\hat{\mathcal{K}} = \frac{\hat{\mathcal{H}} - b\hat{I}}{a}, \qquad \xi_\gamma = \frac{\varepsilon_\gamma - b}{a}, \tag{4.17}$$

where $a = (E_{\max} - E_{\min})/2$ and $b = (E_{\max} + E_{\min})/2$, $E_{\min} \leq \varepsilon_\gamma \leq E_{\max}$, although these numbers can be approximated. As PHS gives $E_{\min} = -E_{\max}$, we have $b = 0$, and as shown in Section 4.1.3 we determine an optimal value of a numerically.

One can define a matrix form by Chebyshev polynomials,

$$[\phi_n(\hat{\mathcal{K}})]_{\alpha\beta} = \sum_{\gamma=1}^{2N} U_{\alpha\gamma} U^*_{\beta\gamma} \phi_n(\xi_\gamma), \tag{4.18}$$

with $\phi_n(\xi_\gamma)$ well-defined in the interval $\xi_\gamma \in [-1, 1]$. Now, substituting the delta function in the definition (4.7) of the spectral density $[\hat{d}(\omega)]$ for the right hand side of Eq. (4.11), noting

that ω should also be rescaled, one finds:

$$[\hat{d}(\omega)]_{\alpha\beta} = -\frac{2\pi i}{a}\sum_{n=0}^{\infty}\frac{W(\omega)}{w_n}\phi_n(\omega)\sum_{\gamma=1}^{2N}U_{\alpha\gamma}U^*_{\beta\gamma}\phi_n(\xi_\gamma) \tag{4.19}$$

$$= -\frac{2\pi i}{a}\sum_{n=0}^{\infty}\frac{W(\omega)}{w_n}\phi_n(\omega)[\phi_n(\hat{\mathcal{K}})]_{\alpha\beta}, \tag{4.20}$$

yielding

$$\boldsymbol{p}^T\hat{d}(\omega)\boldsymbol{q} = -\frac{2\pi i}{a}\sum_{n=0}^{\infty}\frac{W(\omega)}{w_n}\phi_n(\omega)\boldsymbol{p}^T\boldsymbol{q}_n \tag{4.21}$$

for any real $2N$-component vectors $\boldsymbol{p}$ and $\boldsymbol{q}$, where we have defined $\boldsymbol{q}_n = \phi_n(\hat{\mathcal{K}})\boldsymbol{q}$. Using the recursiveness of the Chebyshev polynomials, a sequence of vectors $\boldsymbol{q}_n$ can be recursively generated by

$$\boldsymbol{q}_{n+1} = 2\hat{\mathcal{K}}\boldsymbol{q}_n - \boldsymbol{q}_{n-1} \quad (n \geq 2), \tag{4.22}$$

$$\boldsymbol{q}_1 = \phi_1(\hat{\mathcal{K}})q = \hat{\mathcal{K}}q, \qquad \boldsymbol{q}_0 = \phi_0(\hat{\mathcal{K}})q = q. \tag{4.23}$$

Going back to Eqs. (4.9) and (4.10) for the mean fields, one can now substitute to find

$$\langle c_j^\dagger c_{j'}\rangle = \sum_{n=0}^{\infty}\boldsymbol{e}(j')^T\boldsymbol{e}_n(j)\frac{\mathcal{T}_n}{w_n}, \tag{4.24}$$

$$\langle c_j c_{j'}\rangle = \sum_{n=0}^{\infty}\boldsymbol{e}(j')^T\boldsymbol{h}_n(j)\frac{\mathcal{T}_n}{w_n}, \tag{4.25}$$

where

$$\mathcal{T}_n = \int_{-1}^{1}dx f(ax+b)W(x)\phi_n(x), \tag{4.26}$$

with $\boldsymbol{e}_n(j) = \phi_n(\hat{\mathcal{K}})\boldsymbol{e}(j)$ and $\boldsymbol{h}_n(j) = \phi_n(\hat{\mathcal{K}})\boldsymbol{h}(j)$. The integrals $\mathcal{T}_n$ depend only on temperature and so can be calculated prior to recursively finding $\boldsymbol{e}_n$ and $\boldsymbol{h}_n$ for the mean fields. At zero temperature, one has (recalling also $b = 0$ for the BdG system)

$$\mathcal{T}_0 = \pi - \arccos(-b/a) = \frac{\pi}{2}, \tag{4.27}$$

$$\mathcal{T}_{n\neq 0} = \frac{\sin[n\arccos(-b/a)]}{n} = \frac{\sin(n\pi/2)}{n}. \tag{4.28}$$

The LDOS can be found in a similar manner to the mean fields. In this case, one expands the Green function itself by Chebyshev polynomials. Following [38], define the normal and

anomalous Green functions as

$$\bar{G}^{11}_{\boldsymbol{ij}}(\omega) = \langle c_{\boldsymbol{i}\uparrow}|\hat{G}(\omega)|c^{\dagger}_{\boldsymbol{j}\uparrow}\rangle, \tag{4.29}$$

$$\bar{G}^{12}_{\boldsymbol{ij}}(\omega) = \langle c^{\dagger}_{\boldsymbol{i}\downarrow}|\hat{G}(\omega)|c^{\dagger}_{\boldsymbol{j}\uparrow}\rangle^{*}, \tag{4.30}$$

where $\boldsymbol{i}$ and $\boldsymbol{j}$ denote only spatial site. Again rescaling ω, one finds

$$\bar{G}^{11(12)}_{\boldsymbol{ij}}(\omega) = \frac{-2i}{\sqrt{1-\omega^2}} \sum_{n=0}^{\infty} a_n^{11(12)}(\boldsymbol{i},\boldsymbol{j}) e^{-in \arccos(\omega)}, \tag{4.31}$$

where

$$a_n^{11}(\boldsymbol{i},\boldsymbol{j}) = \langle c_{\boldsymbol{i}\uparrow}|\phi_n(\mathcal{K})|c^{\dagger}_{\boldsymbol{j}\uparrow}\rangle/(1+\delta_{n0}), \tag{4.32}$$

$$a_n^{12}(\boldsymbol{i},\boldsymbol{j}) = \langle c^{\dagger}_{\boldsymbol{i}\downarrow}|\phi_n(\mathcal{K})|c^{\dagger}_{\boldsymbol{j}\uparrow}\rangle/(1+\delta_{n0}). \tag{4.33}$$

The sequence of vectors $\phi_n(\mathcal{K})|c^{\dagger}_{\boldsymbol{j}\uparrow}\rangle$ can be found by recursion as before, noting that index $\boldsymbol{i}$ now refers only to spatial site as spin has been selected, and that $\boldsymbol{e}(\boldsymbol{i}\sigma) \equiv |c_{\boldsymbol{i}\sigma}\rangle$ and $\boldsymbol{h}(\boldsymbol{i}\sigma) \equiv |c^{\dagger}_{\boldsymbol{i}\sigma}\rangle$. In theory, the local density of states can now be calculated from the Green functions, by

$$N^{\uparrow(\downarrow)}(E,\boldsymbol{i}) = -\frac{1}{\pi}\mathrm{Im}\bar{G}^{11(12)}_{\boldsymbol{ii}}(E). \tag{4.34}$$

However, Gibb's oscillations will cause the sum (4.31) to converge slowly. Convoluting the sum with *kernel polynomials* will remedy this effect, such as with the Lorentz kernel which allows for a Lorentzian-broadened delta function. This is easily implemented by multiplying the expansion coefficients by factors given by the Lorentz kernel, so that

$$\tilde{a}_n^{11(12)}(\boldsymbol{i},\boldsymbol{j}) = a_n^{11(12)}(\boldsymbol{i},\boldsymbol{j}) \frac{\sinh\left[\lambda(1-\frac{n}{n_{\max}})\right]}{\sinh(\lambda)}, \tag{4.35}$$

where $n_{\max}$ is the total number of terms used in the expansion, and $\lambda = n_{\max}\epsilon$ if we write the Lorentzian approximation to a delta function as $\delta(x) = 1/\pi \lim_{\epsilon\to 0} \epsilon/(x^2+\epsilon^2)$.

4.1.3 Parameter testing

The Chebyshev polynomial method uses an energy scaling parameter a (see Eq. (4.17)) given in terms of maximum and minimum energies of the system, though in practice these energies are unknown and an approximation of a will work fine. The number of terms used numerically

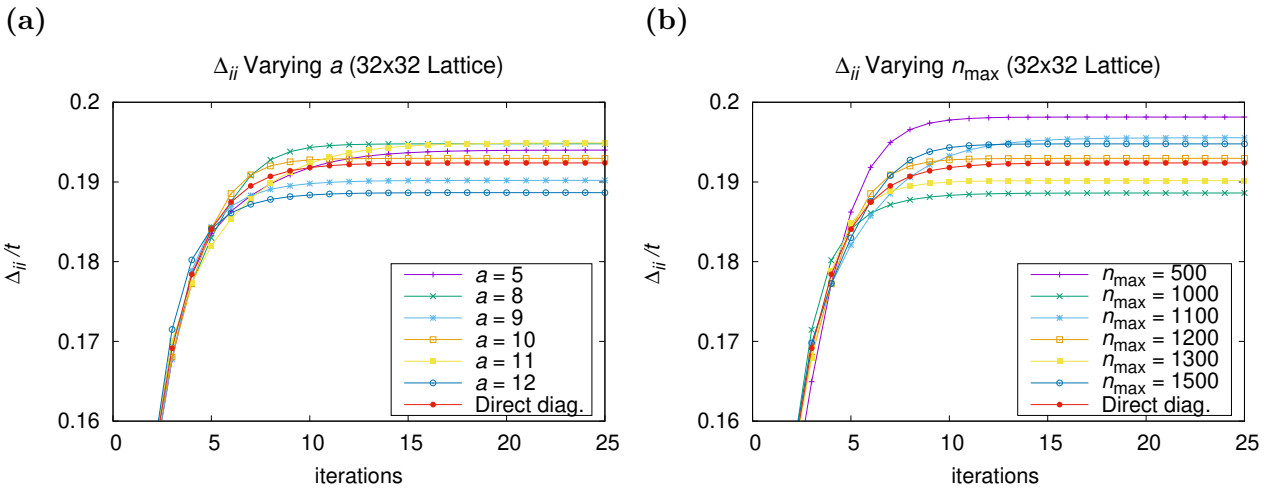

Figure 4.1: Convergence of the order parameter for the homogeneous 32×32 system with $\mu = 0$, $U = -1.5t$, $\alpha = 0$, $h = 0$. comparing the methods of Chebyshev polynomial expansion and direct diagonalization. (a) Varying scaling parameter a ($n = 1200$, $b = 0$). (b) Varying number of terms in the sum, $n_{\max}$ ($a = 10$, $b = 0$).

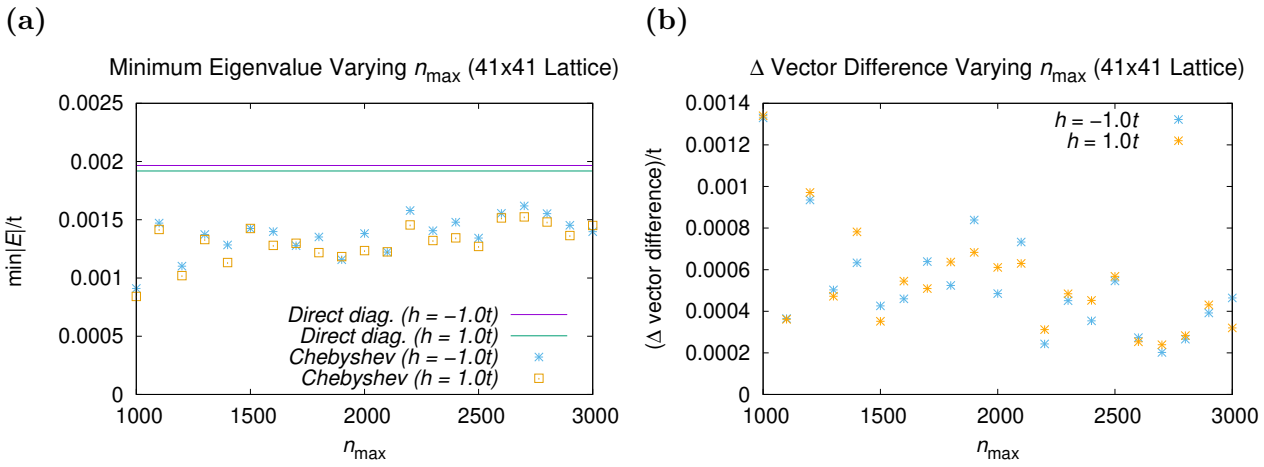

Figure 4.2: Comparison of the Chebyshev polynomial method and direct diagonalization for two 41×41 non-Abelian-phase vortex systems. System parameters are $\mu = 3.5t$, $U = -5.25t$, $\alpha = 1.0t$, and $h = -1.0t$ (blue) or $h = 1.0t$ (orange). (a) Minimum eigenvalue varying $n_{\max}$ ($a = 10$). (b) Vector difference between converged direct diagonalization and Chebyshev order parameters, varying $n_{\max}$ ($a = 10$).

in the Chebyshev method sums, $n_{\max}$, must also be chosen appropriately. In Fig. 4.1 we look at convergence of a homogeneous 32×32 conventional s-wave system with periodic boundary conditions (PBC), comparing the Chebyshev method to direct diagonalization. In part (a), we test for optimal a, and in part (b) for optimal $n_{\max}$. We can see that the parameters $a = 10$ and $n_{\max} = 1200$ work well for this system, as (after several iterations) the order parameter closely matches the direct diagonalization value.

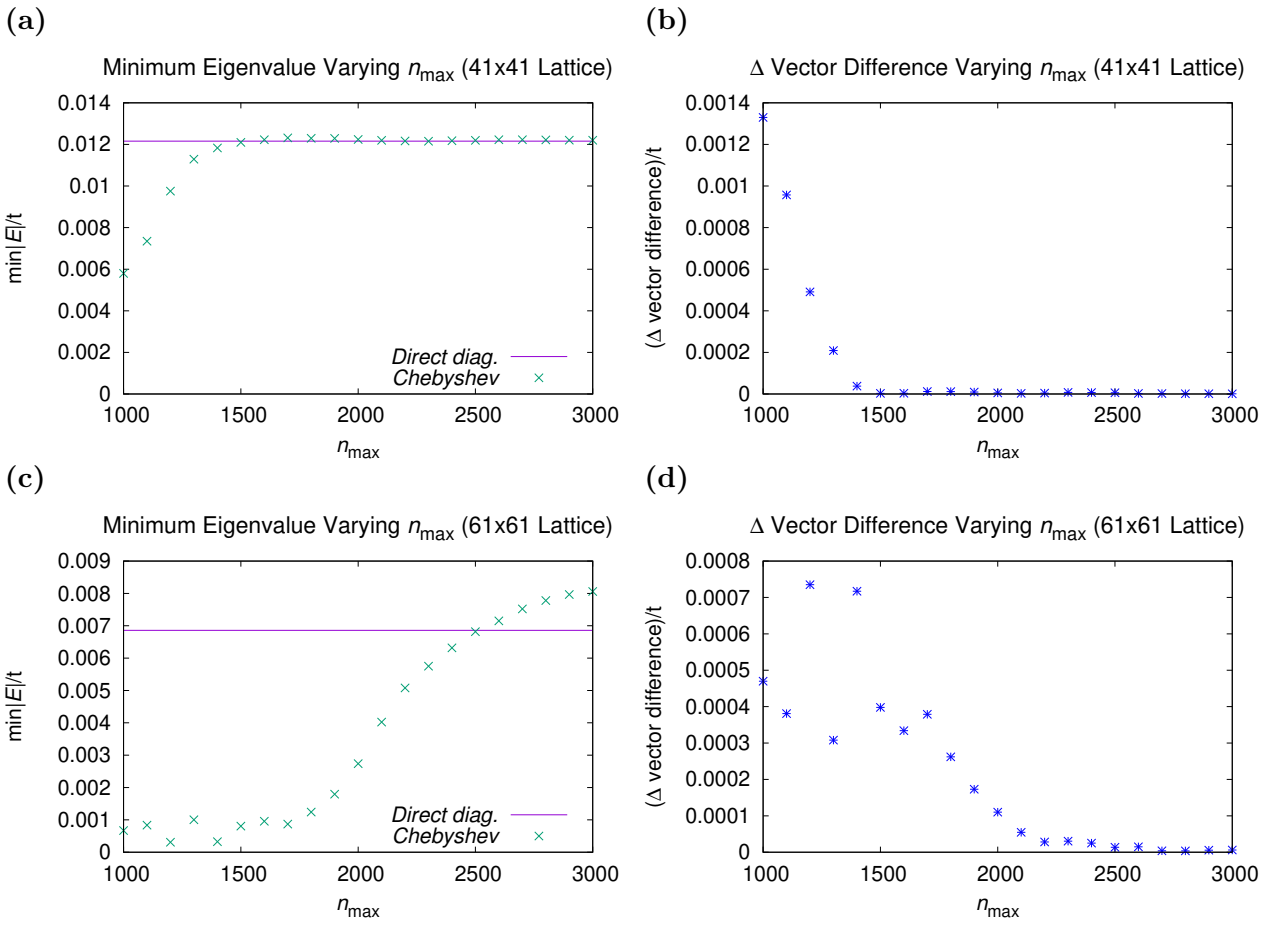

Figure 4.3: Comparison of the Chebyshev polynomial method and direct diagonalization for an Abelian-phase vortex system, for sizes (a) & (b) 41×41 and (c) & (d) 61×61. System parameters are $\mu = -1.0t$, $U = -5.8t$, $\alpha = 2.0t$, $h = -2.0t$. (a), (c) Minimum eigenvalue varying $n_{\max}$ ($a = 10$). (b), (d) Vector difference between converged direct diagonalization and Chebyshev order parameters, varying $n_{\max}$ ($a = 10$).

Most of the systems we wish to study will be vortex systems, of lattice size at least 41×41. In the case of a vortex system, the order parameter will not be constant across the lattice, so we instead look at the converged minimum eigenvalues and the vector difference of the order parameters obtained from Chebyshev expansion and direct diagonalization. PBC was

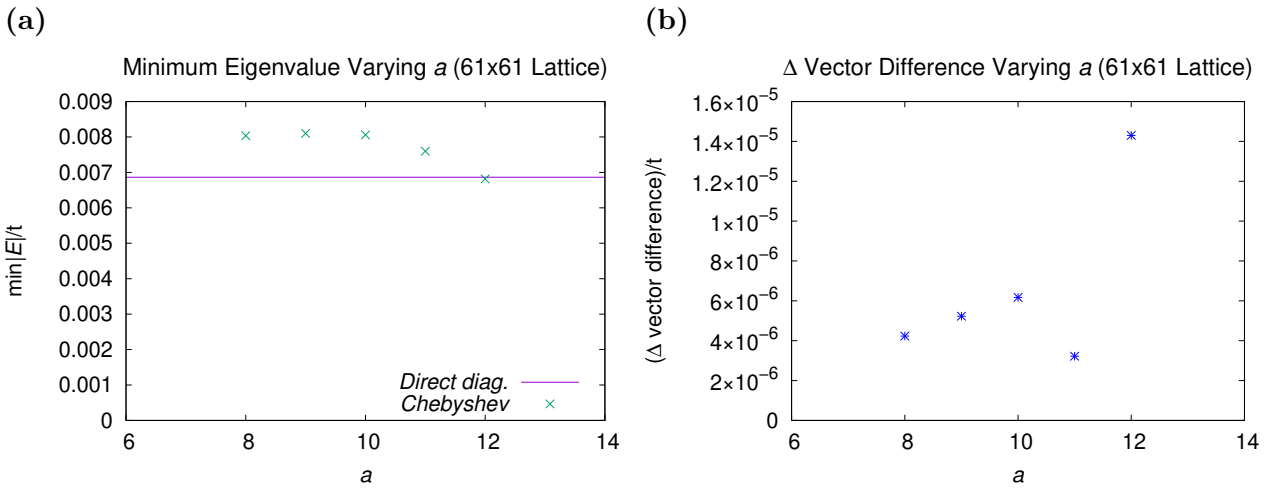

Figure 4.4: Comparison of the Chebyshev polynomial method and direct diagonalization for a 61×61 Abelian-phase vortex system. System parameters are $\mu = -1.0t$, $U = -5.8t$, $\alpha = 2.0t$, $h = -2.0t$. (a) Minimum eigenvalue varying a ($n_{\max} = 3000$). (b) Vector difference between converged direct diagonalization and Chebyshev order parameters, varying a ($n_{\max} = 3000$).

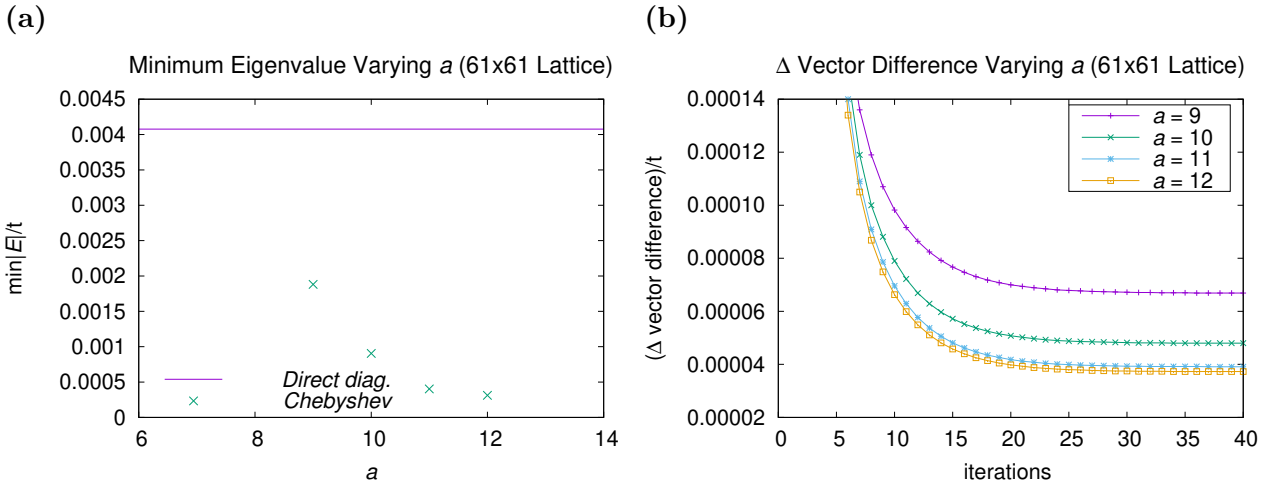

Figure 4.5: Convergence of the order parameter for a 61×61 trivial-phase vortex system, comparing the methods of Chebyshev polynomial expansion and direct diagonalization. System parameters are $\mu = -2.0t$, $U = -5.8t$, $\alpha = 2.0t$, $h = -2.0t$. (a) Minimum eigenvalue varying a ($n_{\max} = 3000$). (b) Running vector difference between Chebyshev and (converged) direct diagonalization order parameters, varying a ($n_{\max} = 3000$).

used in all cases, to simulate the vortex lattice. In Fig. 4.2, we study the effects of varying $n_{\max}$ for two 41×41 non-Abelian-phase ($\mu = 3.5t$, $U = -5.25t$, $\alpha = 1.0t$, and $h = -1.0t$ or $h = 1.0t$) vortex systems, and in Fig. 4.3, we study the effects of varying $n_{\max}$ for an Abelian-phase ($\mu = -1.0t$, $U = -5.8t$, $\alpha = 2.0t$, $h = -2.0t$) vortex system, for sizes 41×41 and 61×61. For size 41×41, the order parameter tends to converge closely enough to the direct diagonalization value by 2000 terms, as seen in Fig. 4.2 (b) and Fig. 4.3 (b), while for size 61×61 it tends to converge closely enough by 3000 terms, as seen in Fig. 4.3 (d). In Figs. 4.4 and 4.5 we look at the effects of varying a for 61×61 Abelian-phase ($\mu = -1.0t$, $U = -5.8t$, $\alpha = 2.0t$, $h = -2.0t$) and trivial-phase ($\mu = -2.0t$, $U = -5.8t$, $\alpha = 2.0t$, $h = -2.0t$) vortex systems, respectively. In Fig. 4.4, we look at converged values only, while in Fig. 4.5 (b) we study the running values of the vector difference between order parameters (with increasing iterations). Fig. 4.4 (a) indicates that $a = 12$ gives the closest minimum eigenvalue, while (b) indicates that $a = 11$ gives the closest order parameter to the direct diagonalization case for the example Abelian-phase system shown, and in Fig. 4.5 similarly $a = 9$ happens to give the closest eigenvalue while $a = 12$ gives the closest order parameter for the example trivial-phase system shown.

Based on our vortex system results, we choose a cut-off for the number of Chebyshev expansion terms $n_{\max} = 2000$ for 41×41 systems, or $n_{\max} = 3000$ for 61×61 or larger systems. However, although the order parameter is slightly closer to the direct diagonalization case for a other than 10 in Figs. 4.4 and 4.5, this does not necessarily translate into closer minimum eigenvalues. Therefore we choose a value of the energy scaling $a = 10$ in all cases for simplicity.

4.1.4 Benchmarking

Now we benchmark to compare runtime using the Chebyshev method versus direct diagonalization of the BdG matrix. In Fig. 4.6, we look at runtimes for direct diagonalization, Chebyshev on a single process, and Chebyshev parallelized on 128 processes. Although different machines were used for different runs allowing for some variability in times, direct diagonalization runtimes go closely to $\mathcal{O}(N^3)$ and Chebyshev runtimes to $\mathcal{O}(N^2)$ (where $N = N_x^2$). Furthermore, parallelizing the computations, not possible with direct diagonaliza-

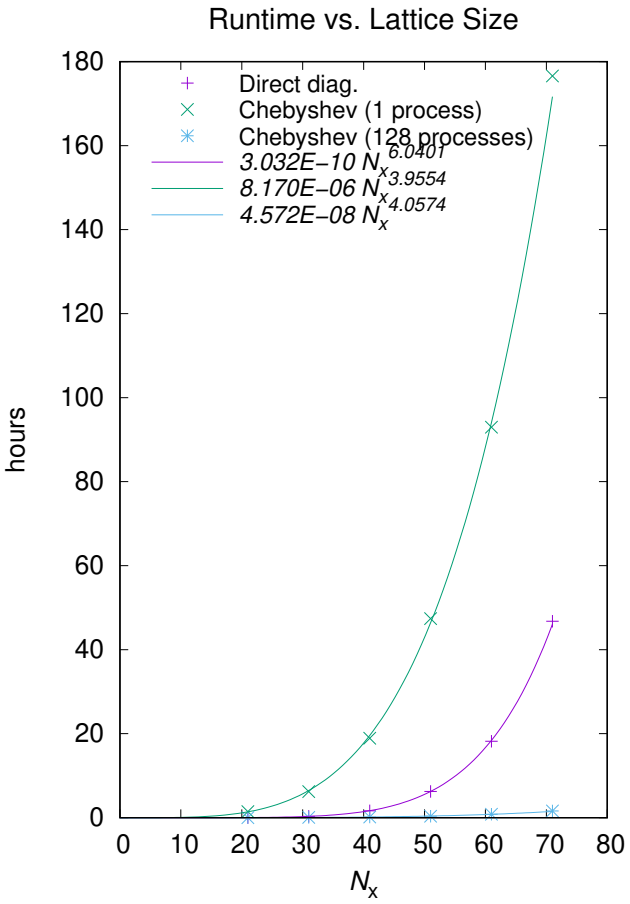

Figure 4.6: Runtimes to converge the mean fields for the homogeneous system with $\mu = -1.0t$, $U = -5.8t$, $\alpha = 2.0t$, $h = -2.0t$ on a square lattice of side length N_x, using direct diagonalization of the BdG matrix, Chebyshev expansion on a single process, or Chebyshev expansion parallelized on 128 processes. Best fit power functions for direct diagonalization and the Chebyshev method go closely to $\mathcal{O}(N_x^6)$ and $\mathcal{O}(N_x^4)$, respectively.

tion, essentially reduces runtime by a factor of the number of processes used.

Converging the mean fields using the Chebyshev method allows for the possibility of parallelization and computation at different lattice sites independently. Therefore one can sample or iterate over lattice sites near vortices (or other inhomogeneities), which tend to converge more slowly, more frequently than other sites. In Fig. 4.7, we look at convergence runtimes (using 192 CPUs) versus the rate of extra sampling of near-vortex sites, for system sizes 41×41 and 61×61 (with parameters $\mu = -1.0t$, $U = -5.8t$, $\alpha = 2.0t$, and $h = -2.0t$). Near-vortex sites were taken simply to be in a square, of differing side length $vsize$, centered around vortices. All calculations for a given system size were done on the same machines for accurate relative runtimes. One can see that the most speedup was gained with a sampling rate for vortex sites double that for other sites, that is, one extra iteration over vortex sites per full lattice iteration. For system size 61×61, this speedup is noticeable, reducing total runtime by around 10% (2 hours) for the system we chose, as one can see in Fig. 4.7 (c).

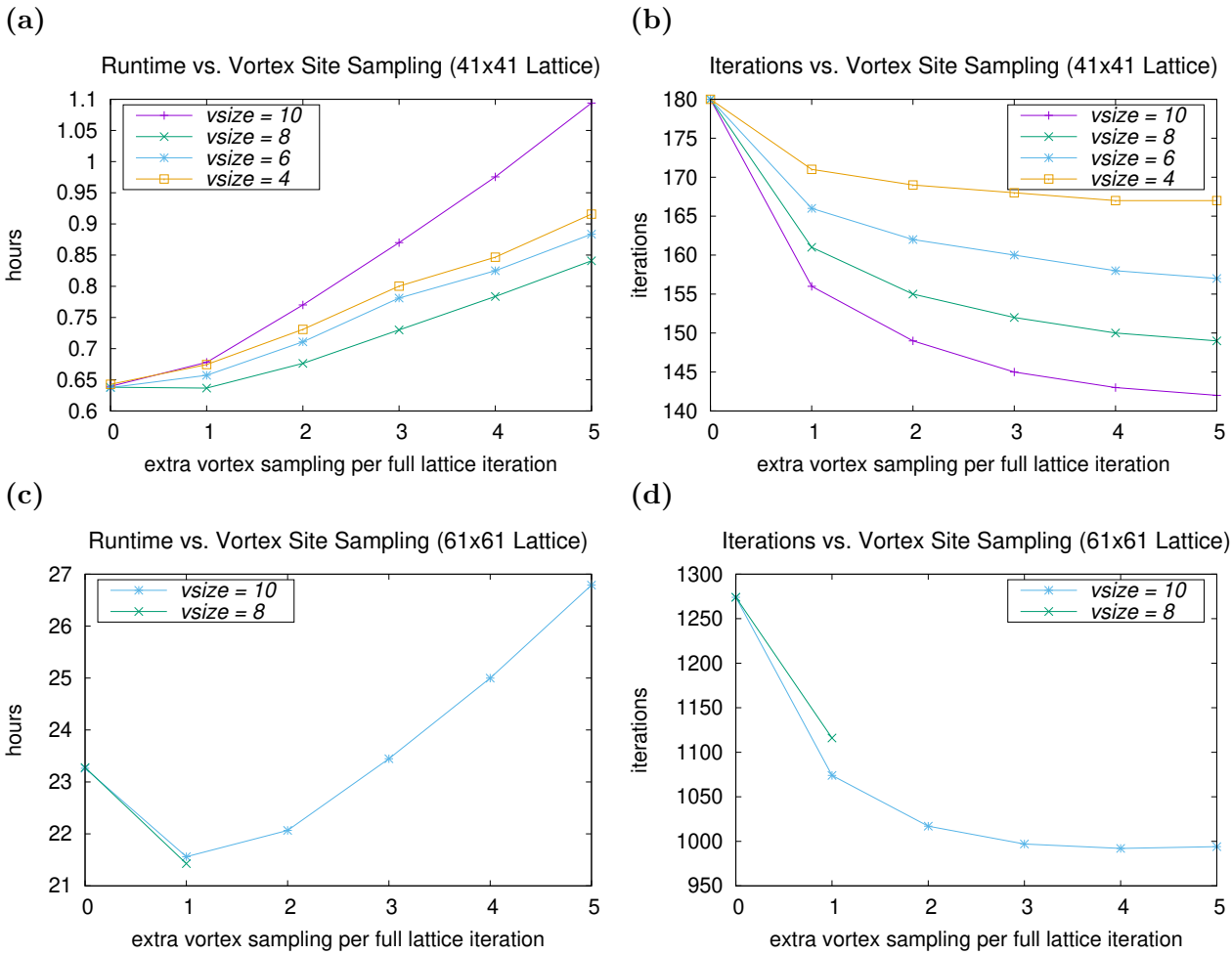

Figure 4.7: Runtimes (using 192 CPUs) and total iterations for convergence of the mean fields, for different sampling rates of lattice sites near vortices. System parameters are $\mu = -1.0t$, $U = -5.8t$, $\alpha = 2.0t$, and $h = -2.0t$, and system size (a) & (b) 41×41, (c) & (d) 61×61. (a), (c) Runtimes versus extra vortex sampling rate. (b), (d) Total iterations versus extra vortex sampling rate.

Finally, we used an efficient method for calculating mean fields at individual lattice sites on different processes, a method sometimes known as the 'master-slave' algorithm. In this algorithm, a single 'master' process oversees and distributes tasks to the other processes, giving a process a new lattice site to run calculations on whenever that process has finished one. This allows for better distribution of calculations among machines of differing processing speeds. In our test of the vortex system with $\mu = -1.0t$, $U = -5.8t$, $\alpha = 2.0t$, and $h = -2.0t$, simply dividing lattice sites up equally between processes (using 160 CPUs) gave runtimes of about 3500s for size 41×41 and 62800s for 61×61, while using the master-slave algorithm on the same machines yielded runtimes of about 3000s for 41×41 and 58300s for 61×61.

4.2 Sakurai-Sugiura Method

The Sakuria-Sugiura method is a method based on Green functions of finding a reduced subspace of the Hamiltonian, allowing one to find the quasiparticle energies and wave functions within an energy window of one's choice. A contour-integral approach allows for finding these eigenpairs, with eigenvalues located in a given domain in the complex plane, from a general matrix. This method is easily parallelized, as it consists of solving a set of independent linear equations.

4.2.1 Projection onto a subspace

The goal of this method is to project onto a (small) subspace of the Hamiltonian. Suppose that the eigenspace of an $n_s \times n_s$ matrix A is spanned by an orthonormal set of vectors $\boldsymbol{x}_j$,

$$A\boldsymbol{x}_j = \varepsilon_j \boldsymbol{x}_j, \qquad \{\boldsymbol{x}_j : j = 1, 2, \ldots, n_s\}. \tag{4.36}$$

Now suppose we have an orthonormal set of vectors $\{\boldsymbol{q}_{j'} : j' = 1, 2, \ldots, m_s\}$, where each $\boldsymbol{q}_{j'}$ is a linear combination of $\{\boldsymbol{x}_j : j = 1, 2, \ldots, m_s\}$. Then the matrix $\tilde{A}$,

$$\tilde{A} = Q^\dagger A Q, \qquad Q = (\boldsymbol{q}_1 \ \boldsymbol{q}_2 \ \ldots \ \boldsymbol{q}_{m_s}), \tag{4.37}$$

contains m_s eigenvalues of the matrix A, with eigenspace spanned by $\{\boldsymbol{x}_j : j = 1, 2, \ldots, m_s\}$. The goal of the Sakuria-Sugiura method is to find a way to project onto this target subspace, that is to find the matrix Q.

To begin, consider an arbitrary (n_s-dimensional) complex vector $\boldsymbol{v}$, which can be expanded in terms of $\boldsymbol{x}_j$'s. Define the *projection operator* $P_\Gamma(A)$ by

$$P_\Gamma(A)\boldsymbol{v} = \sum_{j=1}^{m_s} \alpha_j \boldsymbol{x}_j, \qquad \boldsymbol{v} = \sum_{l=1}^{n_s} \alpha_l \boldsymbol{x}_l. \tag{4.38}$$

This operator projects a vector $\boldsymbol{v}$ onto the m_s-dimensional subspace spanned by $\{\boldsymbol{x}_j : j = 1, 2, \ldots, m_s\}$. As

$$\hat{P}_j = \boldsymbol{x}_j \boldsymbol{x}_j^\dagger \equiv |\boldsymbol{x}_j\rangle\langle\boldsymbol{x}_j| \tag{4.39}$$

is the projection operator onto the (1D) space spanned by $\boldsymbol{x}_j$, we have $P_\Gamma(A) = \sum_{j=1}^{m_s} \hat{P}_j$, or

$$P_\Gamma(A) = \frac{1}{2\pi i} \oint_\Gamma dz \, \frac{1}{z\hat{I} - A}, \tag{4.40}$$

where the closed contour Γ contains only the m_s eigenvalues ε_j desired, each of which corresponds to a simple pole in the so-called resolvent,

$$\frac{1}{z\hat{I} - A} = \sum_{j=1}^{n_s} \frac{\hat{P}_j}{z - \varepsilon_j}. \tag{4.41}$$

4.2.2 Moment vectors and determination of subspace

The moment vectors $\{\boldsymbol{s}_k : k = 0, 1, 2, \ldots, M-1\}$ are defined as

$$\boldsymbol{s}_k = A^k P_\Gamma(A) \boldsymbol{v}. \tag{4.42}$$

These vectors can be seen to be within the subspace associated with $P_\Gamma(A)$, as $P_\Gamma(A)\boldsymbol{v}$ is a linear combination of eigenvectors of A. These moments span what is known as a *Krylov subspace* of order M generated by A. From the above definition we have,

$$\begin{aligned} \boldsymbol{s}_k &= \frac{1}{2\pi i} \oint_\Gamma dz \, A^k \frac{1}{z\hat{I} - A} \boldsymbol{v} = \frac{1}{2\pi i} \oint_\Gamma dz \, A^k \sum_{j=1}^{n_s} \frac{\boldsymbol{x}_j \boldsymbol{x}_j^\dagger}{z - \varepsilon_j} \boldsymbol{v} \\ &= \frac{1}{2\pi i} \oint_\Gamma dz \, \sum_{j=1}^{n_s} \frac{\varepsilon_j^k \boldsymbol{x}_j \boldsymbol{x}_j^\dagger}{z - \varepsilon_j} \boldsymbol{v}, \end{aligned}$$

or finally,

$$\boldsymbol{s}_k = \frac{1}{2\pi i} \oint_\Gamma dz \, \frac{z^k}{z\hat{I} - A} \boldsymbol{v}. \tag{4.43}$$

In the algorithm used, the number M is an input parameter.

As the size of the desired subspace is generally unknown, given by the number of eigenvalues within a contour Γ, first one must calculate the size of the subspace by estimating the trace of the matrix $P_\Gamma(A)$. Recall that, as a projection operator, all eigenvalues of $P_\Gamma(A)$ are either 1 or 0, and the sum of the eigenvalues is therefore the subspace size m_s. The trace of $P_\Gamma(A)$ can be approximated by *stochastic estimation*, that is by a random sampling of input ('source') vectors. Take L_0 n_s-dimensional vectors $\boldsymbol{v}^i$, $i = 1, \ldots, L_0$ (where L_0 is an input

parameter), such that each element of $\boldsymbol{v}^i$ is either -1 or 1 with equal probability. For each $\boldsymbol{v}^i$, one finds,

$$(\boldsymbol{v}^i)^T P_\Gamma(A)\boldsymbol{v}^i = \sum_{j,l} v_j^i (P_\Gamma(A))_{jl}\, v_l^i = \sum_{j=l} v_j^i (P_\Gamma(A))_{jj}\, v_j^i + \sum_{j\neq l} v_j^i (P_\Gamma(A))_{jl}\, v_l^i$$
$$= Tr(P_\Gamma(A)) + \sum_{j\neq l} v_j^i (P_\Gamma(A))_{jl}\, v_l^i,$$

with v_j^i the jth component of $\boldsymbol{v}^i$, so that

$$\tilde{m}_s = \frac{1}{L_0}\sum_{i=1}^{L_0} (\boldsymbol{v}^i)^T P_\Gamma(A)\boldsymbol{v}^i = Tr(P_\Gamma(A)) + \frac{1}{L_0}\sum_{j\neq l}(P_\Gamma(A))_{jl} \sum_{i=1}^{L_0} v_j^i v_l^i$$
$$\to Tr(P_\Gamma(A)), \quad L_0 \to \infty, \tag{4.44}$$

as $\sum_{i=1}^{L_0} v_j^i v_l^i \to 0$ as L_0 becomes large. Therefore we must find the sum on the right-hand side of Eq. (4.44). Using Eq. (4.40) (or Eq. (4.43) with $k = 0$), one has

$$P_\Gamma(A)\boldsymbol{v}^i = \frac{1}{2\pi i}\oint_\Gamma dz\, \boldsymbol{y}^i, \qquad (z\hat{I} - A)\boldsymbol{y}^i = \boldsymbol{v}^i. \tag{4.45}$$

We use the Math Kernel Library (MKL) routine PARDISO to solve the system of equations for each $\boldsymbol{y}^i$. To calculate $P_\Gamma(A)\boldsymbol{v}^i$, the zeroth moment, one can estimate the integral by numerical quadrature,

$$\boldsymbol{s}_k \approx \frac{1}{2\pi i}\frac{2\pi}{N_q}\sum_{j=1}^{N_q} \rho\zeta'(\theta_j) z_j^k \boldsymbol{y}_j^i, \tag{4.46}$$

where the contour is divided into N_q parts, with $(z_j\hat{I} - A)\boldsymbol{y}_j^i = \boldsymbol{v}^i$, and

$$z(\theta) = \gamma + \rho\zeta(\theta), \qquad dz = \rho\frac{d\zeta}{d\theta}d\theta \equiv \rho\zeta'(\theta)\frac{2\pi}{N_q}. \tag{4.47}$$

For our contour we let $\zeta(\theta) = \cos(\theta) + i\alpha\sin(\theta)$ be an ellipse in the complex plane with $0 < \alpha \leq 1$. (Here γ is a shift and ρ is a scaling factor.)

Once an estimate $\tilde{m}_s$ has been calculated, one can construct the subspace. One makes a sequence of the moment vectors $\boldsymbol{s}_k$, varying $\boldsymbol{v}$. Each element of $\boldsymbol{v}^i$, $i = 1, \ldots, L$, is chosen as a random number between $[-1, 1]$. Finding the $n_s \times LM$ matrix $\hat{S}_k = (\boldsymbol{s}_k^1\ \boldsymbol{s}_k^2\ \ldots\ \boldsymbol{s}_k^L)$, for each $k = 0, 1, \ldots, M-1$, one performs singular-value decomposition (SVD) on $\hat{S}_k$ to obtain the singular values $\{\sigma_i\}$. One then finds the effective rank (the number of predominantly linearly

independent vectors) of $\hat{S}_k$ by counting the number of singular values for which $\sigma_i/\sigma_{\max} > \delta$ for a small positive constant δ ($\sim 10^{-14}$). The number L of vectors $\boldsymbol{v}$ that should be chosen, so that the effective rank $m_s \geq \tilde{m}_s$, is given by $LM \geq \tilde{m}_s$, or

$$L = \left\lceil \frac{\kappa \tilde{m}_s}{M} \right\rceil, \qquad \kappa \geq 1. \tag{4.48}$$

where $\lceil x \rceil$ is the smallest integer greater than or equal to x.

Using the LAPACK routine ZGESVD to perform SVD on the matrix $\hat{S}_k$ gives $\hat{S}_k = U\Sigma W^\dagger$ with $\Sigma = \mathrm{diag}(\sigma_1, \sigma_2, \dots)$, where $\sigma_1 \geq \sigma_2 \geq \cdots \geq 0$. Using a submatrix composed of the first m_s columns of U (the left eigenvectors of $\hat{S}_k$), calling this $n_s \times m_s$ submatrix Q, one has

$$\tilde{H} = Q^\dagger H Q. \tag{4.49}$$

This is the reduced Hamiltonian, with m_s eigenvalues of the original Hamiltonian and eigenvectors $\boldsymbol{w}_i$, where $\boldsymbol{x}_i = Q\boldsymbol{w}_i$ are the corresponding eigenvectors of the original Hamiltonian. These eigenpairs can now be easily calculated by diagonalization of the reduced Hamiltonian $\tilde{H}$. In order to check that the correct eigenpairs $(\varepsilon_i, \boldsymbol{x}_i)$ have been found, we compute the residual,

$$\mathrm{res}_i = \frac{||H\boldsymbol{x}_i - \varepsilon_i \boldsymbol{x}_i||}{||H\boldsymbol{x}_i|| + |\varepsilon_i|\,||\boldsymbol{x}_i||}, \tag{4.50}$$

and keep only eigenpairs whose residual is less than 10^{-1}.

4.3 Vortex Lattice

Implementing the vortex lattice under an applied magnetic field requires careful consideration of the boundary conditions, as in practice one must solve for a small section of the full system.

In the presence of a vector potential $\boldsymbol{A}(\boldsymbol{r}, t)$, an electron wave function acquires the Peierls phase factor while traversing from $\boldsymbol{r}_j$ to $\boldsymbol{r}_i$,

$$\exp\left[i \frac{(-e)}{\hbar c} \int_{\boldsymbol{r}_j}^{\boldsymbol{r}_i} d\boldsymbol{r} \cdot \boldsymbol{A}(\boldsymbol{r}, t) \right]. \tag{4.51}$$

This corresponds to the minimal coupling, where the momentum $\boldsymbol{p}$ is modified by the vector potential as $\boldsymbol{p} + (e/c)\boldsymbol{A}$. In the tight-binding model, the matrix elements describing electron

movement between lattice sites (such as the hopping) are modified by this Peierls factor, which can be written as

$$\exp\left[-i\frac{\pi}{\phi_0}\int_{\boldsymbol{r}_j}^{\boldsymbol{r}_i} d\boldsymbol{r}\cdot\boldsymbol{A}\right], \tag{4.52}$$

where $\phi_0 = hc/2e$ is the flux quantum, the smallest magnetic flux the system will allow (so that in traversing around this flux, the wave function is periodic as it must be).

To study the boundary conditions for numerical modelling, gauge transformations must be considered. Under a gauge transformation, $\boldsymbol{A} \to \boldsymbol{A}' = \boldsymbol{A} + \nabla\chi$, where χ is an arbitrary function of spatial coordinate, the electron and hole wave functions u and v acquire the phase factors,

$$\begin{aligned} u'(\boldsymbol{r}_i) &= \exp\left[-i\frac{e}{\hbar c}\chi(\boldsymbol{r}_i)\right]u(\boldsymbol{r}_i), \\ v'(\boldsymbol{r}_i) &= \exp\left[+i\frac{e}{\hbar c}\chi(\boldsymbol{r}_i)\right]v(\boldsymbol{r}_i). \end{aligned} \tag{4.53}$$

The order parameter therefore changes as

$$\Delta'(\boldsymbol{r}_i,\boldsymbol{r}_j) = \exp\left[-i\frac{e}{\hbar c}\Big(\chi(\boldsymbol{r}_i)+\chi(\boldsymbol{r}_j)\Big)\right]\Delta(\boldsymbol{r}_i,\boldsymbol{r}_j). \tag{4.54}$$

The kinetic matrix elements, describing electron motion from site j to site i, change via the Peierls factor by

$$\exp\left[i\frac{e}{\hbar c}(\chi(\boldsymbol{r}_j)-\chi(\boldsymbol{r}_i))\right]. \tag{4.55}$$

The BdG equations are invariant under such a gauge transformation, with all physically observable quantities remaining the same. For self-consistent numerical calculations, this can be implemented by changing the kinetic matrix elements, e.g., the hopping and spin-orbit coupling, as above.

We now study what is required for periodic boundary conditions, to simulate the vortex lattice. Consider a unit cell of the vortex lattice spanned by $\boldsymbol{u}_1$ and $\boldsymbol{u}_2$, where the center of this cell is the origin $\boldsymbol{r} = 0$. Assume there is one vortex at the center. When translated by the Bravais lattice vector,

$$\boldsymbol{R} = m\boldsymbol{u}_1 + n\boldsymbol{u}_2, \tag{4.56}$$

the vector potential in the symmetric gauge, $\boldsymbol{A}(\boldsymbol{r}) = \frac{1}{2}\boldsymbol{H} \times \boldsymbol{r}$, changes as

$$\boldsymbol{A}(\boldsymbol{r} + \boldsymbol{R}) = \boldsymbol{A}(\boldsymbol{r}) + \boldsymbol{A}(\boldsymbol{R}). \tag{4.57}$$

One can regard this transformation as a gauge transformation,

$$\boldsymbol{A}(\boldsymbol{r} + \boldsymbol{R}) = \boldsymbol{A}(\boldsymbol{r}) + \frac{1}{2}\nabla\chi(\boldsymbol{r}, \boldsymbol{R}), \tag{4.58}$$

where

$$\chi(\boldsymbol{r}, \boldsymbol{R}) = 2\boldsymbol{A}(\boldsymbol{R}) \cdot \boldsymbol{r} + C(\boldsymbol{R}) = (\boldsymbol{H} \times \boldsymbol{R}) \cdot \boldsymbol{r} + C(\boldsymbol{R}). \tag{4.59}$$

Under this gauge transformation, u and v acquire the phase factors,

$$\begin{aligned} u'(\boldsymbol{r} + \boldsymbol{R}) &= \exp\left[-i\frac{\pi}{\phi_0}\frac{\chi(\boldsymbol{r}, \boldsymbol{R})}{2}\right] u(\boldsymbol{r}), \\ v'(\boldsymbol{r} + \boldsymbol{R}) &= \exp\left[+i\frac{\pi}{\phi_0}\frac{\chi(\boldsymbol{r}, \boldsymbol{R})}{2}\right] v(\boldsymbol{r}), \end{aligned} \tag{4.60}$$

and the s-wave ($i = j$) order parameter acquires the phase

$$\Delta(\boldsymbol{r} + \boldsymbol{R}) = \exp\left[-i\frac{\pi}{\phi_0}\chi(\boldsymbol{r}, \boldsymbol{R})\right]\Delta(\boldsymbol{r}). \tag{4.61}$$

The constant $C(\boldsymbol{R})$ for a given Bravais lattice vector $\boldsymbol{R} = m\boldsymbol{u}_1 + n\boldsymbol{u}_2$ can be found as follows. Consider translating from $\boldsymbol{r}$ to $\boldsymbol{r} + \boldsymbol{u}_1 + \boldsymbol{u}_2$ by first translating from $\boldsymbol{r}$ to $\boldsymbol{r} + \boldsymbol{u}_1$, then from $\boldsymbol{r} + \boldsymbol{u}_1$ to $\boldsymbol{r} + \boldsymbol{u}_1 + \boldsymbol{u}_2$:

$$\begin{aligned} \chi(\boldsymbol{r}, \boldsymbol{u}_1 + \boldsymbol{u}_2) &= \chi(\boldsymbol{r}, \boldsymbol{u}_1) + \chi(\boldsymbol{r} + \boldsymbol{u}_1, \boldsymbol{u}_2) \\ &= (\boldsymbol{H} \times \boldsymbol{u}_1) \cdot \boldsymbol{r} + C(\boldsymbol{u}_1) + (\boldsymbol{H} \times \boldsymbol{u}_2) \cdot (\boldsymbol{r} + \boldsymbol{u}_1) + C(\boldsymbol{u}_2) \\ &= [\boldsymbol{H} \times (\boldsymbol{u}_1 + \boldsymbol{u}_2)] \cdot r + (\boldsymbol{H} \times \boldsymbol{u}_2) \cdot \boldsymbol{u}_1 + C(\boldsymbol{u}_1) + C(\boldsymbol{u}_2) \\ &= [\boldsymbol{H} \times (\boldsymbol{u}_1 + \boldsymbol{u}_2)] \cdot r + (\boldsymbol{u}_2 \times \boldsymbol{u}_1) \cdot \boldsymbol{H} + C(\boldsymbol{u}_1) + C(\boldsymbol{u}_2) \\ &= [\boldsymbol{H} \times (\boldsymbol{u}_1 + \boldsymbol{u}_2)] \cdot r + (-S\hat{z}) \cdot \left(-\frac{m_\phi \phi_0}{S}\right)\hat{z} + C(\boldsymbol{u}_1) + C(\boldsymbol{u}_2), \end{aligned} \tag{4.62}$$

where $S = |\boldsymbol{u}_1 \times \boldsymbol{u}_2|$ is the area of the unit cell, containing m_ϕ flux quanta so that $HS = m_\phi \phi_0$ with $\boldsymbol{H} = -H\hat{z}$. Comparing this to

$$\begin{aligned} \chi(\boldsymbol{r}, \boldsymbol{u}_1 + \boldsymbol{u}_1) &= \chi(\boldsymbol{r}, \boldsymbol{u}_1) + \chi(\boldsymbol{r} + \boldsymbol{u}_1, \boldsymbol{u}_1) \\ &= [\boldsymbol{H} \times (\boldsymbol{u}_1 + \boldsymbol{u}_1)] \cdot r + (\boldsymbol{H} \times \boldsymbol{u}_1) \cdot \boldsymbol{u}_1 + 2C(\boldsymbol{u}_1) \\ &= [\boldsymbol{H} \times 2\boldsymbol{u}_1] \cdot r + 2C(\boldsymbol{u}_1), \end{aligned} \tag{4.63}$$

and similarly for $\chi(\boldsymbol{r}, \boldsymbol{u}_2 + \boldsymbol{u}_2)$, one sees that the term $m_\phi \phi_0$ is a result only of translation by $\boldsymbol{u}_1$ and $\boldsymbol{u}_2$ together. Therefore,

$$C(m\boldsymbol{u}_1 + n\boldsymbol{u}_2) = mC(\boldsymbol{u}_1) + nC(\boldsymbol{u}_2) + mnm_\phi\phi_0. \tag{4.64}$$

To find $C(\boldsymbol{u}_1)$ and $C(\boldsymbol{u}_2)$, consider the phase change when crossing the vortex at the center of the unit cell, from $-(\boldsymbol{u}_1 + \boldsymbol{u}_2)/2$ to $(\boldsymbol{u}_1 + \boldsymbol{u}_2)/2$:

$$\begin{aligned}\chi(-\frac{1}{2}(\boldsymbol{u}_1 + \boldsymbol{u}_2), \boldsymbol{u}_1 + \boldsymbol{u}_2) &= [\boldsymbol{H} \times (\boldsymbol{u}_1 + \boldsymbol{u}_2)] \cdot \left(-\frac{1}{2}(\boldsymbol{u}_1 + \boldsymbol{u}_2)\right) + C(\boldsymbol{u}_1 + \boldsymbol{u}_2) \\ &= C(\boldsymbol{u}_1 + \boldsymbol{u}_2) = C(\boldsymbol{u}_1) + C(\boldsymbol{u}_2) + \phi_0. \end{aligned} \tag{4.65}$$

The above should equal ϕ_0, so that the phase of the order parameter changes by π as we have wound halfway around the vortex center. Similarly,

$$\chi(-\frac{1}{2}\boldsymbol{u}_1, \boldsymbol{u}_1) = C(\boldsymbol{u}_1), \qquad \chi(-\frac{1}{2}\boldsymbol{u}_2, \boldsymbol{u}_2) = C(\boldsymbol{u}_2), \tag{4.66}$$

should also equal $\pm\phi_0$, so that winding halfway around the vortex from $-\boldsymbol{u}_1/2$ to $\boldsymbol{u}_1/2$ or from $-\boldsymbol{u}_2/2$ to $\boldsymbol{u}_2/2$ gives a phase change of $\pm\pi$. Therefore

$$C(\boldsymbol{u}_1) = -C(\boldsymbol{u}_2) \equiv \phi_0, \tag{4.67}$$

which finally yields

$$\chi(\boldsymbol{r}, \boldsymbol{R}) = 2\boldsymbol{A}(\boldsymbol{R}) \cdot \boldsymbol{r} + [(m - n) + mnm_\phi]\phi_0. \tag{4.68}$$

Shifting the vortex center to $\boldsymbol{r}_c$ and the "center" of the vector potential to $\boldsymbol{r}_A$ gives a phase shift of $-(\boldsymbol{H} \times \boldsymbol{R}) \cdot (2\boldsymbol{r}_c - \boldsymbol{r}_A)$, for a total of

$$\chi(\boldsymbol{r}, \boldsymbol{R}) = 2\boldsymbol{A}(\boldsymbol{R}) \cdot \boldsymbol{r} + [(m - n) + mnm_\phi]\phi_0 - (\boldsymbol{H} \times \boldsymbol{R}) \cdot (2\boldsymbol{r}_c - \boldsymbol{r}_A). \tag{4.69}$$

This $\chi(\boldsymbol{r}, \boldsymbol{R})$ can be used to find the extra phase factors in Eq. (4.60) for implementing periodic boundary conditions.

5 Tight-Binding Index Theorem for Majorana Modes in a Vortex Core

In this chapter we show the existence of two Majorana fermion zero-modes in a vortex core in the Abelian phase, using the 2D model of TSC we study [16, 17]. We adapt to our purposes the continuum model index theorem for the non-Abelian region of Tewari, Sau, and das Sarma [30].

5.1 Hamiltonian

As in the continuum model index theorem [30] (see Appendix B), the single-electron part of the Hamiltonian is first diagonalized in total-angular-momentum basis. In momentum space, the single-electron part, H_0, with Rashba spin-orbit coupling and Zeeman splitting, is given by

$$\begin{aligned} H_0 &= H_K + H_{SO} + H_Z; \\ H_K &= \sum_{\boldsymbol{k}\in BZ} \left[-2t(\cos k_x + \cos k_y) - \mu\right] \left(c^\dagger_{\boldsymbol{k}\uparrow} c_{\boldsymbol{k}\uparrow} + c^\dagger_{\boldsymbol{k}\downarrow} c_{\boldsymbol{k}\downarrow}\right), \\ H_{SO} &= \alpha \sum_{\boldsymbol{k}\in BZ} \left[\left(\sin k_y + i \sin k_x\right) c^\dagger_{\boldsymbol{k}\uparrow} c_{\boldsymbol{k}\downarrow} + H.c.\right], \\ H_Z &= \sum_{\boldsymbol{k}\in BZ} (-h) \left(c^\dagger_{\boldsymbol{k}\uparrow} c_{\boldsymbol{k}\uparrow} - c^\dagger_{\boldsymbol{k}\downarrow} c_{\boldsymbol{k}\downarrow}\right). \end{aligned} \tag{5.1}$$

where $\boldsymbol{k}$ is within the first Brillouin zone, a square (toroidal) region between $\boldsymbol{k} = \pm(\pi, \pi)$ for the square lattice. We set the lattice constant $a \equiv 1$. Around $k \sim 0$, this becomes

$$
\begin{aligned}
H_0^0 &= H_K^0 + H_{SO}^0 + H_Z^0; \\
H_K^0 &\simeq \sum_{k\sim 0} \left[tk^2 - 4t - \mu\right] \left(c_{\boldsymbol{k}\uparrow}^\dagger c_{\boldsymbol{k}\uparrow} + c_{\boldsymbol{k}\downarrow}^\dagger c_{\boldsymbol{k}\downarrow}\right), \\
H_{SO}^0 &\simeq \alpha \sum_{k\sim 0} \left[\left(k_y + ik_x\right) c_{\boldsymbol{k}\uparrow}^\dagger c_{\boldsymbol{k}\downarrow} + H.c.\right], \\
H_Z^0 &\simeq \sum_{k\sim 0} (-h) \left(c_{\boldsymbol{k}\uparrow}^\dagger c_{\boldsymbol{k}\uparrow} - c_{\boldsymbol{k}\downarrow}^\dagger c_{\boldsymbol{k}\downarrow}\right),
\end{aligned}
\tag{5.2}
$$

whereas around $\boldsymbol{k} \sim (\pi, \pi)$, defining $\tilde{\boldsymbol{k}} = \boldsymbol{k} - (\pi, \pi)$, it becomes

$$
\begin{aligned}
H_0^\pi &= H_K^\pi + H_{SO}^\pi + H_Z^\pi; \\
H_K^\pi &\simeq \sum_{\tilde{k}\sim 0} \left[-t\tilde{k}^2 + 4t - \mu\right] \left(c_{\boldsymbol{k}\uparrow}^\dagger c_{\boldsymbol{k}\uparrow} + c_{\boldsymbol{k}\downarrow}^\dagger c_{\boldsymbol{k}\downarrow}\right), \\
H_{SO}^\pi &\simeq -\alpha \sum_{\tilde{k}\sim 0} \left[\left(\tilde{k}_y + i\tilde{k}_x\right) c_{\boldsymbol{k}\uparrow}^\dagger c_{\boldsymbol{k}\downarrow} + H.c.\right], \\
H_Z^\pi &\simeq \sum_{\tilde{k}\sim 0} (-h) \left(c_{\boldsymbol{k}\uparrow}^\dagger c_{\boldsymbol{k}\uparrow} - c_{\boldsymbol{k}\downarrow}^\dagger c_{\boldsymbol{k}\downarrow}\right).
\end{aligned}
\tag{5.3}
$$

The total angular momentum operators are defined as follows [30], with m_J a half-odd-integer:

$$
\begin{aligned}
c_{\boldsymbol{k}\uparrow} &= \frac{1}{\sqrt{2\pi k}} \sum_{m_J=-\infty}^{\infty} c_{m_J,k,\uparrow} e^{i(m_J - \frac{1}{2})\theta_{\boldsymbol{k}}} = \frac{1}{\sqrt{2\pi \tilde{k}}} \sum_{m_J=-\infty}^{\infty} c_{m_J,\tilde{k},\uparrow} e^{i(m_J - \frac{1}{2})\theta_{\tilde{\boldsymbol{k}}}}, \\
c_{\boldsymbol{k}\downarrow} &= \frac{1}{\sqrt{2\pi k}} \sum_{m_J=-\infty}^{\infty} c_{m_J,k,\downarrow} e^{i(m_J + \frac{1}{2})\theta_{\boldsymbol{k}}} = \frac{1}{\sqrt{2\pi \tilde{k}}} \sum_{m_J=-\infty}^{\infty} c_{m_J,\tilde{k},\downarrow} e^{i(m_J + \frac{1}{2})\theta_{\tilde{\boldsymbol{k}}}}.
\end{aligned}
\tag{5.4}
$$

Around $k \sim 0$, m_J is the total (orbital plus spin) angular momentum, whereas around $\boldsymbol{k} \sim (\pi, \pi)$ the relation of m_J to total angular momentum involves an effective mass approximation. The effective mass approximation we use essentially neglects the quickly-oscillating factor $\exp(i(\pi, \pi) \cdot \boldsymbol{r})$ in the electronic wave function. For example, the real-space wave function for a Majorana mode with $\boldsymbol{k} \sim (\pi, \pi)$ can be approximated as

$$
\Psi(\boldsymbol{r}) = e^{i(\pi,\pi)\cdot \boldsymbol{r}} \left(u_\uparrow, u_\downarrow, u_\uparrow^*, u_\downarrow^*\right). \tag{5.5}
$$

The effective mass approximation in terms of operators can be considered as follows. On a square lattice with nearest-neighbour hopping only, look at, for example, the kinetic energy,

$$
H_K = \sum_\sigma \sum_{\langle \boldsymbol{ij} \rangle} \left(-t c_{\boldsymbol{i}\sigma}^\dagger c_{\boldsymbol{j}\sigma}\right) = -t \sum_{\sigma, \boldsymbol{i}} \left(c_{\boldsymbol{i},\sigma}^\dagger c_{\boldsymbol{i}+\hat{\boldsymbol{x}},\sigma} + c_{\boldsymbol{i},\sigma}^\dagger c_{\boldsymbol{i}-\hat{\boldsymbol{x}},\sigma} + c_{\boldsymbol{i},\sigma}^\dagger c_{\boldsymbol{i}+\hat{\boldsymbol{y}},\sigma} + c_{\boldsymbol{i},\sigma}^\dagger c_{\boldsymbol{i}-\hat{\boldsymbol{y}},\sigma}\right),
$$

where $\langle \boldsymbol{ij} \rangle$ denotes nearest neighbour lattice sites $\boldsymbol{i}$ and $\boldsymbol{j}$. Transforming to operators with $\boldsymbol{k} \sim (\pi, \pi)$, one has

$$c^\dagger_{\boldsymbol{i}\sigma} = \frac{1}{\sqrt{N}} \sum_{\boldsymbol{k}} e^{i(\tilde{\boldsymbol{k}}+(\pi,\pi))\cdot \boldsymbol{R}_i} c^\dagger_{\boldsymbol{k}\sigma} = \frac{1}{\sqrt{N}} e^{i(\pi,\pi)\cdot \boldsymbol{R}_i} \sum_{\boldsymbol{k}} e^{i\tilde{\boldsymbol{k}}\cdot \boldsymbol{R}_i} c^\dagger_{\boldsymbol{k}\sigma},$$

where $\boldsymbol{R}_i$ is the vector position of site $\boldsymbol{i}$. Then, substituting the above, the kinetic energy is given by

$$\begin{aligned}
H_K &= -\frac{t}{N} \sum_{\boldsymbol{i},\sigma} \Bigg[e^{i(\pi,\pi)\cdot \boldsymbol{R}_i} e^{-i(\pi,\pi)\cdot(\boldsymbol{R}_i+\hat{\boldsymbol{x}})} \sum_{\tilde{\boldsymbol{k}},\tilde{\boldsymbol{p}}} e^{i\tilde{\boldsymbol{k}}\cdot \boldsymbol{R}_i} e^{-i\tilde{\boldsymbol{p}}\cdot(\boldsymbol{R}_i+\hat{\boldsymbol{x}})} c^\dagger_{\boldsymbol{k}\sigma} c_{\boldsymbol{p}\sigma} + \dots \\
&\quad + e^{i(\pi,\pi)\cdot \boldsymbol{R}_i} e^{-i(\pi,\pi)\cdot(\boldsymbol{R}_i-\hat{\boldsymbol{y}})} \sum_{\tilde{\boldsymbol{k}},\tilde{\boldsymbol{p}}} e^{i\tilde{\boldsymbol{k}}\cdot \boldsymbol{R}_i} e^{-i\tilde{\boldsymbol{p}}\cdot(\boldsymbol{R}_i-\hat{\boldsymbol{y}})} c^\dagger_{\boldsymbol{k}\sigma} c_{\boldsymbol{p}\sigma} \Bigg] \\
&= -\frac{t}{N} \sum_{\boldsymbol{i},\sigma} e^{\pm i\pi} \sum_{\tilde{\boldsymbol{k}},\tilde{\boldsymbol{p}}} e^{i(\tilde{\boldsymbol{k}}-\tilde{\boldsymbol{p}})\cdot \boldsymbol{R}_i} c^\dagger_{\boldsymbol{k}\sigma} c_{\boldsymbol{p}\sigma} \left(e^{-i\tilde{p}_x} + e^{i\tilde{p}_x} + e^{-i\tilde{p}_y} + e^{i\tilde{p}_y} \right) \\
&= \frac{t}{N} \sum_{\boldsymbol{i},\sigma} \sum_{\tilde{\boldsymbol{k}},\tilde{\boldsymbol{p}}} e^{i(\tilde{\boldsymbol{k}}-\tilde{\boldsymbol{p}})\cdot \boldsymbol{R}_i} c^\dagger_{\boldsymbol{k}\sigma} c_{\boldsymbol{p}\sigma} \left(2\cos\tilde{p}_x + 2\cos\tilde{p}_y \right) \\
&= t \sum_{\tilde{\boldsymbol{k}},\sigma} c^\dagger_{\boldsymbol{k}\sigma} c_{\boldsymbol{k}\sigma} \left(2\cos\tilde{k}_x + 2\cos\tilde{k}_y \right).
\end{aligned}$$

Contrasting this with the kinetic energy in terms of $\boldsymbol{k} = (k_x, k_y)$ (Eq. (3.11)), one can see it is the same except for an overall sign change. This follows from the fact that $\boldsymbol{R}_i$ is a quantized coordinate, i.e., that both its components are integer multiples of the lattice constant $a \equiv 1$. All parts of the Hamiltonian, including the vortex part, will have the quickly-oscillating factors cancel out in this fashion (leaving only a possible sign change) around $\boldsymbol{k} \sim (\pi, \pi)$. Therefore, this effective mass approximation is natural to use with the tight-binding model, where the system is on a lattice.

For the vortex (SC pairing) part of the Hamiltonian, we use [30, 40]

$$H_V = -\int d^2R \int d^2r \, e^{i\theta_{\boldsymbol{R}}} h(R) g(\boldsymbol{r}) c^\dagger_{\boldsymbol{R}+\boldsymbol{r},\uparrow} c^\dagger_{\boldsymbol{R}-\boldsymbol{r},\downarrow} + H.c., \tag{5.6}$$

where $\boldsymbol{R}$ and $\boldsymbol{r}$ are the center-of-mass and relative coordinates of a Cooper pair, respectively; $h(R) \sim (1 - e^{-R/\xi})$ describes the amplitude, and $\theta_{\boldsymbol{R}}$ the phase, of SC pairing in the vortex; and $g(\boldsymbol{r})$ is the Fourier transform of the s-wave order parameter $g(\boldsymbol{k}) = \Delta_0 = \text{const}$.

Using the relations

$$c^\dagger_{\boldsymbol{R}\pm\boldsymbol{r},\beta} = 2\pi \sum_{\boldsymbol{k}} c^\dagger_{\boldsymbol{k}\beta} e^{i\boldsymbol{k}\cdot(\boldsymbol{R}\pm\boldsymbol{r})}, \tag{5.7}$$

the vortex part becomes

$$H_V = -(2\pi)^2 \int d^2R \int d^2r\, e^{i\theta_{\boldsymbol{R}}} h(R) g(\boldsymbol{r}) \sum_{\boldsymbol{k}} c^\dagger_{\boldsymbol{k}\uparrow} e^{i\boldsymbol{k}\cdot(\boldsymbol{R}+\boldsymbol{r})} \sum_{\boldsymbol{p}} c^\dagger_{\boldsymbol{p}\downarrow} e^{i\boldsymbol{p}\cdot(\boldsymbol{R}-\boldsymbol{r})} + H.c. \tag{5.8}$$

Around $\boldsymbol{k} \sim (\pi, \pi)$, this yields

$$\begin{aligned} H_V^\pi =& -(2\pi)^2 \int d^2R \int d^2r\, e^{i\theta_{\boldsymbol{R}}} h(R) g(\boldsymbol{r}) \sum_{\boldsymbol{k}\sim(\pi,\pi)} c^\dagger_{\boldsymbol{k}\uparrow} e^{i\tilde{\boldsymbol{k}}\cdot(\boldsymbol{R}+\boldsymbol{r})} e^{i(\pi,\pi)\cdot(\boldsymbol{R}+\boldsymbol{r})} \\ & \cdot \sum_{\boldsymbol{p}\sim(\pi,\pi)} c^\dagger_{\boldsymbol{p}\downarrow} e^{i\tilde{\boldsymbol{p}}\cdot(\boldsymbol{R}-\boldsymbol{r})} e^{i(\pi,\pi)\cdot(\boldsymbol{R}-\boldsymbol{r})} + H.c. \\ =& -(2\pi)^2 e^{i2(\pi,\pi)\cdot\boldsymbol{R}} \int d^2R \int d^2r\, e^{i\theta_{\boldsymbol{R}}} h(R) g(\boldsymbol{r}) \sum_{\boldsymbol{k},\boldsymbol{p}\sim(\pi,\pi)} e^{i\tilde{\boldsymbol{k}}\cdot(\boldsymbol{R}+\boldsymbol{r})} e^{i\tilde{\boldsymbol{p}}\cdot(\boldsymbol{R}-\boldsymbol{r})} c^\dagger_{\boldsymbol{k}\uparrow} c^\dagger_{\boldsymbol{p}\downarrow} + H.c., \end{aligned}$$

where the factor of $e^{i2(\pi,\pi)\cdot\boldsymbol{R}}$ becomes unity. Therefore the vortex part will have the same form whether it is in terms of $\boldsymbol{k}, \boldsymbol{p}$ or $\tilde{\boldsymbol{k}}, \tilde{\boldsymbol{p}}$.

Using the total angular momentum operators, (5.4), we transform to total-angular-momentum space to find

$$\begin{aligned} H_K^0 \simeq& \frac{1}{(2\pi)^2} \sum_{m_J} \int_0^\Omega dk\, \left[-4t - \mu + tk^2\right] \left(c^\dagger_{m_J,k,\uparrow} c_{m_J,k,\uparrow} + c^\dagger_{m_J,k,\downarrow} c_{m_J,k,\downarrow} \right), \\ H_{SO}^0 \simeq& \frac{i\alpha}{(2\pi)^2} \sum_{m_J} \int_0^\Omega dk\, k \left(c^\dagger_{m_J,k,\uparrow} c_{m_J,k,\downarrow} - c^\dagger_{m_J,k,\downarrow} c_{m_J,k,\uparrow} \right), \\ H_Z^0 \simeq& \frac{1}{(2\pi)^2} \sum_{m_J} \int_0^\Omega dk\, (-h) \left(c^\dagger_{m_J,k,\uparrow} c_{m_J,k,\uparrow} - c^\dagger_{m_J,k,\downarrow} c_{m_J,k,\downarrow} \right), \\ H_V^0 \simeq& -i\Delta_0 \sum_m \int_0^\Omega dk \int_0^\Omega dp\, \sqrt{kp}\, u_m(k,p) \left(k c^\dagger_{m+\frac{3}{2},k,\uparrow} c^\dagger_{-m-\frac{1}{2},p,\downarrow} + p c^\dagger_{m+\frac{1}{2},k,\uparrow} c^\dagger_{-m+\frac{1}{2},p,\downarrow} \right) \\ & + H.c., \end{aligned} \tag{5.9}$$

where $\Omega \lesssim \frac{\pi}{2}$ is a cut-off momentum, and u_m is a Fourier component of $1/|\boldsymbol{k}+\boldsymbol{p}|^3$ (see Appendix B).

For all parts of the Hamiltonian, the $m_J = \frac{1}{2}$ channel separates. This is a crucial step to finding the Majorana mode. Taking only the $m_J = \frac{1}{2}$ channel yields

$$H^0_{V,m_J=\frac{1}{2}} \simeq -i \int_0^\Omega dk \int_0^\Omega dp\, \Delta(k,p) c^\dagger_{\frac{1}{2},k,\uparrow} c^\dagger_{\frac{1}{2},p,\downarrow} + H.c., \tag{5.10}$$

where

$$\Delta(k,p) := \Delta_0 \sqrt{kp} (k\, u_{-1}(k,p) + p\, u_0(k,p)). \tag{5.11}$$

As in the continuum model, $\Delta(k,p)$ is real, as all u_m are real (see Eq. (B.26)).

Similarly, around $\boldsymbol{k} \sim (\pi,\pi)$, we have

$$\begin{aligned}
H^{\pi}_{K,m_J=\frac{1}{2}} \simeq & \frac{1}{(2\pi)^2}\int_0^{\Omega} d\tilde{k}\,\left[4t-\mu-t\tilde{k}^2\right]\left(c^{\dagger}_{\frac{1}{2},\tilde{k},\uparrow}c_{\frac{1}{2},\tilde{k},\uparrow}+c^{\dagger}_{\frac{1}{2},\tilde{k},\downarrow}c_{\frac{1}{2},\tilde{k},\downarrow}\right)\\
H^{\pi}_{SO,m_J=\frac{1}{2}} \simeq & -\frac{i\alpha}{(2\pi)^2}\int_0^{\Omega} d\tilde{k}\,\tilde{k}\left(c^{\dagger}_{\frac{1}{2},\tilde{k},\uparrow}c_{\frac{1}{2},\tilde{k},\downarrow}-c^{\dagger}_{\frac{1}{2},\tilde{k},\downarrow}c_{\frac{1}{2},\tilde{k},\uparrow}\right)\\
H^{\pi}_{Z,m_J=\frac{1}{2}} \simeq & \frac{1}{(2\pi)^2}\int_0^{\Omega} d\tilde{k}\,(-h)\left(c^{\dagger}_{\frac{1}{2},\tilde{k},\uparrow}c_{\frac{1}{2},\tilde{k},\uparrow}-c^{\dagger}_{\frac{1}{2},\tilde{k},\downarrow}c_{\frac{1}{2},\tilde{k},\downarrow}\right)\\
H^{\pi}_{V,m_J=\frac{1}{2}} \simeq & -i\int_0^{\Omega} d\tilde{k}\int_0^{\Omega} d\tilde{p}\,\Delta(\tilde{k},\tilde{p})c^{\dagger}_{\frac{1}{2},\tilde{k},\uparrow}c^{\dagger}_{\frac{1}{2},\tilde{p},\downarrow}+H.c.
\end{aligned} \tag{5.12}$$

We now use only this channel, and suppress the subscript $m_J=\frac{1}{2}$.

5.2 Diagonalization, linearization, and Fourier transform of the Hamiltonian

We demonstrate diagonalization, linearization and Fourier transform of the Hamiltonian (channel $m_J=\frac{1}{2}$) around $k\sim 0$. The process for the Hamiltonian around $\boldsymbol{k}\sim(\pi,\pi)$ is very similar. This will put the Hamiltonian in a form similar to the Dirac form and allow for a real-space Majorana solution to be found.

Diagonalizing the single-electron part of the Hamiltonian, $H^0_0 = H^0_K + H^0_Z + H^0_{SO}$, in total-angular-momentum space, gives the energy eigenvalues

$$\begin{aligned}
E^0_{\pm}(k) &= -4t-\mu+tk^2\pm\sqrt{\alpha^2k^2+h^2}\\
&\simeq -4t-\mu\pm|h|+\left(t\pm\frac{1}{2}\frac{\alpha^2}{h}\right)k^2 \qquad k\sim 0.
\end{aligned} \tag{5.13}$$

Linearizing about the Fermi momentum k_F for the upper band gives

$$E^0_+(k_F+q)\simeq \left.\frac{\partial E^0_+}{\partial k}\right|_{k=k_F}\cdot q=\left(2t+\frac{\alpha^2}{h}\right)k_Fq := A_0k_Fq, \tag{5.14}$$

and about $k=0$ for the lower band gives

$$\begin{aligned}
E^0_-(q) &\simeq -4t-\mu-h\\
&\simeq -4t-h, \qquad \mu\approx 0.
\end{aligned} \tag{5.15}$$

Here we have also used the approximation $\mu \approx 0$ (and an implicit approximation of small k_F), as can be true in the Abelian region. Although it is not necessary to take $\mu \approx 0$, this gives a symmetry between the bands at $k \sim 0$ and at $\boldsymbol{k} \sim (\pi, \pi)$,

$$\begin{aligned} E^{\pi}_{-}(k_F + q) &\simeq -\left(2t + \frac{\alpha^2}{h}\right) k_F q \simeq -E^{0}_{+}(k_F + q), \\ E^{\pi}_{+}(q) &\simeq 4t + h \simeq -E^{0}_{-}(q), \qquad\qquad \mu \approx 0,\ q \ll 1, \end{aligned} \tag{5.16}$$

with E^{π}_{-} a function of $\tilde{k}$. Everything is now exactly analogous to the continuum model case, except with the Fermi momentum in the upper band rather than the lower band for $k \sim 0$ (see Fig. 5.1).

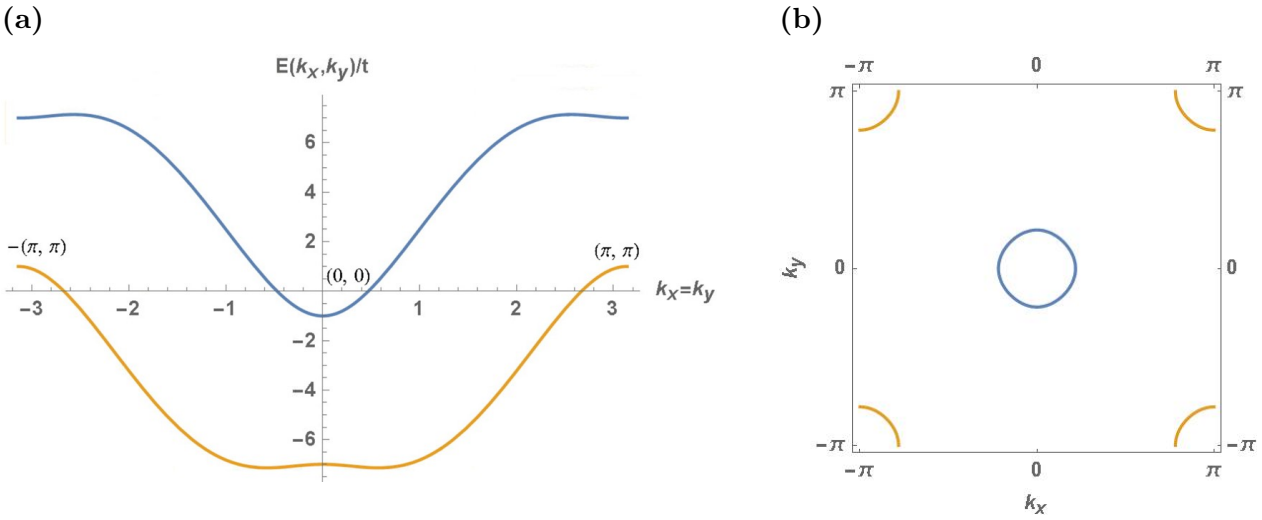

Figure 5.1: Energy bands in the Abelian region for the single-electron part of the Hamiltonian, with parameters $\mu = 0$, $\alpha = 3t$, $h = 3t$. (a) Cross-section of the energy bands for $k_x = k_y$. (b) Fermi surfaces around $k \sim 0$ and $\boldsymbol{k} \sim (\pi, \pi)$. The lattice constant is set to unity.

Using upper- and lower-band operators for the diagonalized Hamiltonian, the single-electron part is given by

$$H^0_0 = \int \frac{dk}{(2\pi)^2} \left[E^0_+(k) f^\dagger_{+,k} f_{+,k} + E^0_-(k) f^\dagger_{-,k} f_{-,k} \right], \tag{5.17}$$

and the vortex part is found to be

$$H^0_V \simeq -\frac{i}{2} \int_0^\Omega dk \int_0^\Omega dp \left[\Lambda_{++}(k,p) f^\dagger_{+,k} f^\dagger_{+,p} + \Lambda_{--}(k,p) f^\dagger_{-,k} f^\dagger_{-,p} + \Lambda_{+-}(k,p) f^\dagger_{+,k} f^\dagger_{-,p} \right] + H.c., \tag{5.18}$$

where Λ_{++} and Λ_{--} are antisymmetric in k and p. As in the continuum model, the phase of Λ_{++} and Λ_{--} functions is arbitrary (Λ_{+-} is always real), depending on a phase factor in how f's are defined in terms of c's (see Appendix B, Eqs. (B.35) and (B.37)).

Limiting the momenta in the upper band to those near the Fermi momentum and momenta in the lower band to those near the band minimum, the total Hamiltonian about $k \sim 0$ is then

$$\begin{aligned} H^0_{Tot} = H^0_0 + H^0_V = \int \frac{dq}{(2\pi)^2} \Big[E^0_+(k_F+q) f^\dagger_{+,k_F+q} f_{+,k_F+q} + E^0_- f^\dagger_{-,q} f_{-,q} \Big] \\ - \frac{i}{2} \iint dq\, dq' \Big[\Lambda_{++}(q-q') f^\dagger_{+,k_F+q} f^\dagger_{+,k_F+q'} + \Lambda_{--}(q-q') f^\dagger_{-,q} f^\dagger_{-,q'} + \Lambda_{+-} f^\dagger_{+,k_F+q} f^\dagger_{-,q} \Big] + H.c. \end{aligned} \tag{5.19}$$

The lower limits on the integrals are $-k_F$ and 0 when the operators correspond to upper and lower bands, respectively. (For $\boldsymbol{k} \sim (\pi, \pi)$, these lower limits will be flipped to 0 and $-k_F$.) Only lowest-order dependence of the functions Λ on q and q', which are consistent with Λ_{++} and Λ_{--} being antisymmetric in q and q', are kept. In the limit of $q, q' \to 0$, $\Lambda_{+-}(k_F+q, q')$ is assumed to be a non-zero constant Λ_{+-} (although, in Appendix C, we will see that actually $\Lambda_{+-} = 0$, simplifying the BdG equations).

After diagonalization and linearization, the Hamiltonian is Fourier transformed to real space. Defining the Fourier operator transforms,

$$\begin{aligned} f^\dagger_+(x) &= \int_{-k_F}^{\Omega} dq\, e^{iqx} f^\dagger_{+,k_F+q}, \\ f^\dagger_-(x) &= \int_0^{\Omega} dq\, e^{iqx} f^\dagger_{-,q}, \end{aligned} \tag{5.20}$$

where $\Omega \lesssim \frac{\pi}{2}$, gives the transformed total Hamiltonian,

$$\begin{aligned} H^0_{Tot} = \int_{-\infty}^{\infty} dx \int_{-\infty}^{\infty} dx' \Big[E^0_+(x-x') f^\dagger_+(x) f_+(x') + E^0_- \delta(x-x') f^\dagger_-(x) f_-(x') \Big] \\ - \frac{i}{2} \int_{-\infty}^{\infty} dx \Big[\Lambda_{++}(x) f^\dagger_+(x) f^\dagger_+(-x) + \Lambda_{--}(x) f^\dagger_-(x) f^\dagger_-(-x) + \Lambda_{+-} \delta(x) f^\dagger_+(x) f^\dagger_-(-x) \Big] + H.c., \end{aligned} \tag{5.21}$$

where $E^0_+(x-x') = iA_0 k_F \partial_x \delta(x-x')$, and $\Lambda_{++}(x)$ and $\Lambda_{--}(x)$ are odd in x.

5.3 BdG equations and zero-energy solution

As with the continuum model [30], the quasiparticle operator for a hypothetical zero-energy mode can be defined as

$$\gamma^\dagger = \int_{-\infty}^{\infty} dx \, \Big(\eta_{+,1}(x) f_+^\dagger(x) + \eta_{-,1}(x) f_-^\dagger(x) + \eta_{+,2}(x) f_+(-x) + \eta_{-,2}(x) f_-(-x) \Big), \tag{5.22}$$

so that one has

$$\big[H_{Tot}^0, \gamma^\dagger \big] = \varepsilon \gamma^\dagger = 0. \tag{5.23}$$

As in Refs. [30, 40], to calculate the commutators in the BdG equations, we need to use the relations,

$$\begin{aligned}
\{ f_+^\dagger(x), f_+(x') \} &= \int_{-k_F}^{\Omega} dq \int_{-k_F}^{\Omega} dq' \, e^{i(qx - q'x')} \{ f_{+,k_F+q}^\dagger, f_{+,k_F+q'} \} = \int_{-k_F}^{\Omega} dq \, e^{iq(x-x')} \\
&\equiv S_+^0(x - x'), \\
\{ f_-^\dagger(x), f_-(x') \} &= \int_{0}^{\Omega} dq \int_{0}^{\Omega} dq' \, e^{i(qx - q'x')} \{ f_{-,q}^\dagger, f_{-,q'} \} = \int_{0}^{\Omega} dq \, e^{iq(x-x')} \equiv S_-^0(x - x'),
\end{aligned} \tag{5.24}$$

and introduce the functions

$$\xi_{\pm,n}(x) = \int_{-\infty}^{\infty} S_\pm(x_1 - x) \eta_{\pm,n}(x_1) dx_1. \tag{5.25}$$

Then, computing the commutator (5.23), the BdG equations take the form

$$\begin{aligned}
E_-^0 \xi_{-,1}(x) - i\Lambda_{--}(x) \xi_{-,2}(x) + \frac{i}{2} \Lambda_{+-} \delta(x) \xi_{+,2}(x) &= 0, \\
i A_0 k_F \partial_x \xi_{+,1}(x) - i\Lambda_{++}(x) \xi_{+,2}(x) - \frac{i}{2} \Lambda_{+-} \delta(x) \xi_{-,2}(x) &= 0, \\
-E_-^0 \xi_{-,2}(x) + i\Lambda_{--}^*(x) \xi_{-,1}(x) + \frac{i}{2} \Lambda_{+-} \delta(x) \xi_{+,1}(x) &= 0, \\
-i A_0 k_F \partial_x \xi_{+,2}(x) + i\Lambda_{++}^*(x) \xi_{+,1}(x) - \frac{i}{2} \Lambda_{+-} \delta(x) \xi_{-,1}(x) &= 0.
\end{aligned} \tag{5.26}$$

Using the first and third of these equations, we have

$$\begin{pmatrix} \xi_{-,1}(x) \\ \xi_{-,2}(x) \end{pmatrix} = \frac{\frac{i}{2}\Lambda_{+-}\delta(x)}{(E_-^0)^2 + |\Lambda_{--}(x)|^2} \begin{pmatrix} -E_-^0 & i\Lambda_{--}(x) \\ -i\Lambda_{--}^*(x) & E_-^0 \end{pmatrix} \begin{pmatrix} \xi_{+,2}(x) \\ \xi_{+,1}(x) \end{pmatrix}, \tag{5.27}$$

and the amplitudes $\xi_{-,1}(x),\ \xi_{-,2}(x)$ for the lower band can be eliminated, giving

$$\begin{aligned} iA_0k_F\partial_x\xi_{+,1}(x) + \frac{1}{4}\frac{E_-^0\Lambda_{+-}^2\delta^2(x)}{(E_-^0)^2+|\Lambda_{--}(x)|^2}\xi_{+,1}(x) - i\left(\Lambda_{++}(x)+\frac{1}{4}\frac{\Lambda_{--}^*(x)\Lambda_{+-}^2\delta^2(x)}{(E_-^0)^2+|\Lambda_{--}(x)|^2}\right)\xi_{+,2}(x) = 0, \\ -iA_0k_F\partial_x\xi_{+,2}(x) - \frac{1}{4}\frac{E_-^0\Lambda_{+-}^2\delta^2(x)}{(E_-^0)^2+|\Lambda_{--}(x)|^2}\xi_{+,2}(x) + i\left(\Lambda_{++}^*(x)+\frac{1}{4}\frac{\Lambda_{--}(x)\Lambda_{+-}^2\delta^2(x)}{(E_-^0)^2+|\Lambda_{--}(x)|^2}\right)\xi_{+,1}(x) = 0. \end{aligned} \tag{5.28}$$

Redefining

$$\psi_n(x) = \exp\left(-\frac{i}{4A_0k_F}\int_0^x dx'\,\frac{E_-^0\Lambda_{+-}^2\delta^2(x')}{(E_-^0)^2+|\Lambda_{--}(x')|^2}\right)\xi_{+,n}(x), \tag{5.29}$$

the equations above become

$$A_0k_F\partial_x\begin{pmatrix}\psi_1(x)\\ \psi_2^*(x)\end{pmatrix} = m(x)\sigma_x\begin{pmatrix}\psi_1^*(x)\\ \psi_2(x)\end{pmatrix}, \tag{5.30}$$

with the mass function $m(x)$ given by

$$m(x) = \left(\Lambda_{++}(x)+\frac{1}{4}\frac{\Lambda_{--}^*(x)\Lambda_{+-}^2\delta^2(x)}{(E_-^0)^2+|\Lambda_{--}(x)|^2}\right). \tag{5.31}$$

Then $m(x)$ is clearly odd in x, as $\Lambda_{++}(x)$ and $\Lambda_{--}(x)$ are odd in x. As in the continuum model, Λ_{+-} is real and $\Lambda_{++}(x)$ and $\Lambda_{--}(x)$ have arbitrary (related) phases dependent on the definition of diagonalized f operators, although the authors of Ref. [30] have chosen $\Lambda_{++}(x)$ and $\Lambda_{--}(x)$ to be real.

Defining $\tilde{m}(x) \equiv \text{sign}(x)|m(x)|$, for $m(x) = e^{i\theta}\tilde{m}(x)$, the general solution to Eq. (5.30) is

$$\begin{aligned} \psi_1(x) &= C\exp\left(\frac{\lambda}{A_0k_F}\int_0^x \tilde{m}(y)dy\right), \\ \psi_2(x) &= Ce^{-i\theta}\text{sign}(\lambda)\exp\left(\frac{\lambda}{A_0k_F}\int_0^x \tilde{m}(y)dy\right), \end{aligned} \tag{5.32}$$

where $\lambda = \pm 1$.

The BdG equations (5.30) are of a form similar to the Dirac equation for a zero-energy mode; in particular, if $\psi(x) = (\psi_1(x), \psi_2^*(x))^T$ is a solution, then $\sigma_x\psi(x)$ is also a solution. Therefore for a unique zero-energy solution about $k \sim 0$ to exist, it must be an eigenspinor of σ_x, with $\sigma_x\psi(x) = \lambda\psi(x)$. This gives $C = e^{i\theta}C^*$, or

$$\begin{aligned} \psi_1(x) &= |C|e^{i\theta/2}\exp\left(\frac{\lambda}{A_0k_F}\int_0^x \tilde{m}(y)dy\right), \\ \psi_2(x) &= |C|e^{-i\theta/2}\text{sign}(\lambda)\exp\left(\frac{\lambda}{A_0k_F}\int_0^x \tilde{m}(y)dy\right), \end{aligned} \tag{5.33}$$

To be Majorana, the unique solution also requires $\lambda = 1$. As in Ref. [30], to see that this gives a Majorana fermion, note that

$$\begin{aligned}
\xi_{+,1}(x) &= |C|e^{i\theta/2} \exp\left(\frac{i}{4A_0k_F}\int_0^x dx' \, \frac{E_-^0\Lambda_{+-}^2\delta^2(x')}{|\Lambda_{--}(x')|^2 + (E_-^0)^2}\right) \exp\left(\frac{1}{A_0k_F}\int_0^x \tilde{m}(y)dy\right), \\
\xi_{+,2}(x) &= |C|e^{-i\theta/2} \exp\left(\frac{i}{4A_0k_F}\int_0^x dx' \, \frac{E_-^0|\Lambda_{+-}|^2\delta^2(x')}{|\Lambda_{--}(x')|^2 + (E_-^0)^2}\right) \exp\left(\frac{1}{A_0k_F}\int_0^x \tilde{m}(y)dy\right).
\end{aligned} \tag{5.34}$$

Then it can be shown that $\xi_{+,1}^*(-x) = \xi_{+,2}(x)$, and using $S_\pm^{0*}(x_1 - x) = S_\pm^0(x - x_1)$ (see Eqs. (5.22), (5.24)), this gives

$$\eta_{+,1}^*(-x) = \eta_{+,2}(x). \tag{5.35}$$

Similarly, one finds that $\eta_{-,1}^*(-x) = \eta_{-,2}(x)$. Therefore PHS is present and $\gamma^\dagger$ is a Majorana fermion operator.

The case for $\boldsymbol{k} \sim (\pi, \pi)$ is very similar, giving BdG equations:

$$-A_0k_F\partial_x \begin{pmatrix} \psi_1^\pi(x) \\ \psi_2^{\pi\,*}(x) \end{pmatrix} = m^\pi(x)\sigma_x \begin{pmatrix} \psi_1^{\pi\,*}(x) \\ \psi_2^\pi(x) \end{pmatrix}, \tag{5.36}$$

where

$$\psi_n^\pi(x) = \exp\left(\frac{i}{4A_0k_F}\int_0^x dx' \, \frac{E_+^\pi(\Lambda_{+-}^\pi)^2\delta^2(x')}{(E_+^\pi)^2 + |\Lambda_{++}^\pi(x')|^2}\right)\xi_{-,n}^\pi(x), \tag{5.37}$$

and the mass function around $\boldsymbol{k} \sim (\pi, \pi)$ is given by

$$m^\pi(x) = \left(\Lambda_{--}^\pi(x) + \frac{1}{4}\frac{\Lambda_{++}^{\pi\,*}(x)(\Lambda_{+-}^\pi)^2\delta^2(x)}{(E_+^\pi)^2 + |\Lambda_{++}^\pi(x)|^2}\right). \tag{5.38}$$

Solving the BdG equations (5.36) around $\boldsymbol{k} \sim (\pi, \pi)$ gives the Majorana solution,

$$\begin{aligned}
\psi_1^\pi(x) &= |C|e^{i\tilde{\theta}/2} \exp\left(-\frac{1}{A_0k_F}\int_0^x \tilde{m}^\pi(y)dy\right), \\
\psi_2^\pi(x) &= |C|e^{-i\tilde{\theta}/2} \exp\left(-\frac{1}{A_0k_F}\int_0^x \tilde{m}^\pi(y)dy\right).
\end{aligned} \tag{5.39}$$

Again it can be shown that the η functions in the zero-mode operator $\gamma^\dagger$ are complex conjugates of each other, giving $\gamma^\dagger$ a Majorana fermion operator.

Note that, as $\tilde{m}(x) = \text{sign}(x)|m(x)|$, the solution (5.39) is normalizable but the Majorana solution (5.33), with $\lambda = 1$, around $k \sim 0$ appears non-normalizable (as in the continuum

model). However, as this is an approximation to the true solution and in practice the Majorana mode will be localized near the vortex core, this Majorana solution is still worth considering.

In Appendix C, we attempt to find the relation between the Majorana modes about $k \sim 0$ and $\boldsymbol{k} \sim (\pi, \pi)$ analytically, that is, whether they are similar or orthogonal, although it is possible that the true relationship between them may not be accurately modelled under the approximations used here.

6 Numerical Results

In this chapter we examine our numerical findings, focusing on the Abelian phase of the 2D topological superconducting system we study. Our index theorem in chapter 5 predicts the existence of two Majorana fermion zero-modes per vortex core in the Abelian phase. In contrast, our numerical results show that there are no Majorana modes in a vortex core in this phase. This is an indication that the Majorana modes in the Abelian phase are similar to each other, that is, their wave functions are not exactly orthogonal, so that when confined in the vortex core they annihilate each other.

6.1 General Considerations and Results

Using two flux quanta in the system for the vortex lattice, our order parameter converges to the solution with half of a vortex at the center of each side. (The precise center of a vortex is located at or just outside the system by one of two opposing sides, and may possibly shift

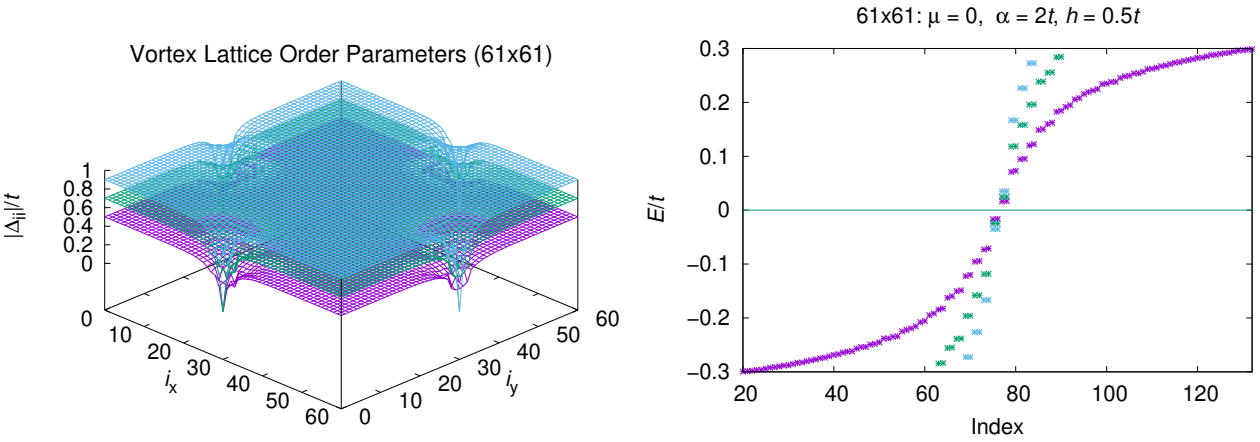

Figure 6.1: Order parameter Δ_{ii}, where $i = (i_x, i_y)$ for a 2D lattice (left), and excitation spectrum (right) for the vortex lattice, for bulk order parameter $\Delta_0 = 0.5t$ (purple), $0.7t$ (green), and $0.9t$ (blue) for the Abelian-phase system with $\mu = t$, $\alpha = 2t$, $h = 2t$. The index numbers the (energy) eigenvalues.

between sides under further convergence.) Vortex lattice order parameters and corresponding excitation spectra are plotted in Fig. 6.1, for an Abelian-phase system ($\mu = t$, $\alpha = 2t$, $h = 2t$) with differing bulk order parameter, $\Delta_0 \equiv \Delta_s$.

Most systems will be studied with the same bulk order parameter, $\Delta_0 \approx 0.34t$, in order to compare results most meaningfully. For this purpose we adjust the coupling constant U for a given set of μ, α and h, and first converge the bulk order parameter to this value in the homogeneous phase. This choice of Δ_0 should not affect results much, as eigenvalues and other properties generally scale linearly with Δ_0 as long as one stays within the same topological region. This is illustrated in Fig. 6.2, where bulk order parameter Δ_0 is plotted as a function of coupling constant U for both Abelian-phase ($\mu = t$, $\alpha = 2t$, $h = 1.5t$, and $\mu = t$, $\alpha = 2t$, $h = 2t$) and non-Abelian-phase ($\mu = -3t$, $\alpha = 1.5t$, $h = 1.5t$) systems, as well as smallest excitation energy as a function of Δ_0 for an Abelian-phase ($\mu = t$, $\alpha = 2t$, $h = 2t$) vortex-lattice system. A near-linear relationship is expected between this smallest energy and Δ_0, although slight deviations occur due to restricted system size.

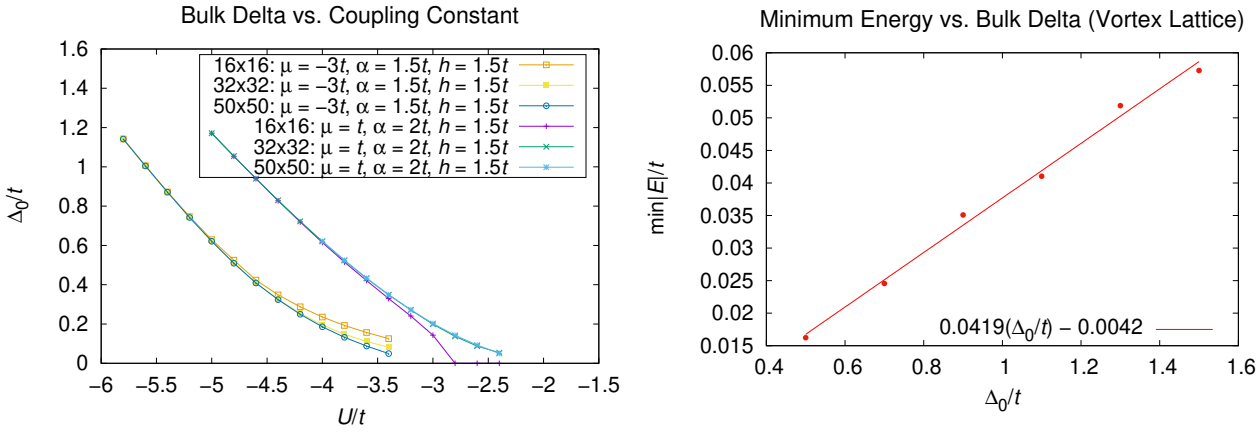

Figure 6.2: *Left:* Bulk (homogeneous) order parameter Δ_0 as a function of coupling constant U for various systems and sizes. The system $\mu = -3t$, $\alpha = 1.5t$, $h = 1.5t$ is within the non-Abelian phase (with $I_{\mathrm{TKNN}} = 1$), and the system $\mu = t$, $\alpha = 2t$, $h = 1.5t$ the Abelian phase, both transitioning to trivial phase around $\Delta_0 \gtrsim 1.12t$. *Right:* Minimum excitation energy versus bulk order parameter, for the 61×61 Abelian-phase system with $\mu = t$, $\alpha = 2t$, $h = 2t$ in the vortex lattice.

The effect of large Zeeman splitting, h, on the order parameter is shown in Figs. 6.3 and 6.4. For $h \gtrsim \alpha$, with α the spin-orbit coupling constant, the order parameter tends not to converge. In some cases, for large Zeeman splitting the order parameter does not converge

to a vortex configuration, especially for smaller lattice sizes, which correspond to stronger magnetic field for the vortex lattice with two flux quanta in the system. In Fig. 6.4 (b), where the order parameter has been converged down to 10^{-8}, superconductivity is nearly destroyed for system size 41×41.

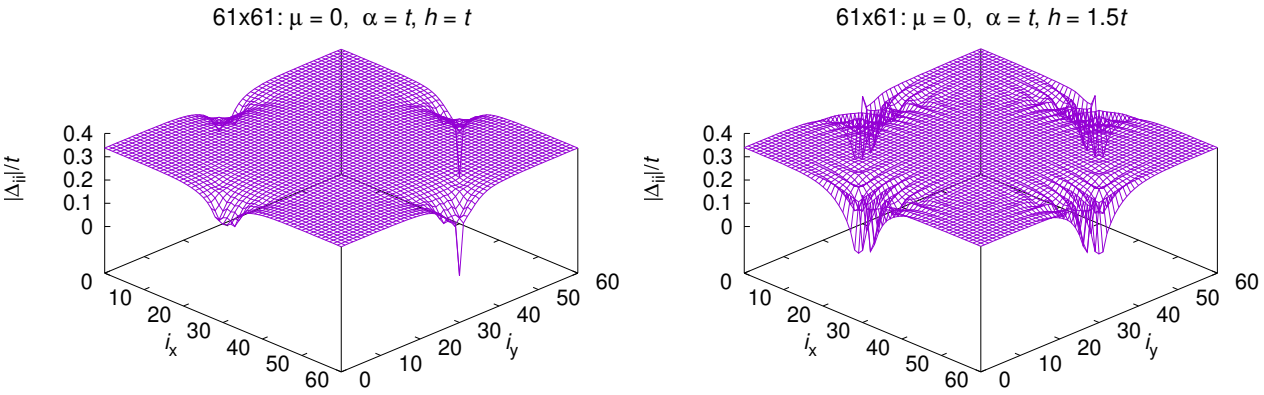

Figure 6.3: Effect of increasing Zeeman splitting on the order parameter for the vortex lattice in Abelian phase, for $h = t$ (left) and $h = 1.5t$ (right) with $\mu = 0$, $\alpha = t$ ($\Delta_0 = 0.34t$, size 61×61).

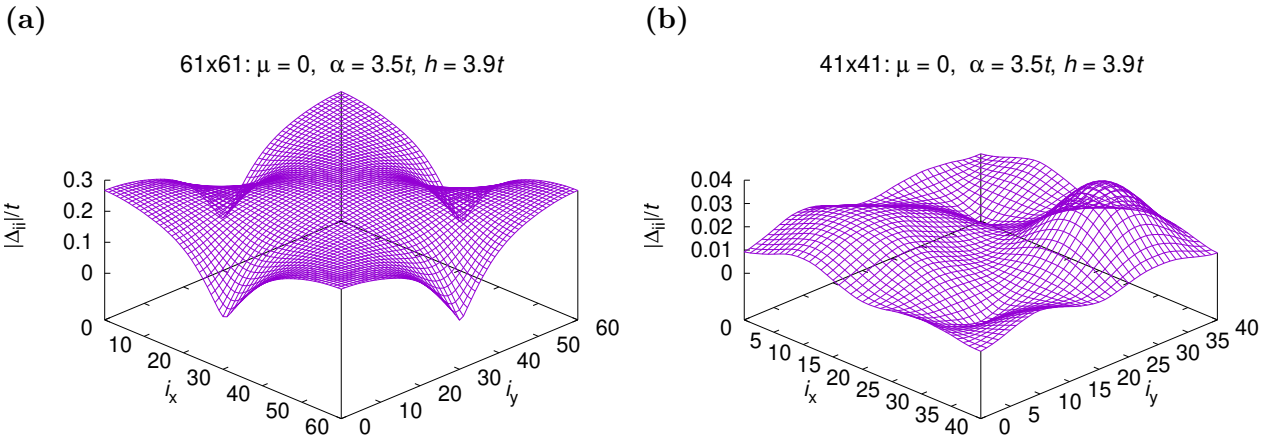

Figure 6.4: Effect of large Zeeman splitting on the order parameter for the vortex lattice in Abelian phase, with $\mu = 0$, $\alpha = 3.5t$, $h = 3.9t$: (a) size 61×61; (b) size 41×41 converged down to 10^{-8}.

In our results here and elsewhere, the order parameter is converged down to at least 10^{-6}, that is, converged until further iterations change the relative vector-magnitude of the order parameter, $||\Delta_{\text{new}} - \Delta_{\text{old}}||/||\Delta_{\text{old}}||$, by less than 10^{-6}.

6.2 Majorana Modes at a Boundary

In numerical calculations of the energy eigenvalues of a system, the lowest energies will never be exactly zero due to restricted system size. Therefore, in order to be able to observe Majorana modes numerically, one must model a system which allows for the presence of an *even* number of Majorana modes – in the homogeneous phase, a system with two separate surfaces works well, or for the vortex lattice a system with two vortices. This ensures the required particle-hole symmetry (PHS) of the Bogoliubov-de Gennes (BdG) equations, with energy eigenvalues symmetric about zero. For each pair of Majorana solutions, one energy will be slightly positive and one (equal-magnitude) energy slightly negative. Each of these energies corresponds to a superposition of the pair of Majorana modes.

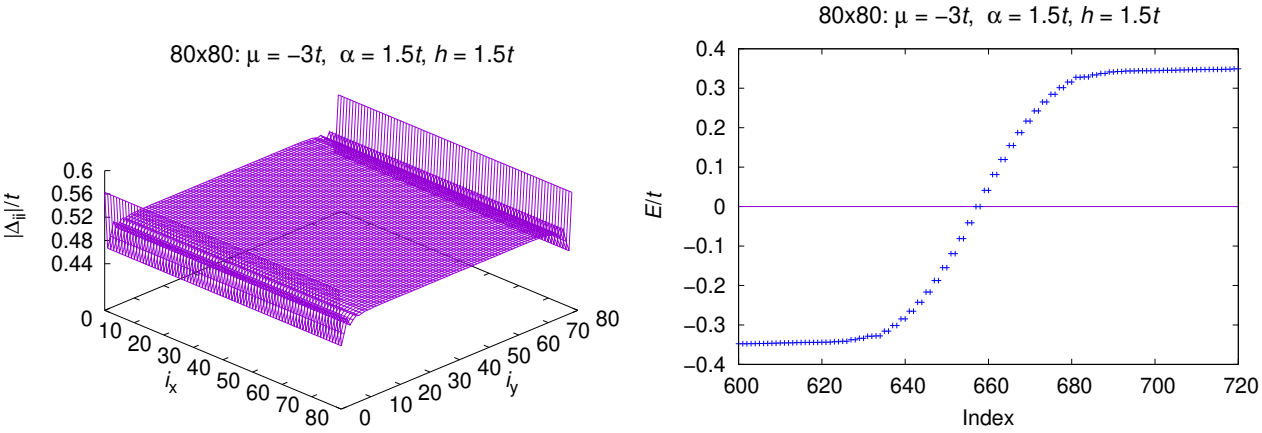

Figure 6.5: *Left:* Order parameter, and *right:* quasiparticle excitation spectrum, for the homogeneous 80×80 non-Abelian-phase system with parameters $\mu = -3t$, $\alpha = 1.5$, $h = 1.5$, $U = -5.5t$ and two boundaries. PBC is used in the x direction and OBC in the y direction, giving one boundary along $i_y = 0$ and one along $i_y = 79$.

The existence of Majorana fermion zero-mode(s) at a boundary occurs in both the non-Abelian and Abelian phases. We study these boundary Majorana modes for the homogeneous phase, that is, in the absence of vortices or impurities. Figure 6.5 (*left*) shows the superconducting order parameter and (b) the quasiparticle excitation spectrum, for a homogeneous 80×80 non-Abelian-phase system ($\mu = -3t$, $\alpha = 1.5$, $h = 1.5$, $U = -5.5t$) with two boundaries. We use periodic boundary conditions (PBC) in the x direction and open boundary conditions (OBC) in the y direction to obtain two boundaries, one along $i_y = 0$ and one along $i_y = 79$. For this non-Abelian-phase system, a single Majorana mode is found along

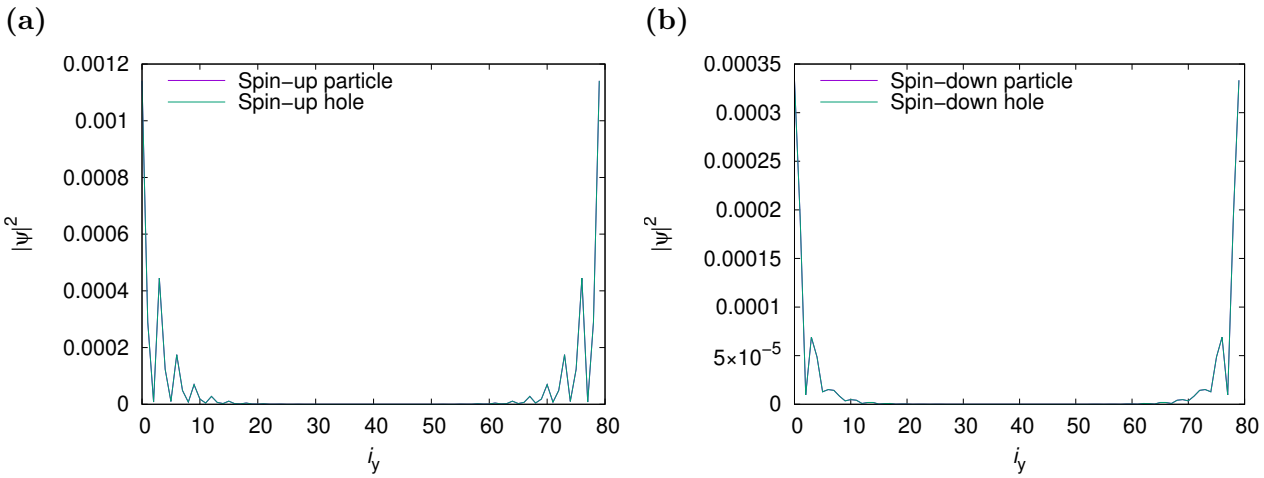

Figure 6.6: Magnitude squared of (a cross-section of) the wave function of the smallest-energy state, for (a) spin-up, and (b) spin-down components, for the homogeneous 80×80 non-Abelian-phase system with parameters $\mu = -3t$, $\alpha = 1.5$, $h = 1.5$, $U = -5.5t$ and two boundaries, one at $i_y = 0$ and one at $i_y = 79$. PHS is present.

each of these two boundaries, with energy $E \simeq \pm 2.7 \times 10^{-6} t$. To confirm that the lowest-energy excitation is a Majorana mode, one must check that the wave function of this state exhibits PHS. In Fig. 6.6 we examine a cross-section of the probability distribution of the (positive) minimum-energy state, and see that it indeed exhibits PHS. The corresponding negative-energy state, with equal-magnitude energy, is also P-H symmetric.

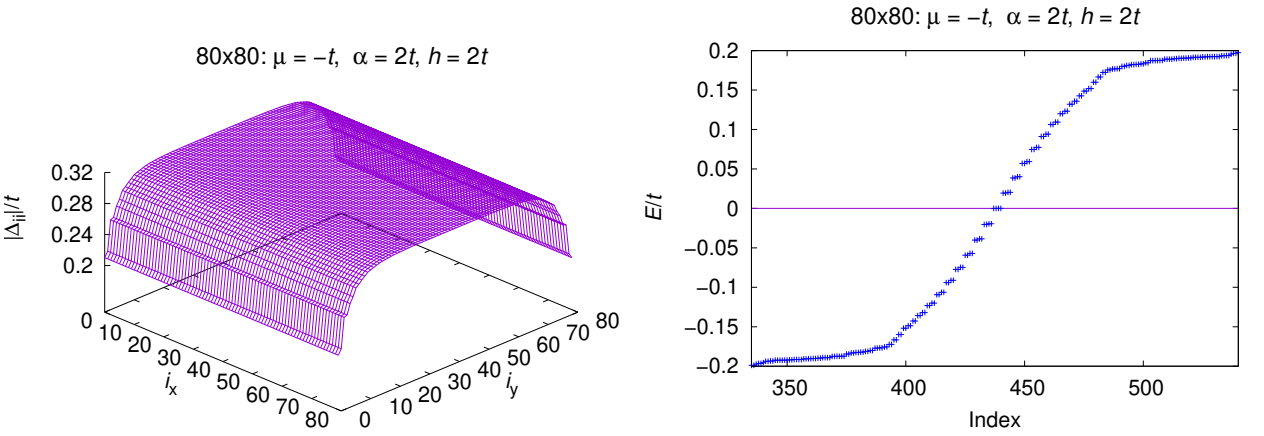

Figure 6.7: *Left:* Order parameter, and *right:* quasiparticle excitation spectrum, for the homogeneous 80×80 Abelian-phase system with parameters $\mu = -t$, $\alpha = 2t$, $h = 2t$, $U = -5.8t$ and two boundaries, one at $i_y = 0$ and one at $i_y = 79$.

In the Abelian phase, one finds *two* Majorana modes per surface. The order parameter and quasiparticle excitation spectrum for a homogeneous 80×80 Abelian-phase system ($\mu = -t$,

$\alpha = 2t$, $h = 2t$, $U = -5.8t$), with two boundaries as before, is shown in Fig. 6.7. The PHS of the two (positive) smallest-energy states, with energies $E_1 \simeq 3.9 \times 10^{-7} t$, $E_2 \simeq 4.6 \times 10^{-6} t$, is examined in Fig. 6.8. The spectral gap for this system is somewhat small – about $0.15t$ – as seen in Fig. 6.7 (b), resulting in some overlap of the Majorana modes and small oscillations in the probability distribution reaching the center of the lattice, in the first excited state. This overlap also perturbs the modes very slightly away from true PHS and hence from being truly Majorana. With a larger spectral gap – and no overlap between zero modes on the two boundaries – these quasiparticle excitations will in general both be true Majorana modes.

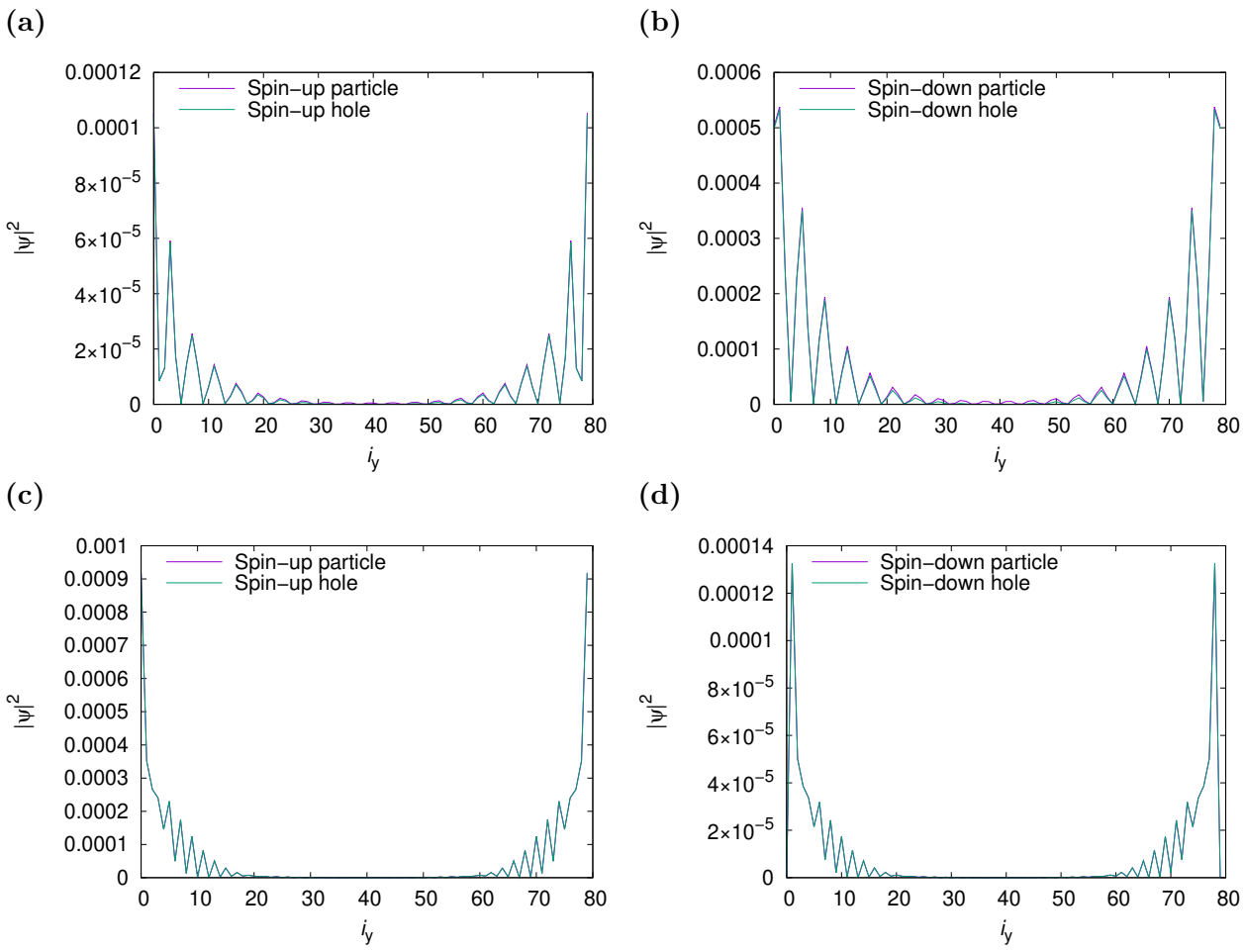

Figure 6.8: Magnitude squared of (a cross section of) wave functions for (a) spin-up and (b) spin-down components of the smallest-energy state, and (c) spin-up and (d) spin-down components of the second-smallest-energy state, for the homogeneous 80×80 Abelian-phase system with parameters $\mu = -t$, $\alpha = 2t$, $h = 2t$, $U = -5.8t$ and two boundaries, one at $i_y = 0$ and one at $i_y = 79$. PHS is slightly broken in the smallest-energy state.

6.3 Majorana Modes in a Vortex Core

As stated in the previous section, modeling a system which allows for an even number of Majorana modes ensures the required PHS of the BdG equations. To study the vortex lattice, we therefore use a system with two vortices (and PBC).

Inter-vortex interactions, which become weaker with increasing distance between vortices, perturb the system energies. If the smallest positive energy (and equal-magnitude negative energy) tends toward zero as the system size increases – that is, as inter-vortex distance increases – this is a good indication of the existence of a Majorana mode.

To confirm that the lowest-energy state is a Majorana mode, one must also check that

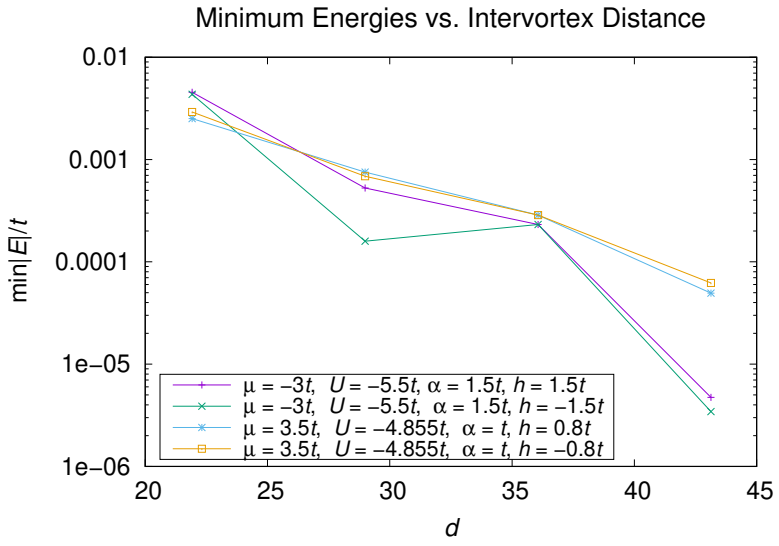

Figure 6.9: Non-Abelian-phase minimum energy eigenvalues (in log scale) versus inter-vortex distance, d. Inter-vortex distances correspond to system sizes 31×31, 41×41, 51×51, and 61×61.

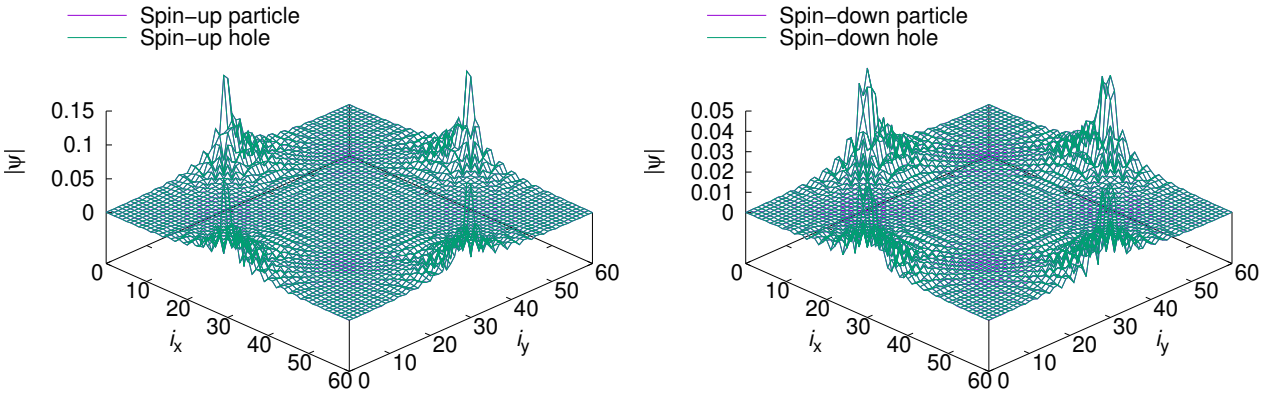

Figure 6.10: Wave function components of the lowest-energy state for the 61×61 non-Abelian-phase system with parameters $\mu = -3t$, $U = -5.5t$, $\alpha = 1.5t$, and $h = 1.5t$. PHS is exhibited. *Left:* spin-up particle and hole, and *right:* spin-down particle and hole components.

the wave function of this state exhibits particle-hole symmetry (PHS). In the non-Abelian region, where there is a single Majorana mode per vortex or boundary, this is what one finds. In Fig. 6.9, we see the minimum excitation energies of the system decreasing with inter-vortex distance for different systems in the non-Abelian region, including the vortex system with the same parameters as the homogeneous-phase system studied in the last section ($\mu = -3t$, $\alpha = 1.5t$, $h = 1.5t$, $U = -5.5t$). In Fig. 6.10 we examine the wave function of the minimum-energy state of this particular system, to see that it indeed exhibits PHS, as in the case of homogeneous phase with two boundaries.

In our data we now focus on the Abelian phase, for which our index theorem predicts the existence of *two* Majorana modes per vortex. Our numerical results, however, indicate that these modes are not exactly orthogonal to each other – and so annihilate each other – we find no Majorana mode in a vortex core numerically in the Abelian phase.

In Fig. 6.11 we examine the dependence of lowest energies on inter-vortex distance for various Abelian-phase systems, and can see that these energies are not going to zero. Included is the system with the same parameters as the homogeneous Abelian-phase system studied in the last section ($\mu = -t$, $\alpha = 2t$, $h = 2t$, $U = -5.8t$). Although size 61×61, as in Fig. 6.10, should be large enough to determine whether PHS of the wave function and therefore Majorana mode(s) exist for the vortex lattice, we examine the minimum-energy wave function of this particular system for size 81×81, in Fig. 6.12. One can see that PHS is not present, in contrast with our results for the homogeneous phase with two boundaries.

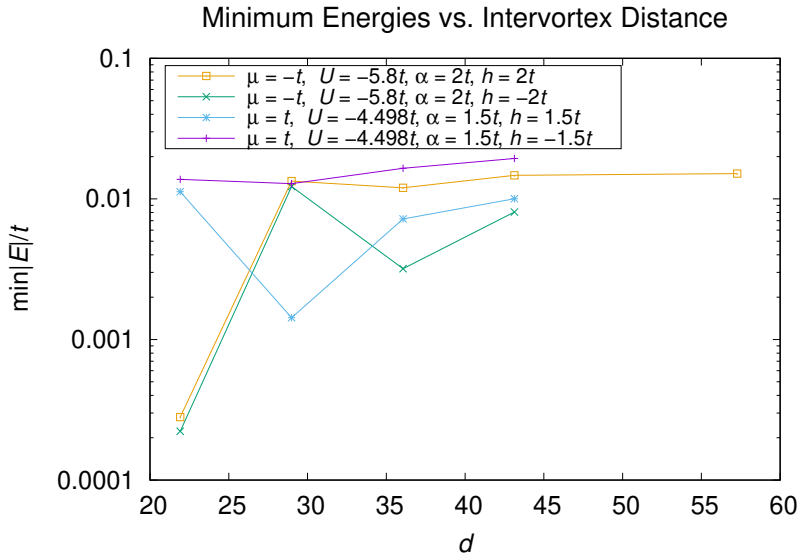

Figure 6.11: Abelian-phase minimum energy eigenvalues (in log scale) versus inter-vortex distance, d. Inter-vortex distances correspond to system sizes 31×31, 41×41, 51×51, 61×61, and 81×81.

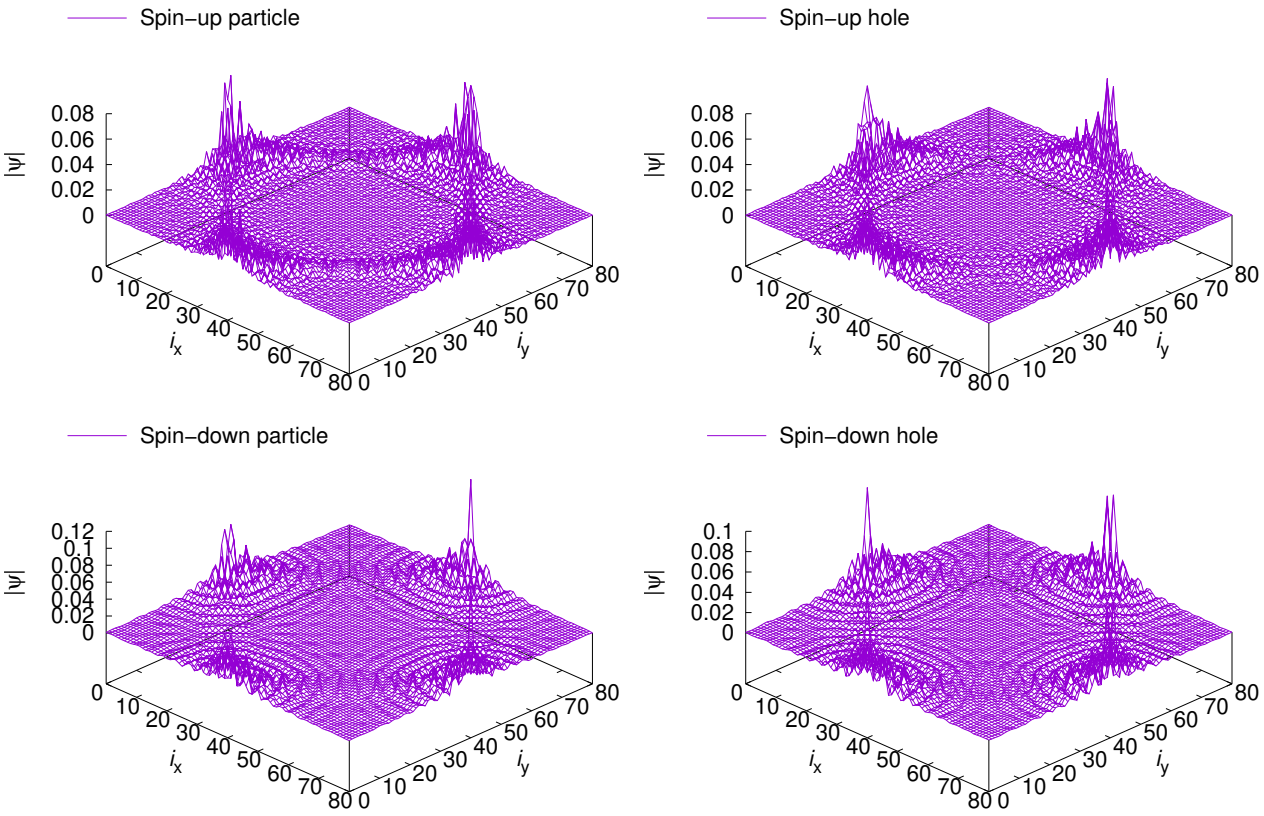

Figure 6.12: Wave function components of the lowest-energy state, for the 81×81 Abelian-phase system with parameters $\mu = -t$, $\alpha = 2t$, $h = 2t$, and $U = -5.8t$. PHS is broken. *Top left:* spin-up particle, *top right:* spin-up hole, *bottom left:* spin-down particle, and *bottom right:* spin-down hole component.

6.4 Exploration of the Abelian Region

From the table of topological regions, Table 3.1, we see that the Abelian phase is given by

$$\mu^2 + \Delta_0^2 < h^2 < (4t - |\mu|)^2 + \Delta_0^2, \qquad |\mu| \leq 2t, \tag{6.1}$$

the region in which the TKNN invariant is -2. We explore this region further in this section.

Shown in Fig. 6.13 is the minimum quasiparticle excitation energy in the vortex lattice as a function of positive Zeeman field, for $\mu = 0$, with bulk Delta $\Delta_0 = 0.34t$ and system size 61×61. In Fig. 6.14 these minimum energies are examined more closely. Although these energies decrease for some systems from system size 41×41 to 61×61, this decrease is relatively small in general. The system $\mu = 0$, $\alpha = 2t$, $h = 0.5t$ shows a significantly small minimum energy for 61×61, of $E_1 \simeq 2.0 \times 10^{-5}t$ ($E_2 \simeq 2.1 \times 10^{-3}t$). The wave functions

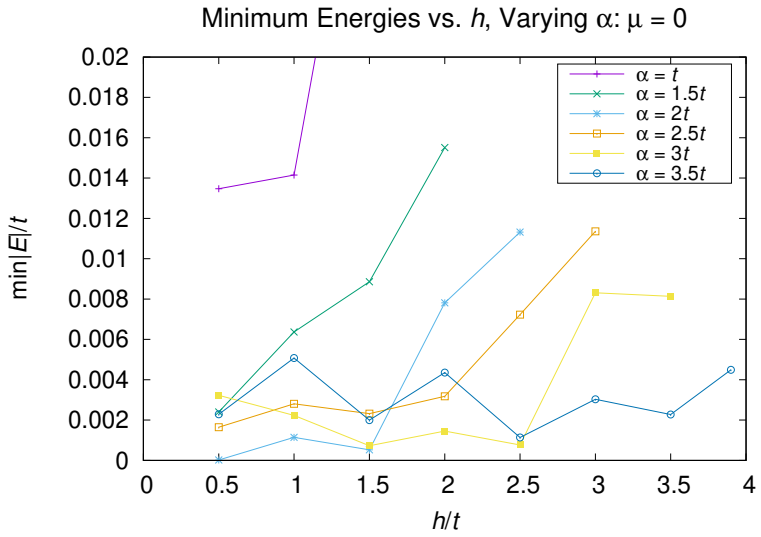

Figure 6.13: Minimum eigenvalues versus Zeeman splitting, h, for varying spin-orbit coupling, α, for the vortex lattice within the Abelian region. Parameters are $\mu = 0$ and $\Delta_0 = 0.34t$, and all system sizes are 61×61. Maximum energy (for $\alpha = t$) is cut off for clarity.

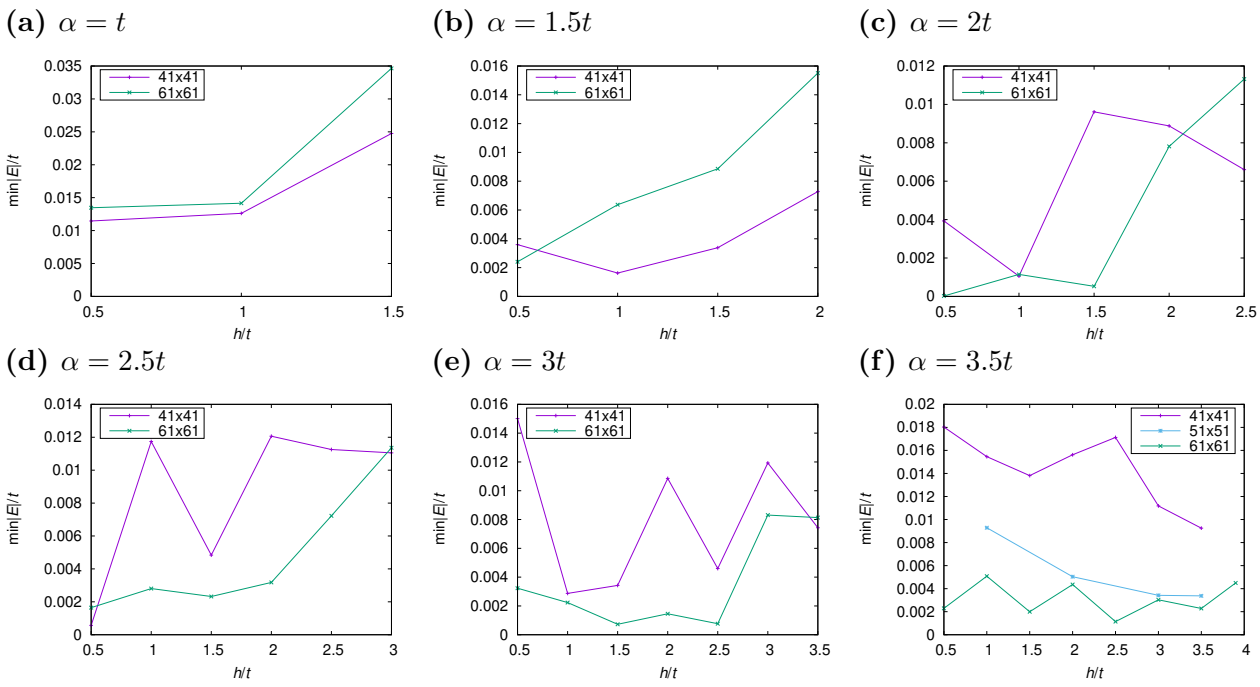

Figure 6.14: Minimum eigenvalues as a function of h for varying α, for the vortex lattice within the Abelian region. Parameters are $\mu = 0$ and $\Delta_0 = 0.34t$.

of this lowest-energy state are shown in Fig. 6.15 – we find that PHS is not present, and therefore this excitation is not a Majorana fermion.

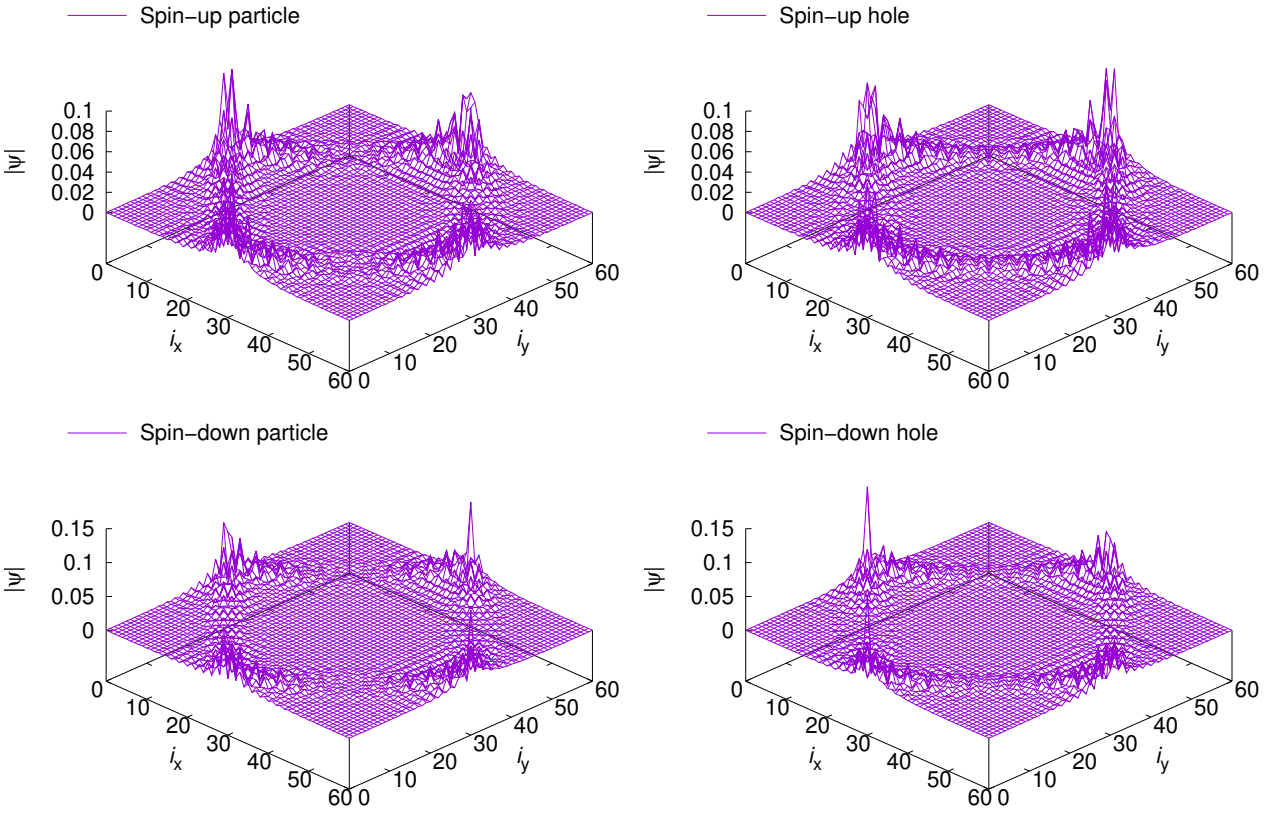

Figure 6.15: Wave function components of the lowest-energy excitation for the Abelian-phase system $\mu = 0$, $\alpha = 2t$, and $h = 0.5t$ ($\Delta_0 = 0.34t$), for size 61×61. PHS is broken. *Top left:* spin-up particle, *top right:* spin-up hole, *bottom left:* spin-down particle, and *bottom right:* spin-down hole component.

The order parameter and the LDOS at a site at the center of one of the sides closest to a vortex center are shown, respectively, in Figs. 6.16 and 6.17, for the same system ($\mu = 0$, $\alpha = 2t$, $h = 0.5t$). The lowest-energy (quasiparticle) states are localized at the vortex center, as reflected in the LDOS.

Looking at the eigenvalue spectrum for this system in Fig. 6.18, we notice something interesting. The smallest two (positive) excitation energies come grouped closely together. We compare non-Abelian and Abelian phase energy spectra in Fig. 6.19. In the non-Abelian phase, a single smallest energy is separated slightly from higher energies, and tends toward zero as the system size increases. Although we do not find energies approaching zero with increasing system size in the vortex lattice in the Abelian phase, the close grouping of the

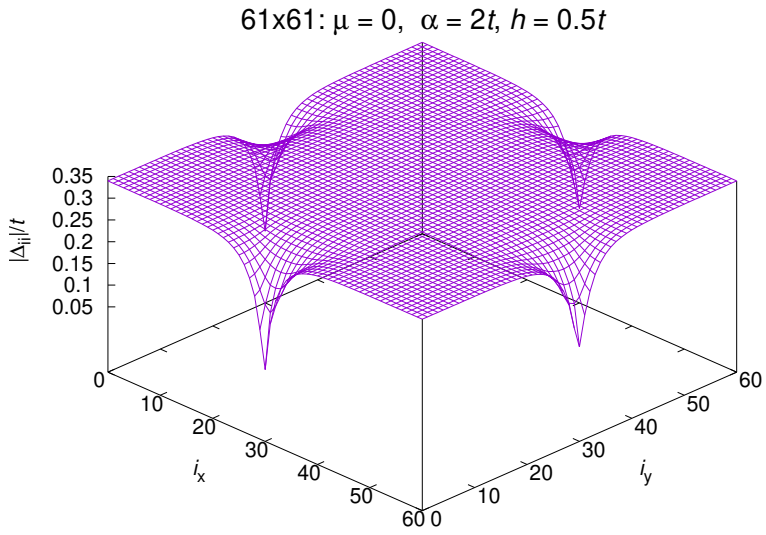

Figure 6.16: Vortex lattice order parameter, for $\mu = 0$, $\alpha = 2t$, $h = 0.5t$ ($\Delta_0 = 0.34t$), for size 61×61.

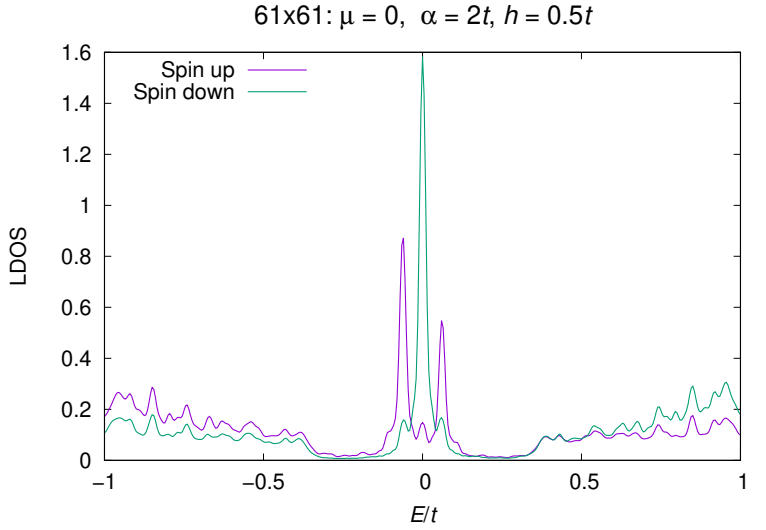

Figure 6.17: LDOS at the center site on one of the sides, closest to one of the vortex centers, for $\mu = 0$, $\alpha = 2t$, $h = 0.5t$ ($\Delta_0 = 0.34t$), size 61×61. The lowest-energy states are localized at the vortex center. For this system, the lowest-energy state is spin-down dominated.

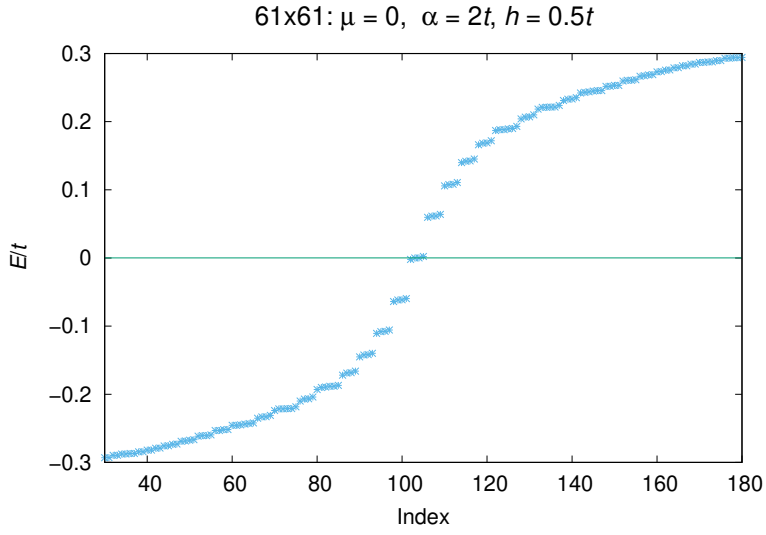

Figure 6.18: Excitation spectrum in the vortex lattice for $\mu = 0$, $\alpha = 2t$, $h = 0.5t$ ($\Delta_0 = 0.34t$), size 61×61.

two smallest energies is reminiscent of what would be found for two Majorana modes (per vortex), should they be able to coexist.

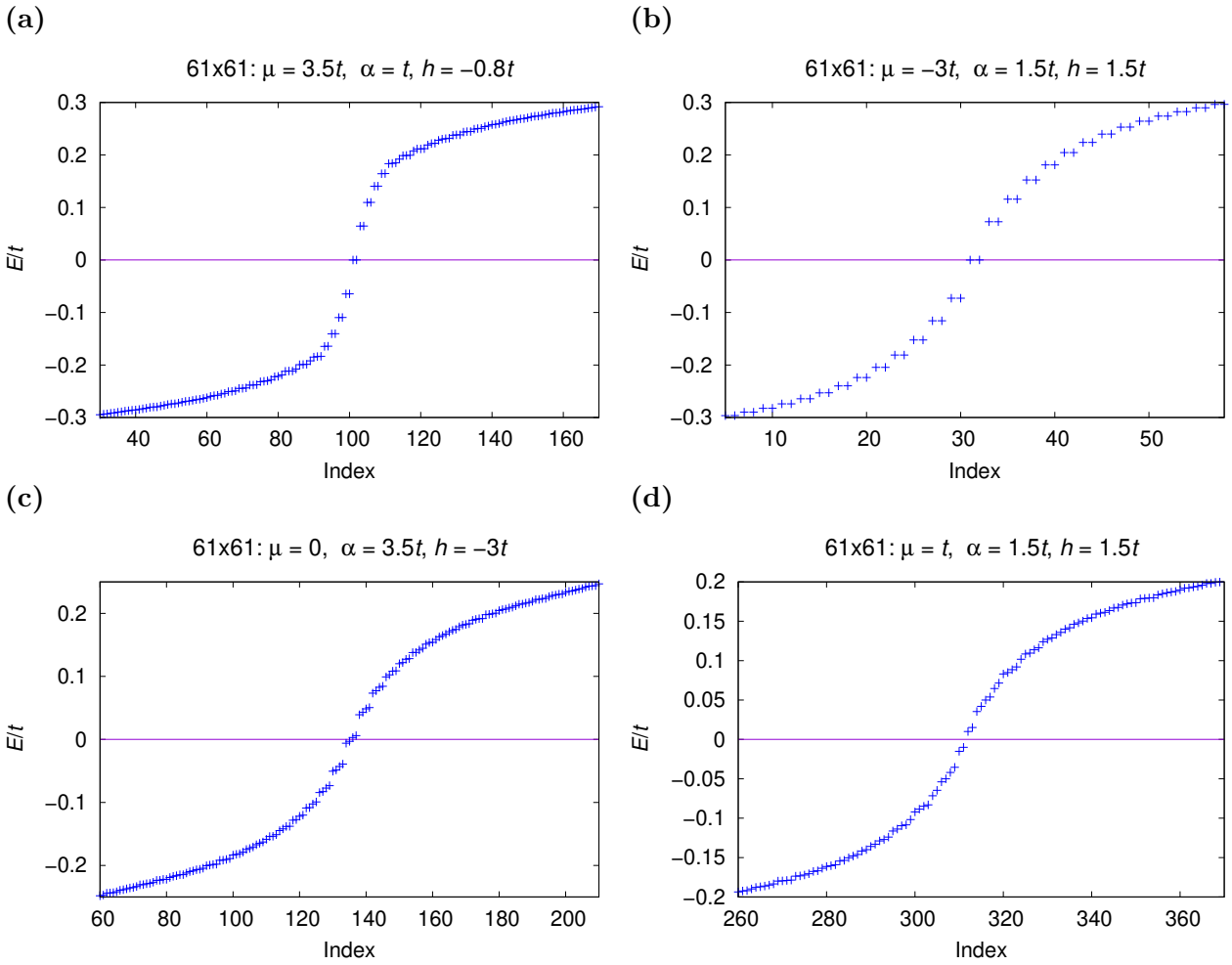

Figure 6.19: Non-Abelian- and Abelian-phase excitation spectra in the vortex lattice. Non-Abelian-phase spectra are for (a) $\mu = 3.5t$, $\alpha = t$, $h = -0.8t$ ($U = -4.855t$) and (b) $\mu = -3t$, $\alpha = 1.5t$, $h = 1.5t$ ($U = -5.5t$). Abelian-phase spectra are for (c) $\mu = 0$, $\alpha = 3.5t$, $h = -3t$ ($U = -10.632t$) and (d) $\mu = t$, $\alpha = 1.5t$, $h = 1.5t$ ($U = -4.498t$). All system sizes are 61×61.

6.4.1 Impurities

We look briefly at the effects of a single, non-magnetic impurity in the vortex center. In Fig. 6.20 the minimum energy eigenvalue is plotted as a function of inverse of the impurity potential, V_{imp}. For the vortex lattice, the order parameter does not converge for large impurity potentials. We find the presence of localized dips in the minimum excitation energy with varying impurity potential, in contrast to the homogeneous phase where minimum

energies tend to vary smoothly with impurity potential [29].

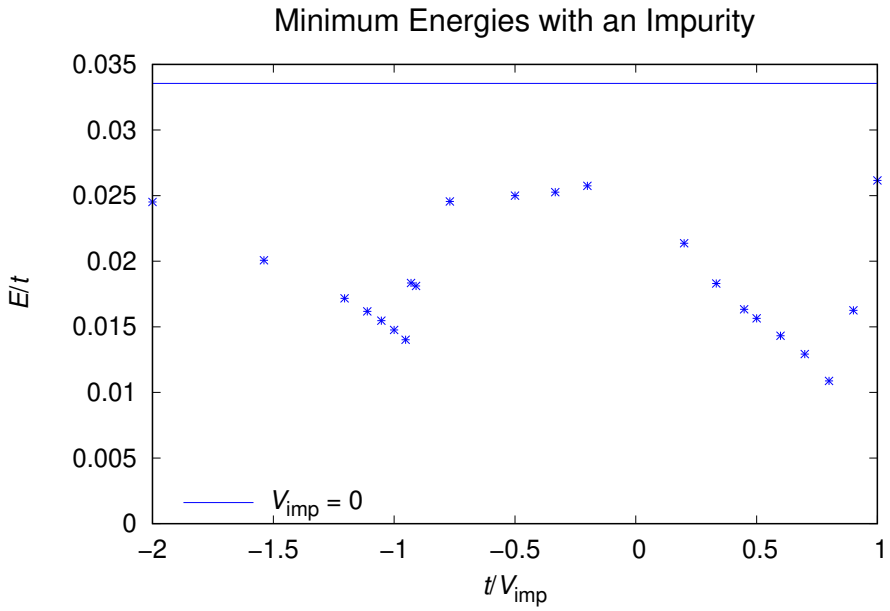

Figure 6.20: Minimum excitation energy with a single, non-magnetic impurity placed at the vortex center, for system parameters $\mu = 0.5t$, $\Delta_0 = 0.34t$, $\alpha = t$, and $h = 1.5t$. The order parameter does not converge for large V_{imp}, or $1/V_{\text{imp}} \approx 0$.

7 Conclusion

In our work, we have focused on the Abelian phase of the model of two-dimensional (2D) topological superconductivity (TSC) that we have studied [16], first described by Sato *et al.* in the context of ultracold fermionic atoms in an optical lattice [17]. Our emphasis was on the vortex lattice, assuming type-II superconductivity. Examining the vortex lattice in the Abelian phase both numerically and analytically, we discerned the properties of this phase, in particular the number of Majorana zero modes localized in a vortex core in this phase. *Bulk-edge correspondence* would predict two Majorana modes per boundary or topological defect for the Abelian phase, due to a Chern (or TKNN) number of -2 in this phase, and the inherent particle-hole symmetry (PHS) of superconductivity. However, bulk-edge correspondence is less-well understood for topological defects such as vortices. Additionally, this correspondence cannot predict the relationship between any Majorana modes and therefore how they present in real systems.

In chapter 5, we adapted an index theorem for the existence of Majorana mode(s) in a vortex core [30] to the Abelian phase of our tight-binding model. While in the non-Abelian phase there is a single Majorana fermion per vortex, we found, in accordance with bulk-edge correspondence, that in the Abelian phase a vortex hosts two Majorana zero modes, one with momentum near the Γ point and the other with momentum near the M point in the Brillouin zone (BZ). In the non-Abelian phase, the energy bands of the normal state have only one Fermi surface, whereas in the Abelian phase there are two Fermi surfaces, one around the Γ point ($k \sim 0$) and one around the M point ($\boldsymbol{k} \sim \pm(\pi, \pi)$) in the BZ. When the Fermi surface(s) are 'gapped out' by the emergence of the superconducting gap, a topological state emerges with one and two Majorana modes for the non-Abelian and Abelian phases, respectively, per surface or topological defect.

To show our index theorem for the tight-binding model (with nearest-neighbour hopping

only), we first approximated the energy bands near the Γ and M points in momentum space to second order, so that the band energies are similar to those in the continuum model. For the M point, this involves an effective mass approximation, equivalent to neglecting the quickly-oscillating factor of $e^{\pm i(\pi,\pi)\cdot \boldsymbol{r}}$ in the electronic wave functions. Neither of these approximations should pose a real problem, as Majorana fermions are zero-energy modes with energies approaching the Fermi energy, and the quickly-oscillating factor above simply causes a sign change in the wave function for every other site on a lattice. However, Sato *et al.* [16] have shown that while Majorana modes in the non-Abelian phase of this model can be composed of quasiparticles with $k \sim 0$ (or $k \sim (\pi, \pi)$) in the long-distance regime far from the vortex, near the vortex core they are likely composed of quasiparticles with a large momentum $k \neq 0, (\pi, \pi)$, as momentum is not a good quantum number in a vortex core. (This large momentum is associated with either the Fermi surface or with the contour in the BZ which, in transitioning from the non-Abelian phase to the Abelian or trivial phase, would become the second Fermi surface.) Therefore our method of treating the modes as either purely near the Γ point or the M point is a simplification, though possibly a good one for the case of both Fermi surfaces in Abelian phase being small, as occurs near half filling.

As in the continuum model index theorem [30], the Hamiltonian is then transformed to total-angular-momentum space, where the total angular momentum channels decouple and one can choose the $m_J = 1/2$ channel. Diagonalization of the Hamiltonian and linearization of the bands about the Fermi momentum or band extremum, followed by Fourier transform to real space, allows one to put the Hamiltonian for channel $m_J = 1/2$ into the Dirac form for a zero-energy mode. Performing this procedure for each of the Γ and M points separately, one finds a unique Majorana solution in each case. Although the solution for the Γ point appears non-normalizable, as in the case of the continuum model (in which the non-Abelian region is the only non-trivial region), this solution is an approximation to the true solution and is therefore still worth considering. This non-normalizability may be an artifact of approximating the Majorana mode as being purely composed of quasiparticles near the Γ point ($k \sim 0$).

An important question we sought to answer was whether these two Majorana modes are similar or orthogonal to each other. Majorana modes which are not spatially confined will

not generally annihilate each other, as can be seen in our numerical results for homogeneous systems with two boundaries. For these systems, each of the two boundaries hosts a single Majorana mode in the non-Abelian phase or two Majorana modes in the Abelian phase, as confirmed numerically. However, in the vortex core where excitations are spatially confined, Majorana modes which are not orthogonal to each other will annihilate. Trying to answer the question of whether these modes are similar or orthogonal analytically is tricky, and not necessarily possible using the results of our index theorem which involves approximations. Analytically, in the limit of decoupled bands our calculations appear to yield orthogonal Majorana modes. However, our numerical results did not show any Majorana modes for the vortex core in the Abelian phase, an indication that these modes are likely not exactly orthogonal to each other.

Numerical calculations involved self-consistently solving the Bogoliubov-de Gennes (BdG) equations for the superconducting order parameter, using efficient numerical algorithms designed for parallel computation including the Chebyshev polynomial expansion and the Sakurai-Suriura (SS) method. The Chebyshev polynomial method to find the mean fields – the order parameter and the Hartree potential(s) – avoids diagonalization of the BdG matrix which is computationally costly for realistic system sizes and hard to parallelize. As the Chebyshev method does not compute the eigenpairs directly, the SS method is useful alongside it to find the energy eigenvalues and corresponding quasiparticle eigenstates within an energy window of one's choice, after convergence of the order parameter.

To compare minimum energies between systems most meaningfully, we chose a bulk order parameter for most systems of $\Delta_0 \approx 0.34t$, by adjusting the coupling constant U for a given set of μ, α and h (chemical potential, spin-orbit coupling and Zeeman splitting), and first checking that the homogeneous phase converged. As properties such as eigenvalues scale linearly with Δ_0 (including for vortex systems) as long as one remains within the same topological phase, this should not affect the usefulness of our results much. Our results showed the presence of the Pauli depairing effect, in which the Zeeman magnetic field (or Zeeman splitting, h) tends to align electronic spins in the field direction, thereby breaking up spin-singlet Cooper pairs and eventually destroying superconductivity for a large enough field. This effect is mitigated by the spin-orbit coupling, with coupling constant α, as was

also apparent in our results. In practice one wants to have a large Zeeman field in order to open a wide-enough gap between the spin-polarized energy bands within which to place the chemical potential, to obtain the topological order. Our results have shown that convergence of the order parameter requires $\alpha \gtrsim h$. For larger h, oscillations tend to appear in the order parameter for the vortex lattice, increasing in amplitude with increasing h; for smaller vortex lattice systems, superconductivity can be destroyed for large enough h.

In calculating energies of the BdG system numerically, one must be careful to allow for the presence of an *even* number of zero-energy modes, as the BdG equations are particle-hole symmetric. This allows there to be an equal-magnitude (small) negative energy for each (small) positive energy – with restricted system size, numerical eigenvalues will never be exactly zero. Each of these energies corresponds to a superposition of the zero-energy modes. Therefore in our calculations we modelled systems with two vortices, with PBC for studying the vortex lattice.

Numerically, we found no Majorana modes in a vortex core for the Abelian phase of this two-dimensional (2D) system. We contrasted this with the non-Abelian phase, where we found one Majorana mode per vortex core, as well as with the homogeneous phase with two boundaries, where we found one or two Majorana modes per boundary in the non-Abelian or Abelian phases, respectively. We observed the Majorana condition by checking both that the minimum energy approached zero with increasing system size, and that the corresponding quasiparticle state exhibited PHS. With increasing system size, the inter-vortex distance increases, weakening inter-vortex tunneling effects which perturb the energies. Our Abelian phase results did not show minimum energies approaching zero with increasing system size; instead energies stayed relatively constant with increasing size. Furthermore, in a vortex system in the Abelian phase, although we did not find Majorana modes, we did observe the close grouping of the *two* smallest (positive) energies for most systems, reminiscent of what would be found for two Majorana modes should they be able to coexist. This is another indication that there are two *similar* Majorana modes per vortex core in the Abelian phase, which annihilate each other.

In the future, further studies could be done to show analytically whether the Majorana modes in the Abelian phase are similar to each other. In our index theorem as well as the

continuum model (non-Abelian) index theorem, an approximation of the interband coupling as a constant leads to this coupling necessarily being zero, by taking the limit of the coupling between the bands at the Fermi momentum and band extremum, respectively (for $\boldsymbol{k} \sim 0$, the Fermi momentum is in the upper band, while for $\boldsymbol{k} \sim \pm(\pi, \pi)$ it is in the lower band). As this approximation appears to give orthogonal Majorana modes in our calculations, this approximation may not properly reflect the real relationship between these modes. One might try using an arbitrary, small interband coupling constant instead. Additionally, one might try to properly account for the fact that a Majorana mode is likely not purely composed of quasiparticles with momentum near the Γ (or M) point, especially close to the vortex core where momentum is not a good quantum number.

References

[1] L. Fu, C. L. Kane, and E. J. Mele. Topological insulators in three dimensions. *Phys. Rev. Lett.*, 98(10):106803, 2007.

[2] D. Hsieh, D. Qian, L. Wray, Y. Xia, Y. S. Hor, R. J. Cava, and M. Z. Hasan. A topological dirac insulator in a quantum spin hall phase. *Nature*, 452(7190):970, 2008.

[3] Y. Xia, D. Qian, D. Hsieh, L. Wray, A. Pal, H. Lin, A. Bansil, D. Grauer, Y.S. Hor, R.J. Cava, and M.Z. Hasan. Observation of a large-gap topological-insulator class with a single dirac cone on the surface. *Nat. Phys.*, 5(6):398–402, 2009.

[4] M. Z. Hasan and C. L. Kane. Colloquium: Topological insulators. *Rev. Mod. Phys.*, 82(4):3045–3067, 2010.

[5] X.-L. Qi and S.-C. Zhang. Topological insulators and superconductors. *Rev. Mod. Phys.*, 83(4):1057–1110, 2011.

[6] Y. Ando. Topological Insulator Materials. *J. Phys. Soc. Japan*, 82:102001, 2013.

[7] Y. Ando and L. Fu. Topological Crystalline Insulators and Topological Superconductors: From Concepts to Materials. *Annu. Rev. Condens. Matter Phys.*, 6:361, 2015.

[8] J. Alicea. New directions in the pursuit of Majorana fermions in solid state systems. *Rep. Prog. Phys.*, 75:076501, 2012.

[9] M. Sato and Y. Ando. Topological superconductors: a review. *Rep. Prog. Phys.*, 80:076501, 2017.

[10] V. Mourik, K. Zuo, S. M. Frolov, S. R. Plissard, E. P. A. M. Bakkers, and L. P. Kouwenhoven. Signatures of Majorana fermions in hybrid superconductor-semiconductor nanowire devices. *Science*, 336(6084):1003–7, 2012.

[11] S. Nadj-Perge, I. Drozdov, J. Li, H. Chen, S. Jeon, J. Seo, A. Macdonald, B. Bernevig, and A. Yazdani. Observation of Majorana fermions in ferromagnetic atomic chains on a superconductor. *Science*, 346(6209):602–607, 2014.

[12] A. Y. Kitaev. Unpaired Majorana fermions in quantum wires. *Physics-Uspekhi*, 44(10S):131–136, 2001.

[13] S. Sasaki, M. Kriener, K. Segawa, K. Yada, Y. Tanaka, M. Sato, and Y. Ando. Topological Superconductivity in Cu(x)Bi(2)Se(3). *Phys. Rev. Lett.*, 107(21):217001, 2011.

[14] H.-H. Sun, K.-W. Zhang, L.-H. Hu, C. Li, G.-Y. Wang, H.-Y. Ma, Z.-A. Xu, C.-L. Gao, D.-D. Guan, Y.-Y. Li, C. Liu, D. Qian, Y. Zhou, L. Fu, S.-C. Li, F.-C. Zhang, and J.-F. Jia. Majorana zero mode detected with spin selective Andreev reflection in the vortex of a topological superconductor. *Phys. Rev. Lett.*, 116(25):257003, 2016.

[15] G. C. Ménard, S. Guissart, C. Brun, M. Trif, F. Debontridder, R. Leriche, D. Demaille, D. Roditchev, P. Simon, and T. Cren. Two-dimensional topological superconductivity in Pb/Co/Si(111). *Nat. Commun.*, 8(1):2040, 2017.

[16] M. Sato, Y. Takahashi, and S. Fujimoto. Non-Abelian topological orders and Majorana fermions in spin-singlet superconductors. *Phys. Rev. B*, 82(13):134521, 2010.

[17] M. Sato, Y. Takahashi, and S. Fujimoto. Non-abelian topological order in s-wave superfluids of ultracold fermionic atoms. *Phys. Rev. Lett.*, 103(2):020401, 2009.

[18] D. Thouless, M. Kohomoto, M. Nightingale, and M. den Nijs. Quantized Hall conductance in a two-dimensional periodic potential. *Phys. Rev. Lett.*, 49:405–408, 1982.

[19] X.-G. Wen. Topological orders and edge excitations in fractional quantum Hall states. *Adv. Phys.*, 44(5):405–473, 1995.

[20] J. Moore. The birth of topological insulators. *Nature*, 464(7286):194–8, 2010.

[21] A. P. Schnyder, S. Ryu, A. Furusaki, and A. W. W. Ludwig. Classification of topological insulators and superconductors in three dimensions. *Phys. Rev. B*, 78:195125, 2008.

[22] Giuseppe Grosso and Giuseppe Pastori Parravicini. *Solid State Physics*. Elsevier Ltd, 2014.

[23] F. Wilczek. Majorana returns. *Nat. Phys.*, 5(9):614–618, 2009.

[24] G. Collins. Computing with quantum knots. *Sci. Am.*, 294(4):56–63, 2006.

[25] S. Das Sarma, M. Freedman, and C. Nayak. Topological quantum computation. *Phys. Today*, 59(7):32–38, 2006.

[26] C. Nayak, S. Simon, A. Stern, M. Freedman, and S. Das Sarma. Non-Abelian anyons and topological quantum computation. *Rev. Mod. Phys.*, 80(3):1083–1159, 2008.

[27] A. Stern. Non-Abelian states of matter. *Nature*, 464(7286):187–93, 2010.

[28] S. L. Goertzen. Self-consistent study of Abelian and non-Abelian order in a two-dimensional topological superconductor. Master's thesis, University of Saskatchewan, 2015.

[29] S. L. Goertzen, K. Tanaka, and Y. Nagai. Self-consistent study of Abelian and non-Abelian order in a two-dimensional topological superconductor. *Phys. Rev. B*, 95(6):064509, 2017.

[30] S. Tewari, J. Sau, and S. Das Sarma. A theorem for the existence of Majorana fermion modes in spin-orbit-coupled semiconductors. *Ann. Phys.*, 325:219–231, 2010.

[31] Emil Prodan and Hermann Schulz-Baldes. *Bulk and Boundary Invariants for Complex Topological Insulators: From K-Theory to Physics*. 2015.

[32] J. R. Schrieffer. *Theory of Superconductivity*. Westview Press, 1999.

[33] P. G. de Gennes. *Superconductivity of Metals and Alloys*. Westview Press, 1999.

[34] Eduardo Fradkin. *Field Theories of Condensed Matter Physics*. Cambridge University Press, second edition, 2013.

[35] R. G. Sharma. *Superconductivity*. Springer, first edition, 2015.

[36] C. Caroli, P. G. De Gennes, and J. Matricon. Bound Fermion states on a vortex line in a type II superconductor. *Phys. Lett.*, 9(4):307–309, 1964.

[37] Y. Nagai, Y. Ota, and M. Machida. Efficient Numerical Self-Consistent Mean-Field Approach for Fermionic Many-Body Systems by Polynomial Expansion on Spectral Density. *J. Phys. Soc. Jpn.*, 81:024710, 2012.

[38] L. Covaci, F. M. Peeters, and M. Berciu. Efficient Numerical Approach to Inhomogeneous Superconductivity: The Chebyshev-Bogoliubov-de Gennes Method. *Phys. Rev. Lett.*, 105:167006, 2010.

[39] Y. Nagai, Y. Shinohara, Y. Futamura, Y. Ota, and T. Sakurai. Numerical Construction of a Low-Energy Effective Hamiltonian in a Self-Consistent Bogoliubov-de Gennes Approach of Superconductivity. *J. Phys. Soc. Jpn.*, 82:094701, 2013.

[40] S. Tewari, S. Das Sarma, and D.-H. Lee. Index Theorem for the Zero Modes of Majorana Fermion Vortices in Chiral p-Wave Superconductors. *Phys. Rev. Lett.*, 99:037001, 2007.

[41] A. P. Schnyder, S. Ryu, A. Furusaki, and A. W. W. Ludwig. Classification of Topological Insulators and Superconductors. *AIP Conf. Proc.*, 1134(1):10–21, 2009.

Appendix A

Chern (TKNN) Number and the Quantum Hall Effect

When the Hamiltonian depends on a parameter, so do its eigenstates. In certain cases, these eigenstates can have a 'twist' in parameter space. (Eigenstates are studied adiabatically, where the parameter is changed slowly enough that at all times the system is approximately in equilibrium.) When a system has translational invariance, for example, it has eigenstates in momentum space [9]:

$$H(\boldsymbol{k})\,|u_n(\boldsymbol{k})\rangle = E_n(\boldsymbol{k})\,|u_n(\boldsymbol{k})\rangle\,, \tag{A.1}$$

where $u_n(\boldsymbol{k})$ is the periodic Bloch function, $H(\boldsymbol{k})$ the corresponding Hamiltonian, and n the band index. One can define a quantity called the Berry connection,

$$A^{(n)}(\boldsymbol{k}) = i\,\langle u_n(\boldsymbol{k})|\partial_{\boldsymbol{k}} u_n(\boldsymbol{k})\rangle\,, \tag{A.2}$$

which measures the rate of change of the wave function in momentum space. As u is undefined up to a phase factor, one can apply a gauge transformation,

$$|u_n(\boldsymbol{k})\rangle \to e^{i\phi_n(\boldsymbol{k})}\,|u_n(\boldsymbol{k})\rangle\,, \qquad A^{(n)}(\boldsymbol{k}) \to A^{(n)}(\boldsymbol{k}) - \partial_{\boldsymbol{k}}\phi_n(\boldsymbol{k}). \tag{A.3}$$

However, the wave function must be single-valued. Integrating A around a closed loop in momentum space can therefore only differ by an integer multiple of 2π, depending on the gauge.

This leads to the definition of the *first Chern number*. The 'field strength' of the Berry connection is its curl in momentum space, which in two dimensions (2D) is given by

$$\mathcal{F}^{(n)}_{ij}(\boldsymbol{k}) = \partial_{k_i} A^{(n)}_{k_j}(\boldsymbol{k}) - \partial_{k_j} A^{(n)}_{k_i}(\boldsymbol{k}). \tag{A.4}$$

The Chern number of the nth band is then defined by

$$Ch^{(n)} = \frac{1}{2\pi}\int_{BZ} dk_x\, dk_y \mathcal{F}^{(n)}_{xy}(\boldsymbol{k}), \tag{A.5}$$

where the total Chern number is given by the sum of Chern numbers over all occupied bands. The Chern number is also known as the TKNN number, named after Thouless, Kohmoto, Nightingale and den Nijs, who first introduced it to classify quantum Hall states [18]. Using Stokes' theorem, and Brillouin zone periodicity (the Brillouin zone for the square lattice is a torus, T^2), this integral vanishes if A is non-singular.

However, if the eigenstates have a 'twist,' giving a singular A, then one can perform a gauge transformation to 'remove' the singularity as in Eq. (A.3). Then the nth Chern number is given by

$$Ch^{(n)} = \frac{1}{2\pi}\oint_{\partial R} d\boldsymbol{k}\cdot\partial_{\boldsymbol{k}}\phi_n(\boldsymbol{k}), \tag{A.6}$$

where the region R encloses the singularity [9]. This boundary integral must give an integer, due to ϕ_n only differing by an integer multiple of 2π after traversing around a closed loop.

In 2D, for a band insulator with no other symmetries of the Hamiltonian, the Chern number will only be non-zero in a system with broken time-reversal symmetry. To see this, one uses the fact that under a transformation $\boldsymbol{k} \to -\boldsymbol{k}$ one has [9]

$$\sum_{E_n<E_F} A^{(n)}(\boldsymbol{k}) \to \sum_{E_n<E_F} A^{(n)}(-\boldsymbol{k}), \qquad \sum_{E_n<E_F} \mathcal{F}_{ij}^{(n)}(\boldsymbol{k}) \to -\sum_{E_n<E_F} \mathcal{F}_{ij}^{(n)}(-\boldsymbol{k}), \tag{A.7}$$

which in 2D gives

$$Ch \to -\frac{1}{2\pi}\int_{BZ} dk_x\, dk_y \sum_{E_n<E_F} \mathcal{F}_{xy}^{(n)}(-\boldsymbol{k}) = -Ch. \tag{A.8}$$

Therefore, if the system has time-reversal symmetry (TRS) its Chern number will be zero.

The state given by broken TRS in this case is the *integer quantum Hall state*, where TRS is broken by the magnetic field. The Chern number is the same as the filling factor ν, the number of filled Landau levels. This also corresponds to the number of gapless, chiral edge states, which propagate around the edge of the material in a single direction determined by the magnetic field. The transverse (Hall) conductivity $\sigma_{xy} = \nu e^2/h$ is quantized, the discovery of which led to the realization that the quantum Hall system was a topological insulator. (The high precision of the quantization, to about 1 part per billion, is used to define standard units of resistance h/e^2 [22, Sec.15.6.1].)

Introducing TRS, although it gives a zero Chern number in this case, can also lead to a non-trivial topological state: the *quantum spin Hall state*. Kramer's theorem shows that a time-reversed, half-integer spin state is orthogonal to the original state, as it has opposite spin. In a system with spin defined on a particular axis, for example the z-axis, the Hamiltonian can be block diagonalized as

$$H(\boldsymbol{k}) = \begin{pmatrix} H_\uparrow(\boldsymbol{k}) & 0 \\ 0 & H_\downarrow(\boldsymbol{k}) \end{pmatrix}. \tag{A.9}$$

Each piece of the Hamiltonian, $H_\uparrow$ and $H_\downarrow$, can have a nonzero 'spin Chern number,' even though the total Chern number vanishes: $Ch_\uparrow + Ch_\downarrow = 0$. In real systems, spin-orbit coupling generally breaks spin conservation; however, one can still define eigensectors by *Kramer's pairs* of time-reversed states rather than spin. Again there are two Chern numbers which sum to zero, say $Ch^I + Ch^{II} = 0$. The classifications I and II are arbitrary however, with no real physical meaning, and members of Kramer's pairs can be exchanged between sectors. The value which does have a real meaning is the *parity* of the Chern numbers:

$$(-1)^{Ch^I} = (-1)^{Ch^{II}}. \tag{A.10}$$

This gives a $\mathbb{Z}_2$ index as the invariant, where -1 is non-trivial [9], that is, the existence of an *odd* number of Kramer's pairs. The protected edge states in the quantum spin Hall state consist of a single Kramers doublet, that is a single pair of modes carrying opposite spin and propagating in opposite directions, which cannot be mixed by any TRS-preserving perturbation [41]. When a $U(1)$ part of the spin is conserved (the spin axis is chosen), these

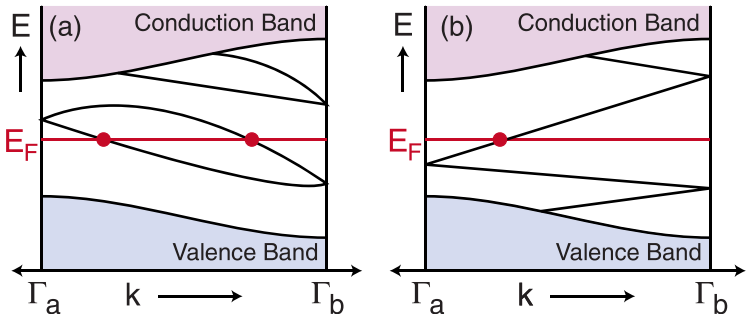

Figure A.1: (a) Trivial TRS system: the two states at $k = 0$ (Γ_a) are connected to the same Kramers doublet at $k = \pi$ (Γ_b), giving an even number of occupied Kramers pairs. (b) Non-trivial TRS system: the two states at $k = 0$ are connected to two different Kramers doublets at $k = \pi$, giving an odd number of Kramers pairs. [4] Copyright (2010) by the American Physical Society. http://dx.doi.org/10.1103/RevModPhys.82.3045

modes correspond to spin-up electrons propagating one way and spin-down electrons the other way.

Quantum Hall states, and topological insulating states in general, resemble both insulators and superconductors. In the integer quantum Hall effect both longitudinal conductance and longitudinal resistance are zero. Topological insulators are insulating in the bulk but host novel metallic states at their boundaries. These edge states cannot be localized by disorder (as in Anderson localization due to impurities) because elastic back-scattering is not allowed.

Another way to view the Chern number is in terms of homotopy [9, 41]. If there are m empty states above the Fermi energy and $(n-m)$ filled states below, one can diagonalize the Hamiltonian using a unitary operation:

$$U^\dagger(\boldsymbol{k})H(\boldsymbol{k})U(\boldsymbol{k}) = \begin{pmatrix} E_1(\boldsymbol{k}) & & \\ & \ddots & \\ & & E_n(\boldsymbol{k}) \end{pmatrix}. \tag{A.11}$$

For a band insulator with no other symmetry, a deformation which preserves the topology (the band gap) is given by

$$U^\dagger(\boldsymbol{k})H(\boldsymbol{k})U(\boldsymbol{k}) = \begin{pmatrix} \mathbf{1}_{m\times m} & \\ & -\mathbf{1}_{(n-m)\times(n-m)} \end{pmatrix}, \tag{A.12}$$

where $\mathbf{1}$ is the identity matrix. This deformed Hamiltonian is often referred to as the projector, as it is similar to the projection operator,

$$P(\boldsymbol{k}) = \sum_{E_n<E_F} |u_n(\boldsymbol{k})\rangle \langle u_n(\boldsymbol{k})|, \tag{A.13}$$

which gives the projection onto filled states. Specifically, one takes the operator

$$Q(\boldsymbol{k}) = \mathbf{1} - 2P(\boldsymbol{k}). \tag{A.14}$$

This 'projector' $Q(\boldsymbol{k})$ gives the deformed Hamiltonian above.

Using this deformation, H is invariant under

$$U(\boldsymbol{k}) \to U(\boldsymbol{k}) \begin{pmatrix} U_{m\times m}(\boldsymbol{k}) & \\ & U_{(n-m)\times(n-m)}(\boldsymbol{k}) \end{pmatrix}, \tag{A.15}$$

where $U_{m\times m}$ and $U_{(n-m)\times(n-m)}$ are arbitrary unitary matrices. The invariance under this transformation holds because the block diagonal unitary and identity matrices commute: the (deformed) Hamiltonian has gauge symmetries of arbitrarily rearranging or taking linear combinations of the m empty states and similarly of the $n-m$ filled states. This transformation of U defines a map from the Brillouin zone to the 'coset space' of $U(n)$,

$$\mathcal{M} = \frac{U(n)}{U(m)\times U(n-m)}. \tag{A.16}$$

In this case, this map has dth homotopy group given by [9]

$$\pi_d(\mathcal{M}) = \begin{cases} 0 & d = 1, 3, \\ \mathbb{Z} & d = 2. \end{cases} \tag{A.17}$$

Homotopy groups define topological properties of a space. The first homotopy group or 'fundamental group' is given by the distinct ways in which to map a cirle with a base point to the space in question. For example, π_1 of the torus is $\mathbb{Z}^2$, as there are two distinct ways to loop around a torus, each of which could be looped around any integer number of times. These distinct ways of looping, that is, of mapping a circle to the torus, cannot be deformed into each other. The second homotopy group is given by distinct ways to map a sphere with base point to the target space, the third homotopy group by distinct ways to map a 3-sphere to the target space, and so on. The space produced in $\mathcal{M}$ by the map from the Brillouin zone can be thought of as the space in which the 'twist' in eigenstates lives.

Appendix B

The Continuum Model Index Theorem for a Majorana Mode in a Vortex Core

This appendix follows the index theorem of Tewari, Sau, and Das Sarma [30] which shows the existence of a single Majorana mode in a vortex core in the non-Abelian phase of a two dimensional (2D) topological superconductor, using the continuum model of momentum space. The model of 2D TSC used here, when extended to a tight-binding model of momentum space, is equivalent to that of Sato *et al.* [16, 17]. We derive equations in more detail.

B.1 Hamiltonian

The problem studied is for the 2D heterostructure combining the ingredients for spin-orbit coupling, Zeeman splitting, and s-wave superconductivity. For example, one can layer a semiconductor next to a ferromagnetic insulator and a superconductor, where the semiconductor provides Rashba spin-orbit coupling, and the ferromagnetic insulator and superconductor induce Zeeman splitting and superconductivity by proximity, respectively. One can also use a superconductor such as lead with intrinsic spin-orbit coupling, layered next to a ferromagnetic insulator [15], or various other set-ups.

The 2D Hamiltonian includes the single-electron part and the SC pairing for a vortex, $H_{Tot} = H_0 + H_V$. The single-electron part is given by $H_0 = H_K + H_{SO} + H_Z$, where (corresponding to Eq. (1) of Ref. [30])

$$\begin{aligned} H_K &= \sum_{\boldsymbol{k},\beta} \left(\frac{k^2}{2m^*} - \mu \right) c^\dagger_{\boldsymbol{k},\beta} c_{\boldsymbol{k},\beta}, \\ H_{SO} &= \alpha \sum_{\boldsymbol{k}} \left[(k_y + ik_x)\, c^\dagger_{\boldsymbol{k},\uparrow} c_{\boldsymbol{k},\downarrow} + H.c. \right], \\ H_Z &= V_Z \sum_{\boldsymbol{k}} \left(c^\dagger_{\boldsymbol{k},\uparrow} c_{\boldsymbol{k},\uparrow} - c^\dagger_{\boldsymbol{k},\downarrow} c_{\boldsymbol{k},\downarrow} \right). \end{aligned} \tag{B.1}$$

Here m^* is the effective electron mass, μ is the chemical potential, α is the spin-orbit coupling constant and V_Z is the Zeeman splitting. The vortex part of the Hamiltonian is given by [30, 40]

$$H_V = -\int d^2R \int d^2r\, e^{i\theta_{\boldsymbol{R}}} h(R) g(\boldsymbol{r}) c^\dagger_{\boldsymbol{R}+\boldsymbol{r},\uparrow} c^\dagger_{\boldsymbol{R}-\boldsymbol{r},\downarrow} + H.c., \tag{B.2}$$

where $\boldsymbol{R}$ and $\boldsymbol{r}$ are the center-of-mass and the relative coordinates of a Cooper pair, respectively; $h(R) \sim (1 - e^{-R/\xi})$ describes the amplitude, and $\theta_{\boldsymbol{R}}$ the phase, of SC pairing in the vortex; and $g(\boldsymbol{r})$ is the Fourier transform of the s-wave order parameter $g(\boldsymbol{k}) \equiv \Delta_0$.

B.2 Fermion zero-mode in 1D Dirac theory

The 2D problem is mapped onto an effectively 1D problem similar to that for the Jackiw-Rebbi zero-mode at a mass domain wall [30]. In the Jackiw-Rebbi problem, which yields an ordinary fermion zero-mode, one uses the Dirac Hamiltonian (Eq. (4) [30]),

$$H_D = \int dx \left[-iv_F \psi^\dagger \sigma_z \partial_x \psi + m(x) \psi^\dagger \sigma_x \psi \right], \tag{B.3}$$

where $\psi^\dagger(x) = (f_1^\dagger(x), f_2^\dagger(x))$, with $f_{1,2}(x)$ two independent fermion fields, and v_F and $m(x)$ are the Fermi velocity and spatially-varying mass of the fermion fields. The two *independent* fermion fields yield a regular fermion zero-mode, as opposed to fields related by Hermitian conjugation and parity reversal which can yield a Majorana fermion zero-mode. In this 1D problem, it can be assumed a quasiparticle excitation has the form (Eq. (5) [30])

$$q^\dagger = \int dx \left[\phi_1(x) f_1^\dagger(x) + \phi_2(x) f_2^\dagger(x) \right]. \tag{B.4}$$

If this quasiparticle has energy ε, one has (Eq. (6) [30])

$$\left[H, q^\dagger \right] = \varepsilon q^\dagger. \tag{B.5}$$

Solving for $\left[H, q^\dagger \right]$ gives:

$$\begin{aligned}
\left[H, q^\dagger \right] &= \int dx \left[-iv_F \left(f_1^\dagger(x), f_2^\dagger(x) \right) \sigma_z \partial_x + m(x) \left(f_1^\dagger(x), f_2^\dagger(x) \right) \sigma_x \right] \begin{pmatrix} f_1(x) \\ f_2(x) \end{pmatrix} \\
&\quad \cdot \int dx' \left(\phi_1(x') f_1^\dagger(x') + \phi_2(x') f_2^\dagger(x') \right) - q^\dagger H \\
&= \int dx\, dx' \left[-iv_F \left(f_1^\dagger(x), f_2^\dagger(x) \right) \sigma_z \partial_x + m(x) \left(f_1^\dagger(x), f_2^\dagger(x) \right) \sigma_x \right] \\
&\quad \begin{pmatrix} \phi_1(x') \left(\delta(x - x') - f_1^\dagger(x') f_1(x) \right) - \phi_2(x') f_2^\dagger(x') f_1(x) \\ -\phi_1(x') f_1^\dagger(x') f_2(x) + \phi_2(x') \left(\delta(x - x') - f_2^\dagger(x') f_2(x) \right) \end{pmatrix} - q^\dagger H \\
&= \int dx\, dx' \Big\{ -iv_F \Big[f_1^\dagger(x) \partial_x \left(\phi_1(x') \left(\delta(x - x') - f_1^\dagger(x') f_1(x) \right) - \phi_2(x') f_2^\dagger(x') f_1(x) \right) \\
&\quad - f_2^\dagger(x) \partial_x \left(-\phi_1(x') f_1^\dagger(x') f_2(x) + \phi_2(x') \left(\delta(x - x') - f_2^\dagger(x') f_2(x) \right) \right) \Big] \\
&\quad + m(x) \Big[f_1^\dagger(x) \left(-\phi_1(x') f_1^\dagger(x') f_2(x) + \phi_2(x') \left(\delta(x - x') - f_2^\dagger(x') f_2(x) \right) \right) \\
&\quad + f_2^\dagger(x) \left(\phi_1(x') \left(\delta(x - x') - f_1^\dagger(x') f_1(x) \right) - \phi_2(x') f_2^\dagger(x') f_1(x) \right) \Big] \Big\} - q^\dagger H.
\end{aligned}$$

Integrating terms with delta functions and rearranging yields

$$
\begin{aligned}
\left[H, q^\dagger\right] &= \int dx \left\{-iv_F \left[f_1^\dagger(x)\partial_x\phi_1(x) - f_2^\dagger(x)\partial_x\phi_2(x)\right] + m(x)\left[f_1^\dagger(x)\phi_2(x) + f_2^\dagger(x)\phi_1(x)\right]\right\} \\
&\quad + \int dx\, dx' \left\{-iv_F \left[f_1^\dagger(x)\left(-\phi_1(x')f_1^\dagger(x')\partial_x f_1(x) - \phi_2(x')f_2^\dagger(x')\partial_x f_1(x)\right)\right.\right. \\
&\quad \left. -f_2^\dagger(x)\left(-\phi_1(x')f_1^\dagger(x')\partial_x f_2(x) - \phi_2(x')f_2^\dagger(x')\partial_x f_2(x)\right)\right] \\
&\quad + m(x)\left[f_1^\dagger(x)\left(-\phi_1(x')f_1^\dagger(x')f_2(x) - \phi_2(x')f_2^\dagger(x')f_2(x)\right)\right. \\
&\quad \left.\left. +f_2^\dagger(x)\left(-\phi_1(x')f_1^\dagger(x')f_1(x) - \phi_2(x')f_2^\dagger(x')f_1(x)\right)\right]\right\} - q^\dagger H \\
&= \int dx \left[-iv_F\left(f_1^\dagger(x), f_2^\dagger(x)\right)\sigma_z\partial_x\begin{pmatrix}\phi_1(x)\\ \phi_2(x)\end{pmatrix} + m(x)\left(f_1^\dagger(x), f_2^\dagger(x)\right)\sigma_x\begin{pmatrix}\phi_1(x)\\ \phi_2(x)\end{pmatrix}\right] \\
&\quad + \int dx\, dx' \left\{-iv_F\left[\left(\phi_1(x')f_1^\dagger(x') + \phi_2(x')f_2^\dagger(x')\right)f_1^\dagger(x)\partial_x f_1(x)\right.\right. \\
&\quad \left. - \left(\phi_1(x')f_1^\dagger(x') + \phi_2(x')f_2^\dagger(x')\right)f_2^\dagger(x)\partial_x f_2(x)\right] + m(x)\left[\left(\phi_1(x')f_1^\dagger(x')\right.\right. \\
&\quad \left.\left. +\ \phi_2(x')f_2^\dagger(x')\right)f_1^\dagger(x)f_2(x) + \left(\phi_1(x')f_1^\dagger(x') + \phi_2(x')f_2^\dagger(x')\right)f_2^\dagger(x)f_1(x)\right]\right\} - q^\dagger H \\
&= \int dx\Big[\ldots\Big] + \int dx' \left[\phi_1(x')f_1^\dagger(x') + \phi_2(x')f_2^\dagger(x')\right]\int dx\left\{-iv_F\left[f_1^\dagger(x)\partial_x f_1(x)\right.\right. \\
&\quad \left.\left. -f_2^\dagger(x)\partial_x f_2(x)\right] + m(x)\left[f_1^\dagger(x)f_2(x) + f_2^\dagger(x)f_1(x)\right]\right\} - q^\dagger H \\
&= \int dx\Big[\ldots\Big] + q^\dagger H - q^\dagger H,
\end{aligned}
$$

or

$$
\left[H, q^\dagger\right] = \int dx\Big[-iv_F\psi^\dagger(x)\sigma_z\partial_x + m(x)\psi^\dagger(x)\sigma_x\Big]\begin{pmatrix}\phi_1(x)\\ \phi_2(x)\end{pmatrix}.
$$

Letting $\phi(x) = (\phi_1(x), \phi_2(x))^T$, Eq. (B.5) becomes

$$
[H, q^\dagger] = \int dx\Big[-iv_F\psi^\dagger(x)\sigma_z\partial_x\phi(x) + m(x)\psi^\dagger(x)\sigma_x\phi(x)\Big] = \varepsilon\int dx\psi^\dagger(x)\phi(x). \tag{B.6}
$$

This implies the real-space BdG equation for $\phi(x)$ (Eq. (7) [30])

$$
\varepsilon\phi(x) = -iv_F\sigma_z\partial_x\phi(x) + m(x)\sigma_x\phi(x). \tag{B.7}
$$

Solving this equation can be done by noting that, because σ_y anticommutes with σ_z and σ_x, for any solution $\phi(x)$ with energy ε there is also a solution $\sigma_y\phi(x)$ with energy $-\varepsilon$:

$$
\begin{aligned}
\sigma_y(\varepsilon\phi(x)) &= \sigma_y(-iv_F\sigma_z\partial_x\phi(x) + m(x)\sigma_x\phi(x)) \\
\Rightarrow \varepsilon\sigma_y\phi(x) &= +iv_F\sigma_z\sigma_y\partial_x\phi(x) - m(x)\sigma_x\sigma_y\phi(x) \\
\Rightarrow -\varepsilon(\sigma_y\phi(x)) &= -iv_F\sigma_z\partial_x(\sigma_y\phi(x)) + m(x)\sigma_x(\sigma_y\phi(x)).
\end{aligned}
$$

For a non-degenerate zero-energy solution to exist, it is therefore required that such a solution have $\phi_0(x) = \lambda\sigma_y\phi_0(x)$, i.e., $\phi_0(x)$ is also an eigenstate of σ_y. Letting $\varepsilon = 0$ and left-multiplying Eq. (B.7) by $i\sigma_z$ gives (Eq. (8) [30])

$$\partial_x\phi_0(x) = \frac{\lambda}{v_F}m(x)\phi_0(x), \tag{B.8}$$

which implies (Eq. (9) [30])

$$\phi_0(x) = \phi_0(0)\exp\left(\frac{\lambda}{v_F}\int_0^x m(y)dy\right). \tag{B.9}$$

For $\tilde{m}(x) = \pm\text{sign}(x)|m(x)|$, ϕ_0 is normalizable for $\lambda = \mp 1$, respectively. Therefore for each sign change of the mass term, $\tilde{m}(x)$, there is a single zero-energy solution (with $x = 0$ shifted to define the point of the sign change). This solution defines the quasiparticle excitation as in Eq. (10) of Ref. [30] (for $\lambda = 1$),

$$q^\dagger = C\int dx\,\exp\left(\frac{1}{v_F}\int_0^x m(y)dy\right)\left[f_1^\dagger(x) + if_2^\dagger(x)\right], \tag{B.10}$$

where C is a normalization constant. As $f_1(x)$ and $f_2(x)$ are two independent fermion fields, $q^\dagger$ is a regular fermion operator with the usual anticommutation relations.

B.3 Map of the Hamiltonian of the 2D semiconductor on an effective 1D theory

In order to map the 2D problem onto an effectively 1D problem, the authors of Ref. [30] use the rotational symmetry of the total Hamiltonian to decouple it into various angular momentum channels. Due to the spin-orbit term, H_{SO}, H_{Tot} is invariant only under simultaneous rotation in real and spin spaces. Therefore a representation of the operators in *total* angular momentum space is used. The annihilation operators in the total-angular-momentum basis are given by the relations (Eq. (11) [30]),

$$\begin{aligned} c_{\boldsymbol{k}\uparrow} &= \frac{1}{\sqrt{2\pi k}}\sum_{m_J=-\infty}^{\infty} c_{m_J,k,\uparrow}e^{i(m_J-\frac{1}{2})\theta_{\boldsymbol{k}}}, \\ c_{\boldsymbol{k}\downarrow} &= \frac{1}{\sqrt{2\pi k}}\sum_{m_J=-\infty}^{\infty} c_{m_J,k,\downarrow}e^{i(m_J+\frac{1}{2})\theta_{\boldsymbol{k}}}, \end{aligned} \tag{B.11}$$

where $k = |\boldsymbol{k}|$ and m_J is the total (orbital plus spin) angular momentum, a half-odd integer for the electron. The relation $\{c_{\boldsymbol{k}\beta}, c^\dagger_{\boldsymbol{p}\gamma}\} = \delta(\boldsymbol{k}-\boldsymbol{p})\delta_{\beta\gamma}$ implies the relation $\{c_{m_J,k,\beta}, c^\dagger_{n_J,p,\gamma}\} = \delta_{m_J,n_J}\delta(k-p)\delta_{\beta\gamma}$, as

$$
\begin{aligned}
\{c_{\boldsymbol{k}\beta}, c^\dagger_{\boldsymbol{p}\gamma}\} &= \frac{1}{\sqrt{2\pi k}}\frac{1}{\sqrt{2\pi p}} \sum_{m_J,n_J=-\infty}^{\infty} \{c_{m_J,k,\beta}, c^\dagger_{n_J,p,\gamma}\} e^{i(m_J\mp\frac{1}{2})\theta_{\boldsymbol{k}}} e^{-i(n_J\mp\frac{1}{2})\theta_{\boldsymbol{p}}} \\
&= \frac{1}{2\pi\sqrt{kp}} \sum_{m_J,n_J=-\infty}^{\infty} \delta_{m_J,n_J}\delta(k-p)\delta_{\beta\gamma} e^{i(m_J\mp\frac{1}{2})\theta_{\boldsymbol{k}}} e^{-i(n_J\mp\frac{1}{2})\theta_{\boldsymbol{p}}} \\
&= \frac{1}{2\pi k}\delta(k-p)\delta_{\beta\gamma} \sum_{m_J=-\infty}^{\infty} e^{im_J(\theta_{\boldsymbol{k}}-\theta_{\boldsymbol{p}})} \\
&= \frac{1}{k}\delta(\theta_{\boldsymbol{k}}-\theta_{\boldsymbol{p}})\delta(k-p)\delta_{\beta\gamma} \\
&= \delta(\boldsymbol{k}-\boldsymbol{p})\delta_{\beta\gamma},
\end{aligned}
\tag{B.12}
$$

where equality of signs for the minus-plus signs is ensured by $\delta_{\beta\gamma}$, and we use the representations for the delta function,

$$
\delta(\theta_{\boldsymbol{k}}-\theta_{\boldsymbol{p}}) = \frac{1}{2\pi}\sum_{m_J=-\infty}^{\infty} e^{im_J(\theta_{\boldsymbol{k}}-\theta_{\boldsymbol{p}})}, \qquad \delta_{n_J,m_J} = \frac{1}{2\pi}\int_0^{2\pi} d\theta_{\boldsymbol{k}} e^{i(n_J-m_J)\theta_{\boldsymbol{k}}}. \tag{B.13}
$$

Transforming the Hamiltonian to total angular momentum space (corresponding to Eqs. (13), (14), and (15) of Ref. [30]), starting with the single-electron part, gives

$$
\begin{aligned}
H_K &= \sum_{\boldsymbol{k},\beta}\left(\frac{k^2}{2m^*}-\mu\right) c^\dagger_{\boldsymbol{k},\beta}c_{\boldsymbol{k},\beta} \\
&= \sum_{\boldsymbol{k},\beta}\left(\frac{k^2}{2m^*}-\mu\right)\cdot\frac{1}{2\pi k}\sum_{m_J} c^\dagger_{m_J,k,\beta}\, e^{-i(m_J\pm\frac{1}{2})\theta_{\boldsymbol{k}}}\cdot\sum_{n_J} c_{n_J,k,\beta}\, e^{i(n_J\pm\frac{1}{2})\theta_{\boldsymbol{k}}} \\
&= \sum_{\beta}\frac{1}{(2\pi)^2}\int dk\, k\int_0^{2\pi} d\theta_{\boldsymbol{k}}\left(\frac{k^2}{2m^*}-\mu\right)\frac{1}{2\pi k}\sum_{m_J}\sum_{n_J} c^\dagger_{m_J,k,\beta}c_{n_J,k,\beta}\, e^{i(n_J-m_J)\theta_{\boldsymbol{k}}}, \\
\therefore H_K &= \frac{1}{(2\pi)^2}\sum_{\beta}\sum_{m_J}\int dk\left(\frac{k^2}{2m^*}-\mu\right) c^\dagger_{m_J,k,\beta}c_{m_J,k,\beta},
\end{aligned}
\tag{B.14}
$$

$$
\begin{aligned}
H_{SO} &= \alpha\sum_{\boldsymbol{k}}\left[(k_y+ik_x)\, c^\dagger_{\boldsymbol{k},\uparrow}c_{\boldsymbol{k},\downarrow} + (k_y-ik_x)\, c^\dagger_{\boldsymbol{k},\downarrow}c_{\boldsymbol{k},\uparrow}\right] \\
&= \frac{\alpha}{(2\pi)^2}\int dk\, k\int_0^{2\pi} d\theta_{\boldsymbol{k}}\,\frac{1}{2\pi k}\Big\{(ike^{-i\theta_{\boldsymbol{k}}})\sum_{m_J} c^\dagger_{m_J,k,\uparrow}\, e^{-i(m_J-\frac{1}{2})\theta_{\boldsymbol{k}}}\cdot\sum_{n_J} c_{n_J,k,\downarrow}\, e^{i(n_J+\frac{1}{2})\theta_{\boldsymbol{k}}} \\
&\quad + (-ike^{i\theta_{\boldsymbol{k}}})\sum_{m_J} c^\dagger_{m_J,k,\downarrow}\, e^{-i(m_J+\frac{1}{2})\theta_{\boldsymbol{k}}}\cdot\sum_{n_J} c_{n_J,k,\uparrow}\, e^{i(n_J-\frac{1}{2})\theta_{\boldsymbol{k}}}\Big\} \\
&= \frac{\alpha}{(2\pi)^2}\int dk\int_0^{2\pi} d\theta_{\boldsymbol{k}}\,\frac{1}{2\pi}ik\sum_{m_J}\sum_{n_J}\left\{c^\dagger_{m_J,k,\uparrow}c_{n_J,k,\downarrow} - c^\dagger_{m_J,k,\downarrow}c_{n_J,k,\uparrow}\right\}e^{i(n_J-m_J)\theta_{\boldsymbol{k}}}, \\
\therefore H_{SO} &= \frac{i\alpha}{(2\pi)^2}\sum_{m_J}\int dk\, k\left[c^\dagger_{m_J,k,\uparrow}c_{m_J,k,\downarrow} - c^\dagger_{m_J,k,\downarrow}c_{m_J,k,\uparrow}\right],
\end{aligned}
\tag{B.15}
$$

and

$$
\begin{aligned}
H_Z &= V_Z \sum_{\boldsymbol{k}} \Big(c^\dagger_{\boldsymbol{k},\uparrow} c_{\boldsymbol{k},\uparrow} - c^\dagger_{\boldsymbol{k},\downarrow} c_{\boldsymbol{k},\downarrow} \Big) \\
&= V_Z \frac{1}{(2\pi)^2} \int dk\, k \int_0^{2\pi} d\theta_{\boldsymbol{k}} \frac{1}{2\pi k} \Big(\sum_{m_J} c^\dagger_{m_J,k,\uparrow}\, e^{-i(m_J-\frac{1}{2})\theta_{\boldsymbol{k}}} \sum_{n_J} c_{n_J,k,\uparrow}\, e^{i(n_J-\frac{1}{2})\theta_{\boldsymbol{k}}} \\
&\quad - \sum_{m_J} c^\dagger_{m_J,k,\downarrow}\, e^{-i(m_J+\frac{1}{2})\theta_{\boldsymbol{k}}} \sum_{n_J} c_{n_J,k,\downarrow}\, e^{i(n_J+\frac{1}{2})\theta_{\boldsymbol{k}}} \Big) \\
&= \frac{V_Z}{(2\pi)^2} \int dk \int_0^{2\pi} d\theta_{\boldsymbol{k}} \frac{1}{2\pi} \sum_{m_J} \sum_{n_J} \Big(c^\dagger_{m_J,k,\uparrow} c_{n_J,k,\uparrow} - c^\dagger_{m_J,k,\downarrow} c_{n_J,k,\downarrow} \Big) e^{i(n_J-m_J)\theta_{\boldsymbol{k}}}, \\
\therefore H_Z &= \frac{V_Z}{(2\pi)^2} \sum_{m_J} \int dk \Big(c^\dagger_{m_J,k,\uparrow} c_{m_J,k,\uparrow} - c^\dagger_{m_J,k,\downarrow} c_{m_J,k,\downarrow} \Big).
\end{aligned} \tag{B.16}
$$

As required, the m_J channels separate for the single-electron Hamiltonian.

To transform the vortex part to total angular momentum channels, the authors of Ref. [30] first substitute the relations

$$
c^\dagger_{\boldsymbol{R}\pm\boldsymbol{r},\beta} = 2\pi \sum_{\boldsymbol{k}} c^\dagger_{\boldsymbol{k},\beta} e^{i\boldsymbol{k}\cdot(\boldsymbol{R}\pm\boldsymbol{r})}, \tag{B.17}
$$

yielding

$$
\begin{aligned}
H_V &= -\int d^2R \int d^2r\, e^{i\theta_{\boldsymbol{R}}} h(R) g(\boldsymbol{r}) c^\dagger_{\boldsymbol{R}+\boldsymbol{r},\uparrow} c^\dagger_{\boldsymbol{R}-\boldsymbol{r},\downarrow} + H.c. \\
&= -(2\pi)^2 \sum_{\boldsymbol{k},\boldsymbol{p}} \int d^2R \int d^2r\, e^{i\theta_{\boldsymbol{R}}} h(R) g(\boldsymbol{r}) c^\dagger_{\boldsymbol{k},\uparrow} e^{i\boldsymbol{k}\cdot(\boldsymbol{R}+\boldsymbol{r})} c^\dagger_{\boldsymbol{p},\downarrow} e^{i\boldsymbol{p}\cdot(\boldsymbol{R}-\boldsymbol{r})} + H.c. \\
&= -(2\pi)^2 \sum_{\boldsymbol{k},\boldsymbol{p}} \int d^2r\, g(\boldsymbol{r}) e^{i(\boldsymbol{k}-\boldsymbol{p})\cdot\boldsymbol{r}} \int d^2R\, e^{i\theta_{\boldsymbol{R}}} h(R) e^{i(\boldsymbol{k}+\boldsymbol{p})\cdot\boldsymbol{R}}\, c^\dagger_{\boldsymbol{k},\uparrow} c^\dagger_{\boldsymbol{p},\downarrow} + H.c.
\end{aligned}
$$

Then, setting (corresponding to Eq. (16) of Ref. [30])

$$
\begin{aligned}
g(\boldsymbol{k}-\boldsymbol{p}) &= \int d^2r\, g(\boldsymbol{r}) e^{i(\boldsymbol{k}-\boldsymbol{p})\cdot\boldsymbol{r}} \equiv \Delta_0, \\
I(\boldsymbol{k}+\boldsymbol{p}) &= \int d^2R\, e^{i\theta_{\boldsymbol{R}}} h(R) e^{i(\boldsymbol{k}+\boldsymbol{p})\cdot\boldsymbol{R}},
\end{aligned} \tag{B.18}
$$

where $g(\boldsymbol{k}-\boldsymbol{p})$ is just the inverse Fourier transform of $g(\boldsymbol{r})$,, the vortex part of the Hamiltonian becomes

$$
H_V = -(2\pi)^2 \sum_{\boldsymbol{k},\boldsymbol{p}} \Delta_0 I(\boldsymbol{k}+\boldsymbol{p})\, c^\dagger_{\boldsymbol{k},\uparrow} c^\dagger_{\boldsymbol{p},\downarrow} + H.c. \tag{B.19}
$$

Now note that, if $(\boldsymbol{k}+\boldsymbol{p})$ is rotated by an angle θ, the quantity $(\boldsymbol{k}+\boldsymbol{p})\cdot\boldsymbol{R}$ is left invariant if $\theta_{\boldsymbol{R}}$ is also rotated by θ. This implies (Eq. (17) [30]) $I(R_\theta(\boldsymbol{k}+\boldsymbol{p})) = e^{i\theta} I(\boldsymbol{k}+\boldsymbol{p})$, where R_θ rotates by θ, as

$$
\begin{aligned}
I(R_\theta(\boldsymbol{k}+\boldsymbol{p})) &= \int d^2R\, e^{i\theta_{\boldsymbol{R}}} h(R) e^{i|\boldsymbol{k}+\boldsymbol{p}|R\cos(\theta_{\boldsymbol{R}}-\theta_{\boldsymbol{k}+\boldsymbol{p}}-\theta)} \\
&= e^{i\theta} \int d^2R\, e^{i\theta'_{\boldsymbol{R}}} h(R) e^{i|\boldsymbol{k}+\boldsymbol{p}|R\cos(\theta'_{\boldsymbol{R}}-\theta_{\boldsymbol{k}+\boldsymbol{p}})},
\end{aligned}
$$

where $\theta'_{\boldsymbol{R}} = \theta_{\boldsymbol{R}} - \theta$. This means the angular dependence of $(\boldsymbol{k}+\boldsymbol{p})$ can be factored out, giving $I(\boldsymbol{k}+\boldsymbol{p}) = e^{i\theta_{\boldsymbol{k}+\boldsymbol{p}}} I(|\boldsymbol{k}+\boldsymbol{p}|)$. The authors of Ref. [30] then choose $(\boldsymbol{k}+\boldsymbol{p})$ along the y-axis, or $\theta = \frac{\pi}{2} - \theta_{\boldsymbol{k}+\boldsymbol{p}}$, giving

$$\begin{aligned} I(\boldsymbol{k}+\boldsymbol{p}) &= e^{-i\theta} I(R_\theta(\boldsymbol{k}+\boldsymbol{p})) \\ &= e^{-i(\frac{\pi}{2}-\theta_{\boldsymbol{k}+\boldsymbol{p}})} \int dR\, R\, h(R) \int d\theta_{\boldsymbol{R}}\, e^{i\theta_{\boldsymbol{R}}} e^{i|\boldsymbol{k}+\boldsymbol{p}|R\sin\theta_{\boldsymbol{R}}} \\ &= -ie^{i\theta_{\boldsymbol{k}+\boldsymbol{p}}} \int dR\, R\, h(R) \cdot 2\pi J_{-1}(|\boldsymbol{k}+\boldsymbol{p}|R) \\ &= ie^{i\theta_{\boldsymbol{k}+\boldsymbol{p}}} \int dR\, R\, h(R) \cdot 2\pi J_1(|\boldsymbol{k}+\boldsymbol{p}|R), \end{aligned}$$

where we have used $J_{-n}(z) = (-1)^n J_n(z)$, and the Bessel function representation,

$$J_n(z) = \frac{1}{\pi}\int_0^\pi \cos\left(-n\phi + z\sin\phi\right) d\phi = \frac{1}{2\pi}\int_{-\pi}^{\pi} e^{-in\phi + iz\sin\phi} d\phi. \tag{B.20}$$

Now, letting $x = |\boldsymbol{k}+\boldsymbol{p}|R$,

$$\begin{aligned} I(|\boldsymbol{k}+\boldsymbol{p}|) &= \frac{2\pi i}{|\boldsymbol{k}+\boldsymbol{p}|^2} \int_0^\infty dx\, x \cdot h\left(\frac{x}{|\boldsymbol{k}+\boldsymbol{p}|}\right) J_1(x) \\ &= \frac{2\pi i}{|\boldsymbol{k}+\boldsymbol{p}|^2} \int_0^\infty dx\, x \cdot \left(1 - e^{-x/\zeta}\right) J_1(x), \end{aligned}$$

with $\zeta = |\boldsymbol{k}+\boldsymbol{p}|\xi$. This integral can be approximated by breaking it into pieces. One has

$$\begin{aligned} \int_0^\infty x e^{-ax} J_1(x) dx &= e^{-ax}\Big[-\frac{x}{a^2+1} J_0(x) - \frac{ax}{1+a^2} J_1(x)\Big]_0^\infty + \frac{1}{a^2+1}\int_0^\infty e^{-ax} J_0(x) dx \\ &= \frac{1}{a^2+1}\Big(\frac{1}{\sqrt{1+a^2}}\Big), \end{aligned} \tag{B.21}$$

and

$$\int_0^\infty x J_1(x) dx = \frac{\pi x}{2}\left[J_1(x)\mathrm{StruveH}_0(x) - J_0(x)\mathrm{StruveH}_1(x)\right]_0^\infty. \tag{B.22}$$

The above integral does not converge to a particular value as the RHS solution is oscillatory at infinity, bounded by $\pm C\sqrt{x}$. However, in practice the vortex does not have infinite extent, so that the upper limit of the above integral can be taken as an arbitrary, large number, and the authors of Ref. [30] approximate the above integral by $\mathcal{O}(1)$.

Therefore Ref. [30] uses the approximation

$$I(\boldsymbol{k}+\boldsymbol{p}) = e^{i\theta_{\boldsymbol{k}+\boldsymbol{p}}} \frac{2\pi i}{|\boldsymbol{k}+\boldsymbol{p}|^2} \mathcal{O}(1). \tag{B.23}$$

Going back to Eq. (B.19), using (B.23), and noting that $e^{i\theta_{\boldsymbol{k}+\boldsymbol{p}}} = (ke^{i\theta_{\boldsymbol{k}}} + pe^{i\theta_{\boldsymbol{p}}})/|\boldsymbol{k}+\boldsymbol{p}|$, one has (Eq. (18) [30])

$$H_V \approx -(2\pi)^3 i\Delta_0 \sum_{\boldsymbol{k},\boldsymbol{p}} \frac{ke^{i\theta_{\boldsymbol{k}}} + pe^{i\theta_{\boldsymbol{p}}}}{|\boldsymbol{k}+\boldsymbol{p}|^3} c^\dagger_{\boldsymbol{k},\uparrow} c^\dagger_{\boldsymbol{p},\downarrow} + H.c. \tag{B.24}$$

Now using the fact that $|\boldsymbol{k}+\boldsymbol{p}|$ is a periodic function of $(\theta_{\boldsymbol{k}}-\theta_{\boldsymbol{p}})$, Fourier-expand as (Eq. (19) [30])

$$\frac{1}{|\boldsymbol{k}+\boldsymbol{p}|^3}=\sum_m u_m(k,p)e^{im(\theta_{\boldsymbol{k}}-\theta_{\boldsymbol{p}})}. \tag{B.25}$$

We note here that all $u_m(k,p)$ are real, as

$$\frac{1}{|\boldsymbol{k}+\boldsymbol{p}|^3}=\left(k^2+p^2-2kp\cos\theta\right)^{-3/2}$$

is an even function of $\theta\equiv\theta_{\boldsymbol{k}}-\theta_{\boldsymbol{p}}$, and so

$$\mathrm{Im}(u_m(k,p))=-\int_{-\pi}^{\pi}\left(k^2+p^2-2kp\cos\theta\right)^{-3/2}\sin m\theta d\theta\equiv 0, \tag{B.26}$$

as $\sin m\theta$ is odd.

Finally, transforming to total angular momentum operators, we have for the vortex (pairing) part of the Hamiltonian,

$$\begin{aligned}
H_V=&-\frac{(2\pi)^3}{(2\pi)^4}i\Delta_0\int dk\,k\int d\theta_{\boldsymbol{k}}\int dp\,p\int d\theta_{\boldsymbol{p}}(ke^{i\theta_{\boldsymbol{k}}}+pe^{i\theta_{\boldsymbol{p}}})\sum_m u_m(k,p)e^{im(\theta_{\boldsymbol{k}}-\theta_{\boldsymbol{p}})}\\
&\cdot\frac{1}{\sqrt{2\pi k}}\sum_{m_J}c^\dagger_{m_J,k,\uparrow}e^{-i(m_J-\frac{1}{2})\theta_{\boldsymbol{k}}}\cdot\frac{1}{\sqrt{2\pi p}}\sum_{n_J}c^\dagger_{n_J,p,\downarrow}e^{-i(n_J+\frac{1}{2})\theta_{\boldsymbol{p}}}+H.c.\\
=&-\frac{i\Delta_0}{(2\pi)^2}\sum_m\int dk\int dp\sqrt{kp}\,u_m(k,p)\int d\theta_{\boldsymbol{k}}\int d\theta_{\boldsymbol{p}}(ke^{i\theta_{\boldsymbol{k}}}+pe^{i\theta_{\boldsymbol{p}}})\sum_{m_J}c^\dagger_{m_J,k,\uparrow}\\
&\cdot e^{-i(m_J-\frac{1}{2}-m)\theta_{\boldsymbol{k}}}\sum_{n_J}c^\dagger_{n_J,p,\downarrow}e^{-i(n_J+\frac{1}{2}+m)\theta_{\boldsymbol{p}}}+H.c.\\
=&-i\Delta_0\sum_m\int dk\int dp\sqrt{kp}\,u_m(k,p)\sum_{m_J,n_J}(k\,\delta_{m_J-\frac{3}{2}-m}\delta_{n_J+\frac{1}{2}+m}+p\,\delta_{m_J-\frac{1}{2}-m}\delta_{n_J-\frac{1}{2}+m})\\
&\cdot c^\dagger_{m_J,k,\uparrow}c^\dagger_{n_J,p,\downarrow}+H.c.,
\end{aligned} \tag{B.27}$$

or (Eq. (20) [30])

$$H_V=-i\Delta_0\sum_m\int dkdp\sqrt{kp}\,u_m(k,p)\left(kc^\dagger_{m+\frac{3}{2},k,\uparrow}c^\dagger_{-m-\frac{1}{2},p,\downarrow}+pc^\dagger_{m+\frac{1}{2},k,\uparrow}c^\dagger_{-m+\frac{1}{2},p,\downarrow}\right)+H.c. \tag{B.28}$$

Therefore the $m_J=\frac{1}{2}$ channel separates from the rest, for all parts of the Hamiltonian: above it is given by taking $m=-1$ in the first term and $m=0$ in the second term.

In the $m_J=\frac{1}{2}$ channel, the total Hamiltonian is given by $H_{Tot,m_J=\frac{1}{2}}=H_{K,m_J=\frac{1}{2}}+H_{SO,m_J=\frac{1}{2}}+H_{Z,m_J=\frac{1}{2}}+H_{V,m_J=\frac{1}{2}}$, where (Eq. (21) [30])

$$
\begin{aligned}
H_{K,m_J=\frac{1}{2}} &= \frac{1}{(2\pi)^2}\sum_{\beta}\int dk\left(\frac{k^2}{2m^*}-\mu\right)c^{\dagger}_{\frac{1}{2},k,\beta}c_{\frac{1}{2},k,\beta},\\
H_{SO,m_J=\frac{1}{2}} &= \frac{i\alpha}{(2\pi)^2}\int dk\,k\Big[c^{\dagger}_{\frac{1}{2},k,\uparrow}c_{\frac{1}{2},k,\downarrow}-c^{\dagger}_{\frac{1}{2},k,\downarrow}c_{\frac{1}{2},k,\uparrow}\Big],\\
H_{Z,m_J=\frac{1}{2}} &= \frac{V_Z}{(2\pi)^2}\int dk\Big(c^{\dagger}_{\frac{1}{2},k,\uparrow}c_{\frac{1}{2},k,\uparrow}-c^{\dagger}_{\frac{1}{2},k,\downarrow}c_{\frac{1}{2},k,\downarrow}\Big),\\
H_{V,m_J=\frac{1}{2}} &= -i\int dkdp\,\Delta(k,p)c^{\dagger}_{\frac{1}{2},k,\uparrow}c^{\dagger}_{\frac{1}{2},p,\downarrow}+H.c.,
\end{aligned}
\tag{B.29}
$$

with

$$
\Delta(k,p) := \Delta_0\sqrt{kp}\,(k\,u_{-1}(k,p)+p\,u_0(k,p))\,. \tag{B.30}
$$

From now on, only the $m_J=\frac{1}{2}$ channel will be taken, and the subscript will be suppressed.

B.4 Demonstration of the zero-energy solution

B.4.1 Diagonalization

The single-electron Hamiltonian (channel $m_J=\frac{1}{2}$) is now diagonalized using a unitary transformation. This will make it possible to linearize band energies around the Fermi surfaces and put the total Hamiltonian in the Dirac form. The single-electron Hamiltonian is diagonalized to the energy eigenbasis by (Eqs. (22) and (23) [30])

$$
\begin{pmatrix}c^{\dagger}_{\uparrow,k}\\ c^{\dagger}_{\downarrow,k}\end{pmatrix}=\begin{pmatrix}a^*_k & -b_k\\ b^*_k & a_k\end{pmatrix}\begin{pmatrix}f^{\dagger}_{+,k}\\ f^{\dagger}_{-,k}\end{pmatrix},\qquad \begin{pmatrix}f^{\dagger}_{+,k}\\ f^{\dagger}_{-,k}\end{pmatrix}=\begin{pmatrix}a_k & b_k\\ -b^*_k & a^*_k\end{pmatrix}\begin{pmatrix}c^{\dagger}_{\uparrow,k}\\ c^{\dagger}_{\downarrow,k}\end{pmatrix}, \tag{B.31}
$$

where $|a_k|^2+|b_k|^2=1$. The $f^{\dagger}_{\pm}$ operators, as they are related to the original operators $c^{\dagger}_{\pm}$ by a unitary transformation, still obey the fermionic anticommutation relations,

$$
\begin{aligned}
\left\{f^{\dagger}_{+,k},f_{+,k}\right\} &= \left\{\left(a_kc^{\dagger}_{\uparrow,k}+b_kc^{\dagger}_{\downarrow,k}\right),\left(a^*_kc_{\uparrow,k}+b^*_kc_{\downarrow,k}\right)\right\}\\
&= |a_k|^2\left\{c^{\dagger}_{\uparrow,k},c_{\uparrow,k}\right\}+|b_k|^2\left\{c^{\dagger}_{\downarrow,k},c_{\downarrow,k}\right\}=|a_k|^2+|b_k|^2=1,\\
\left\{f^{\dagger}_{+,k},f_{-,k}\right\} &= \left\{\left(a_kc^{\dagger}_{\uparrow,k}+b_kc^{\dagger}_{\downarrow,k}\right),\left(-b_kc_{\uparrow,k}+a_kc_{\downarrow,k}\right)\right\}\\
&= -a_kb_k\left\{c^{\dagger}_{\uparrow,k},c_{\uparrow,k}\right\}+a_kb_k\left\{c^{\dagger}_{\downarrow,k},c_{\downarrow,k}\right\}=-a_kb_k+a_kb_k=0,
\end{aligned}
$$

etc.

In the diagonalized basis, the single-electron Hamiltonian, $H_0=H_K+H_{SO}+H_Z$, becomes

$$
H_0=\int\frac{dk}{(2\pi)^2}\left[(E_{+,k}-\mu)f^{\dagger}_{+,k}f_{+,k}+(E_{-,k}-\mu)f^{\dagger}_{-,k}f_{-,k}\right], \tag{B.32}
$$

where $E_{\pm,k}$ are the energy eigenvalues. The vortex part becomes

$$\begin{aligned}
H_V &= -i\int dkdp\Delta(k,p)\left[a_k^* f_{+,k}^\dagger - b_k f_{-,k}^\dagger\right]\left[b_p^* f_{+,p}^\dagger - a_p f_{-,p}^\dagger\right] + H.c. \\
&= -i\int dkdp\Delta(k,p)\left\{a_k^* b_p^* f_{+,k}^\dagger f_{+,p}^\dagger + a_k^* a_p f_{+,k}^\dagger f_{-,p}^\dagger - b_k b_p^* f_{-,k}^\dagger f_{+,p}^\dagger - a_p b_k f_{-,k}^\dagger f_{-,p}^\dagger\right\} + H.c. \\
&= -\frac{i}{2}\int dkdp\Delta(k,p)\left\{a_k^* b_p^* f_{+,k}^\dagger f_{+,p}^\dagger + a_k^* a_p f_{+,k}^\dagger f_{-,p}^\dagger - b_k b_p^* f_{-,k}^\dagger f_{+,p}^\dagger - a_p b_k f_{-,k}^\dagger f_{-,p}^\dagger\right\} \\
&\quad -\frac{i}{2}\int dpdk\Delta(p,k)\left\{a_p^* b_k^* f_{+,p}^\dagger f_{+,k}^\dagger + a_p^* a_k f_{+,p}^\dagger f_{-,k}^\dagger - b_p b_k^* f_{-,p}^\dagger f_{+,k}^\dagger - a_k b_p f_{-,p}^\dagger f_{-,k}^\dagger\right\} + H.c. \\
&= -\frac{i}{2}\int dkdp\Big(\Delta(k,p)a_k^* b_p^* - \Delta(p,k)a_p^* b_k^*\Big) f_{+,k}^\dagger f_{+,p}^\dagger \;-\; \frac{i}{2}\int dkdp\Big(-\Delta(k,p)a_p b_k \\
&\quad + \Delta(p,k)a_k b_p\Big) f_{-,k}^\dagger f_{-,p}^\dagger \;-\; \frac{i}{2}\int dkdp\Big(\Delta(k,p)a_k^* a_p + \Delta(p,k)b_p b_k^*\Big) f_{+,k}^\dagger f_{-,p}^\dagger \\
&\quad -\frac{i}{2}\int dkdp\Big(-\Delta(k,p)b_k b_p^* - \Delta(p,k)a_p^* a_k\Big) f_{-,k}^\dagger f_{+,p}^\dagger + H.c.,
\end{aligned}$$

or, finally (Eq. (24) [30]),

$$\begin{aligned}
H_V = &-\frac{i}{2}\int dkdp\Big(\Delta(k,p)a_k^* b_p^* - \Delta(p,k)a_p^* b_k^*\Big) f_{+,k}^\dagger f_{+,p}^\dagger \\
&-\frac{i}{2}\int dkdp\Big(-\Delta(k,p)a_p b_k + \Delta(p,k)a_k b_p\Big) f_{-,k}^\dagger f_{-,p}^\dagger \\
&-\frac{i}{2}\int dkdp\Big(\Delta(k,p)a_k^* a_p + \Delta(p,k)b_p b_k^*\Big) f_{+,k}^\dagger f_{-,p}^\dagger + H.c.
\end{aligned} \tag{B.33}$$

It can be seen here that the terms with $f_{+,k}^\dagger f_{+,p}^\dagger$ and $f_{-,k}^\dagger f_{-,p}^\dagger$ (the intra-band pairing terms) are antisymmetric in k and p, while the $f_+ f_-$ (inter-band pairing) terms are not. Therefore the total Hamiltonian can be written as (Eq. (25) [30])

$$\begin{aligned}
H_{Tot} = &\int \frac{dk}{(2\pi)^2}\left[(E_{+,k}-\mu)f_{+,k}^\dagger f_{+,k} + (E_{-,k}-\mu)f_{-,k}^\dagger f_{-,k}\right] - \frac{i}{2}\int dkdp\Big\{\Lambda_{++}(k,p)f_{+,k}^\dagger f_{+,p}^\dagger \\
&+ \Lambda_{--}(k,p)f_{-,k}^\dagger f_{-,p}^\dagger + \Lambda_{+-}(k,p)f_{+,k}^\dagger f_{-,p}^\dagger\Big\} + H.c.,
\end{aligned} \tag{B.34}$$

where $\Lambda_{++}(k,p)$ and $\Lambda_{--}(k,p)$ are antisymmetric in k and p,

$$\begin{aligned}
\Lambda_{++}(k,p) &= \Delta(k,p)a_k^* b_p^* - \Delta(p,k)a_p^* b_k^*, \\
\Lambda_{--}(k,p) &= -\Delta(k,p)a_p b_k + \Delta(p,k)a_k b_p, \\
\Lambda_{+-}(k,p) &= \Delta(k,p)a_k^* a_p + \Delta(p,k)b_p b_k^*.
\end{aligned} \tag{B.35}$$

We note that the complex phase of Λ_{++} and Λ_{--} functions can be chosen arbitrarily (Λ_{+-} is always real), depending on a phase factor in how f's are defined in terms of c's. For this system, we have specifically

$$
\begin{aligned}
\mathcal{H}(k) &= \begin{pmatrix} f^\dagger_{+,k} & f^\dagger_{-,k} \end{pmatrix} \begin{pmatrix} E_{+,k} & 0 \\ 0 & E_{-,k} \end{pmatrix} \begin{pmatrix} f_{+,k} \\ f_{-,k} \end{pmatrix} \\
&= \begin{pmatrix} c^\dagger_{\uparrow,k} & c^\dagger_{\downarrow,k} \end{pmatrix} \begin{pmatrix} a_k & -b^*_k \\ b_k & a^*_k \end{pmatrix} \begin{pmatrix} E_{+,k} & 0 \\ 0 & E_{-,k} \end{pmatrix} \begin{pmatrix} a^*_k & b^*_k \\ -b_k & a_k \end{pmatrix} \begin{pmatrix} c_{\uparrow,k} \\ c_{\downarrow,k} \end{pmatrix} \\
&= \begin{pmatrix} c^\dagger_{\uparrow,k} & c^\dagger_{\downarrow,k} \end{pmatrix} \begin{pmatrix} |a_k|^2 E_{+,k} + |b_k|^2 E_{-,k} & a_k b^*_k (E_{+,k} - E_{-,k}) \\ a^*_k b_k (E_{+,k} - E_{-,k}) & |b_k|^2 E_{+,k} + |a_k|^2 E_{-,k} \end{pmatrix} \begin{pmatrix} c_{\uparrow,k} \\ c_{\downarrow,k} \end{pmatrix} \\
&= \begin{pmatrix} c^\dagger_{\uparrow,k} & c^\dagger_{\downarrow,k} \end{pmatrix} \begin{pmatrix} \frac{k^2}{2m^*} - \mu + V_z & i\alpha k \\ -i\alpha k & \frac{k^2}{2m^*} - \mu - V_z \end{pmatrix} \begin{pmatrix} c_{\uparrow,k} \\ c_{\downarrow,k} \end{pmatrix},
\end{aligned}
$$

with eigenvalues $E_{\pm,k}$ given by

$$
E_{\pm,k} = \frac{k^2}{2m^*} - \mu \pm \sqrt{\alpha^2 k^2 + V_z^2}. \tag{B.36}
$$

Therefore we have

$$
\begin{aligned}
a_k &= e^{i\phi} \frac{1}{\sqrt{2}} \sqrt{1 + \frac{V_z}{\sqrt{V_z^2 + \alpha^2 k^2}}}, \\
b_k &= -ie^{i\phi} \frac{1}{\sqrt{2}} \frac{\alpha k}{\sqrt{V_z^2 + \alpha^2 k^2 + V_z \sqrt{V_z^2 + \alpha^2 k^2}}},
\end{aligned} \tag{B.37}
$$

where ϕ is an arbitrary phase. Correspondingly, one has

$$
\begin{aligned}
\Lambda_{++}(k,p) &= ie^{-i2\phi} \operatorname{sign}(\Delta(k,p) - \Delta(p,k)) |\Lambda_{++}(k,p)|, \\
\Lambda_{--}(k,p) &= ie^{i2\phi} \operatorname{sign}(\Delta(k,p) - \Delta(p,k)) |\Lambda_{--}(k,p)|.
\end{aligned} \tag{B.38}
$$

In Ref. [30], it appears that the authors have chosen $\phi = 0$ for simplicity, corresponding to imaginary $\Lambda_{++}(k,p)$ and $\Lambda_{--}(k,p)$.

B.4.2 Linearization

It is assumed that the Fermi level is in the lower $(-)$ band, with Fermi momentum k_F, while the upper $(+)$ band is separated from the Fermi level by an energy gap $E_+ = |V_z| - \mu$ (this is true as long as $|\mu| < |V_z|$, which is implicitly assumed to be true experimentally). Without loss of generality, μ is taken positive. The momenta are now limited to those near the Fermi momentum for the lower band, and near the band minimum at $k = 0$ for the upper band. The total Hamiltonian becomes (Eq. (26) [30])

$$
\begin{aligned}
H_{Tot} = \int \frac{dq}{(2\pi)^2} \left[E_+ f^\dagger_{+,q} f_{+,q} + (E_{-,k_F+q} - \mu) f^\dagger_{-,k_F+q} f_{-,k_F+q} \right] - \frac{i}{2} \iint dq dq' \Big\{ \Lambda_{++}(q,q') f^\dagger_{+,q} f^\dagger_{+,q'} \\
+ \Lambda_{--}(k_F+q, k_F+q') f^\dagger_{-,k_F+q} f^\dagger_{-,k_F+q'} + \Lambda_{+-}(q, k_F+q') f^\dagger_{+,q} f^\dagger_{-,k_F+q'} \Big\} + H.c.
\end{aligned} \tag{B.39}
$$

The lower limits on the momenta q, q' are 0 and $-k_F$ for the upper and lower bands, respectively (upper limits are taken as ∞). The lowest order dependencies of the functions Λ on q and q' which are consistent with Λ_{++} and Λ_{--} being antisymmetric in $(q-q')$ are now taken. Since $\Lambda_{+-}(k,p)$ has no symmetry requirement, it is generically non-zero in the limit $q, q' \to 0$, and it is assumed in Ref. [30] that it is a non-zero constant Λ_{+-} in this limit. (If $\Lambda_{+-}=0$, the bands would decouple, simplifying the final zero-energy solution.) This gives (Eq. (27) [30])

$$H_{Tot} = \int \frac{dq}{(2\pi)^2}\left[E_+ f^\dagger_{+,q} f_{+,q} + (E_{-,k_F+q}-\mu) f^\dagger_{-,k_F+q} f_{-,k_F+q}\right] - \frac{i}{2}\iint dq dq' \Big\{\Lambda_{++}(q-q') f^\dagger_{+,q} f^\dagger_{+,q'} + \Lambda_{--}(q-q') f^\dagger_{-,k_F+q} f^\dagger_{-,k_F+q'} + \Lambda_{+-} f^\dagger_{+,q} f^\dagger_{-,k_F+q'}\Big\} + H.c. \tag{B.40}$$

B.4.3 Fourier transform to real-space

Now that the Hamiltonian has been simplified in this way, it can be Fourier-transformed to real space to find a Majorana solution. The authors of Ref. [30] use the Fourier operator transforms (Eq. (28) [30]),

$$\begin{aligned} f^\dagger_-(x) &= \int_{-k_F}^{\infty} dq\, e^{iqx} f^\dagger_{-,k_F+q}, \\ f^\dagger_+(x) &= \int_0^{\infty} dq\, e^{iqx} f^\dagger_{+,q}. \end{aligned} \tag{B.41}$$

Inserting these transforms into Eq. (29) in Ref. [30] (Eq. (B.45) at the end of this subsection), it is simple to see that the Hamiltonian in q, q'-space is retrieved. In particular,

$$\begin{aligned} \int_{-\infty}^{\infty} dx\, \Lambda_{++}(x) f^\dagger_+(x) f^\dagger_+(-x) &= \int_{-\infty}^{\infty} dx\, \Lambda_{++}(x) \int_0^{\infty} dq\, e^{iqx} f^\dagger_{+,q} \int_0^{\infty} dq'\, e^{-iq'x} f^\dagger_{+,q'} \\ &= \int_0^{\infty} dq \int_0^{\infty} dq' \left(\int_0^{\infty} dx\, \Lambda_{++}(x) e^{ix(q-q')} + \int_{-\infty}^{0} dx\, \Lambda_{++}(x) e^{ix(q-q')}\right) f^\dagger_{+,q} f^\dagger_{+,q'} \\ &= \int_0^{\infty} dq \int_0^{\infty} dq' \left(\int_0^{\infty} dx\, \Lambda_{++}(x) e^{ix(q-q')} + \int_0^{\infty} dx\, (-\Lambda_{++}(x)) e^{-ix(q-q')}\right) f^\dagger_{+,q} f^\dagger_{+,q'} \\ &= \int_0^{\infty} dq \int_0^{\infty} dq' \left(2i \int_0^{\infty} dx\, \Lambda_{++}(x) \sin(x(q-q'))\right) f^\dagger_{+,q} f^\dagger_{+,q'}, \end{aligned} \tag{B.42}$$

giving a function $\Lambda_{++}(q,q')$ in the brackets which is antisymmetric in q and q'. This is only possible if $\Lambda_{++}(x)$ is odd in x, as otherwise $\cos(x(q-q'))$ terms would be present.

Note that the phase of $\Lambda_{++}(q,q')$ ($\Lambda_{--}(q,q')$) is different from the phase of $\Lambda_{++}(x)$ ($\Lambda_{--}(x)$) by a factor of i, meaning (see Eq. (B.38))

$$\begin{aligned} \Lambda_{++}(x) &= \pm e^{-i2\phi} |\Lambda_{++}(x)|, \\ \Lambda_{--}(x) &= \pm e^{i2\phi} |\Lambda_{--}(x)|. \end{aligned} \tag{B.43}$$

In Ref. [30], the authors appear to have chosen $\phi = 0$, yielding real $\Lambda_{++}(x)$ and $\Lambda_{--}(x)$.

Alternatively, to transform the Hamiltonian, one has

$$\begin{aligned} \int dq\, c(q) f^\dagger_{+,q} &= \int_{-\infty}^{\infty} dx\, \tilde{c}(x) f^\dagger_+(x), \\ \tilde{c}(x) &= \int_{-\infty}^{\infty} dq\, c(q) e^{-iqx}, \end{aligned} \tag{B.44}$$

where $c(q)$ can be extended to $q \in (-\infty, \infty)$. We consider the Hamiltonian term by term. The first term (neglecting factors of 2π to some power) gives

$$\begin{aligned} E_+(x,x') &= \int_{-\infty}^{\infty} dq\, E_+ e^{-iqx} e^{iqx'} \\ &= E_+ \delta(x-x') \end{aligned}$$

The second term, noting that $E_{-,k_F+q} - \mu = \nu q$ where ν is the Fermi velocity in the lower band, gives

$$\begin{aligned} E_-(x,x') &= \int_{-\infty}^{\infty} dq\, \nu q e^{-iqx} e^{iqx'} \\ &= \int_{-\infty}^{\infty} dq\, i\nu \partial_x e^{-iq(x-x')} \\ &= i\nu \partial_x \delta(x-x'). \end{aligned}$$

Fourier transforms of the Λ functions are harder to see. Taking the lowest order antisymmetric in q and q', say $\Lambda_{++}(q-q') \approx c_1(q-q')$ for some constant c_1, $\Lambda_{++}(x)$ can be found by

$$\begin{aligned} \int_0^\infty dq\, dq'\, c_1(q-q') f^\dagger_{+,q} f^\dagger_{+,q'} &= \int_{-\infty}^{\infty} dx\, \delta(x) \int_0^\infty dq\, dq'\, c_1(q-q') f^\dagger_{+,q} f^\dagger_{+,q'} \\ &= \int_{-\infty}^{\infty} dx\, \delta(x) \int_0^\infty dq\, dq'\, c_1 \left(-i\partial_x e^{i(q-q')x} \right) f^\dagger_{+,q} f^\dagger_{+,q'} \\ &= \int_{-\infty}^{\infty} dx\, \delta(x) \partial_x \int_0^\infty dq\, dq'\, (-ic_1) e^{iqx} f^\dagger_{+,q} e^{-iq'x} f^\dagger_{+,q'} \\ &= -ic_1 \int_{-\infty}^{\infty} dx\, \delta(x) \partial_x \left(f^\dagger_+(x) f^\dagger_+(-x) \right) \\ &= \int_{-\infty}^{\infty} dx\, \left(ic_1 \partial_x \delta(x) \right) f^\dagger_+(x) f^\dagger_+(-x), \end{aligned}$$

where we have integrated by parts in the last step. The factor in brackets is the function $\Lambda_{++}(x)$, which is odd in x (as the derivative of an even function is odd). The term for the Fourier transform of $\Lambda_{--}(q-q')$ is similar, giving $\Lambda_{--}(x)$, also odd in x. The final term can be found by

$$\begin{aligned} \int_0^\infty dq \int_{-k_F}^{\infty} dq' \Lambda_{+-} f^\dagger_{+,q} f^\dagger_{-,k_F+q'} &= \int_{-\infty}^{\infty} dx\, \delta(x) \int dq\, dq' \Lambda_{+-} f^\dagger_{+,q} f^\dagger_{-,k_F+q'} \\ &= \int_{-\infty}^{\infty} dx\, \delta(x) \Lambda_{+-} \int dq\, dq' e^{ix(q-q')} f^\dagger_{+,q} f^\dagger_{-,k_F+q'} \\ &= \int_{-\infty}^{\infty} dx\, \delta(x) \Lambda_{+-} f^\dagger_+(x) f^\dagger_-(-x), \end{aligned}$$

where in the second last line we have used the fact that $e^{ix(q-q')} = 1$ when x is zero.

The total Fourier-transformed Hamiltonian is, finally (Eq. (29) [30]),

$$\begin{aligned} H_{Tot} = &\int_{-\infty}^{\infty} dx\, dx' \left[E_+\delta(x-x') f_+^\dagger(x) f_+(x') + E_-(x-x') f_-^\dagger(x) f_-(x') \right] \\ &- \frac{i}{2}\int_{-\infty}^{\infty} dx \Big\{ \Lambda_{++}(x) f_+^\dagger(x) f_+^\dagger(-x) + \Lambda_{--}(x) f_-^\dagger(x) f_-^\dagger(-x) \\ &+ \Lambda_{+-}\delta(x) f_+^\dagger(x) f_-^\dagger(-x) \Big\} + H.c. \end{aligned} \tag{B.45}$$

with $\Lambda_{++}(x)$ and $\Lambda_{--}(x)$ odd in x, and $E_-(x-x') = i\nu\partial_x\delta(x-x')$.

B.4.4 BdG equations

One can find the BdG equations from the commutator of H_{Tot} with the operator for a hypothetical excitation, $\gamma^\dagger$. This excitation is defined (Eq. (30) [30]) by

$$\gamma^\dagger = \int_{-\infty}^{\infty} dx \left(\eta_{+,1}(x) f_+^\dagger(x) + \eta_{-,1}(x) f_-^\dagger(x) + \eta_{+,2}(x) f_+(-x) + \eta_{-,2}(x) f_-(-x) \right). \tag{B.46}$$

For $\gamma^\dagger$ a *zero-energy* mode, we have

$$\left[H_{Tot}, \gamma^\dagger \right] = \varepsilon\gamma^\dagger = 0. \tag{B.47}$$

In order to solve this equation, anticommutation relations for $f^\dagger(x)$ operators are needed. These are given by (Eqs. (32) and (33) [30])

$$\begin{aligned} \left\{ f_+^\dagger(x), f_+(x') \right\} &= \int_0^\infty dk\, dk'\, e^{i(kx-k'x')} \left\{ f_{+,k}^\dagger, f_{+,k'} \right\} = \int_0^\infty dk\, e^{ik(x-x')} \equiv S_+(x-x') \\ \left\{ f_-^\dagger(x), f_-(x') \right\} &= \int_{-k_F}^\infty dk\, dk'\, e^{i(kx-k'x')} \left\{ f_{-,k}^\dagger, f_{-,k'} \right\} = \int_{-k_F}^\infty dk\, e^{ik(x-x')} \equiv S_-(x-x'). \end{aligned} \tag{B.48}$$

These anticommutators are not quite delta functions. For example, $S_+(x-x')$ can be found by contour integration in the complex plane to be (Eq. (32) [30])

$$S_+(x-x') = \frac{1}{2}\delta(x-x') + i\mathcal{P}\left(\frac{1}{x-x'}\right), \tag{B.49}$$

where $\mathcal{P}$ stands for the Cauchy principal value. Since these anticommutators are not delta functions, the authors of Ref. [30] define new functions ξ for integrals with S_+ and S_- (Eq. (34) [30]):

$$\xi_{\pm,n}(x) = \int_{-\infty}^{\infty} S_\pm(y-x)\eta_{\pm,n}(y)dy, \tag{B.50}$$

where n takes the values 1, 2. The commutator in Eq. (B.47) can now be calculated. For example, we have

$$
\begin{aligned}
\big[f_+^\dagger(x)f_+(x'),\,\gamma^\dagger\big] &= f_+^\dagger(x)f_+(x')\int_{-\infty}^{\infty} dy\big[\eta_{+,1}(y)f_+^\dagger(y)+\eta_{-,1}(y)f_-^\dagger(y)+\eta_{+,2}(y)f_+(-y)\\
&\qquad +\eta_{-,2}(y)f_-(-y)\big]-\gamma^\dagger f_+^\dagger(x)f_+(x')\\
&=\int_{-\infty}^{\infty} dy\big[\eta_{+,1}(y)f_+^\dagger(x)\Big(S_+(y-x')-f_+^\dagger(y)f_+(x')\Big)+(-1)^2\eta_{-,1}(y)f_-^\dagger(y)f_+^\dagger(x)f_+(x')\\
&\quad -\eta_{+,2}(y)f_+^\dagger(x)f_+(-y)f_+(x')+(-1)^2\eta_{-,2}(y)f_-(-y)f_+^\dagger(x)f_+(x')\big]-\gamma^\dagger f_+^\dagger(x)f_+(x')\\
&=\int_{-\infty}^{\infty} dy\big[\eta_{+,1}(y)\Big(S_+(y-x')f_+^\dagger(x)+f_+^\dagger(y)f_+^\dagger(x)f_+(x')\Big)+\eta_{-,1}(y)f_-^\dagger(y)f_+^\dagger(x)f_+(x')\\
&\quad -\eta_{+,2}(y)\Big(S_+(x-(-y))f_+(x')-f_+(-y)f_+^\dagger(x)f_+(x')\Big)\\
&\quad +\eta_{-,2}(y)f_-(-y)f_+^\dagger(x)f_+(x')\big]-\gamma^\dagger f_+^\dagger(x)f_+(x')\\
&=\int_{-\infty}^{\infty} dy\big[\eta_{+,1}(y)S_+(y-x')f_+^\dagger(x)-\eta_{+,2}(y)S_+(x+y)f_+(x')\big]+\gamma^\dagger f_+^\dagger(x)f_+(x')\\
&\quad -\gamma^\dagger f_+^\dagger(x)f_+(x')\\
&=\xi_{+,1}(x')f_+^\dagger(x)-\xi_{+,2}(-x)f_+(x').
\end{aligned}
$$

Finding other commutators similarly, we have altogether:

$$
\begin{aligned}
\big[f_+^\dagger(x)f_+(x'),\,\gamma^\dagger\big] &= \xi_{+,1}(x')f_+^\dagger(x)-\xi_{+,2}(-x)f_+(x'),\\
\big[f_-^\dagger(x)f_-(x'),\,\gamma^\dagger\big] &= \xi_{-,1}(x')f_-^\dagger(x)-\xi_{-,2}(-x)f_-(x'),\\
\big[f_+^\dagger(x)f_+^\dagger(-x),\,\gamma^\dagger\big] &= \xi_{+,2}(x)f_+^\dagger(x)-\xi_{+,2}(-x)f_+^\dagger(-x),\\
\big[f_-^\dagger(x)f_-^\dagger(-x),\,\gamma^\dagger\big] &= \xi_{-,2}(x)f_-^\dagger(x)-\xi_{-,2}(-x)f_-^\dagger(-x),\\
\big[f_+^\dagger(x)f_-^\dagger(-x),\,\gamma^\dagger\big] &= -\xi_{+,2}(-x)f_-^\dagger(-x)+\xi_{-,2}(x)f_+^\dagger(x),\\
\big[f_+(-x)f_+(x),\,\gamma^\dagger\big] &= \xi_{+,1}(x)f_+(-x)-\xi_{+,1}(-x)f_+(x),\\
\big[f_-(-x)f_-(x),\,\gamma^\dagger\big] &= \xi_{-,1}(x)f_-(-x)-\xi_{-,1}(-x)f_-(x),\\
\big[f_-(-x)f_+(x),\,\gamma^\dagger\big] &= \xi_{+,1}(x)f_-(-x)-\xi_{-,1}(-x)f_+(x).
\end{aligned}
\tag{B.51}
$$

Substituting these into Eq. (B.47), we have in the general case (the authors of Ref. [30] have chosen $\Lambda_{++}(x)$ and $\Lambda_{--}(x)$ to be real: see Eq. (B.43)),

$$\big[H_{Tot},\,\gamma^\dagger\big]=0=\int_{-\infty}^{\infty}dxdx'\Big[E_+\delta(x-x')\Big(\xi_{+,1}(x')f_+^\dagger(x)-\xi_{+,2}(-x)f_+(x')\Big)+i\nu\partial_x\delta(x-x')$$
$$\cdot\Big(\xi_{-,1}(x')f_-^\dagger(x)-\xi_{-,2}(-x)f_-(x')\Big)\Big]-\frac{i}{2}\int_{-\infty}^{\infty}dx\Big[\Lambda_{++}(x)\Big(\xi_{+,2}(x)f_+^\dagger(x)$$
$$-\xi_{+,2}(-x)f_+^\dagger(-x)\Big)+\Lambda_{--}(x)\Big(\xi_{-,2}(x)f_-^\dagger(x)-\xi_{-,2}(-x)f_-^\dagger(-x)\Big)+\Lambda_{+-}\delta(x)$$
$$\cdot\Big(-\xi_{+,2}(-x)f_-^\dagger(-x)+\xi_{-,2}(x)f_+^\dagger(x)\Big)\Big]+\frac{i}{2}\int_{-\infty}^{\infty}dx\Big[\Lambda_{++}^*(x)\Big(\xi_{+,1}(x)f_+(-x)$$
$$-\xi_{+,1}(-x)f_+(x)\Big)+\Lambda_{--}^*(x)\Big(\xi_{-,1}(x)f_-(-x)-\xi_{-,1}(-x)f_-(x)\Big)+\Lambda_{+-}\delta(x)$$
$$\cdot\Big(\xi_{+,1}(x)f_-(-x)-\xi_{-,1}(-x)f_+(x)\Big)\Big].$$

Integrating by parts for the term with $\partial_x\delta(x-x')$, changing $x\to -x$ where needed, and using that $\Lambda_{++}(x)$ and $\Lambda_{--}(x)$ are odd in x, we have

$$\big[H_{Tot},\,\gamma^\dagger\big]=0=\int_{-\infty}^{\infty}dx\Big[E_+\Big(\xi_{+,1}(x)f_+^\dagger(x)-\xi_{+,2}(x)f_+(-x)\Big)+i\nu\Big(\partial_x(\xi_{-,1}(x))f_-^\dagger(x)$$
$$-\partial_x(\xi_{-,2}(x))f_-(-x)\Big)\Big]+\frac{i}{2}\int_{-\infty}^{\infty}dx\Big[-2\Lambda_{++}(x)\xi_{+,2}(x)f_+^\dagger(x)$$
$$-2\Lambda_{--}(x)\xi_{-,2}(x)f_-^\dagger(x)+\Lambda_{+-}\delta(x)\Big(\xi_{+,2}(x)f_-^\dagger(x)-\xi_{-,2}(x)f_+^\dagger(x)\Big)$$
$$+2\Lambda_{++}^*(x)\xi_{+,1}(x)f_+(-x)+2\Lambda_{--}^*(x)\xi_{-,1}(x)f_-(-x)$$
$$+\Lambda_{+-}\delta(x)\Big(\xi_{+,1}(x)f_-(-x)-\xi_{-,1}(x)f_+(-x)\Big).$$

Looking at $f_-^\dagger,\ f_+^\dagger,\ f_-$, and f_+ terms separately, we find the BdG equations (corresponding to Eqs. (35) in Ref. [30], in which Λ functions have been chosen to be real – see Eq. (B.43)):

$$\begin{aligned}
i\nu\partial_x\xi_{-,1}(x)-i\Lambda_{--}(x)\xi_{-,2}(x)+\frac{i}{2}\Lambda_{+-}\delta(x)\xi_{+,2}(x)&=0,\\
E_+\xi_{+,1}(x)-i\Lambda_{++}(x)\xi_{+,2}(x)-\frac{i}{2}\Lambda_{+-}\delta(x)\xi_{-,2}(x)&=0,\\
-i\nu\partial_x\xi_{-,2}(x)+i\Lambda_{--}^*(x)\xi_{-,1}(x)+\frac{i}{2}\Lambda_{+-}\delta(x)\xi_{+,1}(x)&=0,\\
-E_+\xi_{+,2}(x)+i\Lambda_{++}^*(x)\xi_{+,1}(x)-\frac{i}{2}\Lambda_{+-}\delta(x)\xi_{-,1}(x)&=0.
\end{aligned}\tag{B.52}$$

Finding the ξ_+ functions in terms of the ξ_- functions can be done via the second and fourth of these equations, giving (Eq. (36) [30])

$$\begin{aligned}
\frac{i}{2}\Lambda_{+-}\delta(x)\begin{pmatrix}\xi_{-,2}(x)\\ \xi_{-,1}(x)\end{pmatrix}&=\begin{pmatrix}E_+ & -i\Lambda_{++}(x)\\ i\Lambda_{++}^*(x) & -E_+\end{pmatrix}\begin{pmatrix}\xi_{+,1}(x)\\ \xi_{+,2}(x)\end{pmatrix}\\
\Rightarrow\begin{pmatrix}\xi_{+,1}(x)\\ \xi_{+,2}(x)\end{pmatrix}&=\frac{\frac{i}{2}\Lambda_{+-}\delta(x)}{|\Lambda_{++}(x)|^2+E_+^2}\begin{pmatrix}E_+ & -i\Lambda_{++}(x)\\ i\Lambda_{++}^*(x) & -E_+\end{pmatrix}\begin{pmatrix}\xi_{-,2}(x)\\ \xi_{-,1}(x)\end{pmatrix}.
\end{aligned}\tag{B.53}$$

Now we can substitute these into the first and third equations. Similarly to Eqs. (37) [30], the first equation leads to

$$\begin{aligned}
&i\nu\partial_x\xi_{-,1}(x) - i\Lambda_{--}(x)\xi_{-,2}(x) + \frac{i}{2}\Lambda_{+-}\delta(x)\left[\frac{i\Lambda_{+-}\delta(x)}{2(|\Lambda_{++}(x)|^2+E_+^2)}\Big(i\Lambda^*_{++}(x)\xi_{-,2}(x)\right.\\
&\quad\left.-E_+\xi_{-,1}(x)\Big)\right] = 0\\
&\Rightarrow i\nu\partial_x\xi_{-,1}(x) + \frac{1}{4}\frac{\Lambda^2_{+-}\delta^2(x)E_+}{|\Lambda_{++}(x)|^2+E_+^2}\xi_{-,1}(x) - i\left(\Lambda_{--}(x) + \frac{1}{4}\frac{\Lambda^2_{+-}\delta^2(x)\Lambda^*_{++}(x)}{|\Lambda_{++}(x)|^2+E_+^2}\right)\\
&\quad\cdot\xi_{-,2}(x) = 0,
\end{aligned}$$

while the third equation yields

$$\begin{aligned}
&-i\nu\partial_x\xi_{-,2}(x) + i\Lambda^*_{--}(x)\xi_{-,1}(x) + \frac{i}{2}\Lambda_{+-}\delta(x)\left[\frac{i\Lambda_{+-}\delta(x)}{2(|\Lambda_{++}(x)|^2+E_+^2)}\Big(E_+\xi_{-,2}(x)\right.\\
&\quad\left.-i\Lambda_{++}(x)\xi_{-,1}(x)\Big)\right] = 0\\
&\Rightarrow -i\nu\partial_x\xi_{-,2}(x) - \frac{1}{4}\frac{\Lambda^2_{+-}\delta^2(x)E_+}{|\Lambda_{++}(x)|^2+E_+^2}\xi_{-,2}(x) + i\left(\Lambda^*_{--}(x) + \frac{1}{4}\frac{\Lambda^2_{+-}\delta^2(x)\Lambda_{++}(x)}{|\Lambda_{++}(x)|^2+E_+^2}\right)\\
&\quad\cdot\xi_{-,1}(x) = 0.
\end{aligned}$$

Multiplying by $\exp\left(-i\frac{1}{4\nu}\int_0^x dx'\frac{\Lambda^2_{+-}\delta^2(x')E_+}{|\Lambda_{++}(x')|^2+E_+^2}\right)$ and defining

$$\psi_n(x) = \exp\left(-i\frac{1}{4\nu}\int_0^x dx'\frac{\Lambda^2_{+-}\delta^2(x')E_+}{|\Lambda_{++}(x')|^2+E_+^2}\right)\xi_{-,n}(x), \tag{B.54}$$

we find (similarly to Eqs. (39) [30])

$$\begin{aligned}
\nu\partial_x\psi_1(x) - \left(\Lambda_{--}(x) + \frac{1}{4}\frac{\Lambda^2_{+-}\delta^2(x)\Lambda^*_{++}(x)}{|\Lambda_{++}(x)|^2+E_+^2}\right)\psi_2(x) = 0,\\
\nu\partial_x\psi_2(x) - \left(\Lambda^*_{--}(x) + \frac{1}{4}\frac{\Lambda^2_{+-}\delta^2(x)\Lambda_{++}(x)}{|\Lambda_{++}(x)|^2+E_+^2}\right)\psi_1(x) = 0,
\end{aligned} \tag{B.55}$$

or, finally (similarly to Eqs. (40) [30]),

$$\nu\partial_x\begin{pmatrix}\psi_1(x)\\ \psi_2^*(x)\end{pmatrix} = m(x)\sigma_x\begin{pmatrix}\psi_1^*(x)\\ \psi_2(x)\end{pmatrix}. \tag{B.56}$$

Here we have defined a spatially varying mass term,

$$m(x) = \left(\Lambda_{--}(x) + \frac{1}{4}\frac{\Lambda^2_{+-}\delta^2(x)\Lambda^*_{++}(x)}{|\Lambda_{++}(x)|^2+E_+^2}\right). \tag{B.57}$$

Clearly $m(x)$ is odd in x, as $\Lambda_{++}(x)$ and $\Lambda_{--}(x)$ are odd in x.

Note that in general $m(x)$ can have any phase (dependent on the phase of diagonalized f operators in terms of c operators), as $\Lambda_{++}(x)$ and $\Lambda_{--}(x)$ have an arbitrary phase (see

Eq. (B.43)). However, for simplicity, in Ref. [30] $\Lambda(x)$ functions and therefore $m(x)$ have been chosen real.

The general solution to the BdG equations (B.56) is of the form,

$$\begin{aligned}\psi_1(x) &= A_1 \exp\left(\frac{1}{\nu}\int_0^x \tilde{m}(y)dy\right) + B_1 \exp\left(-\frac{1}{\nu}\int_0^x \tilde{m}(y)dy\right),\\ \psi_2^*(x) &= A_2 \exp\left(\frac{1}{\nu}\int_0^x \tilde{m}(y)dy\right) + B_2 \exp\left(-\frac{1}{\nu}\int_0^x \tilde{m}(y)dy\right),\end{aligned} \tag{B.58}$$

where $\tilde{m}(x) \equiv \text{sign}(x)|m(x)|$, and for $m(x) = e^{i\theta}\tilde{m}(x)$ we have

$$A_2 = e^{i\theta}A_1^*, \qquad\qquad B_2 = -e^{i\theta}B_1^*, \tag{B.59}$$

or finally,

$$\begin{aligned}\psi_1(x) &= C \exp\left(\frac{\lambda}{\nu}\int_0^x \tilde{m}(y)dy\right),\\ \psi_2^*(x) &= e^{i\theta}C^* \,\text{sign}(\lambda) \exp\left(\frac{\lambda}{\nu}\int_0^x \tilde{m}(y)dy\right),\end{aligned} \tag{B.60}$$

where $\lambda = \pm 1$.

The BdG equations (B.56) are of a form similar to the Dirac problem. In particular, if $\psi(x) = (\psi_1(x), \psi_2^*(x))^T$ is a solution to (B.56), then $\sigma_x\psi(x)$ is also a solution. Therefore for a unique zero-energy solution to exist, we must have $\psi(x)$ an eigenspinor of σ_x, with $\sigma_x\psi(x) = \lambda\psi(x)$. Setting

$$\sigma_x \begin{pmatrix} C \\ e^{i\theta}C^* \text{sign}(\lambda) \end{pmatrix} = \lambda \begin{pmatrix} C \\ e^{i\theta}C^* \text{sign}(\lambda) \end{pmatrix}, \tag{B.61}$$

we find $C = e^{i\theta}C^*$, or

$$C = |C|e^{i\theta/2}. \tag{B.62}$$

Therefore we have the unique zero-energy solution:

$$\begin{aligned}\psi_1(x) &= |C|e^{i\theta/2} \exp\left(\frac{\lambda}{\nu}\int_0^x \tilde{m}(y)dy\right),\\ \psi_2(x) &= |C|e^{-i\theta/2} \text{sign}(\lambda) \exp\left(\frac{\lambda}{\nu}\int_0^x \tilde{m}(y)dy\right),\end{aligned} \tag{B.63}$$

where θ is determined by the definition of diagonalized f operators in terms of c operators (specifically, we have $\theta = 2\phi \pm \pi$, from Eqs. (B.43) and (B.57)).

Note that, as we chose $\tilde{m}(x) \equiv \text{sign}(x)|m(x)|$, (B.63) is normalizable only for $\lambda = -1$; however, we will see that it is Majorana only for $\lambda = +1$. As this solution is an approximation to the true solution, however, and in practice the Majorana mode will be localized near the vortex core, this Majorana solution is still worth considering.

B.5 Demonstration of the Majorana condition

A Majorana solution is found from (B.63) in the case $\lambda = 1$. To demonstrate that $\gamma^\dagger$ is a Majorana fermion in this case, i.e., $\gamma^\dagger = \gamma$, we need to show that (Eq. (41) [30])

$$\eta^*_{\pm,1}(-x) = \eta_{\pm,2}(x), \tag{B.64}$$

as this would give (see Eq. (B.46))

$$\begin{aligned}\gamma &= \int_{-\infty}^{\infty} dx \left(\eta^*_{+,1}(x)f_+(x) + \eta^*_{-,1}(x)f_-(x) + \eta^*_{+,2}(x)f^\dagger_+(-x) + \eta^*_{-,2}(x)f^\dagger_-(-x)\right)\\ &= \int_{-\infty}^{\infty} dx \left(\eta_{+,2}(x)f_+(-x) + \eta_{-,2}(x)f_-(-x) + \eta_{+,1}(x)f^\dagger_+(x) + \eta_{-,1}(x)f^\dagger_-(x)\right)\\ &= \gamma^\dagger.\end{aligned}$$

To demonstrate (B.64), note that (Eq. (42) [30])

$$\begin{aligned}S^*_+(y-x) &= \int_0^{\infty} dk\, e^{-ik(y-x)} = S_+(x-y),\\ S^*_-(y-x) &= \int_{-k_F}^{\infty} dk\, e^{-ik(y-x)} = S_-(x-y).\end{aligned} \tag{B.65}$$

Then this condition translates into showing (Eq. (43) [30])

$$\xi^*_{\pm,n}(-x) = \xi_{\pm,\bar{n}}(x), \tag{B.66}$$

where $\bar{n} = 1$ for $n = 2$, and vice-versa, as $\xi_{\pm,\bar{n}}(x) = \int_{-\infty}^{\infty} S_\pm(y-x)\eta_{\pm,\bar{n}}(y)dy$, and

$$\begin{aligned}\xi^*_{\pm,n}(-x) &= \int_{-\infty}^{\infty} S^*_\pm(y+x)\eta^*_{\pm,n}(y)dy = \int_{-\infty}^{\infty} S_\pm(-y-x)\eta^*_{\pm,n}(y)dy\\ &= \int_{-\infty}^{\infty} S_\pm(y-x)\eta^*_{\pm,n}(-y)dy.\end{aligned} \tag{B.67}$$

To show that $\xi^*_{\pm,n}(-x) = \xi_{\pm,\bar{n}}(x)$, look at the solution (B.63) to the BdG equations. Then we find, for $\lambda = 1$,

$$\xi_{-,1}(x) = |C|e^{i\theta/2}\exp\left(\frac{i}{4\nu}\int_0^x dx' \frac{|\Lambda_{+-}|^2\delta^2(x')E_+}{|\Lambda_{++}(x')|^2 + E_+^2}\right)\exp\left(\frac{1}{\nu}\int_0^x \tilde{m}(y)dy\right), \tag{B.68}$$

$$\xi_{-,2}(x) = |C|e^{-i\theta/2}\exp\left(\frac{i}{4\nu}\int_0^x dx' \frac{|\Lambda_{+-}|^2\delta^2(x')E_+}{|\Lambda_{++}(x')|^2 + E_+^2}\right)\exp\left(\frac{1}{\nu}\int_0^x \tilde{m}(y)dy\right), \tag{B.69}$$

giving

$$\begin{aligned}\xi^*_{-,1}(-x) &= |C|e^{-i\theta/2}\exp\left(\frac{-i}{4\nu}\int_0^{-x} dx' \frac{|\Lambda_{+-}|^2\delta^2(x')E_+}{|\Lambda_{++}(x')|^2 + E_+^2}\right)\exp\left(\frac{1}{\nu}\int_0^{-x} \tilde{m}(y)dy\right)\\ &= |C|e^{-i\theta/2}\exp\left(\frac{i}{4\nu}\int_0^{x} dx'' \frac{|\Lambda_{+-}|^2\delta^2(x'')E_+}{|\Lambda_{++}(x'')|^2 + E_+^2}\right)\exp\left(\frac{1}{\nu}\int_0^{x} \tilde{m}(y')dy'\right)\\ &= \xi_{-,2}(x),\end{aligned}$$

as the first integrand is even and the second is odd. For the upper band, using Eq. (B.53), one has

$$\begin{aligned}\xi_{+,1}(x) &= \frac{i\Lambda_{+-}\delta(x)}{2(|\Lambda_{++}(x)|^2+E_+^2)}\left(E_+\xi_{-,2}(x)-i\Lambda_{++}(x)\xi_{-,1}(x)\right),\\ \xi_{+,2}(x) &= \frac{i\Lambda_{+-}\delta(x)}{2(|\Lambda_{++}(x)|^2+E_+^2)}\left(i\Lambda_{++}^*(x)\xi_{-,2}(x)-E_+\xi_{-,1}(x)\right).\end{aligned} \tag{B.70}$$

Then

$$\begin{aligned}\xi_{+,1}^*(-x) &= \frac{-i\Lambda_{+-}\delta(-x)}{2(|\Lambda_{++}(-x)|^2+E_+^2)}\left(E_+\xi_{-,2}^*(-x)+i\Lambda_{++}^*(-x)\xi_{-,1}^*(-x)\right)\\ &= -\frac{i\Lambda_{+-}\delta(x)}{2(|\Lambda_{++}(x)|^2+E_+^2)}\left(E_+\xi_{-,1}(x)-i\Lambda_{++}^*(x)\xi_{-,2}(x)\right)\\ &= \xi_{+,2}(x).\end{aligned}$$

Therefore the conditions (B.66) (and (B.64)) hold, and $\gamma^\dagger=\gamma$ is a Majorana fermion operator.

The authors of Ref. [30] go on to show that furthermore, this excitation is topologically protected, so that a Majorana zero-mode will exist even for an anisotropic (i.e., breaking rotational symmetry near the vortex) and strong-pairing Hamiltonian, so long as a bulk phase transition is not crossed, that is, the bulk gap does not close.

Appendix C

Calculation and Comparison of Majorana Wave Functions

C.1 Calculation of Majorana Wave Functions

In this section we calculate the η wave functions of the Majorana modes (see Eq. (5.22)) found in our index theorem in chapter 5. Finding the η wave functions will allow us to compare the Majorana modes about $k \sim 0$ and $\boldsymbol{k} \sim (\pi, \pi)$, which we do in Section C.2.

Computing η's is a long process, as we need to find the Λ functions associated with the SC vortex pairing in momentum space (see Eq. (5.18)), Fourier transform them to real space, substitute them into the ξ functions (see Eqs. (5.31) and (5.34) for $k \sim 0$ and (5.37)-(5.39) for $\boldsymbol{k} \sim (\pi, \pi)$) and finally compute the η wave functions from the definition of ξ's (see Eqs. (5.24) and (5.25)).

C.1.1 Calculation of Lambda functions

To calculate the Λ functions in momentum space, we start with the definitions (see Appendix B, Section B.4.1),

$$\begin{aligned} \Lambda_{++}(k,p) &:= \Delta(k,p)a_k^* b_p^* - \Delta(p,k)a_p^* b_k^*, \\ \Lambda_{--}(k,p) &:= -\Delta(k,p)a_p b_k + \Delta(p,k)a_k b_p, \\ \Lambda_{+-}(k,p) &:= \Delta(k,p)a_k^* a_p + \Delta(p,k)b_p b_k^*, \end{aligned} \tag{C.1}$$

which have the same form whether they are in terms of k or $\tilde{k}$. Here a_k and b_k are components of the matrix diagonalizing the single-electron Hamiltonian, and (see Appendix B Section B.3, Eq. (B.17) onwards)

$$\Delta(k,p) = \Delta_0 \sqrt{kp}(k\, u_{-1}(k,p) + p\, u_0(k,p)), \tag{C.2}$$

with u_m a Fourier component of $1/|\boldsymbol{k}+\boldsymbol{p}|^3$.

To begin, we look at the unitary transformations from the $c_{k,\sigma}^\dagger \equiv c_{m_J=1/2,k,\sigma}^\dagger$ operators to the diagonalized $f_{\pm,k}^\dagger$ operators. In general, we have

$$\begin{pmatrix} f_{+,k}^\dagger \\ f_{-,k}^\dagger \end{pmatrix} = \begin{pmatrix} a_k & b_k \\ -b_k^* & a_k^* \end{pmatrix} \begin{pmatrix} c_{k,\uparrow}^\dagger \\ c_{k,\downarrow}^\dagger \end{pmatrix}, \tag{C.3}$$

with $|a_k|^2 + |b_k|^2 = 1$. For $k \sim 0$, our Hamiltonian (5.9) gives

$$a_k = e^{i\phi}\frac{1}{\sqrt{2}}\frac{\alpha k}{\sqrt{h^2+\alpha^2k^2+h\sqrt{h^2+\alpha^2k^2}}}, \qquad b_k = -ie^{i\phi}\frac{1}{\sqrt{2}}\sqrt{1+\frac{h}{\sqrt{h^2+\alpha^2k^2}}}, \tag{C.4}$$

while for $\boldsymbol{k} \sim (\pi, \pi)$, with $\tilde{\boldsymbol{k}} = \boldsymbol{k} - (\pi, \pi)$, Hamiltonian (5.12) gives

$$\tilde{a}_{\tilde{k}} = e^{i\tilde{\phi}} \frac{1}{\sqrt{2}} \frac{\alpha \tilde{k}}{\sqrt{h^2 + \alpha^2 \tilde{k}^2 + h\sqrt{h^2 + \alpha^2 \tilde{k}^2}}}, \qquad \tilde{b}_{\tilde{k}} = +ie^{i\tilde{\phi}} \frac{1}{\sqrt{2}} \sqrt{1 + \frac{h}{\sqrt{h^2 + \alpha^2 \tilde{k}^2}}}, \tag{C.5}$$

where ϕ and $\tilde{\phi}$ are arbitrary phase factors. This follows from diagonalizing Hamiltonians (5.9) and (5.12):

$$\begin{aligned} \mathcal{H}_0^0(k) &\simeq \left(c_{k,\uparrow}^\dagger, c_{k,\downarrow}^\dagger\right) \begin{pmatrix} (-4t + tk^2 - h) & i\alpha k \\ -i\alpha k & (-4t + tk^2 + h) \end{pmatrix} \begin{pmatrix} c_{k,\uparrow} \\ c_{k,\downarrow} \end{pmatrix} \\ &= \left(f_{+,k}^{\dagger 0}, f_{-,k}^{\dagger 0}\right) \begin{pmatrix} E_+^0(k) & 0 \\ 0 & E_-^0(k) \end{pmatrix} \begin{pmatrix} f_{+,k}^0 \\ f_{-,k}^0 \end{pmatrix}, \end{aligned} \tag{C.6}$$

$$\begin{aligned} \mathcal{H}_0^\pi(\tilde{k}) &\simeq \left(c_{\tilde{k},\uparrow}^\dagger, c_{\tilde{k},\downarrow}^\dagger\right) \begin{pmatrix} (4t - t\tilde{k}^2 - h) & -i\alpha \tilde{k} \\ i\alpha \tilde{k} & (4t - t\tilde{k}^2 + h) \end{pmatrix} \begin{pmatrix} c_{\tilde{k},\uparrow} \\ c_{\tilde{k},\downarrow} \end{pmatrix} \\ &= \left(f_{+,\tilde{k}}^{\dagger \pi}, f_{-,\tilde{k}}^{\dagger \pi}\right) \begin{pmatrix} -E_-^0(\tilde{k}) & 0 \\ 0 & -E_+^0(\tilde{k}) \end{pmatrix} \begin{pmatrix} f_{+,\tilde{k}}^\pi \\ f_{-,\tilde{k}}^\pi \end{pmatrix}, \end{aligned} \tag{C.7}$$

with eigenvalues (setting $\mu \approx 0$)

$$E_\pm^0(k) \approx -4t + tk^2 \pm \sqrt{\alpha^2 k^2 + h^2}, \tag{C.8}$$

where we have used the fact that the upper and lower bands flip orientation between $k \sim 0$ and $\boldsymbol{k} \sim (\pi, \pi)$ (see Eq. (5.16)),

$$E_+^\pi(\tilde{k}) = -E_-^0(\tilde{k}), \qquad E_-^\pi(\tilde{k}) = -E_+^0(\tilde{k}). \tag{C.9}$$

To find the Λ functions, we must also calculate the Fourier components in Eq. (C.2). Using reverse Fourier transforms, we get

$$\begin{aligned} u_m(k,p) &\equiv \int \frac{1}{|\boldsymbol{k} + \boldsymbol{p}|^3} e^{-im(\theta_{\boldsymbol{k}} - \theta_{\boldsymbol{p}})} d(\theta_{\boldsymbol{k}} - \theta_{\boldsymbol{p}}) \\ &= \int_{-\pi}^{\pi} \left(k^2 + p^2 - 2kp\cos\theta\right)^{-3/2} e^{-im\theta} d\theta, \end{aligned}$$

where $\theta = \theta_{\boldsymbol{k}} - \theta_{\boldsymbol{p}}$. Note that all u_m will be real, as the imaginary part of the integrand is odd in θ. First calculating $u_0(k,p)$, we have

$$u_0(k,p) = \int_{-\pi}^{\pi} \left(k^2 + p^2 - 2kp\cos\theta\right)^{-3/2} d\theta = \frac{4\,\mathrm{E}\left[-\frac{4kp}{(k-p)^2}\right]}{(k+p)^2 |k-p|}. \tag{C.10}$$

Now calculating $u_{-1}(k,p)$, we have

$$\begin{aligned} u_{-1}(k,p) &= \int_{-\pi}^{\pi} \left(k^2 + p^2 - 2kp\cos\theta\right)^{-3/2} \cos\theta d\theta \\ &= \frac{2\left((k^2 + p^2)\mathrm{E}\left[-\frac{4kp}{(k-p)^2}\right] - (k+p)^2\,\mathrm{K}\left[-\frac{4kp}{(k-p)^2}\right]\right)}{kp(k+p)^2\,|k-p|}. \end{aligned} \tag{C.11}$$

Here $\mathrm{K}(x)$ and $\mathrm{E}(x)$ are complete elliptic integrals of the first and second kinds, respectively. They can be defined in terms of the hypergeometric function ${}_2F_1$ by

$$\mathrm{K}(x) = \frac{\pi}{2}\,{}_2F_1(\tfrac{1}{2},\tfrac{1}{2};1;x^2) = \frac{\pi}{2}\sum_{n=0}^{\infty}\left(\frac{(2n-1)!!}{(2n)!!}\right)^2 x^{2n},$$

$$\mathrm{E}(x) = \frac{\pi}{2}\,{}_2F_1(-\tfrac{1}{2},\tfrac{1}{2};1;x^2) = \frac{\pi}{2}\left[1-\sum_{n=1}^{\infty}\left(\frac{(2n-1)!!}{(2n)!!}\right)^2\frac{x^{2n}}{(2n-1)}\right].$$

Therefore for $\Delta(k,p)$ (Eq. (C.2)) one finds

$$\begin{aligned}\Delta(k,p) &= \Delta_0\sqrt{kp}\left[k\cdot\frac{2\left((k^2+p^2)\mathrm{E}\left[-\frac{4kp}{(k-p)^2}\right]-(k+p)^2\,\mathrm{K}\left[-\frac{4kp}{(k-p)^2}\right]\right)}{kp(k+p)^2\,|k-p|}+p\cdot\frac{4\,\mathrm{E}\left[-\frac{4kp}{(k-p)^2}\right]}{(k+p)^2|k-p|}\right]\\ &= \Delta_0\sqrt{kp}\left[\frac{2(k^2+3p^2)\,\mathrm{E}\left[-\frac{4kp}{(k-p)^2}\right]}{p(k+p)^2|k-p|}-\frac{2\,\mathrm{K}\left[-\frac{4kp}{(k-p)^2}\right]}{p|k-p|}\right].\end{aligned} \tag{C.12}$$

First let us look at $\Lambda_{+-}(k,p)$. In the continuum model [30], it is assumed that $\Lambda_{+-}(q,k_F+q')$ is a non-zero constant Λ_{+-} in the limit of $q,q'\to 0$. It can be shown, however, that Λ_{+-} is indeed zero, and that the BdG equations simplify in this case. To calculate the constant Λ_{+-}, we use the definition (C.1), where substitution yields

$$\begin{aligned}\Lambda_{+-}(k,p) = \Delta_0\sqrt{kp}\Bigg\{&\left[\frac{2(k^2+3p^2)\,\mathrm{E}\left[-\frac{4kp}{(k-p)^2}\right]}{p(k+p)^2|k-p|}-\frac{2\,\mathrm{K}\left[-\frac{4kp}{(k-p)^2}\right]}{p|k-p|}\right]\frac{1}{2}\frac{\alpha k}{\sqrt{h^2+\alpha^2k^2+h\sqrt{h^2+\alpha^2k^2}}}\\ &\cdot\frac{\alpha p}{\sqrt{h^2+\alpha^2p^2+h\sqrt{h^2+\alpha^2p^2}}}+\left[\frac{2(p^2+3k^2)\,\mathrm{E}\left[-\frac{4kp}{(k-p)^2}\right]}{k(k+p)^2|k-p|}-\frac{2\,\mathrm{K}\left[-\frac{4kp}{(k-p)^2}\right]}{k|k-p|}\right]\\ &\cdot\frac{1}{2}\sqrt{1+\frac{h}{\sqrt{h^2+\alpha^2p^2}}}\sqrt{1+\frac{h}{\sqrt{h^2+\alpha^2k^2}}}\Bigg\}.\end{aligned} \tag{C.13}$$

Around $k\sim 0$ we have the Fermi momentum in the upper band, and so take $k=k_F+q$, $p=q'$ where $q,\ q'\to 0$. In this limit, the argument of the elliptic functions goes to zero. Both elliptic functions give the constant $\pi/2$ in this limit. Therefore, simplifying yields

$$\begin{aligned}\Lambda^0_{+-}(k,p) &\approx \frac{\pi}{2}\Delta_0 k^{1/2}p^{1/2}\Bigg\{\frac{\alpha^2}{\sqrt{2}h}\frac{1}{\sqrt{h^2+\alpha^2k_F^2+h\sqrt{h^2+\alpha^2k_F^2}}}\left(\frac{k(k^2+3p^2)}{(k+p)^2|k-p|}-\frac{k}{|k-p|}\right)\\ &\quad+\sqrt{2}\sqrt{1+\frac{h}{\sqrt{h^2+\alpha^2k_F^2}}}\left(\frac{(p^2+3k^2)}{k(k+p)^2|k-p|}-\frac{1}{k|k-p|}\right)\Bigg\}\\ &= \mathrm{sign}(k-p)\frac{\pi}{2}\Delta_0\frac{k^{1/2}p^{1/2}}{(k+p)^2}\left\{-\frac{\alpha^2}{\sqrt{2}h}\frac{2kp}{\sqrt{h^2+\alpha^2k_F^2+h\sqrt{h^2+\alpha^2k_F^2}}}+2\sqrt{2}\sqrt{1+\frac{h}{\sqrt{h^2+\alpha^2k_F^2}}}\right\},\end{aligned} \tag{C.14}$$

or, substituting for k and p and taking the limit,

$$\Lambda^0_{+-}(q,q') \approx \frac{\sqrt{2}\pi}{k_F^{3/2}}\Delta_0\, q'^{1/2}\sqrt{1+\frac{h}{\sqrt{h^2+\alpha^2k_F^2}}}\,. \tag{C.15}$$

Therefore $\Lambda^0_{+-}(q,q')$ goes to zero as $q'^{1/2}$ as $q' \to 0$. Similarly, for $\boldsymbol{k} \sim (\pi,\pi)$ the Fermi momentum k_F is in the lower band, so we take $\tilde{k} = q$, $\tilde{p} = k_F + q'$ with $q,\ q' \to 0$. This yields the same as (C.14) (but with $\tilde{k}$ and $\tilde{p}$). Substituting and taking the limit yields

$$\Lambda^\pi_{+-}(q,q') \approx -\frac{\sqrt{2}\pi}{k_F^{3/2}}\Delta_0\, q^{1/2}\sqrt{1+\frac{h}{\sqrt{h^2+\alpha^2k_F^2}}}\,. \tag{C.16}$$

which goes to zero as $q^{1/2}$.

One can therefore approximate the BdG equations using $\Lambda_{+-} = 0$. As we will show when calculating the ξ functions in the next subsection, under this approximation the BdG equations for upper and lower bands decouple, and we are left with a mass term (see Eqs. (5.31) and (5.38))

$$m^0(x) \approx \Lambda^0_{++}(x)$$

for $k \sim 0$, and

$$m^\pi(x) \approx \Lambda^\pi_{--}(x)$$

for $\boldsymbol{k} \sim (\pi,\pi)$.

Now let us calculate $\Lambda^0_{++}(q,q')$ and $\Lambda^\pi_{--}(q,q')$. First looking at $\Lambda_{++}(k,p)$, going back to the definition (C.1) and substituting yields

$$\begin{aligned}\Lambda_{++}(k,p) = \pm\Delta_0\sqrt{kp}\,\frac{ie^{-i2\phi}}{2}\Bigg\{&\left[\frac{2(k^2+3p^2)\,\mathrm{E}\left[-\frac{4kp}{(k-p)^2}\right]}{p(k+p)^2|k-p|} - \frac{2\,\mathrm{K}\left[-\frac{4kp}{(k-p)^2}\right]}{p|k-p|}\right]\\ &\cdot\frac{\alpha k}{\sqrt{h^2+\alpha^2k^2+h\sqrt{h^2+\alpha^2k^2}}}\sqrt{1+\frac{h}{\sqrt{h^2+\alpha^2p^2}}} - \Bigg[\frac{2(p^2+3k^2)\,\mathrm{E}\left[-\frac{4kp}{(k-p)^2}\right]}{k(k+p)^2|k-p|}\\ &-\frac{2\,\mathrm{K}\left[-\frac{4kp}{(k-p)^2}\right]}{k|k-p|}\Bigg]\frac{\alpha p}{\sqrt{h^2+\alpha^2p^2+h\sqrt{h^2+\alpha^2p^2}}}\sqrt{1+\frac{h}{\sqrt{h^2+\alpha^2k^2}}}\Bigg\},\end{aligned}$$

where plus and minus signs are for $k \sim 0$ and $\tilde{k} \sim 0$ (substituting $\tilde{k}$ for k and $\tilde{p}$ for p), respectively. Around $k \sim 0$, linearizing by $k = k_F + q$, $p = k_F + q'$, for small $q,\ q'$, yields

$$\begin{aligned}\Lambda^0_{++}(k,p) \approx \frac{ie^{-i2\phi}}{2}\frac{\alpha\Delta_0}{\sqrt{h^2+\alpha^2k_F^2}}k^{1/2}p^{1/2}\Bigg\{&\sqrt{\frac{4kp}{(k-p)^2}}\left[\frac{2(k^2+3p^2)k}{p(k+p)^2|k-p|} - \frac{2(p^2+3k^2)p}{k(k+p)^2|k-p|}\right]\\ &+\sqrt{\frac{(k-p)^2}{4kp}}\left(\frac{1}{2}\log\left(\frac{4kp}{(k-p)^2}\right)+\log 4\right)\left[-\frac{2k}{p|k-p|}+\frac{2p}{k|k-p|}\right]\Bigg\}\end{aligned}$$

where we have used the expansions

$$\begin{aligned} \mathrm{E}(-x) &\approx \sqrt{x} + \mathcal{O}\left(\sqrt{\frac{1}{x}}\log(x)\right), \qquad x \to \infty, \\ \mathrm{K}(-x) &\approx \sqrt{\frac{1}{x}}\left(\frac{1}{2}\log(x) + \log 4\right) + \mathcal{O}\left(\left(\frac{1}{x}\right)^{3/2}\log(x)\right), \qquad x \to \infty. \end{aligned} \tag{C.17}$$

Therefore about $k \sim 0$ we have

$$\Lambda^0_{++}(q,q') \approx \frac{ie^{-i2\phi}}{2}\frac{2\alpha\Delta_0}{\sqrt{h^2+\alpha^2k_F^2}}\left\{\frac{k_F+(q+q')}{(q-q')} - \frac{1}{4}\left(\frac{1}{2}\log\left(\frac{4k_F^2}{(q-q')^2}\right)+\log 4\right)\frac{2(q-q')}{k_F+(q+q')}\right\},$$

or

$$\Lambda^0_{++}(q,q') \approx ie^{-i2\phi}\frac{2\alpha\Delta_0 k_F}{\sqrt{h^2+\alpha^2k_F^2}}\frac{1}{(q-q')}. \tag{C.18}$$

Now, looking at $\Lambda_{--}(k,p)$, substituting into definition (C.1) yields

$$\begin{aligned} \Lambda_{--}(k,p) = \mp\Delta_0\sqrt{kp}\,\frac{ie^{i2\phi}}{2}\Bigg\{ &-\left[\frac{2(k^2+3p^2)\,\mathrm{E}\left[-\frac{4kp}{(k-p)^2}\right]}{p(k+p)^2|k-p|} - \frac{2\,\mathrm{K}\left[-\frac{4kp}{(k-p)^2}\right]}{p|k-p|}\right] \\ &\cdot\frac{\alpha p}{\sqrt{h^2+\alpha^2p^2+h\sqrt{h^2+\alpha^2p^2}}}\sqrt{1+\frac{h}{\sqrt{h^2+\alpha^2k^2}}} + \left[\frac{2(p^2+3k^2)\,\mathrm{E}\left[-\frac{4kp}{(k-p)^2}\right]}{k(k+p)^2|k-p|}\right. \\ &\left. - \frac{2\,\mathrm{K}\left[-\frac{4kp}{(k-p)^2}\right]}{k|k-p|}\right]\frac{\alpha k}{\sqrt{h^2+\alpha^2k^2+h\sqrt{h^2+\alpha^2k^2}}}\sqrt{1+\frac{h}{\sqrt{h^2+\alpha^2p^2}}}\Bigg\}, \end{aligned}$$

with minus sign for $k \sim 0$ and plus sign for $\tilde{k} \sim 0$. For $\boldsymbol{k} \sim (\pi,\pi)$, linearizing with $\tilde{k} = k_F + q$, $\tilde{p} = k_F + q'$, for small $q,\ q'$, one has

$$\begin{aligned} \Lambda^\pi_{--}(\tilde{k},\tilde{p}) \approx -\frac{ie^{i2\phi}}{2}\frac{\alpha\Delta_0}{\sqrt{h^2+\alpha^2k_F^2}}\tilde{k}^{1/2}\tilde{p}^{1/2}\Bigg\{ &\sqrt{\frac{4\tilde{k}\tilde{p}}{(\tilde{k}-\tilde{p})^2}}\left[\frac{2(\tilde{k}^2+3\tilde{p}^2)}{(\tilde{k}+\tilde{p})^2|\tilde{k}-\tilde{p}|} - \frac{2(\tilde{p}^2+3\tilde{k}^2)}{(\tilde{k}+\tilde{p})^2|\tilde{k}-\tilde{p}|}\right] \\ &+\sqrt{\frac{(\tilde{k}-\tilde{p})^2}{4\tilde{k}\tilde{p}}}\left(\frac{1}{2}\log\left(\frac{4\tilde{k}\tilde{p}}{(\tilde{k}-\tilde{p})^2}\right)+\log 4\right)\left[-\frac{2\tilde{p}}{\tilde{p}|\tilde{k}-\tilde{p}|} + \frac{2\tilde{k}}{\tilde{k}|\tilde{k}-\tilde{p}|}\right]\Bigg\}, \end{aligned}$$

or

$$\Lambda^\pi_{--}(q,q') \approx ie^{i2\tilde{\phi}}\frac{2\alpha\Delta_0 k_F}{\sqrt{h^2+\alpha^2k_F^2}}\frac{1}{(q-q')}. \tag{C.19}$$

We now have all the Λ functions that will be needed, and can Fourier-transform them to real space. Due to the definition of the Fourier transforms (e.g., for $k \sim 0$, where transforms

for $\boldsymbol{k} \sim (\pi, \pi)$ will have bands reversed),

$$f_+^\dagger(x) = \int_{-k_F}^{\Omega} dq\, e^{iqx} f_{+,k_F+q}^\dagger,$$
$$f_-^\dagger(x) = \int_0^{\Omega} dq\, e^{iqx} f_{-,q}^\dagger,$$

transformation of the Λ functions is easier to see in reverse. We have the real-space Λ functions:

$$\Lambda_{++}^0(x) = e^{-i2\phi} \frac{\alpha \Delta_0 k_F}{\sqrt{h^2 + \alpha^2 k_F^2}} \mathrm{sign}(x), \qquad \Lambda_{--}^\pi(x) = e^{i2\tilde{\phi}} \frac{\alpha \Delta_0 k_F}{\sqrt{h^2 + \alpha^2 k_F^2}} \mathrm{sign}(x). \tag{C.20}$$

One can see that these are the real-space functions by substituting into the Hamiltonian (5.21) and using definitions above, for example for $k \sim 0$:

$$\begin{aligned}\int_{-\infty}^{\infty} dx\, \Lambda_{++}^0(x) f_+^\dagger(x) f_-^\dagger(-x) &= \int_{-\infty}^{\infty} dx\, C\, \mathrm{sign}(x) \int_{-k_F}^{\Omega} dq\, e^{iqx} f_{+,k_F+q}^\dagger \int_0^{\Omega} dq'\, e^{-iq'x} f_{-,q'}^\dagger \\ &= \iint dq\, dq'\, f_{+,k_F+q}^\dagger f_{-,q'}^\dagger C \int_{-\infty}^{\infty} dx\, \mathrm{sign}(x) e^{ix(q-q')},\end{aligned}$$

with the integral over x given by

$$\begin{aligned}\int_{-\infty}^{\infty} dx\, \mathrm{sign}(x) e^{ix(q-q')} &= \int_0^{\infty} dx\, e^{ix(q-q')} - \int_{-\infty}^{0} dx\, e^{ix(q-q')} \\ &= \int_0^{\infty} dx\, e^{ix(q-q')} - \int_0^{\infty} dx\, e^{-ix(q-q')} \\ &= \left(\frac{1}{2}\delta(q-q') + i\mathcal{P}\left(\frac{1}{q-q'}\right)\right) - \left(\frac{1}{2}\delta(q-q') - i\mathcal{P}\left(\frac{1}{q-q'}\right)\right) \\ &= 2i\mathcal{P}\left(\frac{1}{q-q'}\right),\end{aligned}$$

where $\mathcal{P}$ stands for the Cauchy principal value. Therefore the momentum-space Λ functions are retrieved, and the functions $\Lambda_{++}^0(x)$ and $\Lambda_{--}^\pi(x)$ are given by Eq. (C.20).

C.1.2 Decoupled BdG equations and wave functions

In the previous subsection, we have shown that the constant Λ_{+-} is zero. Therefore we approximate the BdG equations (see Eqs. (5.26)), e.g. about $k \sim 0$, by

$$\begin{aligned} E_-^0 \xi_{-,1}(x) - i\Lambda_{--}^0(x) \xi_{-,2}(x) &= 0, \\ iA_0 k_F \partial_x \xi_{+,1}(x) - i\Lambda_{++}^0(x) \xi_{+,2}(x) &= 0, \\ -E_-^0 \xi_{-,2}(x) + i\Lambda_{--}^{0*}(x) \xi_{-,1}(x) &= 0, \\ -iA_0 k_F \partial_x \xi_{+,2}(x) + i\Lambda_{++}^{0*}(x) \xi_{+,1}(x) &= 0. \end{aligned} \tag{C.21}$$

These equations are decoupled into two lower-band equations and two upper-band equations. The lower-band equations give

$$\xi_{-,1}(x) = i\frac{\Lambda^0_{--}(x)}{E^0_-}\xi_{-,2}(x), \qquad \xi_{-,2}(x) = i\frac{\Lambda^{0*}_{--}(x)}{E^0_-}\xi_{-,1}(x) \tag{C.22}$$

or

$$\xi_{-,1}(x) = i\frac{\Lambda^0_{--}(x)}{E^0_-}\left(i\frac{\Lambda^{*0}_{--}(x)}{E^0_-}\xi_{-,1}(x)\right) = -\frac{|\Lambda^0_{--}(x)|^2}{(E^0_-)^2}\xi_{-,1}(x), \tag{C.23}$$

from which we see that $\xi_{-,1}(x) = 0$ and so the lower band is trivial. The upper-band equations yield

$$A_0 k_F \partial_x \begin{pmatrix}\xi_{+,1}(x)\\ \xi^*_{+,2}(x)\end{pmatrix} = \Lambda^0_{++}(x)\sigma_x \begin{pmatrix}\xi^*_{+,1}(x)\\ \xi_{+,2}(x)\end{pmatrix}. \tag{C.24}$$

The unique solution to the above equation is

$$\begin{aligned}\xi_{+,1}(x) &= |C|e^{-i\phi}\exp\left(\frac{\lambda}{A_0 k_F}\int_0^x \tilde{\Lambda}^0_{++}(y)dy\right),\\ \xi_{+,2}(x) &= |C|e^{i\phi}\mathrm{sign}(\lambda)\exp\left(\frac{\lambda}{A_0 k_F}\int_0^x \tilde{\Lambda}^0_{++}(y)dy\right),\end{aligned} \tag{C.25}$$

where $\tilde{\Lambda}^0_{++}(x) \equiv \mathrm{sign}(x)|\Lambda^0_{++}(x)|$, and we have taken account of the phase factor of $\Lambda^0_{++}(x)$ in Eq. (C.20).

Similarly, around $\boldsymbol{k} \sim (\pi, \pi)$ the upper band becomes trivial and we find lower-band BdG equations,

$$-A_0 k_F \partial_x \begin{pmatrix}\xi^\pi_{-,1}(x)\\ \xi^{\pi*}_{-,2}(x)\end{pmatrix} = \Lambda^\pi_{--}(x)\sigma_x \begin{pmatrix}\xi^{\pi*}_{-,1}(x)\\ \xi^\pi_{-,2}(x)\end{pmatrix}, \tag{C.26}$$

with unique solution,

$$\begin{aligned}\xi^\pi_{-,1}(x) &= |\tilde{C}|e^{i\tilde{\phi}}\exp\left(-\frac{\lambda}{A_0 k_F}\int_0^x \tilde{\Lambda}^\pi_{--}(y)dy\right),\\ \xi^\pi_{-,2}(x) &= |\tilde{C}|e^{-i\tilde{\phi}}\mathrm{sign}(\lambda)\exp\left(-\frac{\lambda}{A_0 k_F}\int_0^x \tilde{\Lambda}^\pi_{--}(y)dy\right).\end{aligned} \tag{C.27}$$

Going back to our real-space Λ functions (C.20) which are proportional to $\mathrm{sign}(x)$, and taking $\lambda = 1$ to provide the Majorana solutions, the ξ functions finally become

$$\begin{aligned}\xi^0_{+,1}(x) \equiv \xi_{+,1}(x) &= |C|e^{-i\phi}\exp\left(\frac{\alpha\Delta_0}{A_0\sqrt{h^2+\alpha^2k_F^2}}|x|\right),\\ \xi^0_{+,2}(x) \equiv \xi_{+,2}(x) &= |C|e^{i\phi}\exp\left(\frac{\alpha\Delta_0}{A_0\sqrt{h^2+\alpha^2k_F^2}}|x|\right),\end{aligned} \tag{C.28}$$

for $k \sim 0$, and

$$\begin{aligned}\xi^\pi_{-,1}(x) &= |\tilde{C}|e^{i\tilde{\phi}}\exp\left(-\frac{\alpha\Delta_0}{A_0\sqrt{h^2+\alpha^2k_F^2}}|x|\right),\\ \xi^\pi_{-,2}(x) &= |\tilde{C}|e^{-i\tilde{\phi}}\exp\left(-\frac{\alpha\Delta_0}{A_0\sqrt{h^2+\alpha^2k_F^2}}|x|\right),\end{aligned} \tag{C.29}$$

for $\boldsymbol{k} \sim (\pi, \pi)$.

C.1.3 Majorana wave functions

The η wave functions in the zero-mode operator,

$$\gamma^\dagger = \int_{-\infty}^{\infty} dx \, \left(\eta_{+,1}(x) f_+^\dagger(x) + \eta_{-,1}(x) f_-^\dagger(x) + \eta_{+,2}(x) f_+(-x) + \eta_{-,2}(x) f_-(-x) \right), \quad \text{(C.30)}$$

are defined in terms of the ξ functions which we have calculated in the previous subsection, by

$$\xi_{\pm,n}(x) = \int_{-\infty}^{\infty} \{ f_\pm^\dagger(x'), f_\pm(x) \} \eta_{\pm,n}(x') dx'. \quad \text{(C.31)}$$

This definition is necessary as the anticommutators of real-space f operators are not quite delta functions. Instead we have, e.g., for $k \sim 0$,

$$\begin{aligned} \{ f_+^\dagger(x), f_+(x') \} &= \int_{-k_F}^{\Omega} dq \int_{-k_F}^{\Omega} dq' \, e^{i(qx - q'x')} \{ f_{+,k_F+q}^\dagger, f_{+,k_F+q'} \} = \int_{-k_F}^{\Omega} dq \, e^{iq(x-x')}, \\ \{ f_-^\dagger(x), f_-(x') \} &= \int_{0}^{\Omega} dq \int_{0}^{\Omega} dq' \, e^{i(qx - q'x')} \{ f_{-,q}^\dagger, f_{-,q'} \} = \int_{0}^{\Omega} dq \, e^{iq(x-x')}, \end{aligned} \quad \text{(C.32)}$$

where $\Omega \lesssim \frac{\pi}{2}$ is a cut-off momentum. Using ξ's in Eq. (C.28), this yields the relation,

$$\xi_{+,1}^0(x) = e^{-i\phi} \exp\left(\frac{\alpha \Delta_0}{A_0 \sqrt{h^2 + \alpha^2 k_F^2}} |x| \right) = \int_{-\infty}^{\infty} dy \int_{-k_F}^{\Omega} dq \, e^{iq(y-x)} \eta_{+,1}^0(y) \quad \text{(C.33)}$$

$$= i \int_{-\infty}^{\infty} dy \, \eta_{+,1}^0(y) \frac{e^{-ik_F(y-x)}}{(y-x)} - i \int_{-\infty}^{\infty} dy \, \eta_{+,1}^0(y) \frac{e^{i\Omega(y-x)}}{(y-x)}. \quad \text{(C.34)}$$

Naively, trying the same form for the η functions as the ξ functions – using $\eta(y) \sim \exp\left[\pm C \, \mathrm{sign}(\mathrm{Re}(y)) y \right]$ which is piecewise holomorphic and a contour which avoids the imaginary axis – one finds, for example for the normalizable functions $\eta^\pi(y) \sim \exp\left[-C \, \mathrm{sign}(\mathrm{Re}(y)) y \right]$,

$$\begin{aligned} \oint dy \, \eta^\pi(y) \frac{e^{-ik_F(y-x)}}{(y-x)} &= -i\pi \mathrm{Res} \left(\eta^\pi(y) \frac{e^{-ik_F(y-x)}}{(y-x)} \right) \Big|_{y=x} = -i\pi e^{-i\phi} \exp\left(-C|x| \right) \\ &= \int_{-\infty}^{\infty} dy \, \eta^\pi(y) \frac{e^{-ik_F(y-x)}}{(y-x)} + 2 \int_0^{\infty} dy \, \frac{\sin(y)}{(iy+x)} e^{-k_F y} \end{aligned} \quad \text{(C.35)}$$

or

$$\int_{-\infty}^{\infty} dy \, \eta^\pi(y) \frac{e^{-ik_F(y-x)}}{(y-x)} = -i\pi e^{-i\phi} \exp\left(-C|x| \right) - 2 \int_0^{\infty} dy \, \frac{\sin(y)}{(iy+x)} e^{-k_F y}. \quad \text{(C.36)}$$

In the future, we hope to find the exact form of the η wave functions.

C.2 Relation between Majorana modes

We now study the relationship between the Majorana modes around $k \sim 0$ and $\boldsymbol{k} \sim (\pi, \pi)$. If they are similar, that is, if their wave functions are not exactly orthogonal, in real systems they will annihilate each other as they have non-zero overlap in the vortex core.

The anticommutator of two Majorana fermion modes, labelled by some parameters α and x, is

$$\{\gamma_{\alpha,x}, \gamma_{\alpha',x'}\} = 2\delta_{\alpha,\alpha'}\delta_{x,x'}. \tag{C.37}$$

The Majorana mode in the continuum model (see Appendix B) has anticommutator with itself

$$\begin{aligned}
\{\gamma, \gamma\} &= \int dx\, dy \Big(\eta_{+,1}(x)\eta_{+,2}(-y) \left\{ f_+^\dagger(x), f_+(y) \right\} + \eta_{-,1}(x)\eta_{-,2}(-y) \left\{ f_-^\dagger(x), f_-(y) \right\} \\
&\quad + \eta_{+,2}(-x)\eta_{+,1}(y) \left\{ f_+(x), f_+^\dagger(y) \right\} + \eta_{-,2}(-x)\eta_{-,1}(y) \left\{ f_-(x), f_-^\dagger(y) \right\} \Big) \\
&= \int dx\, dy \Big(\eta_{+,1}(x)\eta_{+,1}^*(y) S_+(x-y) + \eta_{-,1}(x)\eta_{-,1}^*(y) S_-(x-y) \\
&\quad + \eta_{+,1}^*(x)\eta_{+,1}(y) S_+(y-x) + \eta_{-,1}^*(x)\eta_{-,1}(y) S_-(y-x) \Big) \\
&= \int dy \Big(\xi_{+,1}(y)\eta_{+,1}^*(y) + \xi_{-,1}(y)\eta_{-,1}^*(y) \Big) + \int dx \Big(\eta_{+,1}^*(x)\xi_{+,1}(x) + \eta_{-,1}^*(x)\xi_{-,1}(x) \Big) \\
&= 2 \int dx \Big(\eta_{+,1}^*(x)\xi_{+,1}(x) + \eta_{-,1}^*(x)\xi_{-,1}(x) \Big)
\end{aligned} \tag{C.38}$$

But γ is obviously similar to itself, so this anticommutator should equal 2.

We attempt to find the anticommutator between the Majorana mode around $k \sim 0$, γ_0, and the Majorana mode around $\boldsymbol{k} \sim (\pi, \pi)$, γ_π. To do this, we need the anticommutators between the operators $f_\pm^{\dagger 0}(x)$ and $f_\pm^{\dagger \pi}(x)$.

As before, the unitary transformations from the $c_{k,\sigma}^\dagger$ operators to the diagonalized $f_{\pm,k}^\dagger$ operators yield

$$\begin{pmatrix} f_{+,k}^\dagger \\ f_{-,k}^\dagger \end{pmatrix} = \begin{pmatrix} a_k & b_k \\ -b_k^* & a_k^* \end{pmatrix} \begin{pmatrix} c_{k,\uparrow}^\dagger \\ c_{k,\downarrow}^\dagger \end{pmatrix}, \tag{C.39}$$

where, for $k \sim 0$,

$$a_k = e^{i\phi} \frac{1}{\sqrt{2}} \frac{\alpha k}{\sqrt{h^2 + \alpha^2 k^2 + h\sqrt{h^2 + \alpha^2 k^2}}}, \qquad b_k = -ie^{i\phi} \frac{1}{\sqrt{2}} \sqrt{1 + \frac{h}{\sqrt{h^2 + \alpha^2 k^2}}}, \tag{C.40}$$

while for $\boldsymbol{k} \sim (\pi, \pi)$, with $\tilde{\boldsymbol{k}} = \boldsymbol{k} - (\pi, \pi)$,

$$\tilde{a}_{\tilde{k}} = e^{i\tilde{\phi}} \frac{1}{\sqrt{2}} \frac{\alpha \tilde{k}}{\sqrt{h^2 + \alpha^2 \tilde{k}^2 + h\sqrt{h^2 + \alpha^2 \tilde{k}^2}}}, \qquad \tilde{b}_{\tilde{k}} = +ie^{i\tilde{\phi}} \frac{1}{\sqrt{2}} \sqrt{1 + \frac{h}{\sqrt{h^2 + \alpha^2 \tilde{k}^2}}}, \tag{C.41}$$

where ϕ and $\tilde{\phi}$ are arbitrary phases.

Now, using an effective mass approximation for the operators, we neglect the quickly-oscillating factor for the momentum-space operators, allowing an electron with $k \sim 0$ to be 'similar' to an electron with $\boldsymbol{p} \sim (\pi, \pi)$:

$$\begin{aligned}\left\{c^{\dagger}_{\boldsymbol{k},\sigma}, c_{\boldsymbol{p},\beta}\right\} &= \sum_i e^{i\boldsymbol{k}\cdot\boldsymbol{R}_i} e^{-i(\tilde{\boldsymbol{p}}+(\pi,\pi))\cdot\boldsymbol{R}_i}\delta_{\sigma\beta} \\ &\simeq \sum_i e^{i(\boldsymbol{k}-\tilde{\boldsymbol{p}})\cdot\boldsymbol{R}_i}\delta_{\sigma\beta} = \delta(\boldsymbol{k}-\tilde{\boldsymbol{p}})\delta_{\sigma\beta}. \end{aligned} \tag{C.42}$$

This will allow us to compare wave functions between the Majorana modes. Then for the total angular momentum space operators, we find

$$\left\{c^{\dagger}_{m_J,k,\sigma}, c_{n_J,p,\beta}\right\} \simeq \delta_{n_J,m_J}\delta(k-\tilde{p})\delta_{\sigma\beta}, \tag{C.43}$$

and for the diagonalized-basis f operators in momentum space we have

$$\begin{aligned}\left\{f^{\dagger 0}_{+,k}, f^{\pi}_{+,\tilde{p}}\right\} &= \left\{(|a_k|e^{i\phi}c^{\dagger}_{k,\uparrow} - i|b_k|e^{i\phi}c^{\dagger}_{k,\downarrow}), (|a_{\tilde{p}}|e^{-i\tilde{\phi}}c_{\tilde{p},\uparrow} - i|b_{\tilde{p}}|e^{-i\tilde{\phi}}c_{\tilde{p},\downarrow})\right\} \\ &= e^{i(\phi-\tilde{\phi})}(|a_k||a_{\tilde{p}}| - |b_k||b_{\tilde{p}}|)\delta(k-\tilde{p}), \end{aligned} \tag{C.44}$$

$$\begin{aligned}\left\{f^{\dagger 0}_{-,k}, f^{\pi}_{-,\tilde{p}}\right\} &= \left\{(-i|b_k|e^{-i\phi}c^{\dagger}_{k,\uparrow} + |a_k|e^{-i\phi}c^{\dagger}_{k,\downarrow}), (-i|b_{\tilde{p}}|e^{i\tilde{\phi}}c_{\tilde{p},\uparrow} + |a_{\tilde{p}}|e^{i\tilde{\phi}}c_{\tilde{p},\downarrow})\right\} \\ &= e^{-i(\phi-\tilde{\phi})}(|a_k||a_{\tilde{p}}| - |b_k||b_{\tilde{p}}|)\delta(k-\tilde{p}), \end{aligned} \tag{C.45}$$

$$\begin{aligned}\left\{f^{\dagger 0}_{+,k}, f^{\pi}_{-,\tilde{p}}\right\} &= \left\{(|a_k|e^{i\phi}c^{\dagger}_{k,\uparrow} - i|b_k|e^{i\phi}c^{\dagger}_{k,\downarrow}), (-i|b_{\tilde{p}}|e^{i\tilde{\phi}}c_{\tilde{p},\uparrow} + |a_{\tilde{p}}|e^{i\tilde{\phi}}c_{\tilde{p},\downarrow})\right\} \\ &= -ie^{i(\phi+\tilde{\phi})}(|a_k||b_{\tilde{p}}| + |b_k||a_{\tilde{p}}|)\delta(k-\tilde{p}), \end{aligned} \tag{C.46}$$

$$\begin{aligned}\left\{f^{\dagger 0}_{-,k}, f^{\pi}_{+,\tilde{p}}\right\} &= \left\{(-i|b_k|e^{-i\phi}c^{\dagger}_{k,\uparrow} + |a_k|e^{-i\phi}c^{\dagger}_{k,\downarrow}), (|a_{\tilde{p}}|e^{-i\tilde{\phi}}c_{\tilde{p},\uparrow} - i|b_{\tilde{p}}|e^{-i\tilde{\phi}}c_{\tilde{p},\downarrow})\right\} \\ &= -ie^{-i(\phi+\tilde{\phi})}(|a_k||b_{\tilde{p}}| + |b_k||a_{\tilde{p}}|)\delta(k-\tilde{p}). \end{aligned} \tag{C.47}$$

Then for the real-space f operators we finally have

$$\begin{aligned}\left\{f^{\dagger 0}_{+}(x), f^{\pi}_{+}(y)\right\} &= \int_{-k_F}^{\Omega} dq \int_0^{\Omega} dq'\, e^{i(qx-q'y)}\left\{f^{\dagger 0}_{+,k_F+q}, f^{\pi}_{+,q'}\right\} \\ &= \int_0^{\Omega} dq'\, e^{iq'(x-y)-ik_Fx}e^{i(\phi-\tilde{\phi})}(|a_{q'}|^2 - |b_{q'}|^2), \end{aligned} \tag{C.48}$$

$$\begin{aligned}\left\{f^{\dagger 0}_{-}(x), f^{\pi}_{-}(y)\right\} &= \int_0^{\Omega} dq \int_{-k_F}^{\Omega} dq'\, e^{i(qx-q'y)}\left\{f^{\dagger 0}_{-,q}, f^{\pi}_{-,k_F+q'}\right\} \\ &= \int_0^{\Omega} dq\, e^{iq(x-y)+ik_Fy}e^{-i(\phi-\tilde{\phi})}(|a_q|^2 - |b_q|^2), \end{aligned} \tag{C.49}$$

$$\left\{f_+^{\dagger 0}(x), f_-^{\pi}(y)\right\} = \int_{-k_F}^{\Omega} dq \int_{-k_F}^{\Omega} dq'\, e^{i(qx-q'y)} \left\{f_{+,k_F+q}^{\dagger 0}, f_{-,k_F+q'}^{\pi}\right\}$$
$$= \int_0^{\Omega} dk\, e^{i(k-k_F)(x-y)}(-2i)e^{i(\phi+\tilde{\phi})}|a_k||b_k|, \tag{C.50}$$
$$\left\{f_-^{\dagger 0}(x), f_+^{\pi}(y)\right\} = \int_0^{\Omega} dq \int_0^{\Omega} dq'\, e^{i(qx-q'y)} \left\{f_{-,q}^{\dagger 0}, f_{+,q'}^{\pi}\right\}$$
$$= \int_0^{\Omega} dq\, e^{iq(x-y)}(-2i)e^{-i(\phi+\tilde{\phi})}|a_q||b_q|. \tag{C.51}$$

The anticommutator between the Majorana fermions about $k \sim 0$ and $\boldsymbol{k} \sim (\pi, \pi)$ is given by

$$\{\gamma_0^\dagger, \gamma_\pi^\dagger\} = \Big\{ \int dx \left(\eta_{+,1}^0(x) f_+^{\dagger 0}(x) + \eta_{-,1}^0(x) f_-^{\dagger 0}(x) + \eta_{+,2}^0(-x) f_+^0(x) + \eta_{-,2}^0(-x) f_-^0(x)\right),$$
$$\int dy \left(\eta_{+,1}^{\pi}(y) f_+^{\dagger \pi}(y) + \eta_{-,1}^{\pi}(y) f_-^{\dagger \pi}(y) + \eta_{+,2}^{\pi}(-y) f_+^{\pi}(y) + \eta_{-,2}^{\pi}(-y) f_-^{\pi}(y)\right)\Big\}$$
$$= \Big\{ \int dx \left(\eta_{+,1}^0(x) f_+^{\dagger 0}(x) + \eta_{-,1}^0(x) f_-^{\dagger 0}(x) + H.c.\right),$$
$$\int dy \Big(\eta_{+,2}^{\pi}(-y) f_+^{\pi}(y) + \eta_{-,2}^{\pi}(-y) f_-^{\pi}(y) + H.c.\Big)\Big\}$$
$$= \iint dx\, dy \Big(\eta_{+,1}^0(x)\eta_{+,2}^{\pi}(-y) \left\{f_+^{\dagger 0}(x), f_+^{\pi}(y)\right\} + \eta_{-,1}^0(x)\eta_{-,2}^{\pi}(-y) \left\{f_-^{\dagger 0}(x), f_-^{\pi}(y)\right\}$$
$$+ \ \eta_{+,1}^0(x)\eta_{-,2}^{\pi}(-y) \left\{f_+^{\dagger 0}(x), f_-^{\pi}(y)\right\} + \eta_{-,1}^0(x)\eta_{+,2}^{\pi}(-y) \left\{f_-^{\dagger 0}(x), f_+^{\pi}(y)\right\}\Big) + H.c.,$$

using the fact that $\eta_{\pm,1}^*(-x) = \eta_{\pm,2}(x)$. Using the expressions for the anticommutators above, this finally reduces to

$$\{\gamma_0^\dagger, \gamma_\pi^\dagger\} = \iint dx\, dy \Bigg(\eta_{+,1}^0(x)\eta_{+,2}^{\pi}(-y) e^{-ik_F x} \int_0^{\Omega} dk e^{ik(x-y)} e^{i(\phi-\tilde{\phi})}(|a_k|^2 - |b_k|^2)$$
$$+ \ \eta_{-,1}^0(x)\eta_{-,2}^{\pi}(-y) e^{ik_F y} \int_0^{\Omega} dk e^{ik(x-y)} e^{-i(\phi-\tilde{\phi})}(|a_k|^2 - |b_k|^2)$$
$$+ \ \eta_{+,1}^0(x)\eta_{-,2}^{\pi}(-y) e^{ik_F(x-y)} \int_0^{\Omega} dk e^{ik(x-y)}(-2i)e^{i(\phi+\tilde{\phi})}|a_k||b_k|$$
$$+ \eta_{-,1}^0(x)\eta_{+,2}^{\pi}(-y) \int_0^{\Omega} dk e^{ik(x-y)}(-2i)e^{-i(\phi+\tilde{\phi})}|a_k||b_k|\Bigg) + H.c.$$

or

$$\{\gamma_0^\dagger, \gamma_\pi^\dagger\} = \iint dx\, dy \Bigg(- \left(e^{i(\phi-\tilde{\phi})} e^{-ik_F x} \eta_{+,1}^0(x)\eta_{+,2}^{\pi}(-y) + e^{-i(\phi-\tilde{\phi})} e^{ik_F y} \eta_{-,1}^0(x)\eta_{-,2}^{\pi}(-y)\right)$$
$$\cdot \int_0^{\Omega} dk e^{ik(x-y)} \frac{h}{\sqrt{h^2+\alpha^2k^2}} - i \left(e^{i(\phi+\tilde{\phi})} e^{ik_F(x-y)} \eta_{+,1}^0(x)\eta_{-,2}^{\pi}(-y)\right.$$
$$\left. + e^{-i(\phi+\tilde{\phi})} \eta_{-,1}^0(x)\eta_{+,2}^{\pi}(-y)\right) \int_0^{\Omega} dk e^{ik(x-y)} \frac{\alpha k}{\sqrt{h^2+\alpha^2k^2}}\Bigg) + H.c. \tag{C.52}$$

Under the approximation that the BdG equations for the two energy bands decouple (see Eq. (C.21)), with the lower band wave functions becoming trivial for $k \sim 0$ and the upper band wave functions becoming trivial for $\boldsymbol{k} \sim (\pi, \pi)$, this anticommutator can be simplified somewhat. Using our expressions for the ξ functions under this approximation (see Eqs. (C.28) and (C.29)),

$$\xi^0_{+,1}(x) = |C|e^{-i\phi} \exp\left(\frac{\alpha\Delta_0}{A_0\sqrt{h^2+\alpha^2k_F^2}}|x|\right) = \xi^{0*}_{+,2}(x),$$
$$\xi^\pi_{-,1}(x) = |\tilde{C}|e^{i\tilde{\phi}} \exp\left(-\frac{\alpha\Delta_0}{A_0\sqrt{h^2+\alpha^2k_F^2}}|x|\right) = \xi^{\pi*}_{-,2}(x),$$

and the definition (C.31) for η's, we see that the phase factors containing ϕ and $\tilde{\phi}$ in the anticommutator will all cancel. Additionally, with trivial functions $\xi^0_{-,1}(x) = \xi^0_{-,2}(x) = 0$ and $\xi^\pi_{+,1}(x) = \xi^\pi_{+,2}(x) = 0$, the corresponding η's should be zero, leaving only

$$\{\gamma_0^\dagger, \gamma_\pi^\dagger\} = \iint dx\, dy(-i)e^{i(\phi+\tilde{\phi})}e^{ik_F(x-y)}\eta^0_{+,1}(x)\eta^\pi_{-,2}(-y)\int_0^\Omega dk e^{ik(x-y)}\frac{\alpha k}{\sqrt{h^2+\alpha^2k^2}} + H.c. \tag{C.53}$$

Noting that the anticommutator is real and simplifying, one has

$$\{\gamma_0^\dagger, \gamma_\pi^\dagger\} = 2\int dk\,\frac{\alpha k}{\sqrt{h^2+\alpha^2k^2}}\int_{-\infty}^{\infty}dx\int_{-\infty}^{\infty}dy\,\sin\left((k+k_F)(x-y)\right)\bar{\eta}^0_{+,1}(x)\bar{\eta}^\pi_{-,2}(-y), \tag{C.54}$$

where $\bar{\eta}$'s are the η functions but without phase factors of $\phi,\ \tilde{\phi}$.

A problem now arises with this approximation for comparison between Majorana modes. Our numerical results indicate that the Majoranas are similar to each other. However, as $\sin\left((k+k_F)(x-y)\right)$ is an odd function of $(x-y)$, then if $\bar{\eta}^0_{+,1}(x)\bar{\eta}^\pi_{-,2}(-y)$ is an even function of $(x-y)$, the anticommutator will be zero, indicating orthogonality. Under this approximation of decoupled bands, the ξ functions above are even in x, an indication that η functions are likely also even in x, so that that this condition holds. Therefore this approximation appears to predict that the Majorana modes about $k \sim 0$ and $\boldsymbol{k} \sim (\pi, \pi)$ are orthogonal to each other, a result in contradiction with our numerical results.

Appendix D

Tight-Binding Vortex Model in Real Space

This section uses the vortex model of Sato *et al.* [16], following their derivations for an approximated Majorana solution. Their solution is for the non-Abelian region, with one Fermi surface around $k \sim 0$, while we attempt a similar derivation for the Abelian region, with one Majorana mode for the Fermi surface around $k \sim 0$ and one for the Fermi surface around $\boldsymbol{k} \sim (\pi, \pi)$. However, the asymptotic matching method they use proves unuseful for the Abelian region.

Near a vortex, momentum is not a good quantum number, and it is hypothesized in Ref. [16] that the exact solution for a zero-energy mode should be a combination of quasiparticles with $k \sim 0$ (or $\boldsymbol{k} \sim (\pi, \pi)$ if the Fermi surface lies there instead) and quasiparticles with a large momentum. The large momentum quasiparticles would be dominant near the core of the vortex, while quasiparticles with $k \sim 0$ ($\boldsymbol{k} \sim (\pi, \pi)$) dominate in the long-distance regime far from the vortex.

After describing the model used, we summarize our results for $k \sim 0$, then go into more detail for $\boldsymbol{k} \sim (\pi, \pi)$.

D.1 Vortex model in real space

In the s-wave superconducting state,

$$\mathcal{H}(\boldsymbol{k}) = \begin{pmatrix} \varepsilon(\boldsymbol{k}) - h\sigma_z + \alpha\mathcal{L}_0(\boldsymbol{k}) \cdot \boldsymbol{\sigma} & i\Delta_s\sigma_y \\ -i\Delta_s\sigma_y & -\varepsilon(\boldsymbol{k}) + h\sigma_z + \alpha\mathcal{L}_0(\boldsymbol{k}) \cdot \boldsymbol{\sigma}^* \end{pmatrix}, \tag{D.1}$$

where $\varepsilon(\boldsymbol{k}) = -2t(\cos k_x + \cos k_y) - \mu$ is the kinetic energy, $\mathcal{L}_0(\boldsymbol{k}) = (\sin k_y, -\sin k_x)$ is the Rashba spin-orbit coupling, and h is the Zeeman splitting, as in Eq. (3.24).

For a SC vortex with order parameter $\Delta_s = \Delta e^{in\theta}$, $\Delta = |\Delta_s|$, use the gauge transformation [16, 36],

$$e\boldsymbol{A} \to e\boldsymbol{A} - \frac{n}{2}\boldsymbol{\nabla}\theta, \qquad \Delta e^{in\theta} \to \Delta. \tag{D.2}$$

Then Δ_s is replaced with its magnitude in the vortex, Δ, and the kinetic energy and spin-orbit coupling in the vortex become $\varepsilon(\hat{\boldsymbol{k}} - e\boldsymbol{A} + \frac{n}{2}\boldsymbol{\nabla}\theta)$ and $\mathcal{L}_0(\hat{\boldsymbol{k}} - e\boldsymbol{A} + \frac{n}{2}\boldsymbol{\nabla}\theta)$.

Assuming $H_Z \ll H_{C_2}$, that is the Zeeman magnetic field is much smaller than the upper critical field at which Type-II superconductivity is destroyed, the gauge field $e\boldsymbol{A}$ can be neglected compared to $\frac{n}{2}\boldsymbol{\nabla}\theta$ [36].

D.2 Summary of Majorana equation about $k \sim 0$

Following the model of Sato et al. [16], let $k \sim 0$, giving

$$\varepsilon(\boldsymbol{k}) = \frac{1}{2m}\boldsymbol{k}^2 - \mu_0, \qquad \alpha\mathcal{L}_0(\boldsymbol{k}) = 2\lambda(k_y, -k_x), \tag{D.3}$$

where $m = 1/(2t)$, $\alpha = 2\lambda$, and $\mu_0 = \mu + 4t$. In Ref. [16], $\mu_0 \approx 0$ is set, giving a single Fermi surface near $k \sim 0$. The Abelian region, with two Fermi surfaces, lies between $-2t < \mu < 2t$, so we choose $\mu \approx 0$, giving $\mu_0 \approx 4t$.

Setting

$$\Psi^T = (u_\uparrow, u_\downarrow, u_\uparrow^*, u_\downarrow^*), \tag{D.4}$$

and using $\hat{\boldsymbol{k}} = -i\boldsymbol{\nabla}$, a hypothetical zero-energy solution yields

$$\begin{aligned}
&\left\{ -\frac{1}{2m}\left[\left(\frac{\partial^2}{\partial r^2} + \frac{1}{r}\frac{\partial}{\partial r} + \frac{1}{r^2}\frac{\partial^2}{\partial\theta^2}\right) + i\frac{n}{r^2}\frac{\partial}{\partial\theta} - \frac{n^2}{4r^2}\right] - \mu_0 - h\right\} u_\uparrow \\
&\quad + 2\lambda e^{-i\theta}\left(\frac{\partial}{\partial r} - i\frac{\partial}{\partial\theta} + \frac{n}{2r}\right) u_\downarrow + \Delta\tilde{u}_\downarrow^* = 0, \qquad \text{(D.5)} \\
&\left\{ -\frac{1}{2m}\left[\left(\frac{\partial^2}{\partial r^2} + \frac{1}{r}\frac{\partial}{\partial r} + \frac{1}{r^2}\frac{\partial^2}{\partial\theta^2}\right) + i\frac{n}{r^2}\frac{\partial}{\partial\theta} - \frac{n^2}{4r^2}\right] - \mu_0 + h\right\} u_\downarrow \\
&\quad - 2\lambda e^{i\theta}\left(\frac{\partial}{\partial r} + i\frac{\partial}{\partial\theta} - \frac{n}{2r}\right) u_\uparrow - \Delta\tilde{u}_\uparrow^* = 0. \qquad \text{(D.6)}
\end{aligned}$$

The vortex is modeled by $\Delta = 0$ for $r < r_c$, and $\Delta = \text{const}$ for $r > r_c$. The solutions for the different regions are matched to each other in the asymptotic limit of large r, using the approximation of large spin-orbit coupling, $h \ll m\lambda^2$.

The solutions found for the regions $r < r_c$ and $r > r_c$ in the Abelian phase cannot be matched as for those in the non-Abelian phase studied by Sato *et al.* First of all, to attempt to match solutions asymptotically, it must be assumed that $h^2 > \mu_0^2 \approx (4t)^2$ (to give an imaginary argument in the Bessel functions); however, the Abelian region lies in $\Delta^2 \lesssim h^2 \lesssim \Delta^2 + (4t)^2$. Using this assumption and the approximation $h \ll m\lambda^2$ gives the constants,

$$\gamma_- = \sqrt{-8m^2\lambda^2 - 2m\mu_0 + \sqrt{64m^4\lambda^4 + 4m^2h^2 + 32\lambda^2m^3\mu_0}} \;\sim\; \frac{h}{2\lambda}, \tag{D.7}$$

$$\frac{A_\downarrow}{A_\uparrow} = -i\gamma_- \frac{\left(8\lambda^2m^2 + 2hm + \sqrt{64\lambda^4m^4 + 4h^2m^2 + 32\lambda^2m^3\mu_0}\right)}{8\lambda m^2(h-\mu_0)} \;\sim\; \frac{-ih}{(h-\mu_0)}, \tag{D.8}$$

$$\alpha' = \frac{i}{2}\left(\frac{h-\Delta}{\lambda} \pm \sqrt{\left(\frac{h-\Delta}{\lambda}\right)^2 + 8m\mu_0}\right) \;\sim\; i\left(\frac{h-\Delta}{\lambda} \pm \sqrt{2m\mu_0}\right). \tag{D.9}$$

The solution found for $r < r_c$ is

$$u_\uparrow = A_\uparrow e^{-i\theta/2} H^{(1)}_{(n-1)/2}(i\gamma_- r) \;\sim\; A_\uparrow e^{-i\theta/2} e^{-i\pi(n+1)/4}\sqrt{\frac{2}{\pi\gamma_- r}}\, e^{-h/2\lambda r}, \tag{D.10}$$

$$u_\downarrow = \frac{A_\downarrow}{A_\uparrow} A_\uparrow e^{i\theta/2} H^{(1)}_{(n+1)/2}(i\gamma_- r) \;\sim\; -A_\uparrow \frac{h}{(h-\mu_0)} e^{i\theta/2} e^{-i\pi(n+1)/4}\sqrt{\frac{2}{\pi\gamma_- r}}\, e^{-h/2\lambda r}, \tag{D.11}$$

and the solution for $r > r_c$ is

$$\begin{aligned} u_\uparrow &= -i\frac{C_+}{2}e^{-i\theta/2}e^{i\pi n/4}e^{-\int^r dr'(i\alpha'+(h-\Delta)/2\lambda)}H^{(1)}_{(n-1)/2}(\alpha' r) \\ &\sim -i\frac{C_+}{2}e^{-i\theta/2}e^{-i\pi/4}\sqrt{\frac{2}{\pi|\alpha'|r}}e^{-[(h-\Delta)/2\lambda]r}, \end{aligned} \tag{D.12}$$

$$\begin{aligned} u_\downarrow &= -\frac{C_+}{2}e^{i\theta/2}e^{i\pi n/4}e^{-\int^r dr'(i\alpha'+(h-\Delta)/2\lambda)}H^{(1)}_{(n+1)/2}(\alpha' r) \\ &\sim i\frac{C_+}{2}e^{i\theta/2}e^{-i\pi/4}\sqrt{\frac{2}{\pi|\alpha'|r}}e^{-[(h-\Delta)/2\lambda]r}. \end{aligned} \tag{D.13}$$

Therefore, for the Abelian region with $\mu_0 \approx 4t$, constants for these solutions cannot be asymptotically matched.

D.3 Majorana zero-mode equation about $\boldsymbol{k} \sim \pm(\pi,\pi)$

Now let $\boldsymbol{k} \sim \pm(\pi,\pi)$. Then setting $\tilde{\boldsymbol{k}} = \boldsymbol{k} \mp (\pi,\pi)$, we have

$$\varepsilon(\boldsymbol{k}) = -\frac{1}{2m}\tilde{\boldsymbol{k}}^2 - \tilde{\mu}_0, \qquad \boldsymbol{g}(\boldsymbol{k}) = \alpha\mathcal{L}_0(\boldsymbol{k}) = 2\lambda(-\tilde{k}_y, \tilde{k}_x), \tag{D.14}$$

where $m = 1/(2t)$, $\alpha = 2\lambda$, and $\tilde{\mu}_0 = \mu - 4t$. Again, for the Abelian region we have $\mu \approx 0$, which leads to $\tilde{\mu}_0 \approx -4t$.

Using the effective mass approximation to separate quickly-oscillating plane waves from the slowly varying functions $\tilde{u}_{\uparrow(\downarrow)}$, set

$$\tilde{\Psi}^T = e^{\pm i(\pi,\pi)\cdot\boldsymbol{r}}(\tilde{u}_\uparrow, \tilde{u}_\downarrow, \tilde{u}^*_\uparrow, \tilde{u}^*_\downarrow). \tag{D.15}$$

Using $\hat{\tilde{k}} = -i\boldsymbol{\nabla} \mp (\pi,\pi)$, the kinetic and spin-orbit energies are

$$\begin{aligned} \varepsilon\big(\hat{\boldsymbol{k}} - e\boldsymbol{A} + \frac{n}{2}\boldsymbol{\nabla}\theta\big)e^{\pm i(\pi,\pi)\cdot\boldsymbol{r}}\tilde{u}_{\uparrow(\downarrow)} &= \left\{-\frac{1}{2m}\left(-i\boldsymbol{\nabla} \mp (\pi,\pi) + \frac{n}{2}\boldsymbol{\nabla}\theta\right)^2 - \tilde{\mu}_0\right\}e^{\pm i(\pi,\pi)\cdot\boldsymbol{r}}\tilde{u}_{\uparrow(\downarrow)} \\ &= e^{\pm i(\pi,\pi)\cdot\boldsymbol{r}}\left\{-\frac{1}{2m}\left(-i\boldsymbol{\nabla} + \frac{n}{2}\boldsymbol{\nabla}\theta\right)^2 u_{\uparrow(\downarrow)} - \tilde{\mu}_0\right\}\tilde{u}_{\uparrow(\downarrow)} \\ &= e^{\pm i(\pi,\pi)\cdot\boldsymbol{r}}\left\{-\frac{1}{2m}\left[-\nabla^2 - i\frac{n}{2}\nabla^2\theta - 2i\frac{n}{2}\boldsymbol{\nabla}\theta\cdot\boldsymbol{\nabla} + \frac{n^2}{4}(\boldsymbol{\nabla}\theta)^2\right] - \tilde{\mu}_0\right\}\tilde{u}_{\uparrow(\downarrow)} \\ &= e^{\pm i(\pi,\pi)\cdot\boldsymbol{r}}\left\{-\frac{1}{2m}\left[-\left(\frac{\partial^2}{\partial r^2} + \frac{1}{r}\frac{\partial}{\partial r} + \frac{1}{r^2}\frac{\partial^2}{\partial\theta^2}\right) - i\frac{n}{r^2}\frac{\partial}{\partial\theta} + \frac{n^2}{4r^2}\right] - \tilde{\mu}_0\right\}\tilde{u}_{\uparrow(\downarrow)}, \end{aligned} \tag{D.16}$$

and

$$
\begin{aligned}
&\alpha\mathcal{L}_0(\hat{\boldsymbol{k}} - e\boldsymbol{A} + \frac{n}{2}\boldsymbol{\nabla}\theta)\cdot\boldsymbol{\sigma}\ e^{\pm i(\pi,\pi)\cdot\boldsymbol{r}}\begin{pmatrix}\tilde{u}_\uparrow\\ \tilde{u}_\downarrow\end{pmatrix}\\
&\quad=2\lambda\Big\{-\left(\hat{\tilde{k}}_y + \frac{n}{2}\frac{\partial\theta}{\partial y}\right)\sigma_x + \left(\hat{\tilde{k}}_x + \frac{n}{2}\frac{\partial\theta}{\partial x}\right)\sigma_y\Big\}e^{\pm i(\pi,\pi)\cdot\boldsymbol{r}}\begin{pmatrix}\tilde{u}_\uparrow\\ \tilde{u}_\downarrow\end{pmatrix}\\
&\quad= 2\lambda\Big\{-\left(\mp\pi - i\frac{\partial}{\partial y} + \frac{n}{2}\frac{\partial\theta}{\partial y}\right)\sigma_x + \left(\mp\pi - i\frac{\partial}{\partial x} + \frac{n}{2}\frac{\partial\theta}{\partial x}\right)\sigma_y\Big\}e^{\pm i(\pi,\pi)\cdot\boldsymbol{r}}\begin{pmatrix}\tilde{u}_\uparrow\\ \tilde{u}_\downarrow\end{pmatrix}\\
&\quad= 2\lambda e^{\pm i(\pi,\pi)\cdot\boldsymbol{r}}\Big\{-\left(-i\frac{\partial}{\partial y} + \frac{n}{2}\frac{\partial\theta}{\partial y}\right)\sigma_x + \left(-i\frac{\partial}{\partial x} + \frac{n}{2}\frac{\partial\theta}{\partial x}\right)\sigma_y\Big\}\begin{pmatrix}\tilde{u}_\uparrow\\ \tilde{u}_\downarrow\end{pmatrix}\\
&\quad= 2\lambda e^{\pm i(\pi,\pi)\cdot\boldsymbol{r}}\Big\{\left(i\left(\frac{\cos\theta}{r}\frac{\partial}{\partial\theta} + \sin\theta\frac{\partial}{\partial r}\right) - \cos\theta\frac{n}{2r}\right)\sigma_x\\
&\qquad+\left(-i\left(-\frac{\sin\theta}{r}\frac{\partial}{\partial\theta} + \cos\theta\frac{\partial}{\partial r}\right) - \sin\theta\frac{n}{2r}\right)\sigma_y\Big\}\begin{pmatrix}\tilde{u}_\uparrow\\ \tilde{u}_\downarrow\end{pmatrix}\\
&\quad= 2\lambda e^{\pm i(\pi,\pi)\cdot\boldsymbol{r}}\Big\{\begin{pmatrix}0&1\\0&0\end{pmatrix}\left(i\frac{\cos\theta}{r}\frac{\partial}{\partial\theta} + \frac{\sin\theta}{r}\frac{\partial}{\partial\theta} + i\sin\theta\frac{\partial}{\partial r} - \cos\theta\frac{\partial}{\partial r} - \cos\theta\frac{n}{2r} + i\sin\theta\frac{n}{2r}\right)\\
&\qquad+\begin{pmatrix}0&0\\1&0\end{pmatrix}\left(i\frac{\cos\theta}{r}\frac{\partial}{\partial\theta} - \frac{\sin\theta}{r}\frac{\partial}{\partial\theta} + i\sin\theta\frac{\partial}{\partial r} + \cos\theta\frac{\partial}{\partial r} - \cos\theta\frac{n}{2r} - i\sin\theta\frac{n}{2r}\right)\Big\}\begin{pmatrix}\tilde{u}_\uparrow\\ \tilde{u}_\downarrow\end{pmatrix}\\
&\quad= 2\lambda e^{\pm i(\pi,\pi)\cdot\boldsymbol{r}}\Big\{\begin{pmatrix}0&1\\0&0\end{pmatrix}e^{-i\theta}\left(i\frac{\partial}{\partial\theta} - \frac{\partial}{\partial r} - \frac{n}{2r}\right) + \begin{pmatrix}0&0\\1&0\end{pmatrix}e^{i\theta}\left(i\frac{\partial}{\partial\theta} + \frac{\partial}{\partial r} - \frac{n}{2r}\right)\Big\}\begin{pmatrix}\tilde{u}_\uparrow\\ \tilde{u}_\downarrow\end{pmatrix}\\
&\quad= 2\lambda e^{\pm i(\pi,\pi)\cdot\boldsymbol{r}}\Big\{-e^{-i\theta}\left(\frac{\partial}{\partial r} - i\frac{\partial}{\partial\theta} + \frac{n}{2r}\right)\begin{pmatrix}\tilde{u}_\downarrow\\ 0\end{pmatrix} + e^{i\theta}\left(\frac{\partial}{\partial r} + i\frac{\partial}{\partial\theta} - \frac{n}{2r}\right)\begin{pmatrix}0\\ \tilde{u}_\uparrow\end{pmatrix}\Big\}. \quad \text{(D.17)}
\end{aligned}
$$

Therefore, for a zero-energy solution the first two rows (equivalently the last two rows) of $\mathcal{H}$ in Eq. (D.1) yield

$$
\begin{aligned}
&\left\{\frac{1}{2m}\left[\left(\frac{\partial^2}{\partial r^2} + \frac{1}{r}\frac{\partial}{\partial r} + \frac{1}{r^2}\frac{\partial^2}{\partial\theta^2}\right) + i\frac{n}{r^2}\frac{\partial}{\partial\theta} - \frac{n^2}{4r^2}\right] - \tilde{\mu}_0 - h\right\}\tilde{u}_\uparrow\\
&\quad - 2\lambda e^{-i\theta}\left(\frac{\partial}{\partial r} - i\frac{\partial}{\partial\theta} + \frac{n}{2r}\right)\tilde{u}_\downarrow + \Delta\tilde{u}^*_\downarrow = 0, \quad \text{(D.18)}\\
&\left\{\frac{1}{2m}\left[\left(\frac{\partial^2}{\partial r^2} + \frac{1}{r}\frac{\partial}{\partial r} + \frac{1}{r^2}\frac{\partial^2}{\partial\theta^2}\right) + i\frac{n}{r^2}\frac{\partial}{\partial\theta} - \frac{n^2}{4r^2}\right] - \tilde{\mu}_0 + h\right\}\tilde{u}_\downarrow\\
&\quad + 2\lambda e^{i\theta}\left(\frac{\partial}{\partial r} + i\frac{\partial}{\partial\theta} - \frac{n}{2r}\right)\tilde{u}_\uparrow - \Delta\tilde{u}^*_\uparrow = 0. \quad \text{(D.19)}
\end{aligned}
$$

D.3.1 Equation for $r < r_c$

First we look at the region $r < r_c$, with $\Delta = 0$. Let

$$
\tilde{u}_\uparrow(r,\theta) = e^{-in\theta/2}e^{i(\beta-1)\theta}f^<_\uparrow(r), \qquad \tilde{u}_\downarrow(r,\theta) = e^{-in\theta/2}e^{i\beta\theta}f^<_\downarrow(r), \quad \text{(D.20)}
$$

where β is a constant to be determined. Substituting into Eq. (D.18) gives the radial equation,

$$
\left[\frac{1}{2m}\left(\frac{\partial^2}{\partial r^2} + \frac{1}{r}\frac{\partial}{\partial r} - \frac{(\beta-1)^2}{r^2}\right) - \tilde{\mu}_0 - h\right]f^<_\uparrow - 2\lambda\left(\frac{\partial}{\partial r} + \frac{\beta}{r}\right)f^<_\downarrow = 0, \quad \text{(D.21)}
$$

$$\left[\frac{1}{2m}\left(\frac{\partial^2}{\partial r^2}+\frac{1}{r}\frac{\partial}{\partial r}-\frac{\beta^2}{r^2}\right)-\tilde{\mu}_0+h\right]f_\downarrow^<+2\lambda\left(\frac{\partial}{\partial r}-\frac{(\beta-1)}{r}\right)f_\uparrow^<=0. \tag{D.22}$$

Now let $f_\uparrow^<(r)=A_\uparrow Z_{\beta-1}(\alpha r)$, $f_\downarrow^<(r)=A_\downarrow Z_\beta(\alpha r)$, where $Z_\nu(\alpha r)$ is a Bessel function and α is a constant (different from the spin-orbit coupling constant). The following relation for the Bessel function is used:

$$\frac{\partial Z_\nu(\alpha r)}{\partial r}=\frac{\nu}{r}Z_\nu(\alpha r)-\alpha Z_{\nu+1}(\alpha r)=\alpha Z_{\nu-1}(\alpha r)-\frac{\nu}{r}Z_\nu(\alpha r). \tag{D.23}$$

Substitution gives

$$\left[\frac{\partial^2}{\partial r^2}+\frac{1}{r}\frac{\partial}{\partial r}-\frac{(\beta-1)^2}{r^2}-2m(\tilde{\mu}_0+h)-4m\lambda\frac{A_\downarrow}{A_\uparrow}\alpha\right]Z_{\beta-1}(\alpha r)=0, \tag{D.24}$$

$$\left[\frac{\partial^2}{\partial r^2}+\frac{1}{r}\frac{\partial}{\partial r}-\frac{\beta^2}{r^2}-2m(\tilde{\mu}_0-h)-4m\lambda\frac{A_\uparrow}{A_\downarrow}\alpha\right]Z_\beta(\alpha r)=0. \tag{D.25}$$

These equations are self-consistent (are Bessel differential equations) provided

$$-2m(\tilde{\mu}_0+h)-4m\lambda\frac{A_\downarrow}{A_\uparrow}\alpha=-2m(\tilde{\mu}_0-h)-4m\lambda\frac{A_\uparrow}{A_\downarrow}\alpha=\alpha^2. \tag{D.26}$$

There are two solutions to this self-consistency equation for $\tilde{\mu}_0\approx-4t$, given by

$$\begin{aligned}(i)\ \alpha&=\gamma_+=\sqrt{8m^2\lambda^2-2m\tilde{\mu}_0+\sqrt{64m^4\lambda^4+4m^2h^2-32\lambda^2m^3\tilde{\mu}_0}}\,,\\ \frac{A_\downarrow}{A_\uparrow}&=\frac{\gamma_+\left(-8\lambda^2m^2+2hm+\sqrt{64\lambda^4m^4+4h^2m^2-32\lambda^2m^3\tilde{\mu}_0}\right)}{8\lambda m^2(h-\tilde{\mu}_0)}\,.\end{aligned} \tag{D.27}$$

$$\begin{aligned}(ii)\ \alpha&=i\gamma_-=i\sqrt{-8m^2\lambda^2+2m\tilde{\mu}_0+\sqrt{64m^4\lambda^4+4m^2h^2-32\lambda^2m^3\tilde{\mu}_0}}\,,\\ \frac{A_\downarrow}{A_\uparrow}&=\frac{i\gamma_-\left(8\lambda^2m^2-2hm+\sqrt{64\lambda^4m^4+4h^2m^2-32\lambda^2m^3\tilde{\mu}_0}\right)}{8\lambda m^2(h-\tilde{\mu}_0)}\,.\end{aligned} \tag{D.28}$$

Here it has been assumed that $h^2>\tilde{\mu}_0^2\approx(4t)^2$, in order to attempt to match solutions for $r<r_c$ to those for $r>r_c$ (that is, to give a possible imaginary argument to the Bessel functions).

Therefore we have two solutions for $r<r_c$:

$$\begin{aligned}(i)\ \tilde{u}_\uparrow&=e^{-in\theta/2}e^{i(\beta-1)\theta}A_\uparrow Z_{\beta-1}\left(\gamma_+r\right),\\ \tilde{u}_\downarrow&=e^{-in\theta/2}e^{i\beta\theta}\left(\frac{A_\downarrow}{A_\uparrow}\right)A_\uparrow Z_\beta\left(\gamma_+r\right).\end{aligned} \tag{D.29}$$

$$\begin{aligned}(ii)\ \tilde{u}_\uparrow&=e^{-in\theta/2}e^{i(\beta-1)\theta}A_\uparrow Z_{\beta-1}\left(i\gamma_-r\right),\\ \tilde{u}_\downarrow&=e^{-in\theta/2}e^{i\beta\theta}\left(\frac{A_\downarrow}{A_\uparrow}\right)A_\uparrow Z_\beta\left(i\gamma_-r\right).\end{aligned} \tag{D.30}$$

Solution (i) corresponds to a momentum of approximately $\gamma_+\pm(\pi,\pi)$, with γ_+ not small, while solution (ii) corresponds to a momentum near $\pm(\pi,\pi)$, as γ_- is small in the limit of large spin-orbit coupling ($h\ll m\lambda^2$). Therefore we use solution (ii).

D.3.2 Equation for $r > r_c$

Now we look at the region $r > r_c$, where Δ is nonzero and assumed constant. To separate the θ dependence, choose a solution of the form,

$$\tilde{u}_\uparrow(r,\theta) = e^{-i\theta/2} f_\uparrow^>(r), \qquad \tilde{u}_\downarrow(r,\theta) = e^{i\theta/2} f_\downarrow^>(r). \tag{D.31}$$

In the gauge where Δ_s is real, $\tilde{u}_\sigma(r,\theta)$ is multiplied by $(-1)^n$ when θ is rotated from 0 to 2π, so this form of solution satisfies the correct boundary condition only when the vorticity n is odd. Therefore we solve for odd-vorticity only.

Substitution gives

$$\left[\frac{1}{2m}\left(\frac{\partial^2}{\partial r^2} + \frac{1}{r}\frac{\partial}{\partial r} - \frac{(n-1)^2}{4r^2}\right) - \tilde{\mu}_0 - h\right] f_\uparrow^> - 2\lambda\left(\frac{\partial}{\partial r} + \frac{n+1}{2r}\right) f_\downarrow^> + \Delta f_\downarrow^{>*} = 0, \tag{D.32}$$

$$\left[\frac{1}{2m}\left(\frac{\partial^2}{\partial r^2} + \frac{1}{r}\frac{\partial}{\partial r} - \frac{(n+1)^2}{4r^2}\right) - \tilde{\mu}_0 + h\right] f_\downarrow^> + 2\lambda\left(\frac{\partial}{\partial r} - \frac{(n-1)}{2r}\right) f_\uparrow^> - \Delta f_\uparrow^{>*} = 0. \tag{D.33}$$

Now let

$$f_\uparrow^>(r) = g_\uparrow(r) Z_{(n-1)/2}(\alpha' r), \qquad f_\downarrow^>(r) = g_\downarrow(r), Z_{(n+1)/2}(\alpha' r), \tag{D.34}$$

where $g_{\uparrow,(\downarrow)}$ is a slowly varying function of r, and α' a constant. Substitution yields

$$\begin{aligned}&\frac{1}{m}\frac{dZ_{(n-1)/2}}{dr}\frac{dg_\uparrow}{dr} - \frac{\alpha'^2}{2m} Z_{(n-1)/2} g_\uparrow - (\tilde{\mu}_0 + h) Z_{(n-1)/2} g_\uparrow - 2\lambda Z_{(n+1)/2}\frac{dg_\downarrow}{dr} \\ &\quad - 2\lambda\alpha' Z_{(n-1)/2} g_\downarrow + \Delta Z^*_{(n+1)/2} g_\downarrow^* = 0,\end{aligned} \tag{D.35}$$

$$\begin{aligned}&\frac{1}{m}\frac{dZ_{(n+1)/2}}{dr}\frac{dg_\downarrow}{dr} - \frac{\alpha'^2}{2m} Z_{(n+1)/2} g_\downarrow - (\tilde{\mu}_0 - h) Z_{(n+1)/2} g_\downarrow + 2\lambda Z_{(n-1)/2}\frac{dg_\uparrow}{dr} \\ &\quad - 2\lambda\alpha' Z_{(n+1)/2} g_\uparrow - \Delta Z^*_{(n-1)/2} g_\uparrow^* = 0.\end{aligned} \tag{D.36}$$

The Bessel function $Z_\nu(\alpha' r)$ is now taken to be the first Hankel function, $H_\nu^{(1)}(\alpha' r)$. Using the asymptotic form of the Hankel function $H_\nu^{(1)}(z) \sim \sqrt{\frac{2}{\pi z}} \exp\left[i\left(z - \frac{\pi}{2}\nu - \frac{\pi}{4}\right)\right]$ leads to

$$\frac{Z_{\nu-1}}{Z_\nu} \to i, \qquad \frac{1}{Z_\nu(\alpha' r)}\frac{\partial}{\partial r} Z_\nu(\alpha' r) \to \alpha' i - \frac{\nu}{r}. \tag{D.37}$$

The constant α' will be shown to be a purely imaginary number, which also gives $Z^*_{(n+1)/2}/Z_{(n-1)/2} \to \exp\left[i\frac{\pi}{2}(n+1)\right]$. Then asymptotically we have

$$\frac{i\alpha'}{m}\frac{dg_\uparrow}{dr} + 2i\lambda\frac{dg_\downarrow}{dr} - \frac{\alpha'^2}{2m} g_\uparrow - (\tilde{\mu}_0 + h) g_\uparrow - 2\lambda\alpha' g_\downarrow + \Delta \exp\left[i\frac{\pi}{2}(n+1)\right] g_\downarrow^* = 0, \tag{D.38}$$

$$\frac{i\alpha'}{m}\frac{dg_\downarrow}{dr} + 2i\lambda\frac{dg_\uparrow}{dr} - \frac{\alpha'^2}{2m} g_\downarrow - (\tilde{\mu}_0 - h) g_\downarrow - 2\lambda\alpha' g_\uparrow - \Delta \exp\left[i\frac{\pi}{2}(n+1)\right] g_\uparrow^* = 0. \tag{D.39}$$

Introducing $g_\pm(r) = g_\uparrow \pm i g_\downarrow$, we have

$$\frac{i\alpha'}{m}\frac{dg_+}{dr} - 2\lambda\frac{dg_-}{dr} - \frac{\alpha'^2}{2m}g_+ - (\tilde{\mu}_0 g_+ + h g_-) - 2i\lambda\alpha' g_- - i\Delta\exp\left[i\frac{\pi}{2}(n+1)\right]g_-^* = 0, \quad \text{(D.40)}$$

$$\frac{i\alpha'}{m}\frac{dg_-}{dr} + 2\lambda\frac{dg_+}{dr} - \frac{\alpha'^2}{2m}g_- - (\tilde{\mu}_0 g_- + h g_+) + 2i\lambda\alpha' g_+ + i\Delta\exp\left[i\frac{\pi}{2}(n+1)\right]g_+^* = 0. \quad \text{(D.41)}$$

Examine the following two possible solutions: (a) $g_+ \equiv 0$, and g_- gives a nontrivial solution, (b) $g_- \equiv 0$, and g_+ gives a nontrivial solution. (The first case will give a normalizable solution and the second will not.)

Consider solution (a), and postulate $g_- = \tilde{g}_- \exp\left[i\frac{\pi}{4}(n-2)\right]$, where $\tilde{g}_-$ is a real function. This results in

$$\frac{d\tilde{g}_-}{dr} = \left(-i\alpha' - \frac{h+\Delta}{2\lambda}\right)\tilde{g}_-, \quad \text{(D.42)}$$

$$\frac{d\tilde{g}_-}{dr} = \left(-i\frac{\alpha'}{2} - i\frac{m}{\alpha'}\tilde{\mu}_0\right)\tilde{g}_-. \quad \text{(D.43)}$$

These two equations are equivalent to each other when

$$\alpha' = \frac{i}{2}\left(\frac{h+\Delta}{\lambda} \pm \sqrt{\left(\frac{h+\Delta}{\lambda}\right)^2 - 8m\tilde{\mu}_0}\right). \quad \text{(D.44)}$$

Then we find

$$\tilde{g}_-(r) = C_- \exp\left(\pm\int^r dr'\sqrt{\left(\frac{h+\Delta}{\lambda}\right)^2 - 8m\tilde{\mu}_0}\right). \quad \text{(D.45)}$$

Using $g_\uparrow = g_-/2$ and $g_\downarrow = ig_-/2$ to solve for $g_\uparrow$ and $g_\downarrow$, and α' as in Eq. (D.44), we have finally

$$f_\uparrow^>(r) = \frac{C_-}{2}e^{i\pi(n-2)/4}\exp\left(\pm\frac{1}{2}\int^r dr'\sqrt{\left(\frac{h+\Delta}{\lambda}\right)^2 - 8m\tilde{\mu}_0}\right)H^{(1)}_{(n-1)/2}(\alpha' r), \quad \text{(D.46)}$$

$$f_\downarrow^>(r) = \frac{i}{2}C_- e^{i\pi(n-2)/4}\exp\left(\pm\frac{1}{2}\int^r dr'\sqrt{\left(\frac{h+\Delta}{\lambda}\right)^2 - 8m\tilde{\mu}_0}\right)H^{(1)}_{(n+1)/2}(\alpha' r). \quad \text{(D.47)}$$

The asymptotic form of the Hankel function with imaginary argument is $H_\nu^{(1)}(i\alpha r) \sim \sqrt{\frac{2}{\pi i\alpha r}}\exp\left[-\alpha r - i\frac{\pi}{4}(2\right.$ giving the asymptotic solution,

$$f_\uparrow^>(r) \sim \frac{C_-}{2}e^{-i3\pi/4}\sqrt{\frac{2}{\pi|\alpha'|r}}e^{-[(h+\Delta)/2\lambda]r}, \quad \text{(D.48)}$$

$$f_\downarrow^>(r) \sim \frac{C_-}{2}e^{-i3\pi/4}\sqrt{\frac{2}{\pi|\alpha'|r}}e^{-[(h+\Delta)/2\lambda]r}. \quad \text{(D.49)}$$

D.3.3 Attempt at matching solutions

To attempt to match the solution for $r > r_c$ to the solution for $r < r_c$, take Z_ν to be the first Hankel function, and set $\beta = (n+1)/2$. Then the solution for $r < r_c$ becomes

$$f_\uparrow^<(r) = A_\uparrow H^{(1)}_{(n-1)/2}(i\gamma_- r) \sim A_\uparrow e^{-i\pi n/4}\sqrt{\frac{2}{\pi\gamma_- r}}e^{-\gamma_- r}, \tag{D.50}$$

$$f_\downarrow^<(r) = \left(\frac{A_\downarrow}{A_\uparrow}\right) A_\uparrow H^{(1)}_{(n+1)/2}(i\gamma_- r) \sim \left(\frac{A_\downarrow}{A_\uparrow}\right) A_\uparrow e^{-i\pi(n+2)/4}\sqrt{\frac{2}{\pi\gamma_- r}}e^{-\gamma_- r}. \tag{D.51}$$

Using the approximation $h \ll m\lambda^2$, it follows that $\gamma_- \sim h/(2\lambda)$. In the region $r < r_c$, $\Delta \to 0$. Therefore to match the solutions it only remains to determine constants, which should be given by

$$C_- = 2ie^{-i\pi(n-1)/4}\sqrt{\frac{|\alpha'|}{\gamma_-}}A_\uparrow = 2e^{-i\pi(n-1)/4}\sqrt{\frac{|\alpha'|}{\gamma_-}}\left(\frac{A_\downarrow}{A_\uparrow}\right)A_\uparrow \tag{D.52}$$

$$\Rightarrow \frac{A_\downarrow}{A_\uparrow} = i. \tag{D.53}$$

However, in the limit $h \ll m\lambda^2$, we find (using Eq. (D.28)),

$$\frac{A_\downarrow}{A_\uparrow} \sim \frac{ih}{(h-\tilde{\mu}_0)}. \tag{D.54}$$

Therefore, for the Abelian region with $\tilde{\mu}_0 \approx -4t$, constants for these solutions cannot be asymptotically matched.